IMAGE-ADAPTIVE WATERMARKING UNDER GEOMETRICAL ATTACKS

A Thesis submitted

in fulfilment of the requirement for the award of

the degree of

DOCTOR OF PHILOSOPHY

Submitted by

PREETI BHINDER

(951406001)

Under the Supervision of

Dr. KULBIR SINGH
PROFESSOR, ECED

Dr. NEERU JINDAL
ASSISTANT PROFESSOR, ECED

THAPAR INSTITUTE
OF ENGINEERING & TECHNOLOGY
(Deemed to be University)

DEPARTMENT OF ELECTRONICS AND COMMUNICATION ENGINEERING
THAPAR INSTITUTE OF ENGINEERING & TECHNOLOGY
PATIALA – 147004, INDIA

AUGUST 2021

DECLARATION

I hereby declare that the work being presented in this thesis entitled "**IMAGE-ADAPTIVE WATERMARKING UNDER GEOMETRICAL ATTACKS**' in fulfilment of the requirements for the award of degree of DOCTOR OF PHILOSOPHY submitted in Electronics and Communication Engineering Department, Thapar Institute of Engineering and Technology, Patiala, is an authentic record of my own work carried out under the supervision of Dr. Kulbir Singh, Professor and Dr. Neeru Jindal, Assistant Professor, Department of Electronics and Communication Engineering, Thapar Institute of Engineering and Technology, Patiala and refers other researcher works which are duly listed in the reference section. The matter presented in this thesis has not been submitted for the award of any other degree of this or in any other University.

Preeti

Preeti Bhinder

Registration No 951406001

This is to certify that the above statement made by the candidate is correct and true to the best of my knowledge and belief.

31/8/2021

Dr.Kulbir Singh
(Supervisor)
Professor
Department of Electronics and
Communication Engineering
Thapar Institute of Engineering and
Technology
Patiala-147004, Punjab, India

31/8/2021

Dr Neeru Jindal
(Supervisor)
Assistant Professor
Department of Electronics and
Communication Engineering
Thapar Institute of Engineering and
Technology
Patiala-147004, Punjab, India

ACKNOWLEDGEMENT

First and foremost I thank the Almighty whose divine light provided me the perseverance, guidance, enormous patience, inspiration, faith, and strength to carry out this research work.

It’s my pleasure to pay regards and special thanks to my esteemed and eminent supervisors Dr. Kulbir Singh, Professor, and Dr. Neeru Jindal, Assistant Professor, Department of Electronics and Communication Engineering, Thapar University, Patiala, Punjab, India for all the support, encouragement, guidance and profound efforts without which it was not possible to attain the desired level of achievement. I am extremely indebted to them for providing time to listen and give their valuable suggestions.I also express my sincere thanks to Dr. Alpana Aggarwal, Head, Electronics and Communication Engineering Department, Thapar Institute of Engineering and Technology, Patiala for her support and suggestions. I am grateful to my Doctoral Committee Members: Dr. Ankush Kansal, Dr. Vinay Kumar, and Dr. Mandeep Singh, for their insightful comments and encouragement, but also for the hard question which incented me to widen my research from various perspectives.

Words are inadequate in paying regards to my mother late Smt. Vijay Bhinder who was and has always been my pillar of strength and motivation in this journey. I also pay my regards to my father, Sh. P.S. Bhinder for giving me continuous inspiration. I convey my regards to my parents-in-law, Sh. Ravinder Nath Sharma and Smt. Saroj Sharma for their endless support and encouragement. I too thank my younger brother Gulshan, bhabhi Shubhpreet, brother-in-law Sanjeev and his wife Mamta for their love and selfless support in this journey.

I can't quantify and express in words the constant help and moral support of my dear husband Dr. Rajeev Kamal Sharma. His support and advice have been always pillars of strength not only in this work but at every stage of my life. A loving thanks to our kids -Armaan, Vardaan, Sushant, Ishant, and Jasnoor who acted as invaluable sources of stress busters at the time of mental fatigue. Finally, I would like to express thanks to all my friends and colleagues at Chitkara University, Punjab who made their contribution directly or indirectly during this journey of research work to make my Ph.D. successful.

Preeti Bhinder

ABSTRACT

With the evolution of digital forum and internet telecommunication, multimedia essentialities are becoming more notable and acceptable boost in people's daily life. However, this ascendancy of digital contents of media proves to be a major drawback in terms of copyright contravention and unauthorized use of information content. Digital watermarking has expeditiously progressed during the past two decades, which can provide methodical solutions for protection of proprietorship, identification of trademark, corroboration of data legitimacy, tracing of copies of digital content, reprint and ingress controls, etc. Digital image watermarking is an approach to enclose an undisclosed signal (watermark) within a specific image (cover image) and extricate the untold message at the terminus, thereby fortifying the image from signal filtering attacks during the channelling process. The proposed study concentrates on the research topic of robust image watermarking technique for protection of copyright and imperative authentication under structural and coincidental attacks.

The key specifications of any watermarking technique are robustness, capacity, imperceptibility and security. While the expertise of safeguarding the watermark under several attacks is called as robustness, the foretelling of information implanted in the selected cover work is known as capacity. The security refers to potentiality of the watermarking technique to endure intentional complicity. Though many researchers embraced these stipulations, but an insubstantial balance was achieved between the desired requirements. Hence, an image-adaptive approach was suggested to achieve the favourable characteristics by adapting the features of the digital image to recover the hidden watermark in the best possible manner.

The available literature demonstrated limited statistical approach in image-adaptive watermarking technique to accomplish the extraction of the watermark under various attacks. The main intend of this research is to develop robust and coherent image-adaptive watermarking techniques. Discrete Wavelet Transform (DWT) is used on (8×8) size chunks of the host image, wherein the low coefficients of frequency (LL) are modeled using Gaussian distribution to achieve high Peak Signal to Noise Ratio (PSNR) values of watermarked images with minimum BER (%) of recovered watermarks. Different statistical moments of central tendency have been used to hide the watermarks using a flexible strength factor, which were later extracted using a decoder employing Maximum Likelihood (ML).

With the advent of time, need for multiple watermarking has also proliferated. Therefore, the next proposed technique tendered to insert two watermarks into LL and LH sub bands using

DWT with high PSNR values. Kurtosis is used to insert the watermark bits utilizing an adjustable strength factor. It helps to recover the watermarks with fewer errors. The statistical decoder helps to reclaim both the watermarks by making use of the perspective of Gaussian modeling with minimum Bit Error Rate (BER in %) and Gradient Mean Structural Deviation (GMSD) values.

Though many researchers suggested the use of more than one transform for robust watermarking, again a limited success was achieved against common and geometric attacks. The third proposed technique offered to use a combination of DWT and Fast Walsh Hadamard Transform (FWHT) for obtaining good PSNR values. This hybrid technique outplayed the existing techniques against many geometric attacks using the ML decoder. The values of Normalized Cross Correlation (NCC) and Structural Similarity Index Measure (SSIM) too approached the desirable value of unity utilizing this approach.

Another improved hybrid technique has been proposed to embed two watermarks simultaneously using the transforms DWT and FWHT for high PSNR. Five Hybrid Strength Factors based upon mean, standard deviation, entropy, etc were used for inserting the watermarks. The statistical decoder is again used to recover the watermarks with increased robustness and high imperceptibility. The values of Image Quality Assessment (IQA) parameters, such as, PSNR, NCC, SSIM, GMSD, UIQI and BER (%) too proved good efficacy against other state of art techniques.

The utility of all the proposed techniques lies in real time applications of tele-medicine. Alike the natural images, different sized watermarks are used to hide the information of patients in medical images too. All the proposed techniques are semi blind in nature. Thus, side information is communicated to the receiver for the successful recovery of the watermarks. The security of the side information is also ensured. The study may be broadened for colored images through the utilization of other transform domains too in future.

LIST OF PUBLICATIONS

Published

- Preeti Bhinder, Kulbir Singh, Neeru Jindal, “An improved robust image-adaptive watermarking with two watermarks using statistical decoder,” Multimedia Tools and Applications, 79, pages 183–217 (2020). **(SCIE indexed, Impact Factor 2.757)**.

- Preeti Bhinder, Kulbir Singh, Neeru Jindal, “Image-adaptive watermarking using maximum likelihood decoder for medical images,” Multimedia Tools and Applications, 77, pages 10303–10328 (2018). **(SCIE indexed, Impact Factor: 2.757)**.

Communicated

- Preeti Bhinder, Kulbir Singh, Neeru Jindal, “Robust Image-Adaptive Watermarking Using Hybrid Strength Factors,” Wireless Personal Communications (2022). **(SCIE indexed, Impact Factor: 1.671).**

LIST OF ABBREVIATIONS

2D	Two Dimensional
ASF	Adaptive Strength Factor
AHSF	Adaptive Hybrid Strength Factor
AWGN	Additive White Gaussian Noise
BER	Bit Error Rate
CDMA	Code Division Multiple Access
DCuT	Discrete Curvelet Transform
DMT	Discrete Multiwavelet Transform
DWT	Discrete Wavelet Transform
EPR	Electronic Patient Record
EMD	Empirical Mode Decomposition
FWHT	Fast Walsh-Hadmard Transform
GMSD	Gradient Mean Similarity index
GMM	Gaussian Mixture Model
GDWM	Gradient Direction Watermarking
SSGDWM	Single- Scale GDWM
MSGDWM	Multi scale GDWM
HSF	Hybrid Strength Factor
HVS	Human Visual System
IDWT	Inverse Discrete Wavelet Transform
IQA	Image Quality Assessment
JND	Just Noticeable Difference
JPEG	Joint Photographic Expert Group
LSB	Least Significant Bit
MSE	Mean Square Error
MWT	Multiband Wavelets Transformation
NCC	Normalized Cross Correlation

PSNR	Peak Signal to Noise Ratio
PDF	Probability Density Function
QIM	Quantization Index Modulation
QF	Quality Factor
RDWT	Redundant Discrete Wavelet Transform
SSIM	Structural Similarity Index Measure
UIQI	Universal Image Quality Index
SVD	Singular Value Decomposition
SVR	Support Vector Regression
SVM	Support vector Machine
SURF	Speed Up Robust Features
WHT	Walsh Hadamard Transform
2D	Two Dimensional
BER	Bit Error Rate
CDMA	Code Division Multiple Access
DCuT	Discrete Curvelet Transform
DMT	Discrete Multiwavelet Transform
DWT	Discrete Wavelet Transform
FWHT	Fast Walsh-Hadmard Transform
GMSD	Gradient Mean Similarity index
GMM	Gaussian Mixture Model
HVS	Human Visual System
IDWT	Inverse Discrete Wavelet Transform
IQA	Image Quality Assessment
JND	Just Noticeable Difference
JPEG	Joint Photographic Expert Group
LSB	Least Significant Bit
MSE	Mean Square Error
MWT	Multiband Wavelets Transformation

NCC	Normalized Cross Correlation
PSNR	Peak Signal to Noise Ratio
QIM	Quantization Index Modulation
RDWT	Redundant Discrete Wavelet Transform
SSIM	Structural Similarity Index Measure
UIQI	Universal Image Quality Index
SVD	Singular Value Decomposition
SVR	Support Vector Regression
WHT	Walsh Hadamard Transform

LIST OF FIGURES

LIST OF TABLES

LIST OF SYMBOLS AND NOTATIONS

A	Approximated coefficients of 2D-DWT
$A_{i/0}$	Approximated coefficients of 2D-DWT for bit '0' in i^{th} block
$A_{i/1}$	Approximated coefficients of 2D-DWT for bit '1' in i^{th} block
B	Vertically coefficients of 2D-DWT
C	Horizontally coefficients of 2D-DWT
D	Diagonally coefficients of 2D-DWT
F1	Formula 1
F2	Formula 2
F3	Formula 3
Π	Product representation
Σ	Summation representation
W	Host Image
W'	Watermarked Image
σ	Standard Deviation
σ_{max}	Highest Standard Deviation Standard
$\sigma_{i/0}$	Standard Deviation for bit '0' in i^{th} block
$\sigma_{i/1}$	Standard Deviation for bit '1' in i^{th} block
σ^2	Variance
μ	Mean
μ_j	Mean value of any one of the selected j^{th} 8×8 high entropy blocks
$(\sigma_n)^2$	Noise Variance
α_d	Adjustable Dynamic Strength Factor
ρ	Adjusting parameter of denominator of strength factor
$Kurtosis_j$	merit for kurtosis of approximated coefficients for every j^{th} slab.
$Kurtosis_{max}$	largest merit of kurtosis amidst the entire chosen parameters.
H	Entropy value of any one of the selected 8×8 high entropy blocks
H_j	Entropy value of any one of the selected j^{th} 8×8 high entropy blocks

H1	Hybrid Formula 1
H2	Hybrid Formula 2
H3	Hybrid Formula 3
H4	Hybrid Formula 4
H5	Hybrid Formula 5
H_{max}	Maximum Entropy among all the selected 8×8 high entropy blocks
$P(s_1, s_2, \ldots s_N \| 0)$	Probability distribution with measures s_1, s_2, ….s_N for inserting bit '0'.
$P(s_1, s_2, \ldots s_N \| 1)$	Probability distribution with measures s_1, s_2, ….s_N for inserting bit '0'.

TABLE OF CONTENTS

CHAPTER 1

INTRODUCTION

The spread of digital media and its diffusion has evolved into a convenient and excessive usage of the internet over the current generation. However, with the aforesaid suitable approach, the legal distribution of digital media has become much difficult, which has posed an important challenge on the personalized protection of digital content possessions. Information hiding is a general term encompassing several sub-disciplines, mainly being Steganography and Watermarking [1]. The science of hiding the existence of communication is known as Steganography [2]. Embedding a message into its cover without being perceptible is known as Watermarking [3]. The main intention of steganography is the transfer of contents through match masking in a shielded media without building notable replacements into it. Aforementioned approach mostly requires concealing of the confidential message, viz. audio, text, or image into a cover image to initiate a hidden image [4]. This is settled by applying each of the two domain techniques, namely, spatial [5] or frequency transformation [6]. Similar to the talent of hiding messages in steganography utilizing images, digital watermarking focuses to assure the disguised particulars through safeguarding the digital matter attributes of the personal individual. Figure 1.1(a-b) depicts the block diagrams and examples for steganography and watermarking.

Digital watermarking acts as a medium across which contents like charts, words, videos, images, so forth are hidden within the electronic media invisibly by integrating some unique information, such as, owner name or logo in the digital media [7]. The communication can be perceived to all if the hidden data is visible, thus a threat from a malicious attacker is always possible [8]. Generally, the purpose of steganography is to keep the information secret as hidden, whereas, watermarking aims to hide information which is later imperceptible. While steganography hides a message in point-to-point communication, watermarking is used to hide a message in point-to-multipoint communication. Here, either the watermark was used as a transmission or a verification code. The universal categorization of information hiding is shown in Figure 1.1(c) [9].

1.1 HISTORICAL PERSPECTIVE

The concept of watermarking has emerged seven hundred years back when watermark was used to hide the brand of the paper produced by their mills [9]. By the eighteenth

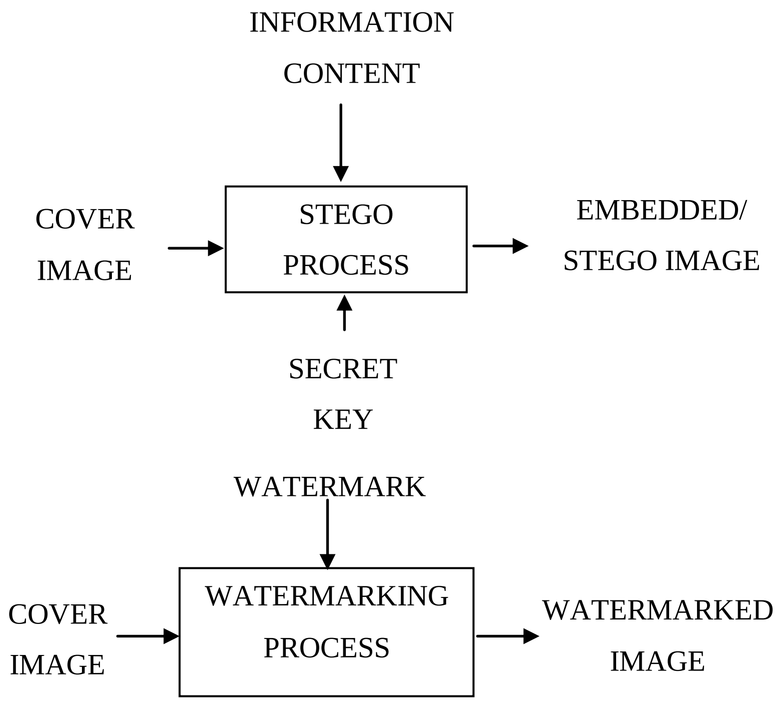

Figure 1.1(a) Block Diagram(s) of Steganography and Digital Watermarking

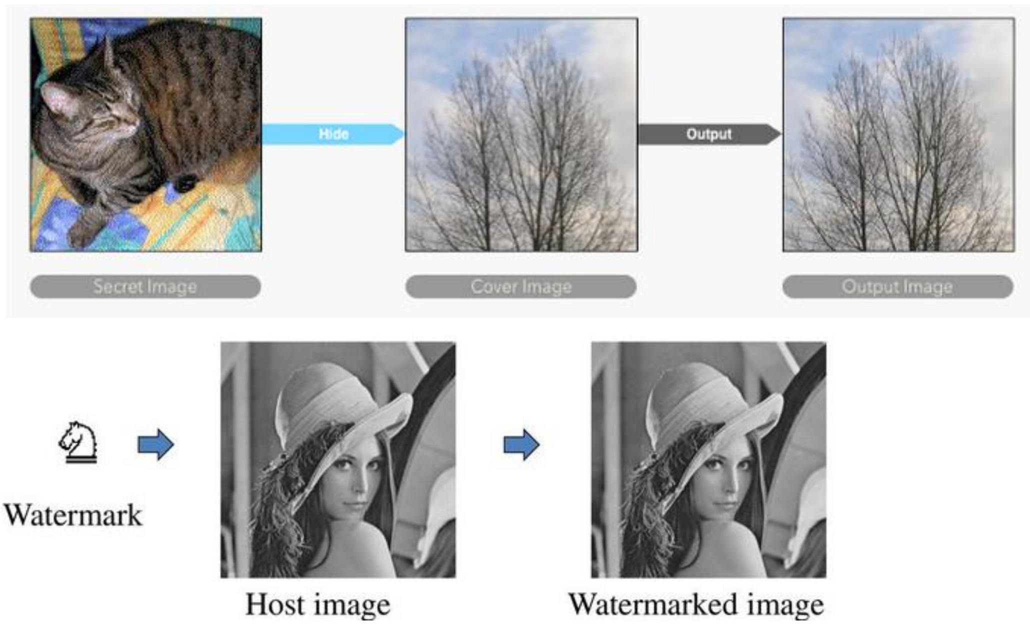

Figure1.1 (b) Examples of Steganography and Digital Watermarking

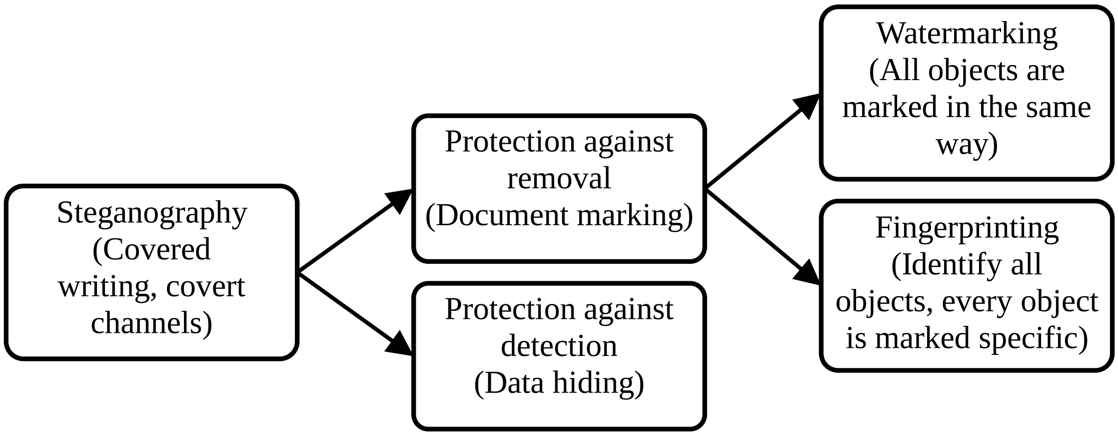

Figure1.1(c) Data Hiding Classification.

century, it was used on currency and other documents. Towards the end of the eighteenth century, the term watermark was introduced, since the marks were found to be similar to the impressions of water on paper [10]. The phrase "digital watermarking" was first utilized by Komatsu and Tominaga in 1988 [11]. Around 1995, the research on digital watermarking increased [12]. However, with the passage of time, the objective of watermarking shifted towards optimum detection of the watermark in the data. This led to the development of various optimum detection techniques like correlation, maximum likelihood, etc.

Similarly, the history of steganography also goes back to pre-Christian era, when messages were written on shaved heads, which disappeared with growing hair. Around the First and the Second World War, invisible ink and blocks of text or images were also used to send messages [2].

Thus, brief reviews of the historic perspective of the above discussed techniques indicate towards the classification of digital watermarking.

1.2 CLASSIFICATION OF DIGITAL WATERMARKING

Digital watermarking displays convenience for claiming the recognition as well as confirming the possession of the electronic media [13]. It provides many applications like security of copyright [14], finger tracing [15], content legitimating, and health protection [18]. Such techniques of watermarking are categorized as spatial [17] as well as transform domain [16] methods.

The criterion of classification of data hiding is generally disjointed towards spatial and frequency domain [19]. The spatial domain techniques refer to manipulations done at the pixel level by varying the intensity values, whereas the techniques of frequency domain refer to the manipulations done at the coefficient level by using frequency transforms [20]. The transform field processes are robust since the attacker is unfitted to easily influence the transfigured coefficients [21]. Nevertheless, numerous transforms, like, Discrete Cosine Transform (DCT) [22], Discrete Fourier Transform (DFT), have already been utilized, even now DWT proves its advantages. These comprise fine regions of frequency as well as space, presentation of multiple designs, investigation of scaling, and versatility [23]. Some of the important techniques existing under spatial and frequency domains are illustrated in Figure1.2.

Depending upon the nature of the application, digital watermarking needs to fulfil different requirements, so that it can be used for different purposes, such as security of identity cards, detection of watermark based on statistical techniques of correlation, likelihood estimation, etc. The classification of watermarking can be understood from Figure 1.3.

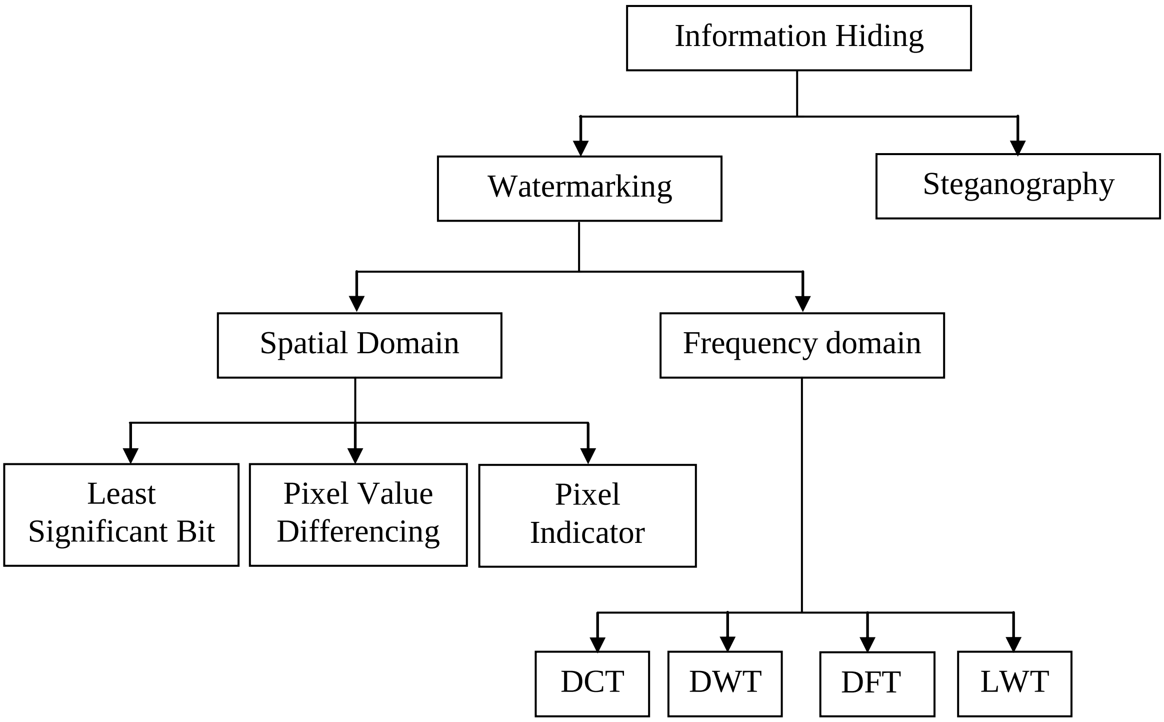

Figure 1.2 Data hiding classification based on domain.

Generally, such applications are divided into two categories viz., detection of watermark and decoding of watermark [24]. The detection of the watermark is used to verify the integrity by determining the appearance of the watermark. The decoding of the watermark deals with the accurate determination of the hidden unknown message. The emphasis of this research work is focused on the second category that is, watermarking for the purpose of data hiding. The techniques of embedding the watermark can also be broadly classified into two classes in the frequency domain, namely Quantization Index Modulation (QIM) and Spread Spectrum (SS) [25].

The embedding of the watermark from the original signal of the media is the fundamental principle of QIM based approaches. Based upon the bit of the information to be placed, the content of the host is quantized to the nearest point of a lattice. However, the direct summation of the watermark to the genuine signal of media is the underlying approach of spread spectrum. Since the hidden information is spread over the host signal, it is doubtlessly the most famous perspective for hiding data.

The embedding in spread spectrum can be done either by additive or Multiplicative Spread Spectrum (MSS) approaches. The information bit is uniformly spread over the host signal in the additive spread spectrum approach. Due to non-availability of the host signal at the decoder, blind decoders are used. Blind decoders suffer from the limitation of performance degradation due to the effects of interference of the host signal, even though they are simple and robust to design. This is a major issue of concern in additive SS (or conventional SS).

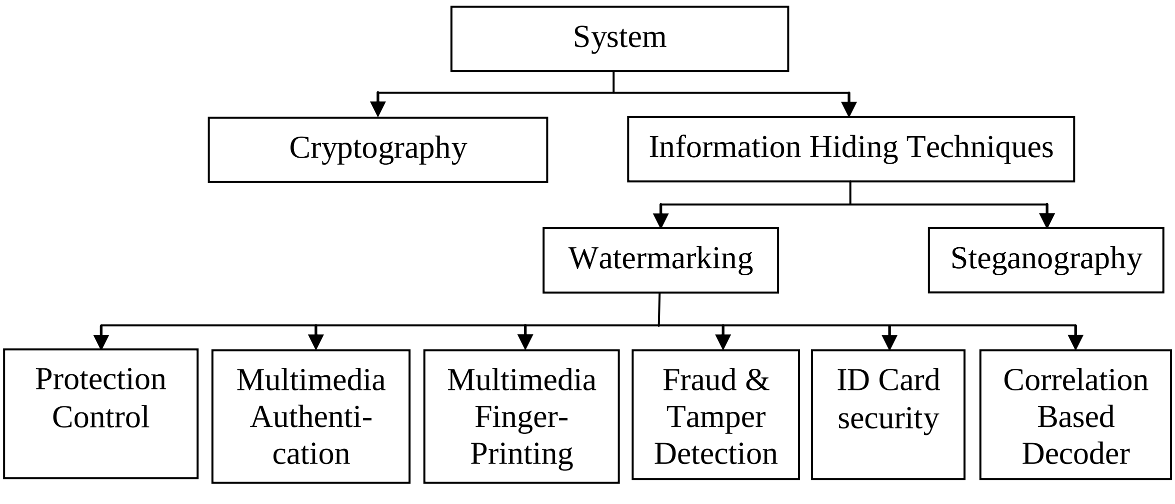

Figure 1.3 Data hiding classification based on techniques used.

An Improved Spread Spectrum (ISS) was also proposed to reduce the interference effects in additive spread spectrum approaches [3]. However, the bits are spread according to the host content in MSS, that is, they are image content dependent, due to which it has higher security features. Later an Improved MSS (IMSS) was also proposed.

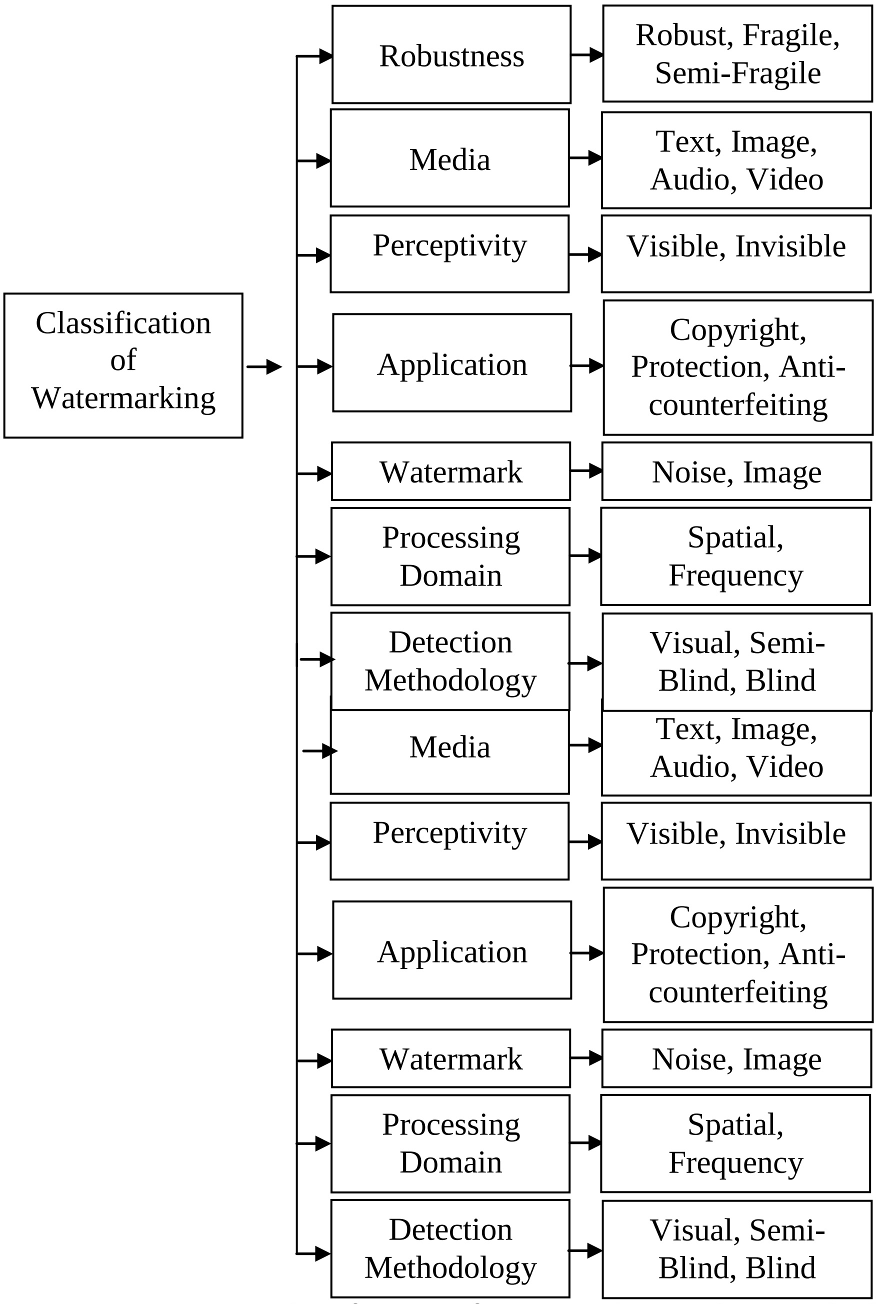

Figure 1.4 Classification of Watermarking techniques [26].

Recently, to increase the strength for providing higher resistance to attacks, new scaling based MSS have been used. Thus, multiplicative watermarking is preferred over additive watermarking methods for protecting copyrights. All types of techniques discussed must be secure against malicious or non-malicious attacks when used in any of the medium or channels. The various classification techniques indicate important characteristics of digital watermarking, as shown in Figure 1.4.

1.3 CHARACTERISTICS OF DIGITAL WATERMARKING

Certain important characteristics [1] of digital watermarking system are

- Embedding Capacity: Refers to the maximum information which can be placed without degrading the image standards.
- Robustness: Refers to destroying the embedded information using various attacks without affecting the blind or semi-blind detection of the cover image [14]. It can be increased by using many statistical approaches such as scaling based strength factor [18], correlation [27], maximum likelihood estimation [28], etc.
- Imperceptibility: The inability to distinguish between the original and the stego-image by a person.
- Security: It is the degree of originality maintained after being treated by intentional or non-intentional attacks.
- Embedding Complexity (desirable).
- Detection complexity (desirable).

However, a trade-off always exists between capacity, invisibility, and robustness of a watermark hiding system [29]. This can be well depicted through a Magic Triangle as shown in Figure 1.5.

1.4 ATTACKS OF DIGITAL WATERMARKING

According to the suitability and compatibility of the application, once the choice of transform has been finalized, the most important requirement is to confirm the stability of the embedding algorithm. When the embedded image withstands various intentional and unintentional (like noise) attacks intervening in the communication channel, it is said to possess the best stability. The different intentional attacks are cropping, filtering, scaling, rotating, compression, etc. as they are done in an attempt to destroy or retrieve the information in some way or the other. Thus, it is important to ensure the stability of the embedding algorithm by assessing the robustness of the attacked watermarked image [3]. The various attacks may be classified as shown in Figure1.6.

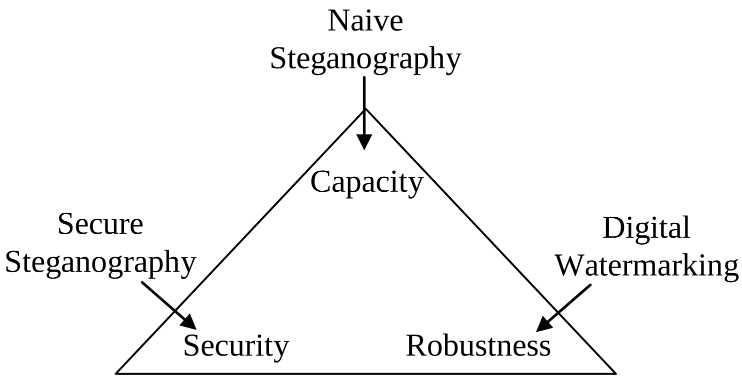

Figure1.5 Magic Triangle to depict trade-off between capacity, robustness, and security [30].

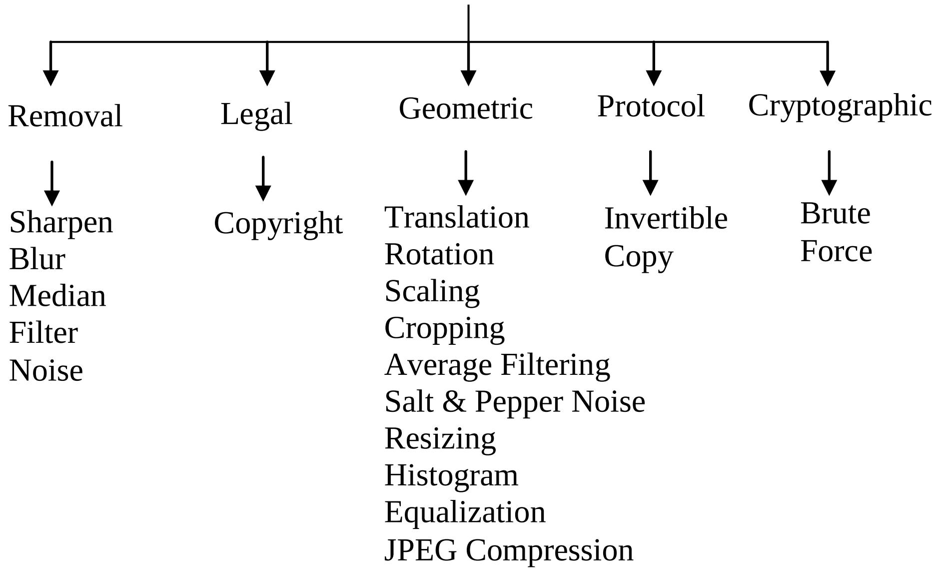

Figure 1.6 Classification of attacks on digital watermarking.

This research study is focused especially on testing the stability and robustness of the watermarked images against geometric attacks. They are very simple but difficult to handle. In these assaults, the main objective of the attacker is to extract the watermark with minimum effect on the performance parameters of the system. These attacks destroy the synchronization between the embedded and extracted watermark resulting in failure of detection and make the entire process of watermarking useless. However, there are many applications of digital watermarking using geometric attacks.

1.5 APPLICATIONS OF DIGITAL WATERMARKING

Data hiding practices are an integration of the applications of its sub-fields of steganography and watermarking. There are many applications of steganography, such as, circulation of confidential information in defense organizations, intelligence departments, military offices, etc. It can also be used for embedding personal details in the photographs of identity cards, medical diagnosis, online voting system, internet banking using mobiles, etc.

Similarly, watermarking applications include the most prominent being copyright protection, where a high level of robust information is embedded about the individual who owns the cover. It is indeed difficult to secure the information against various intentional attackers for medical images also. It can be used in copy protection where the watermark is embedded to avoid the unauthorized copy of the cover, as well as in content authentication, where a less robust and fragile watermark is embedded to detect modifications to the cover. Thus, the applications of digital watermarking [1] can be elaborated but not limited to personal communication, authentication of images, fingerprinting (or traitor-tracing), fraud detection of images, copy protection in Digital Video Discs, smart browsing, viewing movies in a given version of rating, and telemedicine etc. The research is mainly focused on the application of copyright protection of images for further applications in medical watermarking.

1.6 IMAGE-ADAPTIVE WATERMARKING

There are three desirable traits of a universal watermarking set-up viz. High ruggedness, invisibility, and capacity [28]. The watermark of adequate length [29] must be undetectable [30] and strong in opposition to several attacks [31]. A compromise always subsists between high ruggedness with acceptable undetectability and huge volume [32]. This is attained by employing the approach of image-adaptive watermarking which offers the best possible solution [33].

The image-adaptive approach aids the calculation of the statistical parameters to proportionally change with the unique characteristics of the image, thus easing the insertion of the data. Generally the analytical parameters again obtained at the receiver for extraction provide less deviation which helps in detecting or decoding the hidden information at the receiver accurately.

There still exists a wide scope to explore many image-adaptive options [34] to achieve high robustness of the extracted watermark [35] against different assaults [36].

1.7 AIM OF THE RESEARCH WORK

Most of the image watermarking applications emphasized upon the protection of copyright [37] . This was better achieved by using frequency or transform domain techniques based on Spread Spectrum (SS). This approach offered improved robustness and high security against various common and non-malicious attacks. The SS approaches of watermarking also authorized embedding of multiple watermarks with less complexity. The need of a robust watermarking technique has been increasing day by day with the growth of digital media and spread of information.

A limited study has been found for image-adaptive watermarking in telemedicine applications. Hence, a statistical decoder is designed using Maximum Likelihood Estimation (MLE) for successful extraction of medical watermarks. The efficient image- adaptive watermarking technique based on an adjustable, flexible and dynamic strength factor is developed with the best imperceptibility and high robustness. The proposed method effectively recovers the watermarks against various common and geometric attacks.

1.8 CONTRIBUTIONS OF THESIS

- This thesis provides the introduction to an image-adaptive watermarking technique using a flexible strength factor. The notion of spread spectrum was utilized to hide the watermark. A statistical approach has been used to extract the watermark successfully under various attacks.
- In this work, (8×8) block segmentation was used with DWT, wherein the low-low coefficients of frequency were modeled utilizing Gaussian distribution. Statistical moments of central tendency (like, mean, standard deviation, kurtosis, etc.) were used to embed the watermarks. Later, these were extracted using the ML decoder with minimum error.
- The presented work also proposed to embed two watermarks (image and text) concurrently into Low-Low and Low-High coefficients correspondingly. These specifications were diversified in uphill (a bit of watermark as‘1’) or downhill orientation (a bit of watermark as ‘0’) through changeable merit familiar as Adjustable Strength Factor (ASF). Kurtosis was used to compute the mentioned factor, which was further utilized for placing the watermark bits and calibrating along with the properties of the image.

- A hybrid technique using DWT and FWHT was also proposed in the research work. This technique gave better performance and robustness than the earlier techniques against common and geometric attacks.
- Another improved technique using DWT and FWHT was proposed to insert two watermarks simultaneously with increased robustness and high imperceptibility.
- In addition to the performance metrics of PSNR, NCC, and SSIM of watermarked images and BER of recovered watermark, other metrics GMSD as well as UIQI were also used to display the effectiveness of the proposed techniques.
- Lastly, all the proposed techniques found real time applications in the field of telemedicine. Similar to the natural images used in the study, different sized watermarks were used to embed the patient information in medical images. The techniques displayed good imperceptibility and high robustness with desirable capacity and high security.

1.9 THESIS ORGANIZATION

Chapter 1 presents the historical prospective, classification, characteristics, attacks, and applications of digital watermarking. It also includes aim of the research work, contributions and organization of the thesis.

Chapter 2 presents the various techniques, design requirements, and challenges of image watermarking technique. The research gaps, objectives, and research methodology are also described in the chapter.

Chapter 3 presents a new image- adaptive technique for medical images using DWT. An adjustable dynamic strength factor is calculated for watermark extraction using the statistical ML decoder. The approach is partially blind where the attempt is also to secure the side information. The results of execution with common assaults and comparison with existing techniques are also given in detail in the chapter.

Chapter 4 focuses on the improved image-adaptive watermarking technique utilizing two watermarks. The adjustable dynamic strength factor is calculated using the fourth statistical moment known as Kurtosis. The performance of the method is tested against various attacks. The results are compared with techniques embedding single as well as multiple watermarks. The proposed approach found suitable applications in the field of telemedicine.

Chapter 5 presents a hybrid image-adaptive watermarking technique using DWT and FWHT. Four hybrid dynamic strength factors are calculated to confirm the robustness of the suggested approach. The technique is again compared with several existing hybrid watermarking techniques and is found to be worthy for medical images too.

In **Chapter 6**, another modified hybrid image-adaptive watermarking technique is introduced to embed two watermarks simultaneously. The scheme is again compared with latest watermarking techniques of the literature and those proposed in the previous chapters.

Chapter 7 presents the conclusion of the research work and also gives the future direction to improve the performance for the further applications of watermarking.

The next chapter presents the literature survey of the existing techniques of digital watermarking.

CHAPTER 2

LITERATURE SURVEY

In this chapter, the related literature review of image watermarking has been discussed. The different techniques of image watermarking related to spatial, frequency and hybrid domains are elaborated. Several common and important attacks for testing the robustness of the techniques along with various performance metrics are also discussed. The chapter concludes the review with research gaps, objectives.

2.1 INTRODUCTION

The outspread of digital media has significantly increased with the convenient usage of the Internet in the modern era. However, with such an advantageous ingress, nearly all electronic implementations claim various techniques for hiding the knowledge and defending them. These techniques help to protect digital knowledge against unauthorized exploitation and access. Various applications, such as substantiation, protection of trademark, safety, etc. use these techniques, which may be further classified depending upon the type of domain used [38]. The next section describes the types of domain, such as spatial, frequency, and hybrid techniques of image watermarking.

2.2 TECHNIQUES OF IMAGE WATERMARKING

All the techniques of image watermarking depend upon the type of domain for inserting multimedia information using different algorithms [19]. This section helps to analyze the latest methods of watermarking through a summary of the spatial, frequency, and hybrid techniques.

2.2.1 Spatial Domain

These techniques help to insert the watermark bits in the time domain by directly modifying the original pixels of the image [36]. The intensities of the pixels determine either a visible or an invisible watermark [39]. A variety of methods such as, Least Significant Bit (LSB), Intermediate Significant bits (ISB) and patchwork algorithms have been used [38], to achieve a desirable performance [40]. Though these techniques help to hide a large amount of information, yet it may be detected easily if the data is exposed to different attacks [41].

2.2.2 Frequency Domain

Since spatial domain techniques of watermarking can be manipulated easily, thus transform (or frequency) domain techniques are considered as more robust against different attacks [20]. These techniques hide the information effectively in a transform rather than the time space of the signal [21]. The coefficients of transform domain of the original image may be changed by using various transforms, such as Discrete Cosine Transform (DCT), Discrete Wavelet Transform (DWT), Hadamard transform, Fresnel transform, etc. Many researchers have used transform domain techniques of image watermarking for proving better requirement parameters for grayscale, color, and medical images.

2.2.3 Hybrid Domain

Nowadays, the most recent trends in watermarking algorithms are the study of hybrid domain techniques [42]. These watermarking techniques use the combination of spatial and frequency domain algorithms [43].This helps to offer the advantages of both domain techniques [44] by ensuring to achieve both robustness [45] and increased data insertion properties [46]. These methods also help to increase [47] the capacity of the original images [48]. A lot of research has been carried out on the hybrid domain watermarking techniques for medical [49] and security applications [50].

2.3 DESIGN REQUIREMENTS OF IMAGE WATERMARKING

The techniques of digital watermarking system aim to successfully hide a watermark into multimedia information [51]. This is done for ensuring the authenticity and protection of copyright against unauthorized manipulation. Hence, the characteristics of image watermarking system play a very important role in developing an efficient watermarking technique for various applications [52]. These requirements are detailed below.

2.3.1 Imperceptibility

Watermarking techniques hide the bits of the information into an image in such a way that the perceptual differences are invisible to the human eye. Here, the watermarked image appears almost indistinguishable to the humans though there are a few degradation changes in the brightness or the contrast of the image. Thus, imperceptibility refers to the requirement of preserving the image quality of the watermarked image to seem similar to the original image. The best techniques of image watermarking ensure complete invisibility to the human visual system and generate no visual differences between the original and watermarked images [53].

2.3.2 Robustness

Generally watermarked images are manipulated intentionally or unintentionally for extraction of the watermarks. When these watermarks survive such attacks, they are known as robust watermarks. Hence, robustness refers to a key requirement of detecting a watermark under different applications of common and uncommon signal processing operations. Robust watermarking techniques may be either classified into robust, fragile or semi fragile [54].

While robust techniques help to successfully extract the watermark without any alteration of the data, fragile watermarking techniques result in acceptable effects in the visual quality to human eye. However, semi-fragile watermarking techniques resist some common transformations but fail to recover the watermark under malicious attacks. Thus a good watermarking technique must be robust against various attacks.

2.3.3 Security

Security is a significant requirement in digital watermarking techniques. Various techniques have been used to ensure the confidentiality, integrity and authenticity of the inserted watermark through different encryption techniques. This requirement helps to prevent any unauthorized access for distinguishing, retrieving or modifying the hidden watermark. The degree of security confirms the quality of the various digital image watermarking techniques [55].

2.3.4 Capacity

The capacity of the watermarking technique refers to the maximum number of redundant information bits to be inserted into the host image. It is also called as payload and depends upon the size of the watermark bits. Similar to imperceptibility and robustness, capacity is too an important requirement as it determines the maximum information to be carried by any host image with less distortion [56]. It challenges the limitations of the watermark information while trying to achieve a desirable balance between imperceptibility and robustness. Hence desirable watermarking techniques should aim to minimize distortion with greater information embedding capacity.

From the above discussion, it seems difficult to achieve a simultaneous balance between the desirable requirements of digital image watermarking techniques. Due to their limiting and conflicting characteristics, an increase in robustness and capacity may lead to a decrease in imperceptibility, or a decrease in robustness may lead to an increase in the payload. Though most of the techniques try to maintain a good trade off amongst these requirements, still limited set of desirable properties are satisfied by many watermarking approaches. Some of these techniques are given in Table 2.1.

Most of the above latest image watermarking techniques is used for protection of copyright and ownership applications, but a limited sphere exists for field of telemedicine. This requires the need for robust techniques using transforms, such as DWT. However, it is observed that only a limited robustness is achieved against various geometric attacks. Though these techniques offer good imperceptibility with minimum security and less capacity, still a wide scope exists for further research using natural and medical images.

2.3.5 Techniques of Image-Adaptive Watermarking

Robustness, imperceptibility and capacity are the desirable characteristics of any watermarking system in general. But a trade-off always exists between high robustness with good imperceptibility and large capacity. This is achieved by using image-adaptive watermarking approach. It is indeed one of the best solutions used to balance the desirable features.

Cox et al. [3] used a simple approach of additive watermarking to hide the information in specific parts of the image using spread spectrum method so that the watermark became slightly robust towards common transformations. Podilchuk et al. [33] proposed another approach of watermarking based on visual models for copyright protection to maintain a difficult balance between opposing requirements of imperceptibility and robustness of watermarking system. Models for image-adaptive watermarking using human visual system were also proposed by Watson [35] and Barni et al [32] for limited robustness. Akhaee et al. [27] suggested a robust, semi blind, and scaling based image-adaptive approach for embedding the bits of watermark in blocks of high entropy of the host image. The block coefficients were modeled using Gaussian distribution which was scaled in an up or down direction in each block with a fixed strength factor only, which was indeed difficult to change.. The data was extracted using the ML decoder. A similar approach was also used by Amirmazlaghani et al. [31], where the block coefficients were modeled by Gaussian Mixture Model (GMM) to achieve improved robustness with limited capacity. Yadav and Singh [14] also proposed a robust and semi-blind image-adaptive technique of watermarking. They used the concept of spread spectrum by making the strength factor variable with the general characteristics of the image based on standard deviation. Blocks of high entropy were used for embedding data which were extracted using a non statistical correlation decoder. Yadav et al. [16] also provided a brief review on popular transform domain techniques of robust image adaptive watermarking techniques. He used different models based on HVS (Human Visual System), transform properties and limited statistical approaches. He also distributed transform coefficients based on entropy and extractions from natural host image. Thus, most of the research was detailed for natural images and a limited amount of work is done in medical image–adaptive watermarking. Hence the suggested technique may find a suitable application in the area of telemedicine.

2.3.6 Watermark Extraction using Statistical Decoders

Depending upon the nature of the application, digital watermarking needs to fulfill different requirements, so that it can be used for different purposes, such as security of identity cards, detection of watermark based on statistical techniques of correlation, likelihood estimation, etc. Generally, such applications are divided into two categories viz. detection of watermark and decoding of watermark [24] The detection of the watermark is used to verify the integrity by determining the appearance of the watermark [25]. The decoding of the watermark deals with the accurate determination of the hidden unknown message [26]. The emphasis of this research work is focused on the second category that is, watermarking for the purpose of data hiding.

According to the suitability and compatibility of the application, once the choice of transform has been finalized, the most important requirement is to confirm the stability of the embedding algorithm [57]. When the embedded image withstands various intentional and unintentional (like noise) attacks intervening in the communication channel, it is said to possess the best stability [58]. The different intentional attacks, cropping [59], filtering [60], scaling [61], rotating [62],

compression [63], etc, are done in an attempt to destroy or retrieve the information in some way or the other. Thus, it is important to ensure the stability of the embedding algorithm [64] by assessing the robustness of the attacked watermarked image [65].
The role of watermark detector became very important especially when watermarks were attacked by malicious or non-malicious users to retrieve or corrupt information [20]. Several researchers proposed different techniques to test the robustness of watermark extraction by either using correlation based [23] or decision based approaches. Barni et al. [32] used statistical decision theory technique based on the criteria of Neyman-Pearson to decode 1-bit and multi-bit watermarks using the limited features of Weibull distribution. Ng and Garg [66] proposed the use of maximum likelihood for only detecting the presence of digital watermark by using Generalized Gamma and Laplacian models [67]. Akhaee et al. [68] also used maximum likelihood decision rule in an image watermarking system using multiplicative embedding to determine the watermarked coefficients using Generalized Gaussian Distribution (GGD) and Quantization Index Modulation (QIM) [69] techniques with limited robustness against various attacks.. Zhu [70] used information entropy to embed the Discrete Wavelet Transform (DWT) coefficients modeled by GGD and only detected the watermark using hypothesis testing based on Likelihood Ratio Test (LRT). Cogranne et al. [71] too used hypothesis testing theory to design a Generalized Likelihood Ratio Test Local Adaptive Model (GLRT-LAM) to predict the false alarm probability by using statistical properties of the designed test.

In addition, some researchers [72] have also utilized the principle of Maximum Likelihood Estimation (MLE) for watermark extraction [73]. This approach is based upon statistical modeling [31] of the transform coefficients for better extraction of watermark bits [74], as compared to correlation detectors. The unbiased estimation of this approach helps to recover the watermark more efficiently [64]. A comparative analysis of the latest state of art techniques has also been presented in Table 2.2.

2.4 TRANSFORMS USED

A brief characterization of the Transforms utilized in the proposed work is presented in this section.

2.4.1 Discrete Wavelet Transform (DWT)

The concept of wavelet transform was first incepted by Haar [75] in 1910. Grossman et.al [76] were the first to report the development of wavelets in 1984. Later in 1988 and 1989, Daubechies [77] and Meyer [78] gave the concept of orthogonal wavelet and multi-resolution analysis, respectively.

DWT divided an image within four frequency sub bands. The Low-Low sub band carried the lowest frequency coefficients that can be further decomposed to embed watermark bits. DWT offered excellent multi-resolution and localization characteristics which allowed information to be inserted in any of the sub bands. It also exhibited similarity with the HVS (Human Visual System) model which helped to hide the watermark imperceptibly.

2.4.2 Fast Walsh Hadamard Transform (FWHT)

FWHT is an orthogonal transform that offers the simplicity of implementation due to low computational cost and superior performance [79]. It is best suited for image processing applications because of fast computation by successive doubling methods [80]. Generally, Hadamard Transform uses a Hadamard square matrix which is orthogonal and contains only +1 and -1 values, as shown below.

$$H_2k = \begin{bmatrix} H_{2^{k-1}} & H_{2^{k-1}} \\ H_{2^{k-1}} & -H_{2^{k-1}} \end{bmatrix}, \text{for } k=1,2,3.....\text{and } H_1=1 \text{ for } k=0 \qquad (2.5)$$

Similarly, the Hadamard Transform of order 2 (for k=1) and 4 (for k=2) are related respectively as,

$$H_2 = \begin{bmatrix} 1 & 1 \\ 1 & -1 \end{bmatrix} \text{ and } H_4 = \begin{bmatrix} H_2 & H_2 \\ H_2 & -H_2 \end{bmatrix} \qquad (2.6)$$

Here, most of the energy is concentrated in the upper section of the transformed pattern. These square matrices are orthogonal and contain only integer values. This helps in the fast calculation as implementation needs M $\log_2 M$ additions and subtractions, where M is the dimension of the image. Since these coefficients are also very less affected by noise, the concentration of FWHT coefficients into a very small area offers a perfect hiding place for watermark bits. This helps to implant the watermark bits imperceptibly in the small frequency components and also increases the robustness against various attacks.

Due to the numerous benefits offered by DWT and FWHT, the proposed work utilized them in watermarking of medical images.

2.5 CHALLENGES

The above key requirements of a digital image watermarking technique are indeed a difficult task to be implemented. Moreover, the alteration or detection of a hidden watermark becomes easier when such information is passed through a communication channel. The watermark may be manipulated or impaired by an intentional or unintentional attack. This poses a great threat to the hidden information and another challenge for successful extraction of the watermark amidst different attacks.

2.5.1 Attacks

In digital image watermarking, an attack may be assumed as any activity which may cause a harmful modification of the watermark information. Such a processed watermark is also known as attacked information or data [36]. However, it is desired that watermarking techniques must be enough robust against these attacks [37]. Attacks may be generally classified into Active and Passive attacks. They may be further sub classified into Removal attacks, Geometric attacks, Protocol attacks and Cryptographic attacks.

Active attacks occur when the watermark is adversely exploited for the purpose of removal or destruction leading to a distortion in the watermarked image. Such attacks may process the watermark to make the detection either imperceptible or unauthenticated even in a case of validated watermarked image [81].

Passive attacks relate to obtaining the watermark information without the destruction, deletion or manipulation of the same. No resources of the watermark are modified for accessing the hidden information [82].

Removal attacks aim to remove the watermark data without using the security key of the watermark embedding algorithm. The watermark information is altered to an extent that it becomes more difficult for the original owner to retrieve through extraction algorithm. Such attacks decrease the robustness of the watermark data by adding different types of noise (Gaussian noise, salt pepper noise, etc.), blurring, sharpening or filters to the watermarked signal. Though these attacks are unable to remove the watermark completely, still they attempt to the damage the information contained in the watermark to a considerable extent [83].

Geometry attacks do not attempt to remove the watermark but instead attempt to distort the synchronization of the detector of the watermark. These attacks convert the structural pattern between the original and the recovered watermark during the detection process [84]. These are known as are the most difficult attacks as the image geometry is deeply manipulated. Despite the challenge, the watermark is still extracted as it lies hidden in the watermarked image. Watermarking techniques must be robust against these transformation attacks such as, rotation, scaling, translation, cropping and compression. The proposed work also presented excellent robustness against geometrical attacks.

Protocol attacks aim to replace or copy the original, valid watermark to deeply affect the applications of watermarking techniques. In such attacks, the original watermark may never be extracted as the attacker may pose the original owner of the hidden information [85]. These attacks may be either invertible or non-invertible in nature.

Cryptographic attacks aim to break or crack the security of a watermarking algorithm by removing the inserted information. They may either inset a secret information for misleading the watermark or create a non-watermarked signal for public detection [86]. These attacks are highly complicated and are used in restricted applications.

2.5.2 Robustness against Geometric attacks

Recently, the focal point of the research in watermarking has shifted towards robustness against geometric distortions [36]. These manipulations [87] uniformly affect the coordination between pixels of the image and deform them to a severe extent [88]. They also cause difficult recovery of watermarks [52] and lead to prominent performance losses [53]. The robustness of the watermarking techniques is evaluated against different geometrical attacks, such as, compression [89], scaling, rotation and filtering [90], etc.

While the compression attack deals with coding of the transform, the scaling attacks modify the aspect ratio of the images by changing their sizes either uniformly or non uniformly [85]. Filtering attacks also degrade the watermark quality and decrease the strength of the security [73]. However, the rotation attacks apply different geometrical angles of rotation in a clockwise or an anticlockwise direction, with recovery of the watermark being a great challenge [91].

Though many approaches have been suggested, still the performance of the watermarking techniques draws a significant attention. The evaluation of the robustness is confirmed from the following performance metrices.

2.5.3 Performance Metrics

An important criterion to recognize the performance of watermarked images is the quality of the watermarked images under various attacks. This may be measured through the evaluation of various performance metrices [92]. The objective values of these parameters justify the effectiveness of the watermarking techniques. Some of the Image Quality Assessment (IQA) parameters are as follows.

Peak signal to Noise Ratio (PSNR) relates to the similarity between watermarked and host images and is measured in decibels (dB) [93]. Greater the value of PSNR superior is the sensitivity of the inserted watermark upon the host image. It is a great challenge to obtain the desirable features of imperceptibility and robustness simultaneously. It is calculated using Mean Squared error (MSE) between the watermarked and original images, as

$$PSNR = 10\, log\left(\frac{max_i^2}{MSE}\right)_{10} \tag{2.1}$$

$$MSE = \frac{1}{M \times N} \sum_{x=0}^{M-1} \sum_{y=0}^{N-1} (\, B(x, y) - B_w(x, y))^2 \tag{2.2}$$

Here, B is the original image, B_w is the watermarked image, M represents the rows and N represents the columns of an image.

The values of *Normalized Cross Correlation (NCC)* and *Structural Similarity Index Measure (SSIM)* are calculated using (2.3) and (2.4) [94]. While NCC measures the degree of alikeness (or unlikeness) among the watermarked image $\left(w^*(x, y)\right)$ and host image $\left(w(x, y)\right)$, SSIM calculates the perceptual difference between two similar images. The value of NCC is normalized in scale 0 to 1 and indicates how well a pattern of the host image matches with that of a watermarked image [95]. However, the value of SSIM relates to visible structures and tries to quantify the data losses in an image when watermark bits are embedded in it, which are compared with the structure of an original reference image [96]. These scruples approach the perfect value of unity.

$$NCC = \frac{\sum_{z=1}^{M}\sum_{y=1}^{N} w(x,y)Xw^{*}(x,y)}{\sum_{x=1}^{M}\sum_{y=1}^{N} w^{2}(x,y)} \tag{2.3}$$

$$SSIM = \frac{\left(2\mu_{w}\mu^{*}{}_{w}+C1\right)(2\sigma_{ww^{*}}+C2))}{\left(\mu_{w}^{2}+\mu_{w^{*}}+C1\right)(\sigma_{w}^{2}+\sigma_{w^{*}}^{2}+C2)} \tag{2.4}$$

The robustness of the techniques is also measured by the pixel-wise geometric similarity approach of GMSD, which also proves an important subjective image quality performance metric. By capturing the local host image characteristics, GMSD calculated the average diversity using the concept of standard deviation in the watermarked image [97]. Ideally, the deviation must be zero.

Another subjective Image Quality Assessment (IQA) parameter, namely UIQI is also used to prove the robustness of the techniques [98]. This perception-based quality measure used the characteristics of the Human Visual System (HVS) in calculating the change in quality due to distortions in correlation, luminance, and contrast between two images [99]. Ideally, the value of UIQI lies within the dynamic range of [-1, 1] but desirably must approach unity. Since the approach of the measurement does not depend either upon the image to be tested or its conditions, thus it is called as universal [98].

Finally, the performance is also measured by Bit Error Rate (BER) which is generally calculated as the ratio of received noisy watermarked bits to the total number of initial watermark bits and expressed in percentage [100]. It is generally calculated as a proportion of received noisy bits of the watermark to the total count of bits for the initial watermark and is expressed in percentage. This value lies in the range [0, 1]. The lesser the value of BER (%), the higher is the accomplishment of the suggested techniques with regard to a good watermark extraction [101].

It is indeed a great challenge to obtain desirable Image Quality Assessment (IQA) parameters under different attacks. Many researchers have tried to achieve the desirable performance metrics against the challenging scenarios of various common and geometric attacks.

Table 2.1 Comparative analysis of design requirements of image watermarking techniques.

Author, Reference no., Year, Domain	Technique Used	Imperce-ptibility	Robustness	Capacity	Security	Applications
Pizzolante et.al, [102], 2014 Spatial	Blind extraction		✓		✓	Protection of Microscopic images
Zhou et.al, [55], 2017, Transform	DCT	✓	✓		✓	Protection of Copyright information
Singh et.al, [56], 2016, Spatial	Back Propagation Neural Networks (BPNN)		✓	✓	✓	Protection of digital information
Zear et.al, [49], 2016, Hybrid	DWT, DCT and SVD	✓	✓	✓	✓	Health care and diagnosis
Zhang et.al, [81], 2017, Transform	All Phase Bi orthogonal Transform (APBT) and SVD	✓	✓			Authentication and protection of copyrights
Liu et.al, [103], 2017, Transform	DCT and Fractal Coding	✓	✓	✓	✓	Protection of copyright
Jia et.al, [104], 2017, Transform	DWT, QR Decomposition	✓	✓	✓		Copyright protection in color images
H.Vo et.al,[105], 2017,Transform	DCT, SVD	✓	✓			Copyright protection for stereo images
AL-Haj et. al,[82], 2017, Transform	DWT, SVD	✓	✓		✓	Protection of copyright for E-government transactions
Ernawan et.al,[83], 2017, Transform	DCT using psycho visual threshold	✓	✓		✓	Protection of Copyright
Harjito et.al,[106], 2017,Transform	DWT , SVD	✓	✓		✓	Protection of ownership rights
Sandoval et.al,[107], 2017, Spatial	Just Noticeable Distortion (JND) and Gamma Correction Factor (GCF)	✓	✓			Watermarking of visible images for

						protection of copyright
Loan et.al, [93], 2018, Transform	Discrete Cosine Transform(DCT), Arnold Transform and Chaotic Encryption	✓	✓		✓	Telemedicine and E-healthcare
Varma et.al,[94], 2018, Spatial	Correlation Coefficient matrix	✓	✓			Authentication of data
Arrasyid.et.al,[95], 2018, Transform	DCT, DWT, and SVD	✓	✓			Improvement in performance of copyright protection
Takore et.al,[48], 2018, Hybrid	Particle Swarm Optimization algorithm	✓	✓			Authentication of Images
Zhou et.al,[96], 2018, Transform	All Phase Discrete Cosine Bi orthogonal Transform (APDCBT), DWT ,SVD	✓	✓			Protection of copyright
Phadikar et.al,[108], 2019, Transform	Lifting and Companding using DWT	✓		✓	✓	Digital Imaging and Communications in Medicine
Lei et.al,[84], 2019, Hybrid	Integer Discrete Wavelet Transform (IDWT), Artificial Bee Colony (ABC) and Quantization Index Modulation (QIM)	✓	✓		✓	Protection of Copyright and Authentication of images
Chen et.al,[109], 2019, Transform	Lifting Wavelet Transform	✓	✓	✓		Protection of Copyright
Errawan et.al,[100], 2018, Transform	RDWT and SVD	✓	✓			Protection of Copyright
Abraham et.al,[110], 2019, Spatial	LSB modification using Simple Image Region Detector (SIRD)	✓	✓	✓		Protection of Copyright
Ambadikar et.al,[85], 2019, Transform	DWT	✓		✓	✓	Protection of Copyright and authentication of

						Content
Khan et.al, [111], 2019, Spatial	Image scanning using Neighbouring Distance Difference (NDD)	✓	✓			
Koley et.al,[86], 2019, Transform	Reversible and feature based watermarking using LWT	✓	✓			Protection of copyright and ownership
Sharmin et.al, [92], 2019, Transform	Blind watermarking using Hadamard Transform	✓	✓			Copyright fortification
Ariatmanto et.al, [61], 2020, Transform	DCT coefficients were utilized for embedding with different scaling factors.	✓	✓		✓	Protection of Copyright
Ariatmanto et.al,[62], 2020, Transform	Adaptive scaling factors used with DCT	✓	✓	✓	✓	Improvement in performance of copyright protection
Malayil et.al,[112], 2021, Transform	Zero watermarking	✓	✓	✓	✓	Transmission of medical images
Zheng et.al,[63], 2020, Transform	Adaptive strengths used for embedding with DWT and NSST	✓	✓			Image and Video watermarking
Srivastava et.al,[57], 2021, Hybrid	DCT-DWT used with Arnold Transform	✓	✓	✓	✓	Video watermarking
Xiang-Yang et.al,[58], 2021, Transform	Statistical BKF modeling using blind approach with NSST for adaptive watermarking	✓	✓			Protection of Copyright

Table 2.2 Performance summary of latest state of the art image watermarking techniques against various attacks.

Author, Reference no., Year, Domain	**Technique used for embedding**	**Technique used for watermark extraction**	**Size of host image and watermark**	**IQA parameters used**	**Attacks performed**	**Performance of Robustness against various attacks**
Su et.al, [87], 2014, Transform	Algorithm based on colored host images and watermarks using QR decomposition	Blind approach	512 × 512 32 × 32	PSNR NCC SSIM	JPEG Compression, Geometric attacks	Highly imperceptible and robust with limited security and capacity.
Su et.al, [36], 2018, Spatial	Approximate Schur based decomposition for colored imaged	Blind approach	512 × 512 32 × 32	PSNR NCC SSIM	JPEG Compression, Filtering, Noise, scaling, rotation	Good imperceptibility and robustness but limited real time applications.
Su et.al, [88], 2015, Transform	Two level DCT used for colored images	Correlation detection	512 × 512 64 × 64	PSNR NCC SSIM	JPEG Compression, Filtering, Noise, blurring, cropping, rotation	Excellent robustness against JPEG compression attacks with good security and capacity.
Su et.al ,[39], 2019, Hybrid	2-D-DFT used to obtain DC component for quantization in spatial domain	Correlation detection	512 × 512 32 × 32	PSNR NCC SSIM	JPEG Compression, Filtering, Noise, cropping,	Good imperceptibility with limited robustness in real time applications.

Su, [113], 2016, Transform	Algorithm based on colored host images and watermarks using Hessenberg decomposition.	Blind approach using Correlation detection	512 × 512 32 × 32	PSNR NCC SSIM	image compression, filtering, cropping, rotation, adding noise, blurring, scaling, sharpening and rotation	Good imperceptibility and robustness.
Qin et.al,[38], 2016, Spatial	Self-embedding scheme for tampering recovery applications was used for gray scale images.	Correlation detection	512 × 512 32 × 32	PSNR, SSIM	Analysis of effects under different embedding strengths only	-------------
Roy et.al, [40], 2018, Spatial	Change in pixel geometry	Blind approach	Host images of size 613 × 833 and 512 × 512 with Binary watermarks of sizes , 100 × 91 148 × 72 100 × 128 150 × 149 549 × 85 438 × 115	PSNR, BER	cropping, rotation, scaling and crop-and-rescaling attacks were used for testing.	Validated Robustness
Mir, [114], 2014, Spatial	HASH function used to embed watermarks with encryption	Correlation detection	------	------	-------	Robust using cryptography and encryption techniques.
Huynh	Selective MSB and LSB	Detection using	512 × 512	PSNR,	median filtering,	Limited robustness

et.al,[89], 2018, Transform	embedding (SMLE) method used with DWT	Otsu thresholding.	64 × 64	NCC, SSIM, BER	average filtering, linear motion blurring, size scaling, rotation, cropping, additional noise (Gaussian and Salt & Pepper), histogram equalization, and lossy JPEG compression	against JPEG Compression and Rotation attacks.
Agarwal et.al,[90], 2015, Transform	DWT and Redundant DWT were used	Blind ,invisible approach	512 × 512 64 × 64	PSNR, NC	cropping, Gaussian filtering, Gaussian noise, salt and pepper noise, rotation, JPEG compression and resize	Limited robustness against Rotation attack
Ambadekar et.al,[85], 2019, Transform	DWT	Non Blind approach using Correlation detection	228 × 228 90 × 90	PSNR MSE CC (Correlation Coefficient)	salt-and-pepper noise, geometrical attack through rotation and JPEG compression attack	Limited robustness against Rotation attack
Rosiyadi et.al,[115], 2012,	DCT and SVD using Genetic Algorithm(GA) combination used to	Correlation detection	512 × 512 256 × 256	PSNR Correlation Coefficient	JPEG 50, rotation 60, median filtering,	Good robustness in DCT-SVD using GA than original

Transform	compare performance with original DCT-SVD combination				Gaussian noise 0.5.	combination.
Sarreshtedarie t.al,[116], 2015, Spatial	Source coding algorithm using Set partitioning in hierarchical trees (SPIHT) encoding was used to protect against tampering	Decoder using correlation detection principle	512 × 512 ----	PSNR	---------	
Akhaee et.al,[73], 2015, Transform	Scaling based strengths for watermarking with different transform domains	ML Decoder	512 × 512 64 × 64	PSNR NCC SSIM BER	JPEG Compression, Gaussian noise, Salt & pepper noise, Gauss Filter, Scaling, Cropping, and Rotation.	Limited robustness against geometric attacks
Amirmazlagh ani et. al,[31], 2015, Transform	Blind watermarking approach using Gaussian Mixture modeling and scaling factors	ML Decoder	512 × 512 Different PN sequences of variable lengths		JPEG Compression, Gaussian noise, Median filter, Gauss Filter, Scaling, Rotation	Acceptable robustness than partially blind approach.
Hu et.al,[44], 2017, Hybrid	QIM application with DWT-DCT scheme with adjustable embedding strength	Blind approach	512 × 512 64 × 64	PSNR SSIM	JPEG Compression, Gaussian noise, Salt & pepper noise, Median filter, Gauss Filter, Scaling, Cropping	Robustness failure against desynchronization attacks.

Zear et.al,[49], 2018, Hybrid	Multiple watermarking using DWT, DCT ,SVD and BPNN for medicine applications	Correlation Detection	512 × 512 256 × 256	PSNR NCC BER	JPEG Compression, Gaussian noise, Salt & pepper noise, Median filter, Gauss Filter, Scaling, Cropping, Rotation	Improved robustness using BPNN
Sadreazami et.al,[74], 2016, Spatial	Contourlet domain	ML decoder based on Normal Inverse Gaussian distribution	512 × 512 Different PN sequences of variable lengths	PSNR, NCC, SSIM, BER	JPEG Compression, Gaussian Noise, Rotation, Filtering, Cropping	Limited time complexity
Wang et.al,[91], 2016, Transform	Blind approach using NSST	ML decoder based on Bessel K Form (BKF) modeling used	512 × 512 128 bits of watermark data used	PSNR, NCC, SSIM, BER	JPEG Compression, white Gaussian noise, Salt &Pepper Gaussian Filter, Scaling, Rotation	Limited robustness against geometric attacks
Amini et.al,[117], 2017, Transform	DWT	Statistical modeling using HMM	512 × 512 and PN sequences of various lengths.	PSNR, NCC, SSIM, BER	JPEG Compression, white Gaussian noise, Gaussian Filter, Sharpening	Sensitivity in shifting of wavelets
Ahmaderaghi	Blind watermarking	Statistical	512 × 512	PSNR,	JPEG	Good performance

et.al,[118], 2018, Transform	approach using Discrete Shearlet Transform (DST)	decoder using Laplacian modeling	------	MSE, BER	Compression, white Gaussian noise, Rotation, Cropping	under limited payload capacity
Amini et.al,[119], 2019, Spatial	Blind watermarking using HMM and contourlets	Statistical detection using binary Hypothesis testing	512 × 512 And PN sequences	PSNR	JPEG Compression, white Gaussian noise,Filtering, Rotation, Cropping	Good robustness against common attacks
Garg et.al,[50], 2019, Hybrid	Discrete Stationary Wavelet Transform (DSWT), DCT and SVD using Arnold Transform	Correlation Detection	256 × 256 256 × 256	PSNR NC	JPEG Compression, Salt &Pepper Wiener Filter, Median Filter, Rotation	Good robustness achieved with less values of NC.
Zhang et.al,[51], 2019, Hybrid	DWT, DCT using Spread transform quantization index modulation (STQIM) and Orthogonal matching pursuit (OMP)	Correlation Detection	256 × 256 32 × 32	PSNR, BER	JPEG Compression, Gaussian Noise, Salt &Pepper noise	Good robustness against most of the attacks
Elsafty et.al,[52], 2019, Hybrid	Discrete Curvelet Transform (DCuT) and Redundant Discrete Wavelet Transform (RDWT)	Blind approach using correlation detection	512 × 512 64 × 64	PSNR, NCC, SSIM, BER	JPEG Compression, Scaling, Filtering, Cropping, Rotation, Flipping, Scaling	Limited robustness against rotation, flipping and scaling attacks.
Yu et.al,[53], 2019, Hybrid	All Phase Discrete Cosine Bi Orthogonal Transform (APDCBT) and Shuffling	Correlation Detection	512 × 512 64 × 64	PSNR, NCC, SSIM,	JPEG compression, Gaussian noise,	Limited robustness against geometric attacks

	Singular Value decomposition (SSVD) were used with Fibonacci transform			BER	salt and pepper noise, average filter, median filter, Gaussian filter, sharpening, scaling and rotation Attacks.	
Niu et.al,[65], 2020, Transform	Blind approach using Non Sub-Sampled Shearlet transform (NSST)	Cauchy statistical distribution used in statistical decoder with multiplicative approach	512 × 512 and PN sequences of lengths 32, 64,128, 256 and 512 bits.	PSNR, NCC, SSIM, BER	JPEG compression, Gaussian noise, salt and pepper noise, median filter, Gaussian filter, Rotation and Scaling Attacks.	Limited time complexity
Wang et.al,[64], 2021 Transform	Local Radial harmonic Fourier moments (RHFMs) using the Beta exponential distribution	Modified Max. Likelihood Estimation (MMLE)was used	512 × 512 and PN sequences of lengths 128, 256, 512, 1024 and 2048 bits.	PSNR, BER	JPEG compression, Gaussian noise, median filter, Gauss Filter, Cropping, Rotation	PSNR ranges from 39-52 dB, Limited time complexity
Niu et.al,[59], 2021 Transform	Local Quaternion Polar Complex Exponential Transform (QPCET)	Cauchy Rayleigh distribution statistical decoder was utilized.	512 × 512 ------	PSNR, BER	JPEG compression, Gaussian noise, Filtering attacks	Improved robustness
Wang et.al,[60],	Combination of Stationary Wavelet Transform (SWT)	Modeling of Exponent-	512 × 512 64 × 64	PSNR, NCC,	JPEG compression,	Good robustness against most of the

2021, Transform		Fourier moments used for statistical extraction.		SSIM, BER	Gaussian noise, median filter, Gauss Filter, Cropping, Rotation	attacks
Thakkar et.al,[120], 2021, Transform	Adaptive approach using combination of DWT-SVD and Particle Swarm Optimization (PSO)	Correlation decoder	512 × 512 32 × 32	PSNR, Normalized Similarity Ratio (NSR)	JPEG compression, Gaussian noise, salt and pepper noise, average filter, median filter, Gaussian filter, sharpening, scaling and rotation Attacks.	PSNR ranges from 34-47 dB

2.6 RESEARCH GAPS

From the above discussion, the following gaps in literature survey have been observed.

(a) Many image-adaptive techniques and their hybrid forms have been used for watermark hiding like DWT, DFT, DCT, DWT-DFT, Ridgelets, Contourlets etc. with a limited robustness only. Still, there is a further need to improve the robustness from various attacks.

(b) Most of the watermarking schemes developed till now, are resistant to a limited number of geometric attacks, such as translation, rotation, scaling, etc. Hence, there is a further scope to improve the performance of watermarking approaches from more geometric attacks.

(c) Most of the work is done in watermark detection with various approaches based on QIM, LSB, HVS, etc. but a limited research is done in detecting image-adaptive watermarks using statistical methods.

(d) A large amount of work has been done in watermarking using images as watermarks only. Still, different kinds of watermark(s) can also be used for watermarking to make effective use of technology in real world applications.

(e) Objective parameters such as PSNR (Peak Signal to Noise Ratio), MSE (Mean Squared Error) etc. have been used to evaluate performance of different watermarking techniques. There is a further need of more number of objective parameters to evaluate the performance of watermark detection techniques.

2.7 OBJECTIVES

Based upon the discussion of literature survey and research gaps, the following research objectives have been formulated:

1. To implement and analyze various existing image-adaptive watermarking techniques with various attacks.
2. To propose an image-adaptive watermarking scheme using a statistical approach.
3. To validate the robustness of the proposed technique using different performance analysis parameters.

4. To evaluate the performance of proposed watermarking scheme with the existing technique against different types of geometric attacks

2.8. RESEARCH METHODOLOGY

In the proposed scheme, an existing image-adaptive watermarking technique was analyzed to be modified into a new image-adaptive watermarking technique by using a statistical approach of watermarking detection.

The local properties of the image were used by the image-adaptive approach to embed a watermark. Four standard host images and five medical host images were used. Different sizes of watermark were also used for the analysis.

The host subset used for watermarking was segmented into smaller blocks (e.g. 8 × 8 pixel blocks), and entropy of each block was calculated. Only those blocks with sufficient entropy were chosen for watermark embedding. The threshold entropy for selecting the blocks was also calculated using the local properties of the image.

Frequency transforms were applied to the host subset so that the information may be stored in the lower frequency values. The modification of transform coefficients was done by a constant value called strength factor. The performance of the scheme was also evaluated against various geometric attacks.

For data extraction, the watermarked sequence used the statistical approach for extracting the watermark. All simulations and analysis are done using MATLAB (R2013b) software.

CHAPTER 3

IMAGE-ADAPTIVE WATERMARKING FOR MEDICAL IMAGES USING MAXIMUM LIKELIHOOD DECODER

The main objective of watermarking is to hide the data securely by protecting the copyrights of digital media of the individuals, which helps to serve many applications. A powerful demand existed to evolve a mature strategy scheme of watermarking utilizing medical images. This chapter focuses upon the significant application of an image-adaptive watermarking technique in the area of tele-health using spread spectrum.

3.1. INTRODUCTION

The methodology of digital watermarking plays a salient role in controlling the rising thefts and crime of medicinal images [112]. The watermark to be placed must be safe and robust to premeditated or unintentional attacks for retrieving the information of the patient. The aspect of the watermark detector also became significant mostly when watermarks were striked by hostile or unfriendly users to redeem or corrupt the information of patients.

In this chapter, the suggested image watermarking scheme used the latest rugged, analytical, and image-adaptive technique centered on spread spectrum. The power factor used for embedding the watermark inside the image was regulated through the internal properties of the image. The image-adaptivity was procured by breaking up the natural image into minute dimension chunks followed by sorting of blocks with high entropy only for the basis of watermarking. In every block, the wavelet coefficients of little frequency were ascended either in an uphill or a downhill orientation by an adjustable value based upon the merit of the bits of the watermark. This flexible value was known as the adjustable zestful strength factor that assisted to mould the low frequency wavelet measures utilizing Gaussian dispensation. The watermark was extracted by utilizing a Maximum Likelihood decoder. The suggested strategy was partially blind in nature, wherefore supportive information accommodating a scarcity characteristics of the authentic host image were dispatched to the decoder for extracting the watermark of the patient with less inaccuracy. The mathematical properties of the Gaussian dissemination were used for inserting identically and independently distributed (i.i.d.) selected attributes of watermark specifics. The technique was distinctly strong as well as firm at odds with several geometric assaults which made it further justifiable and worthy for tele-medical utilizations.

3.2 PROPOSED METHOD

3.2.1 Watermark Embedding

The host image was partitioned into chunks of dimension (8×8). The blocks with high entropy were selected for watermark insertion. Each bit of a twofold watermark was inserted within a single high level entropy slab. 2-D DWT was appealed on the same as it afforded the finest temporal design. The transform contained approximated, horizontally, vertically, and diagonally recurrence parameters. Every sole bit of merit '0' as well as '1' was lodged in each slab by altering the approximated parameters (A) in consonance with the inserting strategy given as:

$$A = A.(1 + \alpha_d) \text{ For inserting 1} \quad (3.1)$$

$$A = A.(1 - \alpha_d) \text{ For inserting 0} \quad (3.2)$$

At this moment α_d was the adjustable dynamic strength factor that was enumerated through entropies, standard deviations, or rather the means of the approximation counts of chunks with peak entropy. The coefficients of the block procured the watermarked image through Inverse DWT. Eventually; the chunks of high over entropy were united along with the leftover blocks. The suggested process of watermarking is shown in Figure 3.1.

3.2.1.1 Calculation of Adjustable dynamic strength factor

The value of α_d for a distinct large entropy bar was determined through mean, standard deviation as well as entropy. These were expressed utilizing the following equations.

$$\alpha_d = \mu_j / (\mu_{max})^{\rho} \quad (3.3)$$

$$\alpha_d = \sigma_j / (\sigma_{max})^{\rho} \quad (3.4)$$

$$\alpha_d = H_j / (H_{max})^{\rho} \quad (3.5)$$

where, μ_j, σ_j, and H_j were the mean, std. deviation as well as the entropy of fewer quantities of each slab. μ_{max}, σ_{max}, and H_{max} were recognized as the highest mean, standard deviation as well as entropy of the sought slabs correspondingly. ρ was the changeable or versatile value in the denominator. When ρ increased for a specific natural image, there was an upsurge in PSNR for the watermarked image along with a distinct consequence upon the merit of BER for a withdrawn watermark. This merit of α_d through (3.3), (3.4), or (3.5) was utilized as a fragment for support information collected for watermark recovery. These expressions were mentioned as phrases F_1, F_2, and F_3 consequently.

3.2.2 Maximum Likelihood (ML) Decoder

In the eradication of watermark, the collated image was sub divided into slabs of dimension (8×8), and the greater entropy bars were recognized utilizing the supportive information. The decoder demonstrated in Figure 3.2 profited through three kinds of side information linked with the location of blocks with high entropy, the variance as well as mean of every high entropy slab along with α_d .

To recover every concealed segment of the watermark through its block, a perfect decoder was applied. Mihcak et al. [121] assumed that Gaussian disintegration was owned by large pass wavelet coefficients. Likewise, the approximation coefficients of every high entropy bar could be replicated by a Gaussian disintegration by carrying out the Kolmogorov-Smirnoff test was also pre-assumed [122]. This analytical way aided to accurately ascertain the standard deviation and mean of the aforementioned coefficients of high entropy chunks. These variables assisted to craft the attributes utilizing the Probability Density Function (PDF). The correct assessment of PDF helped to instrument the decoder utilizing the idea of maximum likelihood. Therefore, superior the validity of PDF of these coefficients utilized at the decoder, the larger was the authenticity of recovering the watermark utilizing α_d. Thus, an ML decoder was employed to extract the watermark. The PDF of a Normal distribution is designated as

$$f(z|\mu\,,\sigma^2) = \frac{1}{\sqrt{2\pi\sigma^2}} e^{\frac{-(z-\mu)^2}{2\sigma^2}} \tag{3.6}$$

Before inserting a watermark bit onto a large entropy bar, the approximated coefficients were constituted through mean μ and variance σ^2 utilizing Normal disintegration. Subsequently inserting bits ‘0’ or ‘1’, the merits of approximation measures were magnified with the adaptive vigorous strength factor as $(1-\alpha_d)$ as well as $(1+\alpha_d)$ consequently. Therefore, the dissemination of A for '0' and '1' implantation was stated like:

$$A_{i/0} = A_i.(1-\alpha_d) \sim N(\mu_{i/0}, \sigma_{i/0}) \quad (3.7)$$

$$A_{i/1} = A_i.(1+\alpha_d) \sim N(\mu_{i/1}, \sigma_{i/1}) \quad (3.8)$$

In case the collected approximated measures were stirred through null mean 'Additive White Gaussian Noise (AWGN)', it followed that $\sigma_{z|1}^2 = (1+\alpha_d)^2\sigma^2 + \sigma_n^2$ and$\sigma_{z|0}^2 = (1-\alpha_d)^2\sigma^2 + \sigma_n^2$.

In the given representation, the wavelet coefficients were 'i.i.d' for each disintegration in their first level. Hence the dissemination of the approximated measures in every slab with N measures z_1, z_2, z_3,…..z_N for embedding bit '0' was given as,

$$P(z_1, z_2, z_3, \ldots z_N|0) = \prod_{j=1}^{N} \sqrt{2\pi\sigma_{z|0}^2}\frac{1}{e^{-(z_j-(1-\alpha_d)\mu)^2}/2\sigma_{z|0}^2} \quad (3.9)$$

And the distribution of embedding bit '1' was given as,

$$P(z_1, z_2, z_3, \ldots z_N|1) = \prod_{j=1}^{N} \sqrt{2\pi\sigma_{z|1}^2}\frac{1}{\frac{e^{-(z_j-(1+\alpha_d)\mu)^2}}{2\sigma_{z|1}^2}} \quad (3.10)$$

For the maximum-likelihood decision

$$P(z_1, z_2, z_3, \ldots \{zN|1\}) \underset{<0}{\overset{>1}{}} P(z_1, z_2, z_3, \ldots zN|0) \quad (3.11)$$

Thus by replacing (3.7) and (3.8) in (3.9), it has been found

$$\prod_{i=1}^{N} \sqrt{2\pi\sigma_{z|1}^2}\frac{1}{e^{-(z_j-(1+\alpha_d)\mu)^2}/2\sigma_{z|1}^2} \underset{<0}{\overset{>1}{}} \prod_{j=1}^{N} \sqrt{2\pi\sigma_{z|0}^2}\frac{1}{e^{-(z_j-(1-\alpha_d)\mu)^2}/2\sigma_{z|0}^2} \quad (3.12)$$

Taking logarithm on both sides,

$$\frac{(-N)}{2}\ln\left(\sigma_{z|1}^2\right) - \frac{1}{\sigma_{z|1}^2}\sum_{j=1}^{N}(z_j - (1+\alpha_d)\mu)^2 \underset{<0}{\overset{>1}{}} \frac{(-N)}{2}\ln\left(\sigma_{z|0}^2\right) - \frac{1}{\sigma_{z|0}^2}\sum_{j=1}^{N}(z_j -$$

$$1-\alpha d\mu)2 \quad (3.13)$$

Simplifying equation (3.13),

$$\left(\frac{1}{\sigma_{z|0}^2} - \frac{1}{\sigma_{z|1}^2}\right)\sum_{j=1}^{N} z_j^2 - 2\mu\left\{\frac{(1-\alpha_d)}{\sigma_{z|0}^2} - \frac{(1+\alpha_d)}{\sigma_{z|1}^2}\right\}\sum_{j=1}^{N} z_j \underset{<0}{\overset{>1}{}} N\ln\left(\frac{\sigma_{z|1}^2}{\sigma_{z|0}^2}\right) - N\mu^2\left\{\frac{(1-\alpha_d)^2}{\sigma_{z|0}^2} -\right.$$

$$1+\alpha d2\sigma z|12 \quad (3.14)$$

The finest resolution of retrieving portions '1' as well as '0'of watermark was firmly linked with the approximate assessment for the variance of the noise σ_n^2. Considering an inhibiting instance of elevated SNR for $\sigma_n \rightarrow 0$,

$$\sigma_{z|1}^2 = (1+\alpha)^2\sigma^2 \text{ and } \sigma_{z|0}^2 = (1-\alpha_d)^2\sigma^2$$

Thus (3.14) was altered for bit '0' and '1'consequently as,

$$\frac{1}{\sigma^2(1-\alpha_d)^2}\sum_{j=1}^{N} z_j^2 - \frac{2\mu}{(1-\alpha_d)\sigma^2}\sum_{j=1}^{N} z_j < (-2N)\{\ln\sigma + \ln(1-\alpha_d)\} - N\frac{\mu^2}{\sigma^2} \tag{3.15}$$

$$\frac{(-1)}{\sigma^2(1+\alpha_d)^2}\sum_{j=1}^{N} z_j^2 + \frac{2\mu}{(1+\alpha_d)\sigma^2}\sum_{j=1}^{N} z_j > (2N)\{\ln\sigma + \ln(1+\alpha_d)\} + N\frac{\mu^2}{\sigma^2} \tag{3.16}$$

It was noticed that for greater SNR, the merit of α_d approached zero thereby making the decoder self-reliant on the dynamic power factor. Hence the watermark was removed fortuitously.

Three standard natural images, namely, 'Barbara', 'Lena' as well as 'Baboon' with dimension (512 × 512) including three variable watermarks of mini, moderate and large dimensions of (18 × 25), (20 × 50), and (20 × 80) were utilized. Entire 4096 chunks of dimension (8 × 8) were figured through a (512 × 512) natural image. So, these watermarks were utilized such that their identical segments of variable duration were inserted in the comparable numeral of blocks with elevated entropy. The original images along with watermarks are exhibited in Figures 3.3 and 3.4.

From the charts, it was noticed when ρ increased, the merits of PSNR and BER escalated at the same time. The watermark became entirely invisible and extremely robust at such levels. The merit of the parameter was improved to preserve the watermark invisibility beyond 45dB along with justifiable merit of BER (%) for the recuperated watermark. It was noticed too from Figure 3.5 to Figure 3.13. (iii) when the quantity of watermark pieces expanded, the peak of PSNR for watermarked image (in dB) utilizing F_1, F_2, and F_3 lessened in contrast to Figure 3.5 to Figure 3.13 (i) and (ii) individually. Correspondingly, the peak of BER for recuperated watermark (%) utilizing F_1, F_2, and F_3 incremented in contrast to Figure 3. 4 (a-c) (i) and (ii) individually. The highest merit for ρ was 2.10, 2.30, and 5.50 for (17-19) separately beyond which the merit of PSNR became infinite. This pointed no watermark was planted into the original image. Hence ρ was diversified in the middle of 1 and 2 for (17-18) and 1 to 5 for (19). Likewise, the merit of α_d extended from 10^{-3} to 10^{-4} for advisable PSNR for (3.3), (3.4), and (3.5). So, the PSNR was settled perfectly by

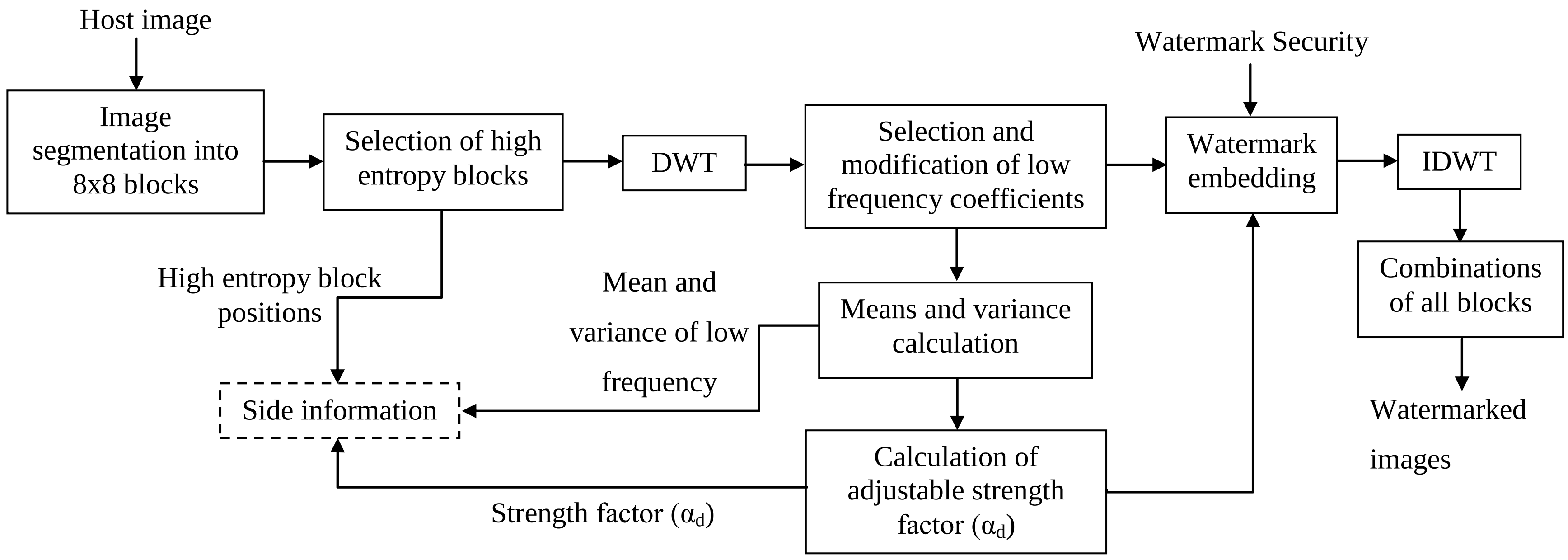

Figure 3.1 Outline of the suggested Encoder in the watermarking strategy.

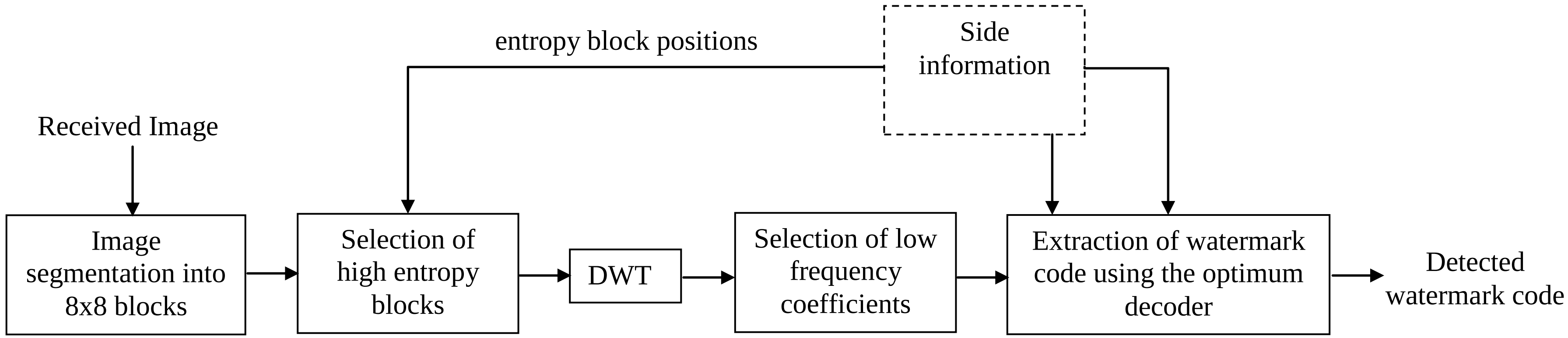

Figure 3.2 Outline of the suggested Decoder in the watermarking strategy.

Figure 3.3 Original images used (i) ‘Barbara’ (ii) ‘Lena’ (iii) ‘Baboon’.

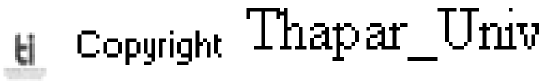

Figure 3.4 Watermarks utilized (i) ‘TIET (18 × 25)’ (ii) ‘Copyright (20 × 50)’, (iii) ‘Thapar_Univ (20 × 80)’.

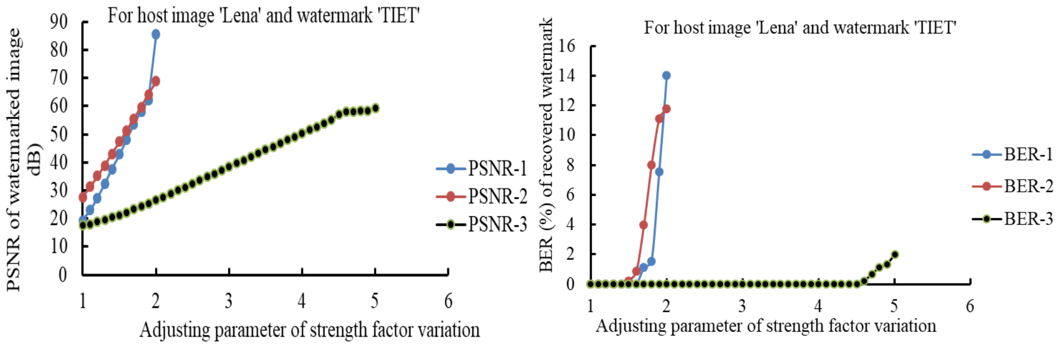

Figure 3.5 Plot of ‘PSNR (in dB)’ for watermarked image ‘Lena’ and ‘BER (%)’ of retrieved watermark employing watermark ‘TIET’.

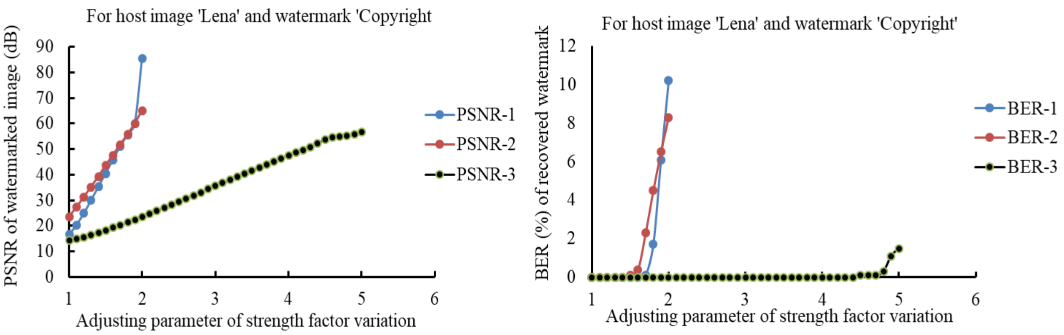

Figure 3.6 Plot of ‘PSNR (in dB)’ for watermarked image ‘Lena’ and ‘BER (%)’ of retrieved watermark employing watermark ‘Copyright’.

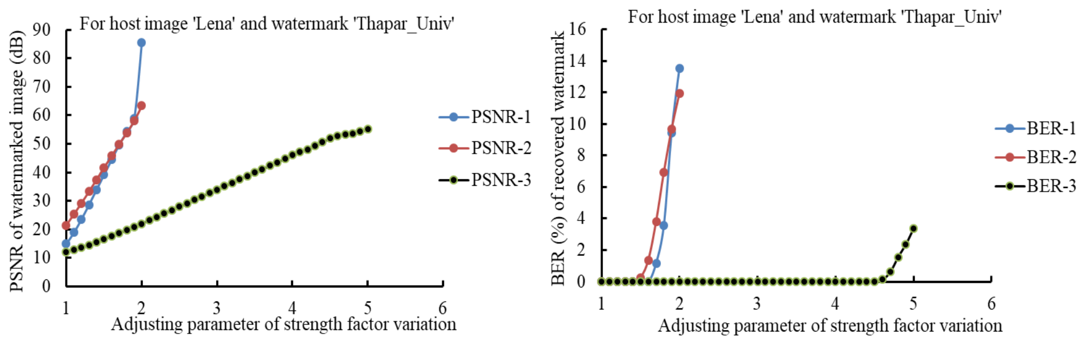

Figure 3.7 Plot of ‘PSNR (in dB)’ for watermarked image ‘Lena’ and ‘BER (%)’ of retrieved watermark employing watermark ‘Thapar_Univ’.

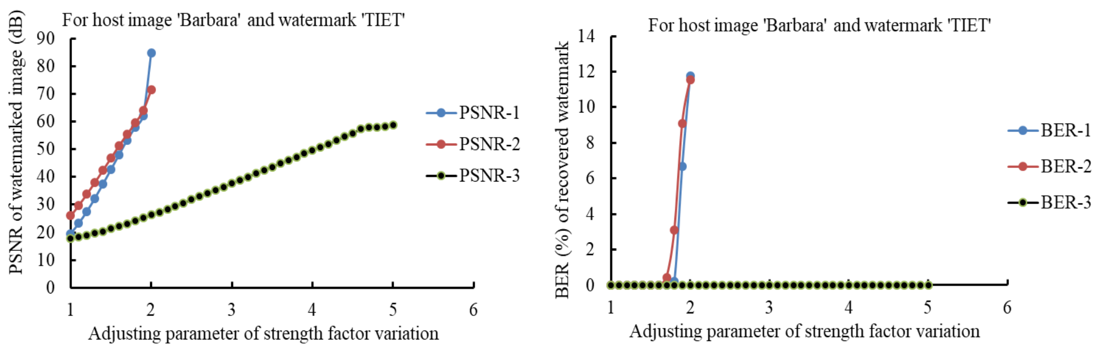

Figure 3.8 Plot of ‘PSNR (in dB)’ for watermarked image ‘Barbara’ and ‘BER (%)’ of retrieved watermark employing watermark ‘TIET’.

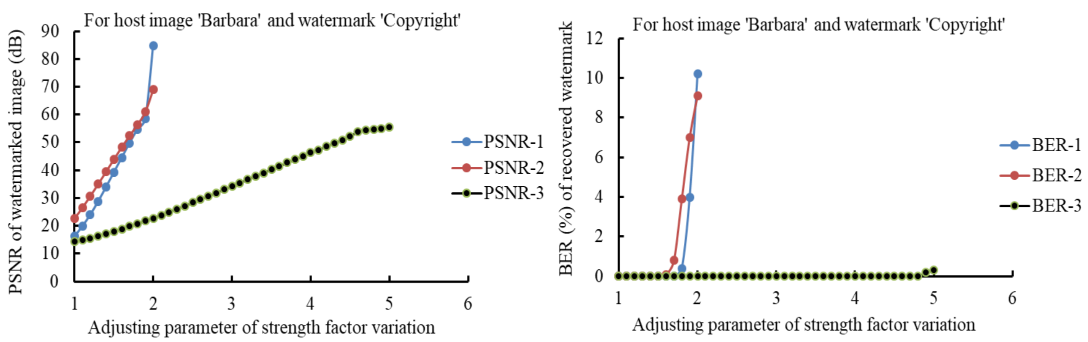

Figure 3.9 Plot of ‘PSNR (in dB)’ of watermarked image ‘Barbara’ and ‘BER (%)’ of retrieved watermark employing watermark ‘Copyright’.

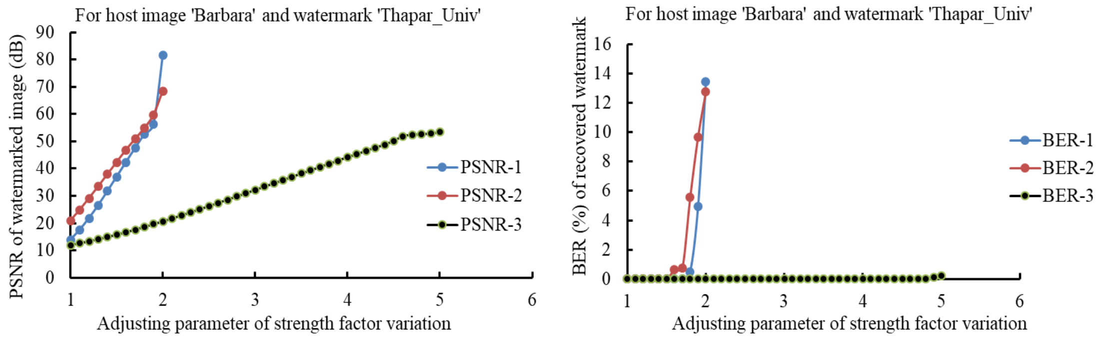

Figure 3.10 Plot of 'PSNR (in dB)' for watermarked image 'Barbara' and 'BER (%)' of retrieved watermark employing watermark 'Thapar_Univ'.

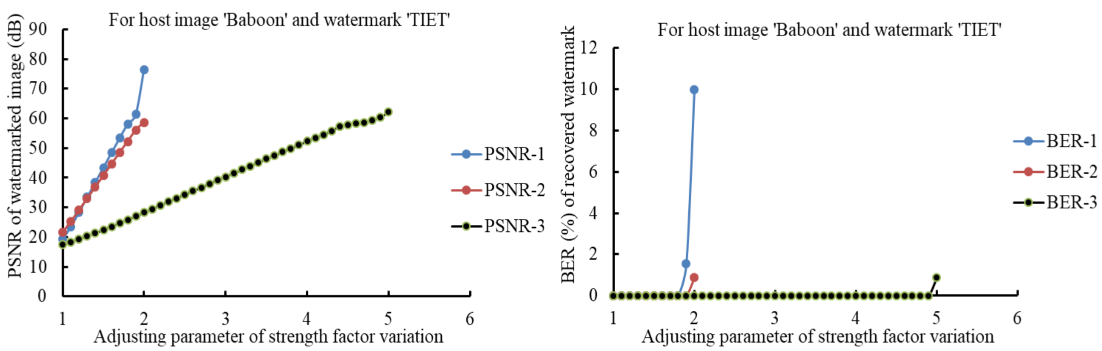

Figure 3.11 Plot of 'PSNR (in dB)' for watermarked image 'Baboon' and 'BER (%)' of retrieved watermark employing watermark 'TIET'.

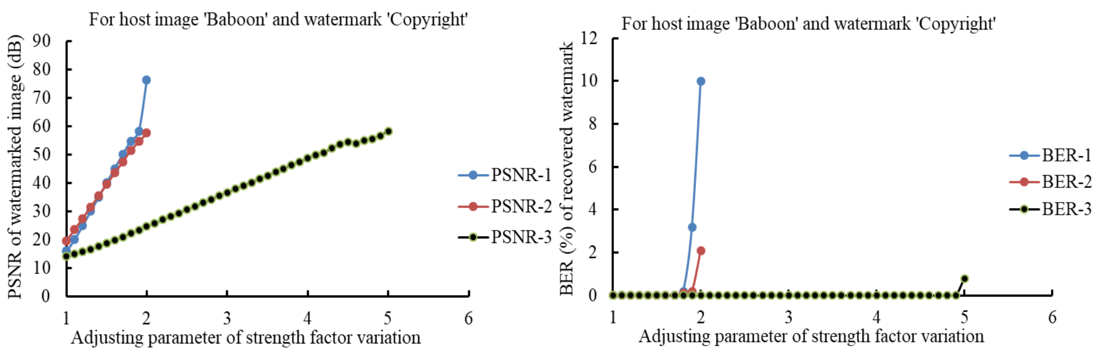

Figure 3.12 Plot of 'PSNR (in dB)' for watermarked image 'Baboon' and 'BER (%)' of retrieved watermark employing watermark 'TIET'.

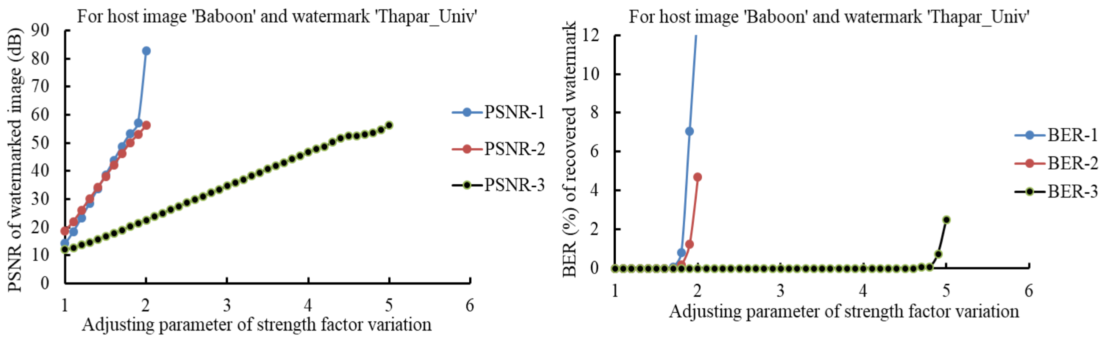

Figure 3.13 Plot of 'PSNR (in dB)' for watermarked image 'Baboon' and 'BER (%)' of retrieved watermark employing watermark 'TIET'.

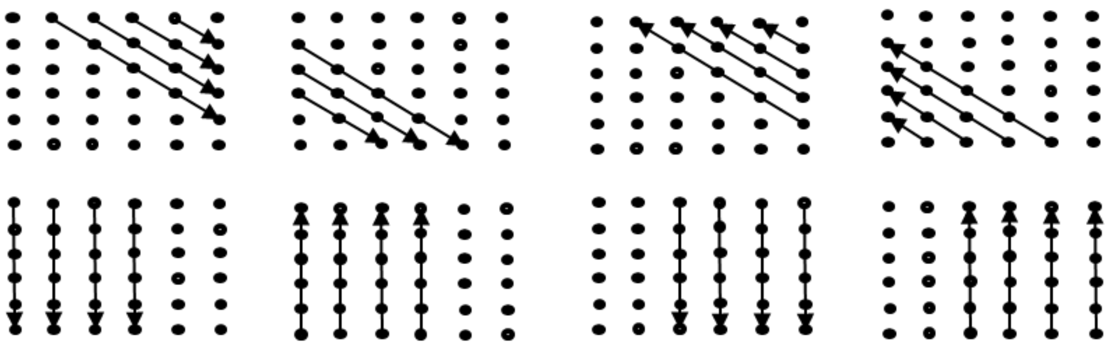

Figure 3.14 Eight options through which blocks of dimension (8 × 8) were chosen next to arrows and diagonal stocking within a cubicle arrangement.

modifying the merit for ρ. Superior the merit of PSNR, smaller was the value of BER for the recovered watermark, and hence greater was the toughness with advisable un-detectability.

3.3 SECURITY OF WATERMARK

The supporting information accommodated means, variances, and location of every block with large entropy and α_d. It was conveyed through the process of insertion of the watermark to the decoder for the watermark removal to circumvent any intentional attack for eradicating the watermark. This was confirmed when the locations of blocks with large entropy in a cubicle arrangement didn't directly respond to the medicinal image. Every single bar from an image of dimension (8 × 8) was sorted out through any of the 16 methods and laid down in the cubicle arrangement by the other 13 sideways. Figure 3.14 showed eight options through which blocks were sorted out next to diagonal and side rows. Likewise, the leftover eight sideways accounted for the choice of blocks alongside the other diagonal and columns. Thus every individual dot constituted an image bar of dimension (8 × 8), whereupon the directions of the arrow depicted the chosen blocks.So, the possibility (p) through which an intentional assailant might have correctly guessed the locations of the block with large entropy utilizing the supporting information within a watermarked image was computed as

$$p = \left({}^{01}/_{16}\right) \times \left({}^{01}/_{13}\right) = {}^{01}/_{208} = 0.480\%.$$

01 × 4096	02 × 2048	04 × 1024	08 × 512	016 × 256
4096 × 01	2048 × 02	1024 × 04	512 × 08	256 × 016
032 × 128	128 × 032	64.0 × 64.0		

It was noticed the merit of accomplishment was about lower than 0.5%, which meant ample attempts were required to be submitted for eradicating the watermark well. For greater security in opposition to watermark destruction, the side data could also be sent in the concealed state.

3.4. RESULTS AND DISCUSSION

In the entire study, the suggested algorithm was tried out in opposition to numerous attacks to assess the performance. Figure 3.15 demonstrates ‘Lena’, ‘Barbara’ as well as ‘Baboon’ after watermarking and their extracted watermarks utilizing α_d from (3.3), (3.4), and (3.5). Table 3.1 indexes the allowable merits of ‘PSNR’ fulfilling the un-noticeability benchmark at minimal ‘BER (%)’ for the retrieved watermark having sizes (512 × 512) and (1024 × 1024) respectively.

Figure 3.15 ‘Lena’, ‘Barbara’, as well as ‘Baboon’ after watermarking and retrieved watermarks.

Table 3.1 'PSNR (in dB)' for images with various dimension watermarks for parameter ρ utilizing F_1, F_2, and F_3.

'Lena'(512 × 512)			
Water mark	F_1	F_2	F_3
'TIET (25 × 18)'	49.7	47.3	57.9
'Copyright (50 × 20)'	51.0	47.6	53.8
'Thapar_Univ(80 × 20)'	45.9	45.7	53.2
'Barbara'(512 × 512)			
Water mark	F_1	F_2	F_3
'TIET (25 × 18)'	47.9	48.2	49.7
'Copyright (50 × 20)'	48.1	48.2	49.8
'Thapar_Univ (80 × 20)'	47.2	48.0	50.1
'Baboon'(512 × 512)			
Watermark	F_1	F_2	F_3
'TIET (25 × 18)'	48.4	45.7	52.9
'Copyright (50 × 20)'	45.1	44.8	49.8
'Thapar_Univ (80 × 20)'	43.7	45.3	47.7
'Lena'(1024 × 1024)			
Water mark	F_1	F_2	F_3
'TIET (25 × 18)'	64.1	50.0	59.5
'Copyright (50 × 20)'	63.3	45.2	57.7
'Thapar_Univ (80 × 20)'	64.0	41.9	60.3
'Barbara'(1024 × 1024)			
Water mark	F_1	F_2	F_3
'TIET (25 × 18)'	61.2	61.8	56.3
'Copyright (50 × 20)'	60.4	57.2	54.3
'Thapar_Univ (80 × 20)'	61.3	54.3	56.8
'Baboon'(1024 × 1024)			
Water mark	F_1	F_2	F_3
'TIET (25 × 18)'	59.1	63.4	53.9
'Copyright (50 × 20)'	58.4	55.9	52.4
'Thapar_Univ (80 × 20)'	59.5	56.1	54.9

.

Table 3.2 'BER (%)'for recuperated watermark undergoing various assaults for 'Lena', 'Barbara' as well as 'Baboon' (512 × 512).

LENA									
Watermark	*For.*	*G. Fil. (3 × 3)*	*G. Fil. (5 × 5)*	*Med. Fil. (3 × 3)*	*Med. Fil. (5 × 5)*	*Med. Fil. (7 × 7)*	*Wien. Fil. (3 × 3)*	*Wien. Fil. (5 × 5)*	*Sharp*
'TIET'	F_1	2.0	2.0	2.60	5.770	9.770	1.550	4.220	9.770
	F_2	1.3	1.3	1.3	6.2	11.1	0.8	2.80	6.66
	F_3	3.7	3.7	4.6	12.8	18.80	2.8	14.40	16.22
'Copyright'	F_1	4.30	4.40	14.60	21.40	26.80	04	12.0	20.12
	F_2	3.60	3.70	8.40	17.90	23.90	3.10	8.790	16.4
	F_3	4.30	4.30	14.6	21.40	26.80	2.60	14.70	10.2
'Thapar_ Univ'	F_1	1.37	1.312	11.56	22.18	27.370	2.187	8.12	19.43
	F_2	3.87	3.81	10.680	22.37	28.93	4.31	10.6	20.31
	F_3	05	4.687	19.560	30.43	35.6	7.4	22.50	13.5
BARBARA									
Watermark	*For.*	*G. Fil. (3 × 3)*	*G. Fil. (5 × 5)*	*Med. Fil. (3 × 3)*	*Med. Fil. (5 × 5)*	*Med. Fil. (7 × 7)*	*Wien. Fil. (3 × 3)*	*Wien. Fil. (5 × 5)*	*Sharp*
'TIET'	F_1	2.22	2	4	18.4	28.2	1.55	5.77	11.4
	F_2	6.88	7.11	3.33	19.5	32	1.77	9.77	14
	F_3	4	4	4.44	19.1	32.2	0.88	7.55	14
'Copyright'	F_1	5.5	5.6	7.19	20	29	2	12	10.2
	F_2	5.5	5.6	6.4	22.6	31.2	2.9	16.1	10.2

	F_3	6.7	6.7	6.1	221.8	30.7	1.6	15.6	10.2
‘Thapar_ Univ’	F_1	5.43	5.5	9.187	23.37	31.56	2.62	5.62	13.5
	F_2	4.37	4.37	7.12	22.18	32	2.75	15.81	13.5
	F_3	4.87	4.87	10.5	25.87	34.37	3.25	19.43	13.5
BABOON									
Watermark	*For.*	*G. Fil. (3 × 3)*	*G. Fil. (5 × 5)*	*Med. Fil. (3 × 3)*	*Med. Fil. (5 × 5)*	*Med. Fil. (7 × 7)*	*Wien. Fil. (3 × 3)*	*Wien. Fil. (5 × 5)*	*Sharp*
‘TIET’	F_1	1.55	1.55	31.55	44.88	50.22	0.22	5.11	11.77
	F_2	0	0	21.33	37.55	45.11	0	2	11.77
	F_3	5.55	5.77	37.7	51.77	54	0.44	12.44	11.77
‘Copyright’	F_1	1.1	1.2	27.6	39	43.7	0.4	6	10.2
	F_2	0.3	0.3	23.7	38.9	42.4	0.5	5.2	10.2
	F_3	5.5	5.7	36	47.5	49.1	1.9	16.2	10.2
‘Thapar_ Univ’	F_1	1	1.062	25.06	34.93	39.56	1.062	8.87	13.5
	F_2	1.562	1.75	27	38.12	42.12	2.43	13.12	13.5
	F_3	3.93	4.12	31.5	41.18	45.18	2.93	18,31	13.5

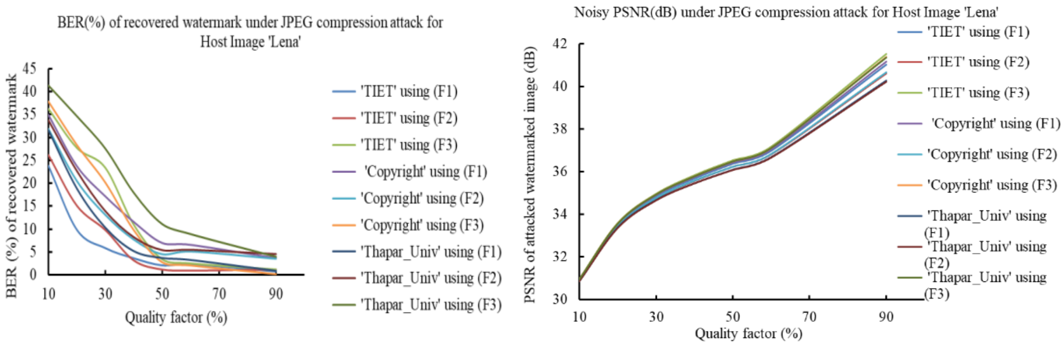

Figure 3.16 Plot of 'BER (%)' for recuperated watermark with 'PSNR (in dB)' of noisy 'Lena' for different Quality factors of 'JPEG Compression' assault.

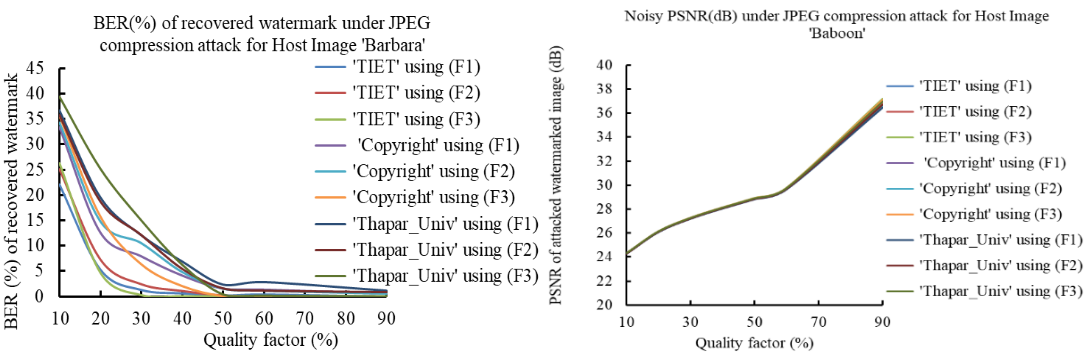

Figure 3.17 Plot of 'BER (%)' for recuperated watermark with 'PSNR (in dB)' of noisy 'Barbara' for different Quality factors of 'JPEG Compression' assault.

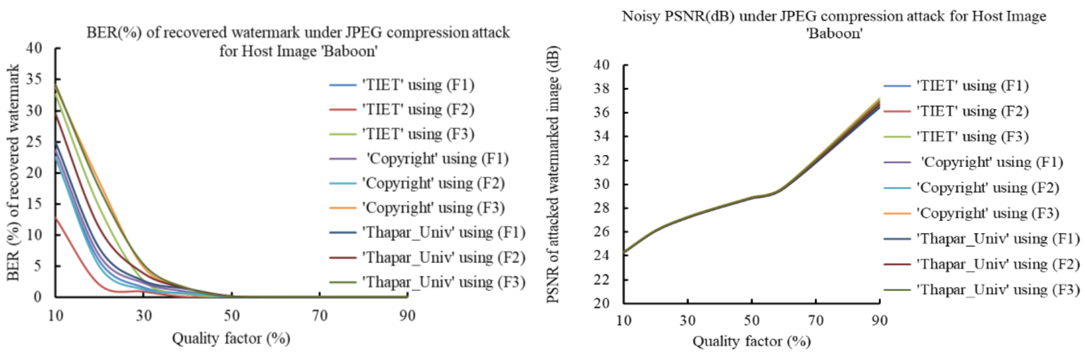

Figure 3.18 Plot of 'BER (%)' for recuperated watermark with 'PSNR (in dB)' of noisy 'Baboon' for different Quality factors of 'JPEG Compression' assault.

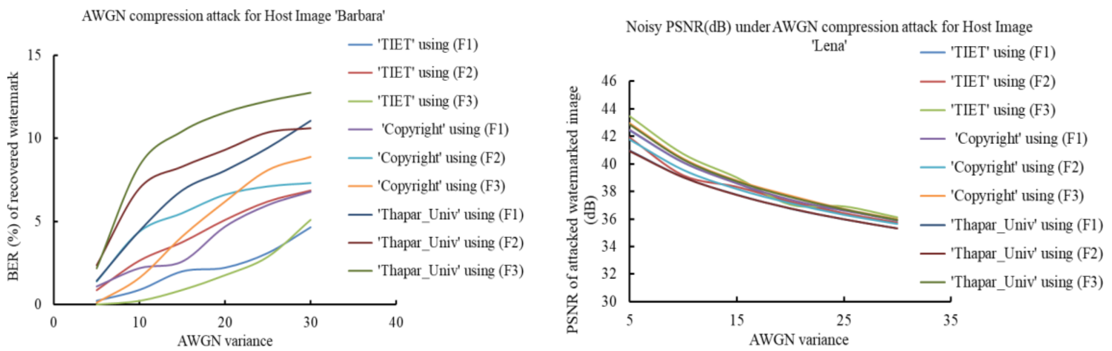

Figure 3.19 Plot of 'BER (%)' for recuperated watermark with 'PSNR (in dB)' of noisy 'Lena' for different variances of 'AWGN' assault.

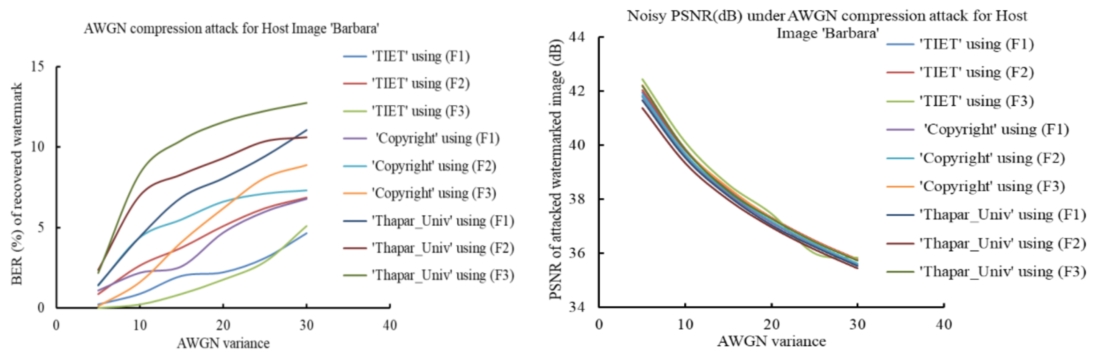

Figure 3.20 Plot of 'BER (%)' for recuperated watermark with 'PSNR (in dB)' of noisy 'Barbara' for different variances of 'AWGN' assault.

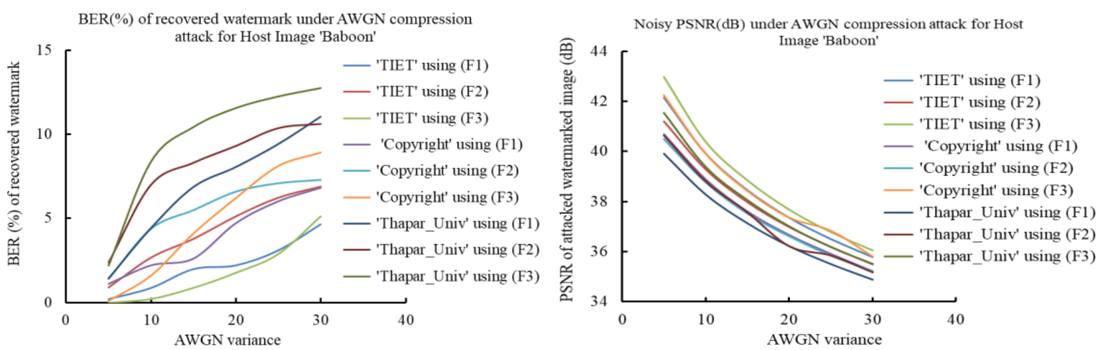

Figure 3.21 Plot of 'BER (%)' for recuperated watermark with 'PSNR (in dB)' of noisy 'Baboon' for different variances of 'AWGN' assault.

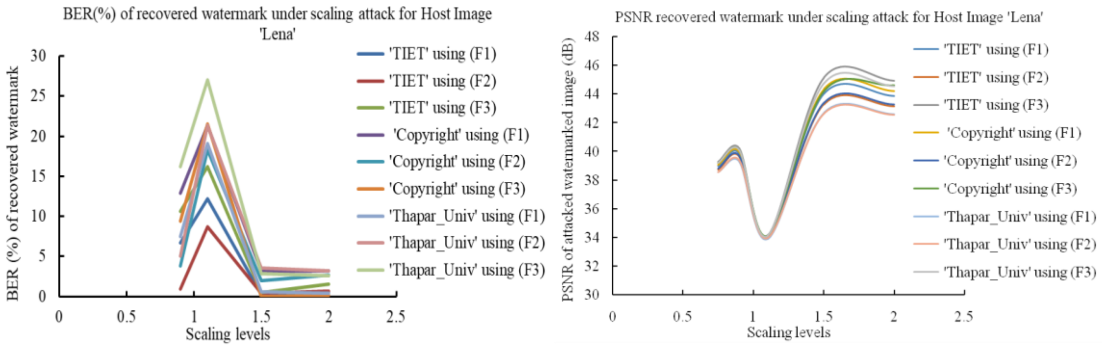

Figure 3.22 Plot of 'BER (%)' for recuperated watermark with 'PSNR (in dB)' of noisy 'Lena' for different degrees of 'Scaling' assault.

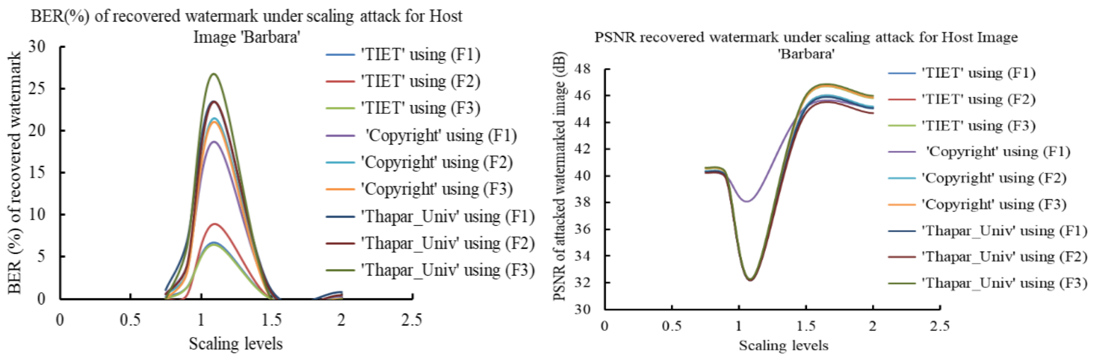

Figure 3.23 Plot of 'BER (%)' for recuperated watermark with 'PSNR (in dB)' of noisy 'Barbara' for different degrees of 'Scaling' assault.

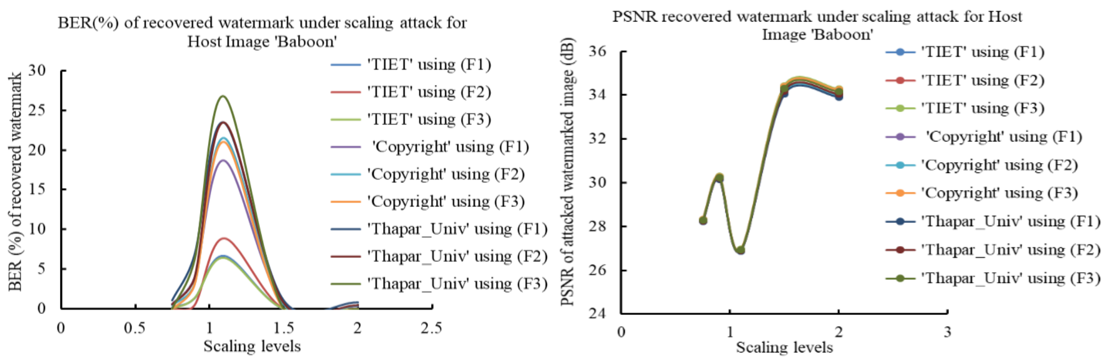

Figure 3.24 Plot of 'BER (%)' for recuperated watermark with 'PSNR (in dB)' of noisy 'Baboon' for different degrees of 'Scaling' assault.

.

Figure 3.25 ‘Lena’ under various assaults of Gauss Fil. (3×3), ‘AWGN’ (σ^2=5, 20), ‘JPEG Comp’. (10%) as well as Scale degrees (0.9, 1.1) and their recuperated watermarks.

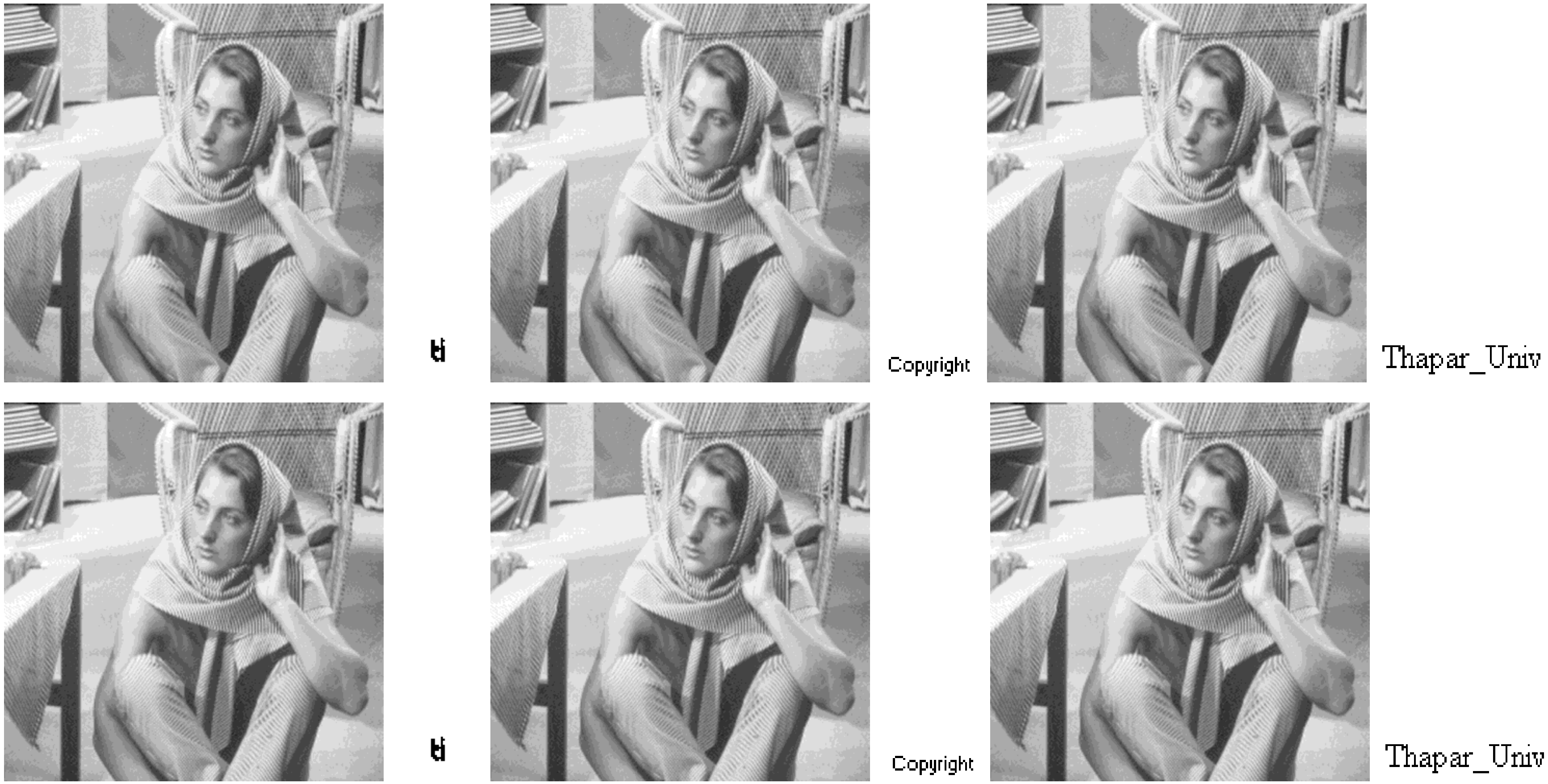

Figure 3.26 ‘Barbara’ under various assaults of Gauss Fil. (3×3), ‘AWGN’ (σ^2=5, 20), ‘JPEG Comp.’ (Q=10%) as well as Scale degrees (0.9, 1.1) and their recuperated watermarks.

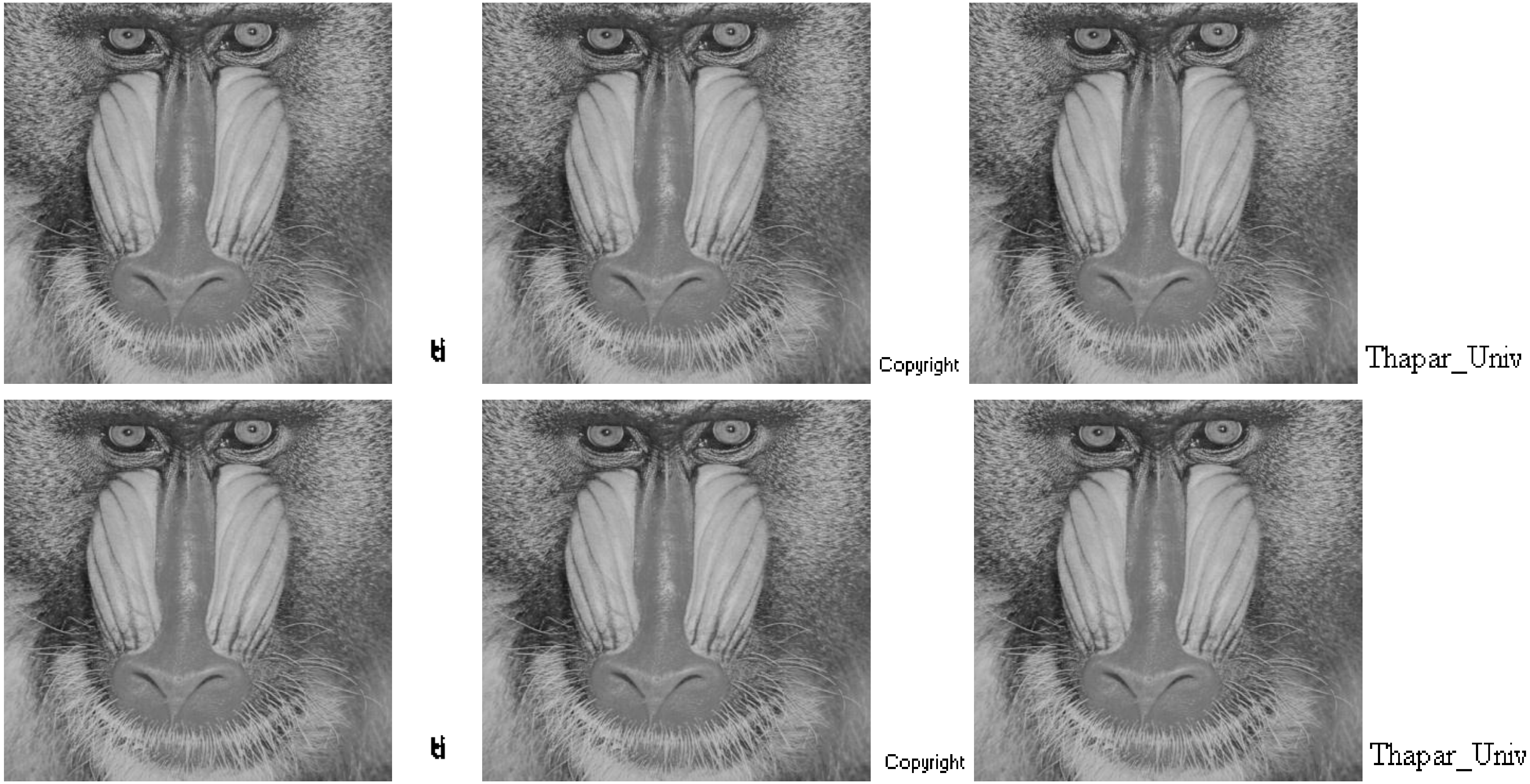

Figure 3.27 ‘Baboon’ under various assaults of Gauss Fil. (3×3), ‘AWGN’ (σ^2=5, 20), ‘JPEG Comp.’ (Q=10%) as well as Scale degrees (0.9, 1.1) and their recuperated watermarks.

3.4.1 Analysis of execution with common assaults

Every watermark was used for analyzing the performance with numerous attacks that is AWGN, JPEG compression, Scaling, and Sharpening. The merits of BER (%) of recuperated watermark for unalike assaults are expressed in Table 3.2. It affirms the suggested technique is strong. The merits of BER were noticed to be minimal for Gauss filter attacks but analogously larger for Wiener Filter assaults. For AWGN assault, as variances of noise enhanced, the merit of BER also expanded. The outcome improved when the watermark dimension was decreased. The merit of 'BER (%)' for eradicated watermark lessened too when JPEG Comp. quality factors expanded. However, for Scale attack, the merits of BER were perceived as rising and falling for growing scale extents.

Plots of 'BER (%)' for recuperated watermark with their noisy 'PSNR (in dB)' for assaulted images 'Lena', 'Barbara' and 'Baboon' considering different attacks are displayed in Figures 3.16 to Figure 3.24. Outstanding performance for BER results was achieved in figures and tables for 'Scaling', 'JPEG Compression', 'Median Filter', and 'Sharpening' assaults utilizing F_1. Similar values of BER were best attained for 'Gauss Filter', 'Wiener Filter' as well as 'AWGN' assaults utilizing F_2 and F_3 correspondingly. The different assaulted images and their recuperated watermarks are also displayed in Figures 3.25, 3.26, and 3.27 respectively.

3.4.2 Comparison of Results with existing Techniques

In this Segment, the suggested technique was collated with six various watermarking techniques. Results emphasized in bold values distinctly stipulated the superior presentation of the proposed approach.

3.4.2.1 Comparison with Yadav et al. [14]

Firstly, the suggested scheme was collated against the recent approach utilized by Yadav et al. [14], utilizing DWT as they were partially sightless as well as image-adaptive. The practices used blocks of dimension (8 × 8) with large entropy for inserting the watermark with support information to recover the same. The watermarks utilized were too of similar bit dimensions. The low frequency coefficients were modeled using Gaussian distribution and the strength factor was adaptively calculated from the parameters of mean and standard deviation. Finally the watermarks were extracted using correlation decoder. Tables 3.3 and 3.4 attest to the robust behavior of the suggested technique under different standard factors of 'JPEG Compression' and 'AWGN' noise variances.

Table 3.3 Comparison of 'BER (%)' for recuperated watermark betwixt suggested technique and Yadav et al [14] with different watermark extents for 'Barbara' of dimension (512 × 512) utilizing F_1, F_2, and F_3.

'TIET'								
	'JPEG Comp.' With Qual. Factor =10%	'AWGN' with variance=20	G. Filter (3 × 3)	Scaling degree				
				0.75	0.9	1.1	1.5	2
Yadav et al. [14] at 45dB	15.33	4	1.56	0	0.22	5.33	0	0
Proposed Utilizing 'F_1'	**14.8**	**1.3**	**2**	0	0.22	**4.88**	0	0
Proposed Utilizing 'F_2'	**12.4**	**1.33**	**0.44**	0	0.66	**4.66**	0	0
Proposed Utilizing 'F_3'	**6.22**	**0.22**	**0.22**	0	0.22	**3.11**	0	0

	' Copyright'			' Thapar_Univ'		
	'JP EG Comp.' with QF=10%	'AWGN' with variance=20	G. Filter (3 × 3)	'JPEG Comp.' with QF=10%	'AWGN' with variance=20	G. Filter (3 × 3)
Yadav et al. [14] at 45dB	26.1	4.2	3.6	31.5	7.25	4.06
Proposed Utilizing 'F_1'	**25.5**	4.1	**3.4**	**31.31**	7.5	**3.31**
Proposed Utilizing 'F_2'	**23.5**	**1.7**	**1.2**	**29.875**	**4.5**	**2.6875**
Proposed Utilizing 'F_3'	**21.5**	**0.7**	**0.2**	**29**	**2.375**	**2.375**

Table 3.4 Comparison of 'BER (%)' for recuperated watermark betwixt suggested technique and Yadav et al. [14] with different standard factors of 'JPEG' assault utilizing watermark with duration 256 bits for 'Lena'.

	10%	20%	30%	40%	50%
Yadav et al. [14] at 45dB	18.750	8.980	4.3	0.780	0.0
Proposed Utilizing 'F_1'	**7.81**	**3.9062**	**1.171**	**0.390**	0.0
Proposed Utilizing 'F_2'	**18.350**	**7.812**	**3.515**	1.17	0.0
Proposed Utilizing 'F_3'	**0.0**	**0.0**	**0.0**	**0.0**	0.0

Table 3.5 Comparison of 'BER (%)' for recuperated watermark betwixt suggested technique, Akhaee et al. [27] as well as Yadav et al. [14] for various watermark extents for 'Barbara'.

W. duration '128 bits'			
	'JPEG Comp.' with QF=10%	'AWGN' with variance=20	G. Filter (3 × 3)
Akhaee et al. [27]	5.9	5.9	3.3
Yadav et al. [14] at 45 dB	3.1	0.0	0.0
Proposed Utilizing 'F_1'	**1.562**	0.0	0.0
Proposed Utilizing 'F_2'	**2.34**	0.0	0.0
Proposed Utilizing 'F_3'	**0.0**	0.0	0.0
W. duration '256 bits'			
	'JPEG Comp.' with QF=10%	'AWGN' with variance=20	G. Filter (3×3)
Akhaee et al. [27]	7.8	6.3	3.1
Yadav et al. [14] at 45 dB	11.7	0.0	0.3
Proposed Utilizing 'F_1'	**5.85**	**0.3906**	**0.0**
Proposed Utilizing 'F_2'	13.28	**0.3906**	0.3906
Proposed Utilizing 'F_3'	**2.34**	**0.0**	**0.0**
W. duration '512 bits'			
	'JPEG Comp.' with QF=10%	'AWGN' with variance=20	G. Filter (3×3)
Akhaee et al. [27]	16.740	10.730	3.610
Yadav et al. [14] at 45 dB	15.82	0.780	2.930
Proposed Utilizing 'F_1'	**14.8**	**0.39**	**0.39**
Proposed Utilizing 'F_2'	**16.6**	**0.976**	**3.12**
Proposed Utilizing 'F_3'	**8.98**	**0.195**	**0.195**

W. duration ‘1024 bits’			
	JPEG Comp. with QF=10%	AWGN with variance=20	G. Filter (3 × 3)
Akhaee et al. [27]	22.240	14.390	3.750
Yadav et al. [14] at 45 dB	25.880	4.780	3.610
Proposed Utilizing ‘F_1’	**24.70**	**2.24**	**1.26**
Proposed Utilizing ‘F_2’	26.36	**2.63**	**3.41**
Proposed Utilizing ‘F_3’	**23.04**	**1.36**	**0.29**
W. duration ‘2048 bits’			
	‘JPEG Comp.’ with QF=10%	‘AWGN’ with variance=20	G. Filter (3×3)
Akhaee et al. [27]	24.680	18.220	4.670
Yadav et al. [14] at 45 dB	34.170	20.650	3.420
Proposed Utilizing ‘F_1’	**30.32**	**1.22**	**2.9**
Proposed Utilizing ‘F_2’	**32.47**	**2.05**	**3.8**
Proposed Utilizing ‘F_3’	**30.32**	**1.31**	**2.9**

Table 3.6 Comparison of ‘BER (%)’ for recuperated watermark betwixt suggested technique and Kalantari et al. [123] with different ‘JPEG Comp.’ as well as ‘Med. Filter’ assaults utilizing watermark with duration 256 bits for ‘Lena’.

	‘Med. F’		‘JPEG Comp.’ Q. Factor (%)				
	3 × 3	5 × 5	10	20	30	40	50
Kalantari et al.[123]	10.160	21.480	9.240	1.740	0.780	0.130	0.0
Proposed Utilizing ‘F’	**0.390**	**2.340**	**7.812**	3.906	1.171	0.390	0.0
Proposed Utilizing ‘F’	**0.390**	**2.340**	18.350	7.812	3.515	1.1718	0.0
Proposed Utilizing ‘F’	**0.0**	**0.0**	**0.0**	**0.0**	**0.0**	**0.0**	0.0

Table 3.7 Comparison of BER (%) for recuperated watermark betwixt suggested technique and Nezhadarya et al. [124] with Gauss, Med. Filter as well as JPEG compression assaults utilizing watermark duration of 256 bits.

‘Barbara’								
	‘JPEG Comp.’ Q. Factor (%)					Med. Fil.		G. Fil.
	20	30	40	50	60	3 × 3	5 × 5	5 × 5
Nez.et al. [124]	1.690	0.160	0.050	0.0	0.0	1.1	8.140	0.130
Proposed Utilizing ‘F’	**0.0**	**0.0**	**0.0**	0.0	0.0	**0.0**	**0.78**	**0.0**
Proposed Utilizing ‘F’	**0.39**	**0.0**	**0.0**	0.0	0.0	**0.78**	12.89	1.950

Proposed Utilizing	**0.0**	**0.0**	**0.0**	0.0	0.0	**0.0**	**4.29**	**0.0**
‘Lena’								
	‘JPEG Comp.’ Q. Factor (%)					Med. Fil.		G. Fil.
	20	30	40	50	60	3 × 3	5 × 5	5 × 5
Nez.et al. [124]	1.650	0.410	0.220	0.1	0.0	0.0	7.10	0.17
Proposed Utilizing	**1.56**	**0.39**	**0.0**	0.0	0.0	**0.0**	**1.71**	**0.0**
Proposed Utilizing	**3.51**	0.781	0.39	0.0	0.0	**0.0**	**1.71**	**0.0**
Proposed Utilizing ‘F_3’	**0.0**	**0.0**	**0.0**	0.0	0.0	**0.0**	**0.781**	**0.0**

Table 3.8 Comparison of ‘BER (%)’ for recuperated watermark betwixt suggested technique as well as [31] with ‘Gauss’ and ‘Med. Filters’, ‘JPEG Comp’ as well as ‘AWGN’ assaults utilizing watermark with duration 128 bits for ‘Barbara’.

	‘AWGN’ (with variance)			‘JPEG Comp.’ Q.Factor (%)			
	10	20	30	10	30	50	70
Amirmazlaghani et al. [31]	0.070	0.480	2.030	0.0	0.0	0.0	0.0
Proposed Utilizing ‘F_1’	**0.0**	**0.0**	**0.0**	0.78	0.780	0.0	0.0
Proposed Utilizing ‘F_2’	**0.0**	**0.0**	**0.0**	0.78	0.0	0.0	--
Proposed Utilizing ‘F_3’	**0.0**	**0.0**	**0.0**	0.0	0.0	0.0	--
	Med. Fil.		G. Fil.		Scale degree		
	3 × 3	5 × 5	3 × 3	5 × 5	2	1.5	0.9
Amirmazlaghani et al. [31]	1.210	5.9	0.0	0.780	0.0	0.0	0.160
Proposed Utilizing ‘F_1’	**0.0**	**0.156**	0.0	0.0	0.0	0.0	**0.0**
Proposed Utilizing ‘F_2’	**0.0**	**1.56**	0.0	0.0	0.0	0.0	**0.0**
Proposed Utilizing ‘F_3’	**0.0**	**0.781**	0.0	0.0	0.0	0.0	**0.0**

Table 3.9 Comparison of ‘BER (%)’ for recuperated watermark betwixt suggested technique and Hamghalam et al. [125] with ‘JPEG Comp.’, ‘Med. Fil.’ as well as ‘AWGN’ assaults utilizing watermark with duration 256 bits.

	‘Barbara’	‘Lena’
Med. Fil. (3 × 3)		
Hamghalam et al. [125]	19.520	6.240
Proposed Utilizing ‘F_1’	**0.0**	**0.0**

Proposed Utilizing ‘F_2’	**0.781**	**0.0**
Proposed Utilizing ‘F_3’	**0.0**	**0.0**
‘AWGN’ with variance = 10		
Hamghalam et al. [125]	11.47	5.01
Proposed Utilizing ‘F_1’	**0.0**	**1.171**
Proposed Utilizing ‘F_2’	**0.0**	**1.56**
Proposed Utilizing ‘F_3’	**0.0**	**0.0**

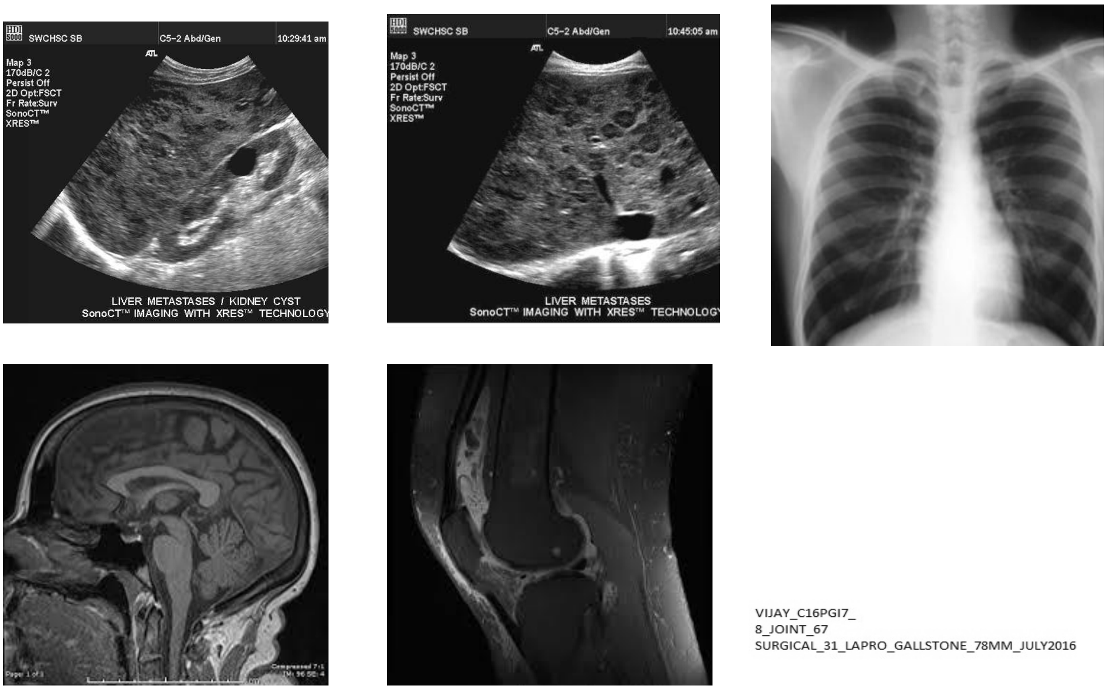

Figure 3.28 (i) Medical images utilized (a) ‘Liver-1’, (b) ‘Liver-2’, (c) ‘X –ray’ (d) ‘MRI brain’ (e) ‘Knee Joint’ (ii) ‘Patient watermark’ (18 × 25).

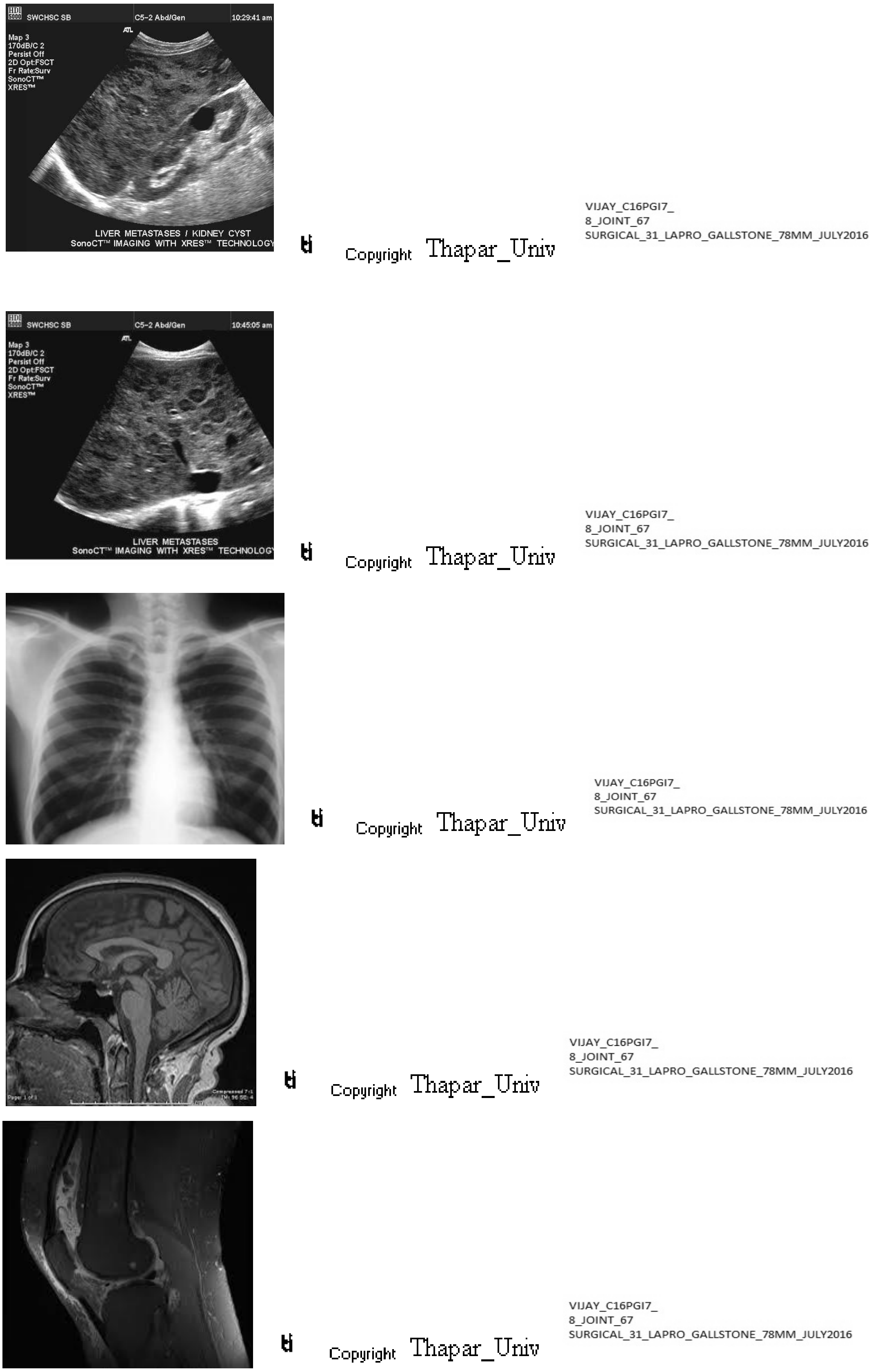

Figure 3.29 Watermarked image(s) as well as recuperated watermark(s).

Table 3.10 'PSNR (in dB)' for various dimension watermark(s) utilizing F_1, F_2 and F_3.

'Liver-1'			
Water mark	Utilizing F_1	Utilizing F_2	Utilizing F_3
'TIET' (18 × 25)	46.10	45.50	55.70
'Copyright' (20 × 50)	48.060	45.90	52.020
'Thapar_Univ' (20 × 80)	46.080	42.780	53.500
'Patient Watermark' (18 × 25)	45.63	43.26	53.44
'Liver2'			
Water mark	Utilizing F_1	Utilizing F_2	Utilizing F_3
'TIET' (18 × 25)	48.010	42.740	57.860
'Copyright (20 × 50)	45.50	42.50	53.40
'Thapar_Univ' (20 × 80)	45.40	43.210	51.220
'Patient Watermark' (18 × 25)	47.31	43.43	52.84
'X-ray'			
Water mark	Utilizing F_1	Utilizing F_2	Utilizing F_3
'TIET' (18 × 25)	46.720	53.10	57.40
'Copyright' (20 × 50)	45.090	50.090	53.640
'Thapar_Univ' (20 × 80)	44.230	48.17	52.680
'Patient Watermark' (18 × 25)	42	49.85	52.70
'MRI brain'			
Water mark	Utilizing F_1	Utilizing F_2	Utilizing F_3
'TIET' (18 × 25)	46.740	47.670	57.780
'Copyright' (20 × 50)	46.0	44.35	53.950
'Thapar_Univ' (20 × 80)	44.710	43.560	53.430
'Patient Watermark' (18 × 25)	44.27	45.16	57.78
'Knee Joint'			
Water mark	Utilizing F_1	Utilizing F_2	Utilizing F_3
'TIET' (18 × 25)	45.090	46.20	56.310
'Copyright' (20×50)	45.320	42.660	50.580
'Thapar_Univ; (20×80)	42.80	44.270	48.90
'Patient Watermark' (18×25)	44.19	44.35	55.18

3.4.2.2 Comparison with Akhaee et al. [27]

A juxtaposition of the suggested technique was executed with distinct partially impaired and image-adaptive approach presented by Akhaee et al. [27] also. The practices again used blocks of dimension (8 × 8) with large entropy for inserting the watermark with support information to recover the same.

Watermarks of various spans of 512, 256, and 128 bits were inserted in 'Barbara'. These were put through 'Gauss filter', 'AWGN' as well as 'JPEG Compression' assaults. A notable change in BER for recuperated watermark was noticed for the suggested technique against Yadav et al. [14] in Table 3.5 for greater watermark dimensions of 2048 and 1024 bits.

3.4.2.3 Comparison with Kalantari et al. [123] and Nezhadarya et al. [124]

The performance of the suggested watermarking scheme was also collated with the Ridgelet domain technique proposed by Kalantari et al. [123] and a QIM approach suggested by Nezhadarya et al. [124]. The techniques utilized watermark spans of 256 bits with 'Lena' and 'Barbara' of dimension (512 × 512). Table 3.6, as well as 3.7, have displayed competent performance of the suggested technique in opposition to 'Median filter' and various standard factors of 'JPEG Compression' assaults.

3.4.2.4 Comparison with Amirmazlaghani et al. [31] and Hamghalam et al. [125]

A collation was also done with the recent progressive methods presented by Amirmazlaghani et al. [31] and Hamghalam et al. [125] with watermark extents of 256 as well as 128 bits. The suggested technique demonstrated superior values in opposition to 'Median & Gauss filter', 'JPEG Compression' as well as 'AWGN' assaults as displayed in Table 3.8 as well as 3.9.

3.5. IMPLEMENTATION FOR TELE-MEDICINE

Since the suggested watermarking technique showed excellent achievement in terms of watermark length capacity, enhanced security, robustness, and accurate watermark extraction, thus the scheme had found potential applications in the field of telemedicine. In this Section, medical images, namely 'Liver-1', 'Liver-2' [126], 'X-ray' [127], 'MRI brain' [128] and 'Knee Joint' [129] were used for watermarks, 'TIET', 'Copyright' and 'Thapar_Univ' .A medical watermark known as 'Patient watermark'(25 × 18) was also used. Figure 3.28 shows the medical host images and

Table 3.11 'BER (%)' for recuperated watermark beneath various assaults for medicine images of dimension (512 × 512).

Attacks	'TIET'			'Copyright'			'Thapar_Univ'			Medicine image
	Utilizing F_1	Utilizing F_2	Utilizing F_3	Utilizing F_1	Utilizing F_2	Utilizing F_3	Utilizing F_1	Utilizing F_2	Utilizing F_3	
G. Filter (3 × 3)	2.2	5.3	13.3	6.9	5.2	7	6	3.12	11.31	Liver- 1
G. Filter (3 × 3)	6.4	4	17.3	3.7	3.1	8.69	4.93	4.25	6.37	Liver- 2
G. Filter (3 × 3)	35.5	24.4	26.6	9.19	9.3	2.5	11.43	20	4	Knee Joint
Med. Filter (7 × 7)	11.77	16.44	19.7	22.1	23	16.2	25.68	37.31	22.56	Knee Joint
Wien. Filter (5 × 5)	16.8	11.55	29.3	18	18	28.6	22.5	23.06	29.4	Liver- 2
Wien. Filter (5 × 5)	5.55	6.44	10.22	14.7	14.5	6.2	15.9	27.56	7.87	Joint
AWGN with Var=10	4.2	5.7	10.44	6.3	6.7	7.5	7.62	7.12	12.31	Liver- 1
AWGN with Var=10	5.55	8.88	11.3	5.5	6.3	6	8.06	9.56	8.43	Knee Joint
JPEG Comp. with QF = 20%	16.4	19.5	32	26.2	25.5	30.3	33.5	20.06	33.56	Liver- 1
JPEG Comp. with QF = 20%	19.11	25.5	32.2	26.1	27.1	26.1	25.9	33.2	25.31	Joint
Scaling degree 0.75	7.3	4	17.1	5.5	3.1	8.1	5.62	5	5.06	Liver – 2
Scaling degree 0.75	2.88	4.8	3.3	11.1	11.8	2.9	14.8	21.8	4.8	Knee Joint
Scaling degree 2	2.66	2.66	2	7.3	6.2	2.3	3.25	16.25	3.25	Knee Joint
Scaling degree 2	1.33	1.3	1.11	3.5	2.5	2.3	4.5	3.62	4.3	X-ray
Sharpening	14	14	10.2	10.2	10.2	10.2	13.5	13.5	13.5	Knee Joint
Sharpening	14	14	14	10.2	10.2	10.2	13.5	13.5	13.5	MRI brain

Table 3.12 Watermarked Medical images and recuperated watermarks underneath different assaults of 'Gauss Filter' (5 x 5), 'Scaling' (2), 'JPEG' (QF=30%) and 'AWGN' (σ_n=20).

				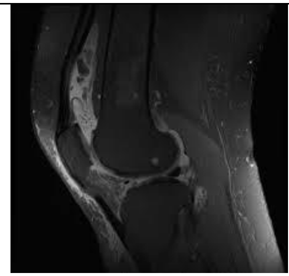
	Thapar_Univ		Copyright	
Copyright		VIJAY_C16PGI7_ 8_JOINT_67 SURGICAL_31_LAPRO_GALLSTONE_78MM_JUL	Thapar_Univ	Copyright
Thapar_Univ	Thapar_Univ	Copyright		VIJAY_C16PGI7_ 8_JOINT_67 SURGICAL_31_LAPRO_GALLSTONE_78MM_JULY2016
	VIJAY_C16PGI7_ 8_JOINT_67 SURGICAL_31_LAPRO_GALLSTONE_78MM_JULY2016	Copyright	VIJAY_C16PGI7_ 8_JOINT_67 SURGICAL_31_LAPRO_GALLSTONE_78MM_JULY2016	Thapar_Univ

patient watermark respectively. Alike to the experiment carried out earlier, the first degree of dissolution of Daube chies wavelets was utilized for calculating 2-Dimension DWT. Bits for patient watermark were inserted in the minimal frequency quantum of every chosen slab in the earliest degree. The watermarked genre of medicinal images as well as their recuperated watermark(s) utilizing various rules for estimating α_d is demonstrated in Figure 3.29.

The peak value of PSNR for watermarked medicinal image(s) is demonstrated in Table 3.10. The presentation of the atop debated approach utilizing medicine images was also examined under various assaults as displayed in Table 3.11. It was noticed that merit of BER (%) for the recuperated watermark was low for 'AWGN' variances, 'JPEG compression', 'Sharpening', 'Scaling', 'Wiener', 'Median' and 'Gauss Fil'. assaults. The assailed watermarked images as well as their recuperated watermarks are presented in Table 3.12.

3.6. SUMMARY

In this chapter, an image-adaptive watermarking technique for medical images was introduced making use of blocks of large entropy belonging to the original image. The inserting of the bits of the watermark was settled into less frequency coefficients ×of (8 × 8) blocks using statistical modeling. The accurate and efficient approach of maximum likelihood using Gaussian distribution was utilized for embedding as well as extraction of the watermark(s) correspondingly. The different extents of watermark, such as, (18 × 25) , (20 × 50) and (20 × 80) were utilized to accommodate information (or data of patients) in their corresponding natural as well as medicine images. For comparing the performance, the proposed technique also utilized various watermark dimensions of 128, 256, 512, 1024 and 2048 bits. In the suggested technique, the dynamic strength factor α_d was altered with the image characteristics utilizing three formulae concurrently. The calculated merits of α_d confirmed the finest outcomes for exorbitant PSNR (45-57dB) and enervated BER (0-1%). Extortionate resistance to geometric assaults was also detected. This justified the suggested technique was robust with the best invisibility for natural images. The technique secured watermark insertion against malicious and non-malicious assaults in tele-medicine applications too and achieved excellent equilibrium between invisibility and robustness of the watermark.

The next chapter focuses upon the improvement of the proposed watermarking technique using two watermarks for the purpose of enhancing the robustness and security of telemedicine applications.

CHAPTER 4

IMPROVED IMAGE-ADAPTIVE WATERMARKING FOR DUPLET WATERMARKS UTILIZING MATHEMATICAL DECODER

This chapter represents an upgraded image-adaptive watermarking method wherein a pair of watermarks was implanted in the elevated entropy 8×8 blocks of approximation and vertical coefficients of the host image using DWT. Fourth order analytical moment familiar as kurtosis was used to calculate Adjustable Strength Factor (ASF) for insertion of watermarks. This helped to improve the capacity and robustness of the suggested watermarking technique. Related to the semi blind process used in the previous chapter, restricted support information was again communicated besides the watermarked image. Similarly, Gaussian (or Normal) distribution was utilized for modeling and analyzing the disseminated features which assisted the ML decoder in retrieving the watermarks profitably utilizing a mathematical procedure. The effectiveness of the suggested work was assessed and compared through superior results of simulation by making use of PSNR, SSIM, NCC, and GMSD for various assaults. Finally, the suggested work was carried out on medicinal practices due to superior performance over existing methods [49].

4.1 INTRODUCTION

A watermark must be strong, invisible as well as indifferent in opposition to the variations in the transit signal undergoing different intended or unintended assaults [130]. In this chapter, duplet undetectable watermarks were inserted for the motive of protection of copyright, intensification of security, and refined durability. The essence of the suggested technique was partially impaired that didn't require authentic features of the image at the destination for recovery of the watermark. The unit arrangement displays that less support information as collated to [27] and [131] were broadcasted with the image after watermarking for watermark eradication. Such facts were communicated at the receiver prior to the procedure of watermark insertion.

Results of simulation for the suggested plan were estimated upon general images. However, the medical images were contemplated as one of the implementations of the proposed watermarking method owing to their unusual features, like, high safety, robustness, and limited capacity. The utmost originality was supported through watermarking of the medicinal image (having bounded range) along with its associated content into the only image, which helped in lessening the possibilities for incorrect prognosis. The safety issues of the healthcare sector were also controlled as the proposed scheme was gauged with different assaults. Lastly, the suggested watermarking methodology focused on sustaining the balance within robustness, capacity, and imperceptibility of the watermarked images using the standard judgment features of PSNR, SSIM, NCC, and GMSD. ML decoder centered on mathematical modeling helped in watermark eradication with outstanding completion.

Side Information	**Akhaee et al. [27]**	**Yadav et al. [131]**	**Intended**
Information1	High level entropy block locations	High level entropy block locations	High level entropy block locations
Information2	Mean and variance of less pass scaling features	Means of WHT features	Mean and variance of Low Low and Low High features
Information3	Strength factor	Dimension of watermark	----

4.2 SIGNIFICANCE OF ADJUSTABLE STRENGTH FACTOR UTILIZING KURTOSIS

Fourth order analytical moment familiar as kurtosis is considered in union with noise and design measure. It is used to discover more information about the shape. Large positive merits for kurtosis designate images having less noise with low resolution. With a usual scattering, kurtosis [132] is expressed mathematically as

$$Kurtosis = \frac{(1/n)\sum_{j=0}^{n}\left(I_j - \bar{I}\right)^4}{\left(\sqrt{(1/n)\sum_{j=0}^{n}\left(I_j - \bar{I}\right)^2}\right)^4} \tag{4.1}$$

Here, I_j and I' represented the image and mean of the block j, and n represented the total numeral of blocks. The merit of kurtosis was significant since it assisted in collating various slabs of the original image in the suggested technique. This was rightly associated with the relationship of noise as well as resolution of the image. The various blocks hold equal merit of means, std. deviation and skewness, but unalike merits of kurtosis. The differences with DWT parameters was better realized through the assistance of merits of kurtosis by attaining a strong approach. Kurtosis has contemplated a gauge for insufficiency that assisted to ascertain if the approximated (8 × 8) slab parameters of the original image developed a consistent or the highest point disposition. Such peak value was linked to the impressive outlook of scarce codes. In a usual disintegration, there is no value of Kurtosis. These may be indicated as either flat-tailed (Leptokurtic) or thin tailed (Platy-kurtic) disseminations if their merits are larger or lower than three correspondingly. Though in the first case, most of the particulars lie in the rear end, however the same rely longer upon the crest for the other case. Lastly, these positive merits for every slab also assisted for lowering the computations. Thus, the greater the mathematical moments utilized, the superior are the parameters for the objective standard for images in the procedure for watermarking. A flexible and adjustable strength factor was again utilized for placing the watermark bits in large entropy blocks, familiarized as the ASF. It was evaluated and expressed utilizing kurtosis as,

$$ASF = \frac{Kurtosis_{\ j}}{(Kurtosis_{\ max})^{\rho}} \tag{4.2}$$

Here, $Kurtosis_j$ was the merit for kurtosis of approximated coefficients for every j^{th} slab. $Kurtosis_{max}$ was the largest merit of kurtosis amidst the entire chosen parameters. ρ was the inconstant criterion for the power factor utilized in insertion. The settlement procedure to finalize acceptable blocks was banked upon kurtosis. The highest merit for a preferred slab showed the existence of commotion, which assisted in the computation of ASF. This outlook avoided the probability of losing the bits of watermark and assisted in proving robustness for the suggested technique. The fourth degree analytical feature, kurtosis provided the benefit of intolerance for brilliant modifications in pictures and manifested normal centralized and similar disparities. Hence, it was favoured in watermarking though its use for inserting duplet watermarks slightly lowered the preferable merit for PSNR.

4.3 PROPOSED KURTOSIS BASED WATERMARKING TECHNIQUE

4.3.1 Embedding of Watermark

The suggested scheme for inserting duplet watermarks is demonstrated in Figure 4.1. The detailed method is described in the given steps:

1: Segmented the natural image into blocks of dimension (8 × 8).

The (N × N) dimension of the natural image was partitioned into slabs of dimension (8 × 8). At this moment, N represented the numeral for rows as well as numeral of columns correspondingly.

2: Choice of the large blocks of entropy.

The value for entropy was determined in every block for the calculation of the value for the mean. The present value assisted in showing the inclination of parameters in clustering near a confined worth in the dispensation. The slabs having entropy larger than the average value of combined merit were carried solely by the cubicle arrangement. The sequence for these blocks was created by examining every row separately, which shaped the initial supporting information inside step 8.

3: Appealed DWT upon preferred blocks in achieving prevalent parameters.

2-D DWT was employed upon blocks with large entropy in achieving approximated (A), vertically (B), horizontally (C), and diagonally (D) recurrence parameters. Low-Low sub-band holds an uneven detail about the image [13] since it was the outcome for low passing refining for all rows as well as columns [133]. The Low-High sub-band was utilized for watermark insertion [15] since desirable attainment of invisibility and toughness was obtained [134].

4: Modeled the Low-Low and Low-High parameters utilizing means, the variance of Gaussian disintegration.

It was supposed that the approximated as well as vertically recurrence parameters feasibly be modeled through a Gaussian disintegration analogous to [121]. In general, the Gaussian mathematical procedure entangled PDF into watermarking [27]. Yet, an alternative method to determine specifications, μ and σ was also examined through 4.3 and 4.4.

$$\bar{X} = \frac{\sum_{j=1}^{N} x_j}{N} \tag{4.3}$$

$$\sigma = \sqrt{\frac{\sum_{j=1}^{N}(x_j - \bar{X})}{N}} \tag{4.4}$$

This was the second most significant supporting information utilized inside step 8.

5: Enumerated the numerals of ASF utilizing the Low-Low and Low-High measures.

The ASF was enumerated utilizing kurtosis which was converged using (4.2). The merit of ASF was unique for these parameters.

6: Inserting the bits of the initial watermark into the Low-Low parameters.

The recurrence parameters of the approximated band, ‘A’ were altered with every bit (0 or 1) for the earliest watermark, in consonance with the specified technique for inserting as given in (4.5) and (4.6),

Inserting ‘1’,

$$A = A\,.(1 + ASF) \quad (4.5)$$

Inserting ‘0’,

$$A = A\,.(1 - ASF) \quad (4.6)$$

7: Inserting the bits of the next watermark into the Low-High parameters.

Similar to the previous step, the horizontally recurrence parameters, ’B’ were too altered with every bit (0 or 1) for the following watermark in (4.7) and (4.8) as,

Inserting ‘1’,

$$B = B.(1 + ASF) \quad (4.7)$$

Inserting ‘0’,

$$B = B.(1 - ASF) \quad (4.8)$$

8: Arranged the supporting details.

The details contained positions of the block with entropy and mean, the variance of Low-Low and Low-High parameters. This was obtained from Step2 and Step4 correspondingly.

9: Applied Inverted DWT.

After inserting, the Inverted transform was appealed upon the altered slabs. The numeral of bits of the watermark to be concealed was consistently equivalent to the numeral of blocks with high entropy. It was chosen as one bit was inserted in each slab. The practice of choosing the blocks with high entropy blocks was obtained through scrutinizing every row separately, given in Step2. Finally, every altered block with high entropy was reconnected along the leftover slabs to obtain the image after watermarking.

10: Communicated the image after watermarking.

After watermarking, the image was communicated when entire blocks were collected with the supporting details as conceived in Step8.

4.3.2 Removal of Watermark and Mathematical designing of decoder

The analytical procedure for modeling features of the decoder assisted in attaining exact as well as strong results. The demonstration of the suggested decoder is displayed in Figure 4.2. The subsequent steps set out the detailed extraction of watermarks:

1: Division of the accepted Watermarked image in blocks of dimension (8 × 8).

The accepted watermarked image with dimension N × N was separated in slabs of dimension (8 × 8). Again, N represented the numeral for rows as well as the numeral of columns correspondingly.

2: Selection of the large blocks of entropy.

The positions of blocks with large communicated in the supporting information were utilized for achieving the blocks with large entropy in the accepted image after watermarking.

3: Implemented DWT upon the chosen blocks with large entropy in achieving prevalent parameters.

Closer to the procedure for insertion, 2-D DWT was implemented upon blocks with large entropy of the accepted image for achieving approximated (A'), vertically (B'), horizontally (C') and diagonally (D') recurrence parameters. Low-Low, as well as Low-High sub-bands were utilized as introduced in Step 3 of Section 4.3.1

4: Modeled the Low-Low and Low-High parameters utilizing means, the variance of Gaussian disintegration.

Alike to Step 4 of Section 4.3.1, $\mu^{'}$ as well as $\sigma^{'2}$ were too procured as significant features from these parameters of the accepted image utilizing Gaussian disintegration as a supposition.

4.3.3 Decoder Modeling using Statistical approach

The distribution of Gaussian features, viz, μ as well as σ^2 (communicated in supporting details) were collated with features of modeling, viz, $\mu^{'}$ as well as $\sigma^{'2}$of the accepted image. An ideal decoder established on the idea of highest feasibility was utilized in watermark eradication due to growing dependability and rightness.

The strategy for embedding the watermark utilizing the multiplicative approach assisted in inserting bits of the watermark. This was done appropriately in approximating and horizontally recurrence parameters with superior toughness.

$$A_{j/0} = A_j.(1 - ASF) \sim N(\mu_{\frac{j}{0}}, \sigma_{\frac{j}{0}} \text{and} B_{j/0} = B_j.(1 - ASF) \sim N\left(\mu_{\frac{j}{0}}, \sigma_{\frac{j}{0}}\right) \quad (4.9)$$

$$A_{j/1} = A_j.(1 + ASF) \sim N(\mu_{j/1}, \sigma_{j/1}) \text{and} B_{j/1} = B_j.(1 + ASF) \sim N(\mu_{j/1}, \sigma_{j/1}) \quad (4.10)$$

It was undertaken that approximating and horizontally recurrence parameters were 'i.i.d' for every form with an initial degree.

Hence the splitting of the approximating (and horizontally) recurrence parameters for every block having N coefficients s_1, s_2, s_3,…..s_N (and t_1, t_2, t_3,…..t_N) for embedding bit '0' was written as,

$$P(s_1, s_2, \dots s_N|0) \text{or } P(t_1, t_2, \dots t_N|0) =$$

$$\prod_{j=1}^{N} \sqrt{2\pi\sigma^2_{s(ort)|0}} \frac{1}{e^{-(s(or\ t)_j-(1-ASF)\mu)^2}/2\sigma^2_{s(or\ t)|0}} \quad (4.11)$$

and the division of placing bit '1' was written as,

$$P(s_1, s_2, s_3, \dots s|1) \text{or} P(t_1, t_2, t_3, \dots t_N|1) =$$

$$\prod_{j=1}^{N} \sqrt{2\pi\sigma^2_{s(or\ t)|1}} \frac{1}{e^{-s(or\ t)_j-(1+ASF)\mu)^2}/2\sigma^2_{s(or\ t)|1}} \quad (4.12)$$

For the Maximum Likelihood settlement, for approximating (and horizontally) recurrence parameters,

$$P\left(s(or\ t)_1, s(or\ t)_2, s(ort)_3, .\{s(ort)_N|1\}\right)$$

$$\underset{<0}{>1} P(s(or\ t)_1, s(or\ t)_2, s(or\ t)_3, .\ s(ort)_N|0) \quad (4.13)$$

Substituting (4.11), (4.12) in (4.13), we get

$$\prod_{j=1}^{N} \sqrt{2\pi\sigma^2_{s(ort)|1}} \frac{1}{\frac{e^{-(s(ort)_j-(1+ASF)\mu)^2}}{2\sigma^2_{s(ort)|1}}}$$

$$\underset{<0}{>1} \prod_{j=1}^{N} \sqrt{2\pi\sigma^2_{s(or\ t)|0}} \frac{1}{\frac{e^{-(s(ort)-(1-ASF)\mu)^2}}{2\sigma^2_{s(ort)|0}}} \quad (4.14)$$

Taking logs on both sides of (4.16),

$$\frac{(-N)}{2} \ln\left(\sigma^2_{s(ort)|1}\right) \frac{1}{\sigma^2_{s(ort)|1}} \sum_{j=1}^{N} (s(ort)_j - (1+ASF)\mu)^2$$

$$\underset{<0}{>1} \frac{(-N)}{2} \ln\left(\sigma^2_{s(ort)|0}\right) \frac{1}{\sigma^2_{s|0}} \quad (4.15)$$

Simplifying (4.15)

$$\left(\frac{1}{\sigma^2_{s(or\ t)|0}} - \frac{1}{\sigma^2_{s(or\ t)|1}}\right) \sum_{j=1}^{N} s(or\ t)_j^2 - 2\left\{\frac{(1-ASF)}{\sigma^2_{s(or\ t)|0}} -\right.$$

$$\left.\frac{(1+ASF)}{\sigma^2_{s(or\ t)|1}}\right\} \sum_{j=1}^{N} s(or\ t)_j \underset{<0}{>1} N \ln\left(\frac{\sigma^2_{s(or\ t)|1}}{\sigma^2_{s(or\ t)|0}}\right) - N\mu^2 \left\{\frac{(1-ASF)^2}{\sigma^2_{s(or\ t)|0}} - \frac{(1+ASF)^2}{\sigma^2_{s(or\ t)|1}}\right\} \quad (4.16)$$

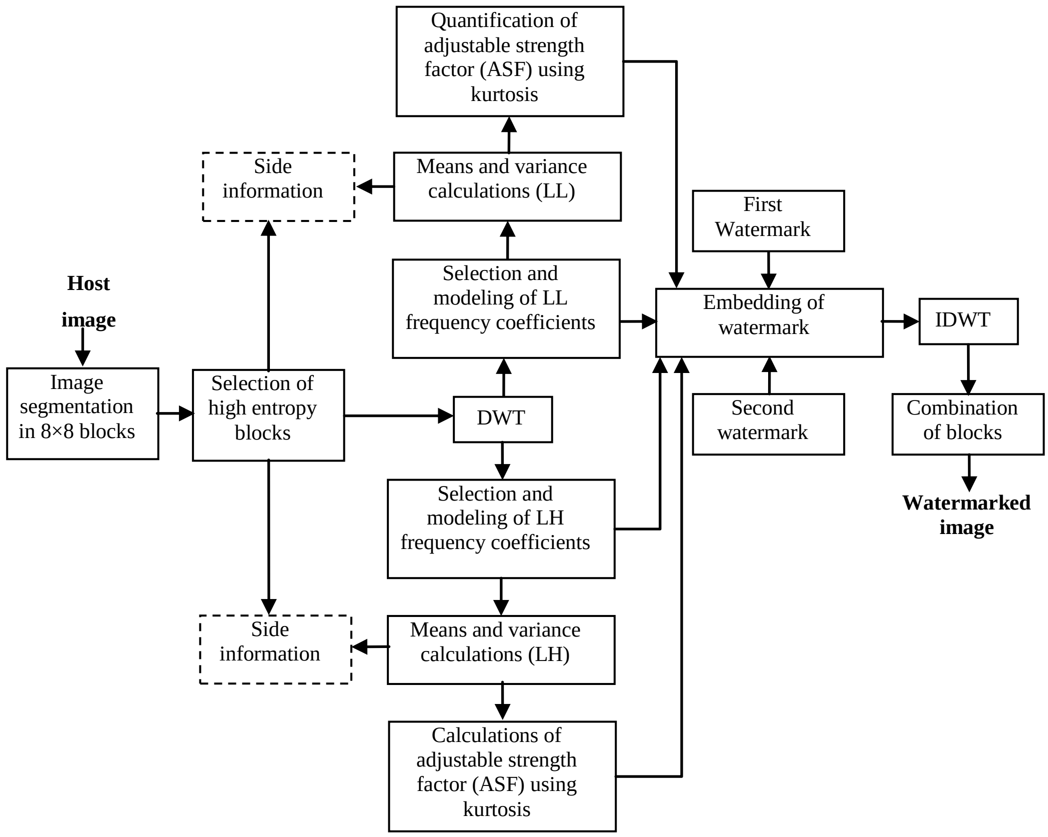

Figure 4.1 Block Diagram for Suggested task for watermarks insertion.

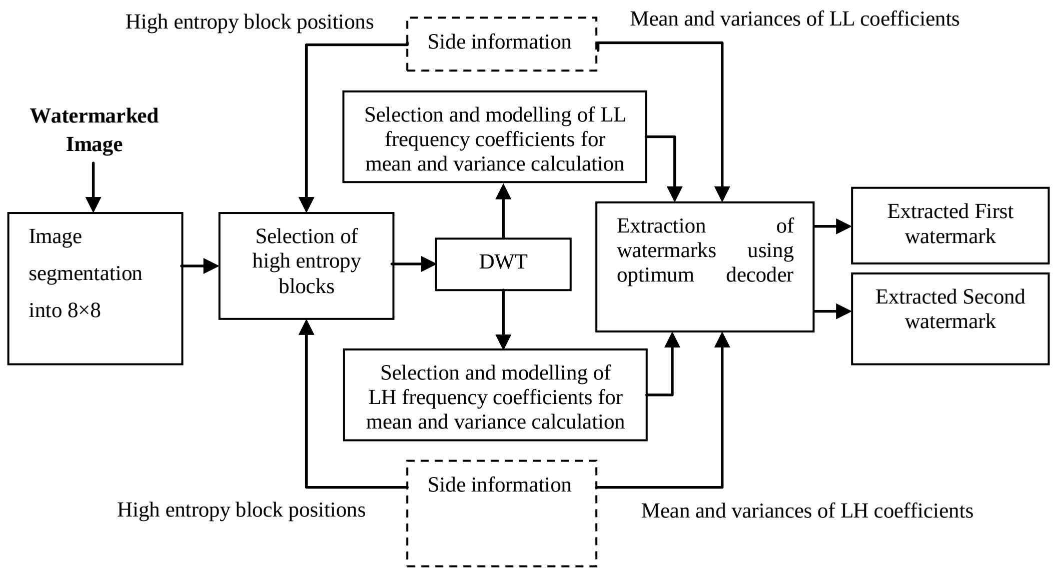

Figure 4.2 Block Diagram for Suggested task for watermark withdrawal.

Assuming the merit of noisy variance approaching to nothing for a restricting instance of soaring SNR, $\sigma_{s|1}^2(or\ \sigma_{t|1}^2) = (1 + ASF)^2\sigma^2$ and $\sigma_{s|0}^2(or\ \sigma_{t|1}^2) = (1 - ASF)^2\sigma^2$ equation (4.16) was altered with bit '0' as well as '1' in approximating (and horizontally) recurrence parameters as,

$$\frac{1}{\sigma^2(1-ASF)^2}\sum_{j=1}^{N} s(or\ t)_j^2 - \frac{2\mu}{(1-ASF)\sigma^2}\sum_{j=1}^{N} s(or\ t)_j < (-2N)\{\ln\sigma + \ln(1 - ASF)\} - N\frac{\mu^2}{\sigma^2} \quad (4.17)$$

$$\frac{(-1)}{\sigma^2(1+ASF)^2}\sum_{j=1}^{N} s(or\ t)_j^2 + \frac{2\mu}{(1+ASF)\sigma^2}\sum_{j=1}^{N} s(or\ t)_j > (2N)\{\ln\sigma + \ln(1 + ASF)\} + N\frac{\mu^2}{\sigma^2} \quad (4.18)$$

The merit for ASF was approximated to zero, as SNR approached to a high range. Hence the decoder was validated to gain independence of ASF for correct extraction of watermarks.

4.4 SAFETY OF WATERMARKING APPROACH

The offered technique utilized supporting details for assisting the decoder in purposeful watermark redemption. These supporting details by and large composed of formerly, locations for large blocks with entropy and secondarily, the variances as well as means for the parameters. The arrangement of block locations having large entropy had no direct association with the original image. The short lived orientation of these slabs in the arrangement was never permanent. This aided in ensuring safety for the suggested method in circumventing intentional attacks. This became a significant provocation to approximate the slabs location of large entropy properly by the attacker. The safety of the supporting details [135] could be increased through coding.

4.5 INVESTIGATION AND OUTCOMES

In this section, the efficacy of the proposed approach was examined by conducting several attacks on standard images of size (512 × 512). Thus, the potency of the suggested method was justified through simulation outputs acquired by utilizing natural images for dimension (1024 × 1024). The experiment utilized quaternary monochrome watermarks for various dimensions. To start with, a sole 'TIET', 'Copyright' or 'Thapar_Univ' was placed in the Low-Low recurrence parameters for the quality original image. Afterward, insertion of duplet watermarks was done concurrently into approximating and horizontally recurrence parameters in Figure 4.1, The initial watermark was selected amongst the three dissimilar dimensions raised above, though the subsequent watermark utilized was 'Logo' of dimension (64 × 64). Therefore, ternary watermark amalgamations specifically ('TIET' with 'Logo'), (‘Copyright’ with ‘Logo’) as well as (‘Thapar_Univ with ‘Logo’) were utilized in inserting both watermarks as displayed in Figure 4.3 to Figure 4.5. Similarly, medical watermarks, ‘Patient watermark’ as well as ‘Joint’ of dimensions, (18 × 25) and (32 × 32) [32] correspondingly were the sole amalgamation utilized. The above images and amalgamations are exhibited in Figure 4.6.

Various plots for PSNR (in dB) and BER (in %) were also exhibited with various merits for ρ in Figures 4.7 correspondingly for placing a sole watermark. As ρ utilizing (4.2) increases, the merit for PSNR also intensifies as displayed in charts.

Figure 4.3 Natural images utilized, ‘Lena’, ‘Barbara’, ‘Baboon’, ‘Peppers’.

Figure 4.4 Use of watermarks, “first image watermark”: ‘TIET’ of dimension (18 × 25), ’Copyright’ of dimension (50 × 20), ‘Thapar_Univ’ of dimension (80 × 20) , “second image watermark” : ‘Logo’ of dimension (64 × 64).

(a) (b) (c)

Figure 4.5 Amalgamations of watermarks utilized: (a) (‘TIET’, with ‘Logo’) (b) (‘Copyright’, with ‘Logo’) (c) (‘Thapar_Univ’, with ’Logo’).

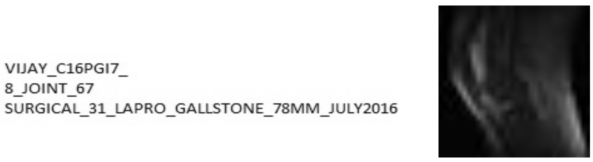

(a) (b)

Figure 4.6 Medical Image watermarks (a) ‘Patient watermark’ exhibiting particulars for the doctor, code of hospital, number of images, details of patientscan (b) ‘Joint’.

The merit for BER too enhanced in the exponential direction though it remained unaffected initially. Utilizing (4.2), ρ merits were (2.1, 2.2, 2.3), (2.7, 2.6, 2.7), (2.2, 2.1, 2.1) and (2.2, 2.4, 2.5) for inserting sole watermarks ‘TIET’, ‘Copyright’, 'Thapar_Univ' within natural images 'Lena', 'Barbara', 'Peppers' and 'Baboon' correspondingly. But, when the first watermark amalgamation 'TIET with Logo' was placed concurrently within every natural image, the merits for ρ changed for every sub band correspondingly. The factors for each sub band were altered jointly in obtaining an excellent invisible image after watermarking with minimal BER (%) for eradicated watermarks. The merits chosen for ρ in approximating and vertically recurrence parameters were (2.40, 0.70), (2.60, 0.90), (2.40, 0.90) and (2.40, 0.90) for images 'Lena', 'Barbara', 'Peppers' and 'Baboon' consequently utilizing 'TIET' (in Low-Low sub band) and 'Logo'(in Low-High sub band). Similarly, while inserting 'Copyright' as well as 'Thapar_Univ'(in Low-Low sub band) and Logo (in Low-High sub-band) within the similar images, the ρ merits were collected as (2.40, 0.70), (2.60,0.90), (2.20,0.90), (2.40,0.90) and (2.40, 0.70), (2.60, 0.90), (2.20, 0.90) and (2.20, 0.90) correspondingly. ASF merits lie within the scale of 0.0040 to 0.07. The approach guaranteed images with high imperceptibility, robustness, and minimal BER (%).

Table 4.1 and Table 4.2 set down the purposeful quality merits of 'PSNR', 'BER', 'SSIM', 'NCC' as well as 'GMSD' of the different images utilizing sole watermark for 450, 1000, or 1600 bits being inserted in the approximately recurrence parameters for the natural image having blocks with large entropy. Superior invisibility of images after watermarking was observed as the suggested method used PSNR with 47 dB. The merits of SSIM and NCC neared the highest merit of one after watermarks were inserted in the blocks with large entropy. BER (%) for the recuperated watermarks neared minimal values, which was advantageous as per watermark quality. The merits of GMSD too marked the least divergence in images after watermarking. The objective framework was again measured in Table 4.3 and 4.4 when the alternative watermark 'Logo' was inserted concurrently with either of the initial watermark(s) in the vertically recurrence parameters.

It was observed, the images 'Lena', 'Peppers' as well as 'Baboon' exhibited values for NCC when two watermarks were inserted in them. Merits for 'BER (%)' for the initial recuperated watermark did not change much while the later watermark was being placed. However, these values expressed significant variations during the insertion of the initial watermark. Besides GMSD merits too furnished superb effects for images with different watermark amalgamations. Table 4.5 shows these images with their recovered watermarks.

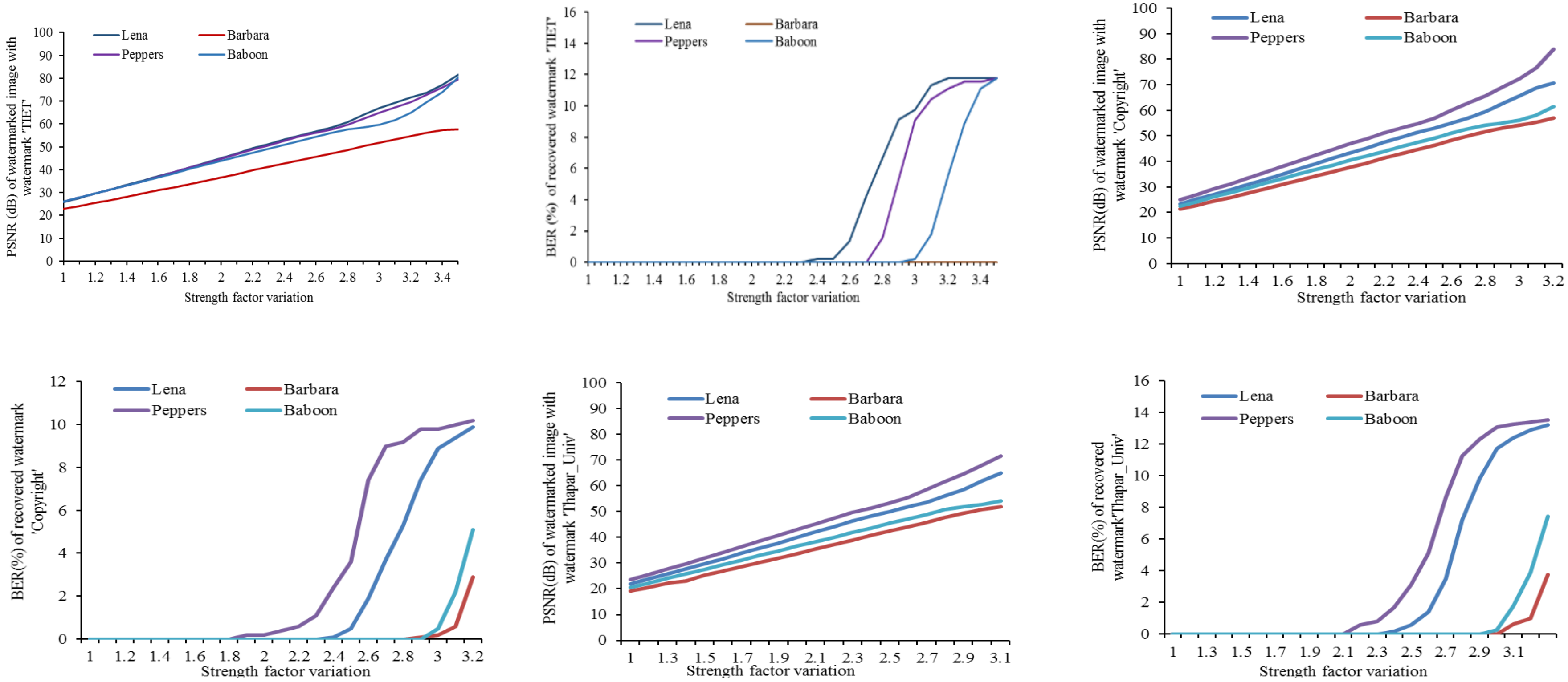

Figure 4.7 Plots for ‘PSNR (in dB)’ for images with ‘BER (%)’ for recuperated watermarks ‘TIET’, ‘Copyright’ as well as ‘Thapar_Univ’.

Table 4.1 ‘PSNR’, ‘NCC’, ‘SSIM’ as well as ‘GMSD’ frameworks for images with dimension (512×512) and ‘BER (%)’ for recuperated watermarks ‘TIET’, ‘Copyright’, ‘Thapar_Univ’ appropriately.

→ Standard Quality Criterions ↓ Natural image (watermark)	Dimension	‘PSNR’	‘NCC’	‘SSIM’	‘BER(%)’ for recuperated watermark	‘GMSD’ ($\times 10^{-3}$)
‘Lena’	512 × 512					
(with ‘TIET’)		47.23	0.9978	0.99814	0	12.3
(with ‘Copyright’)		47.4	0.99816	0.99739	0	8.55
(with ‘Thapar_Univ’)		48.27	0.9984	0.9973	0	5.81
‘Barbara’	512 × 512					
(with ‘TIET’)		47.24	0.9993	0.99849	0	6.513
(with ‘Copyright’)		48.14	0.99931	0.99791	0	4.2206
(with ‘Thapar_Univ’)		47.71	0.99907	0.99749	0	4.165
‘Peppers’	512 × 512					
(with ‘TIET’)		48.76	0.99890	0.99829	0	6.27
(with ‘Copyright’)		48.91	0.9989	0.9974	0.4	4.84
(with ‘Thapar_Univ’)		47.51	0.9983	0.9967	0.56	5.944
‘Baboon’	512 × 512					
(with ‘TIET’)		47.41	0.9997	0.9982	0	4.476
(with ‘Copyright’)		47.43	0.99774	0.9971	0	3.4230
(with ‘Thapar_Univ’)		48.99	0.99974	0.9972	0	2.237

Table 4.2 'PSNR', 'NCC', 'SSIM' as well as 'GMSD' frameworks for images with dimension (1024 × 1024) and BER (%) for recuperated watermarks 'TIET', 'Copyright' and 'Thapar_Univ' consequently.

→ Standard Quality Criterions ↓ Natural image (watermark)	Dimension	'PSNR'	'NCC'	'SSIM'	'BER(%)' for recuperated watermark	'GMSD' ($\times 10^{-3}$)
'Lena' (with 'TIET') (with 'Copyright') (with 'Thapar_Univ')	1024× 1024	51.03 49.72 49.44	0.9994 0.9988 0.9986	0.9989 0.9985 0.9981	0 0 0	8.7 8.5 8.05
'Barbara' (with 'TIET') (with 'Copyright') (with 'Thapar_Univ')	1024× 1024	39.48 46.62 37.85	0.9977 0.9986 0.9956	0.9966 0.9989 0.9927	0 0 0	2.073 7.484 2.835
'Peppers' (with 'TIET') (with 'Copyright') (with 'Thapar_Univ')	1024× 1024	51.14 51.82 49.92	0.9996 0.9990 0.9986	0.9997 0.9992 0.9987	0 0 0.125	2.495 4.842 5.955
'Baboon' (with 'TIET') (with 'Copyright') (with 'Thapar_Univ')	1024× 1024	52.11 51.95 52.57	0.9994 0.9991 0.9990	0.9999 0.9998 0.9998	0 0 0	2.384 1.906 1.501

Table 4.3 'PSNR', 'NCC', 'SSIM', as well as 'GMSD' parameters for images of dimension (512 × 512) and 'BER (%)' for amalgamations ('TIET' with 'Logo'), ('Copyright' with 'Logo') and ('Thapar_Univ' with 'Logo') correspondingly.

→Standard Grade Criterion ↓ Natural image (watermark)	Dimension	'PSNR'	'NCC'	'SSIM'	'BER(%)' for recuperated watermark 1	'BER(%)' for recuperated watermark 2	'GMSD' ($\times 10^{-3}$)
'Barbara'							
(' TIET with Logo')	512 × 512	46.930	0.9993	0.9967	0	5.88	1.6
('Copyright with Logo')		47.030	0.9985	0.9970	0	11.74	2.175
('Thapar_Univ with Logo')		44.370	0.9977	0.9970	0.0625	17.08	4.72
'Peppers'							
(' TIET with Logo')	512 × 512	44.08	0.9990	0.9958	0.4	8.83	2.24
('Copyright with Logo')		44.08	0.9979	0.9961	0.2	14.42	3.57
('Thapar_Univ with Logo')		44.44	0.9971	0.9963	0.43	20.62	4.01
'Baboon'							
(' TIET with Logo')	512 × 512	36.62	0.9981	0.9875	0.2	5.41	0.472
('Copyright with Logo')		37.98	0.9980	0.9899	0.89	11.20	0.542
('Thapar_Univ with Logo')		39.00	0.9970	0.9920	0.125	18.16	2.58
'Lena'							
(' TIET with Logo')	512 × 512	43.22	0.9912	0.9933	0.4	8.39	2.149
('Copyright with Logo')		43.27	0.9982	0.9941	0.4	11.88	2.915
('Thapar_Univ with Logo')		43.75	0.9974	0.9948	0.6875	18.57	4.97

Table 4.4 'PSNR', 'NCC', 'SSIM', as well as 'GMSD' parameters for images with dimension (1024 × 1024) and 'BER (%)' for amalgamations ('TIET' with 'Logo'), ('Copyright' with 'Logo') and ('Thapar_Univ' with 'Logo') respectively.

→Standard Grade Criterion ↓ Natural image (watermark)	Dimension	'PSNR'	'NCC'	'SSIM'	'BER(%)' for recuperated watermark 1	'BER(%)' for recuperated watermark 2	'GMSD' ($\times 10^{-3}$)
'Barbara'							
(' TIET with Logo')	1024 × 1024	43.84	0.9987	0.9978	0	7.12	11.3
('Copyright with Logo')		45.99	0.9986	0.9982	0	13.62	7.48
('Thapar_Univ with Logo')		44.82	0.9981	0.9977	0	20.97	9.44
'Peppers'							
(' TIET with Logo')	1024 × 1024	54.80	0.9998	0.9995	0.2	10.57	1.1
('Copyright with Logo')		52.03	0.9992	0.9991	0	16.4	3.22
('Thapar_Univ with Logo')		50.91	0.9988	0.9989	0.125	22.90	3.95
'Baboon'							
(' TIET with Logo')	1024 × 1024	47.79	0.9995	0.9989	0	5.54	1.34
('Copyright with Logo')		47.42	0.9990	0.9990	0	11.62	1.9
('Thapar_Univ with Logo')		45.57	0.9982	0.9989	0	18.82	4,38
'Boat'							
(' TIET with Logo')	1024 × 1024	51.20	0.9998	0.9991	0	6.86	6.7
('Copyright with Logo')		50.92	0.9995	0.9990	0	12.93	2.8
('Thapar_Univ with Logo')		50.78	0.9992	0.9989	0	20	3.4

4.5.1 Robustness Analysis

The images were initially inserted using watermark ‘TIET’, ‘Copyright’or ‘Thapar_Univ’ in the approximated recurrence parameters. These were exposed to Median (3 × 3), (5 × 5), (7 × 7), Gauss (3 × 3), (5 × 5), Wiener (3 × 3), (5 × 5) filters, and Sharp assaults. Similarly, the water marked images having duplet watermarks were too exposed to similar assaults. Table 4.6 demonstrates the collation for merits of ‘PSNR’, ‘NCC’, ‘SSIM’, as well as ‘GMSD’ for assaulted images with watermarks ‘TIET’, ‘Copyright’ or ‘Thapar_Univ’ and their amalgamations, (‘TIET’ and ‘Logo’), (‘Copyright’ and ‘Logo’) or (‘Thapar_Univ’ and ‘Logo’). Bold numerals designated superior outputs.

The images were exposed to AWGN, Scale as well as JPEG Comp. assaults too. Plots depicting changes in ‘PSNR’, ‘NCC’, ‘SSIM’ or ‘GMSD’ were devised for different watermark instances were plotted in Figure 4.8 to Figure 4.10. The scripts mentioned in the charts conveyed separate meanings for every watermark and its amalgamation. For instance, Lena1 designated outputs for insertion with initial watermark in ‘Lena’, while Lena2 stipulated the image after watermarking with watermark amalgamations.

From Table 4.4, watermark ‘TIET’ gave better results for images ’Lena’ and ‘Barbara’ for Median (3 × 3, 5 × 5, 7 × 7) as well as Gauss (3 × 3, 5 × 5) filter assaults. ’Barbara’ too depicted finer outcomes for Wiener (3 × 3, 5 × 5) and Sharp assaults. Improvement in outcomes was also noticed in ’Barbara’ as well as ‘Lena’ when the watermark ‘Copyright’ was utilized. Limited variations were noticed while using the watermark ‘Thapar_Univ’. However, the outcomes of NCC utilizing duplet watermarks were superior against those utilizing one watermark only. Superior performance was too noticed for values of SSIM underneath Wiener (3 × 3, 5 ×5) assaults with full-size watermarks. Besides, it was observed for all host images, GMSD merits gave superior performance utilizing both watermarks than those with the only watermark under no assaults. Results were better under Gauss attacks too, but average improvement was noticed under Median attacks. It was true correct for every type of watermark utilized. Through these charts, it was noticed that assaulted merits for ‘PSNR’ with duplet watermarks reduced under AWGN assault for different watermark amalgamations in contrast with the merits achieved utilizing one watermark. These merits displayed better outcomes with JPEG Comp. assaults but displayed perfect results under various changes for Scale assault. The merits of NCC utilising watermark amalgamation involving ‘TIET’ and ‘Copyright’ gave superior outcomes under AWGN assault. The values of NCC demonstrated outstanding results for every watermark type with JPEG Comp. and Scale assaults. The merits of SSIM utilising watermark combinations for AWGN as well as JPEG assaults declined, yet displayed superior outcomes for earliest dissimilarities for Scale assault. Finally, GMSD merits utilising watermark combinations displayed outstanding outputs in contrast with those utilising one watermark under different assaults for every type of watermark dimension.

Consequently, the suggested approach utilising one and two watermarks demonstrated excellent achievements for different assaults. The fulfilment standards

Table 4.5 Water marked images with their recuperated watermarks

i		ti	Copyright	Thapar_Univ	HAPAR NIVERSITY
ii		ti	Copyright	Thapar_Univ	HAPAR NIVERSITY
iii		ti	Copyright	Thapar_Univ	HAPAR NIVERSITY
iv	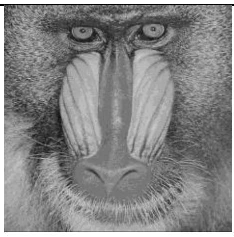	ti	Copyright	Thapar_Univ	HAPAR NIVERSITY

Table 4.6 ‘PSNR’, ‘NCC’, ‘SSIM’, as well as ‘GMSD’ constants for assaulted images

Noisy ‘PSNR’ (in dB)										
Images	Watermark union	Under no attack	Gauss F (3 × 3)	Gauss F (5 × 5)	Med. F (3×3)	Med. F (5×5)	Med. F (7×7)	Sharpening	Wien. F (3×3)	Wien. F (5×5)
Barbara	‘TIET’	47.240	39.910	39.870	33.80	29.110	26.860	9.880	35.450	31.10
	‘TIET’ with ‘Logo’	46.930	**40.340**	**40.30**	**33.870**	**29.140**	**26.870**	**9.890**	**35.690**	**31.180**
Lena	‘Copyright’	47.40	40.50	40.480	36.070	32.15	30.060	8.640	38.350	35.540
	‘Copyright’ with ‘Logo’	43.270	**40.590**	**40.570**	**35.970**	32.130	30.050	**8.650**	38.070	35.490
Peppers	‘Thapar_Univ’	47.510	39.250	39.230	34.880	32.240	30.310	9.390	36.360	34.590
	‘Thapar_Univ’ with ‘Logo’	44.440	39.170	39.150	34.790	32.210	30.30	9.380	36.160	34.450
Baboon	‘TIET’	47.410	32.920	32.90	25.040	22.630	21.910	8.630	28.60	26.150
	‘TIET’ with ‘Logo’	36.620	32.760	32.740	24.910	22.570	21.880	8.620	28.440	**26.160**
Noisy ‘NCC’										
Barbara	‘Copyright’	0.9979	0.9992	0.99923	0.9992	0.9991	0.9987	0.6882	0.999	0.9998
	‘Copyright’ with ‘Logo’	**0.9985**	**0.9998**	**0.9998**	**0.9998**	**0.9998**	**0.9993**	**0.6886**	**0.9997**	**01**
Lena	‘Thapar_Univ’	0.9973	0.9986	0.9986	0.9984	0.9993	0.9998	0.6026	0.998	0.9987
	‘Thapar_Univ’ with ‘Logo’	0.9974	0.9988	0.9988	0.9986	0.9995	01	0.6029	0.9982	0.9989
Peppers	‘TIET’	0.9982	0.9994	0.9999	0.9987	0.9995	01	0.6086	0.9994	01
	‘TIET’ with ‘Logo’	0.999	**01**	**01**	**0.9996**	**01**	**01**	**0.6086**	**01**	**01**
Baboon	‘Copyright’	0.9971	01	01	0.999	0.9999	0.9999	0.587	01	01
	‘Copyright’ with ‘Logo’	**0.9980**	01	01	**01**	**01**	**01**	**0.587**	01	01

Noisy 'SSIM'										
Barbara	'Thapar_Univ'	0.9990	0.99004	0.9899	0.924	0.7937	0.6949	0.9742	0.9320	0.819
	'Thapar_Univ' with 'Logo'	0.9970	0.9889	0.9888	0.9232	0.7931	0.6943	0.5675	**0.9334**	**0.82**
Lena	'TIET'	0.9978	0.9863	0.9862	0.9347	0.88368	0.8433	0.626	0.942	0.9043
	'TIET' with 'Logo'	0.9933	0.9863	0.9862	0.9337	0.8836	0.8431	0.6122	0.942	**0.9056**
Peppers	'Copyright'	0.9989	0.9742	0.9742	0.889	0.8516	0.8259	0.5328	0.8966	0.86053
	'Copyright' with 'Logo'	0.9961	**0.9743**	0.9742	0.8878	0.8508	0.8254	0.5245	0.8962	0.8601
Baboon	'Thapar_Univ'	0.99974	0.9627	0.9625	0.7298	0.5076	0.4167	0.5265	0.8215	0.6706
	'Thapar_Univ' with 'Logo'	0.992	0.9623	0.9621	0.7269	0.5058	0.4156	0.5131	**0.8243**	**0.6751**
Noisy 'GMSD'										
Barbara	'TIET'	6.51×10^{-3}	1.61×10^{-2}	1.62×10^{-2}	1.99×10^{-2}	7.26×10^{-2}	0.1296	0.2588	1.61×10^{-2}	6.19×10^{-2}
	'TIET' with 'Logo'	$\mathbf{1.6\ 10^{-3}}$	$\mathbf{1.49\times10^{-2}}$	$\mathbf{1.50\times10^{-2}}$	$\mathbf{0.89\times10^{-2}}$	7.3×10^{-2}	0.1313	**0.2563**	$\mathbf{1.45\times10^{-2}}$	$\mathbf{6.18\times10^{-2}}$
Lena	'Copyright'	8.55×10^{-3}	1.88×10^{-2}	1.89×10^{-2}	1.64×10^{-2}	1.96×10^{-2}	8.83×10^{-2}	1.86×10^{-2}	1.056×10^{-2}	3.168×10^{-2}
	'Copyright' with 'Logo'	$\mathbf{2.91\times10^{-3}}$	$\mathbf{1.74\times10^{-2}}$	$\mathbf{1.75\times10^{-2}}$	$\mathbf{1.53\times10^{-2}}$	5.02×10^{-2}	8.89×10^{-2}	**0.1835**	$\mathbf{8.15\times10^{-3}}$	$\mathbf{3.07\times10^{-2}}$
Peppers	'Thapar_Univ'	5.94×10^{-3}	1.2×10^{-2}	1.20×10^{-2}	1.38×10^{-2}	3.73×10^{-2}	6.713×10^{-2}	0.1768	8.579×10^{-2}	2.652×10^{-2}
	'Thapar_Univ' with 'Logo'	$\mathbf{4.01\times10^{-3}}$	$\mathbf{1.13\times10^{-2}}$	$\mathbf{1.13\times10^{-2}}$	$\mathbf{1.37\times10^{-2}}$	$\mathbf{3.73\times10^{-2}}$	6.74×10^{-2}	**0.1754**	$\mathbf{7.83\times10^{-3}}$	$\mathbf{2.62\times10^{-2}}$
Baboon	'TIET'	$4.47\text{x}10^{-3}$	$1.08\text{x}10^{-2}$	$1.08\text{x}10^{-2}$	$5.55\text{x}10^{-2}$	0.1179	$1.69\text{x}10^{-2}$	$1.59\text{x}10^{-2}$	$2.653\text{x}10^{-2}$	$7.515\text{x}10^{-2}$
	'TIET' with 'Logo'	$\mathbf{4.72\times10^{-4}}$	$\mathbf{9.86\times10^{-3}}$	$\mathbf{9.92\times10^{-3}}$	5.98×10^{-2}	0.118	**0.169**	0.162	2.7×10^{-2}	7.53×10^{-2}

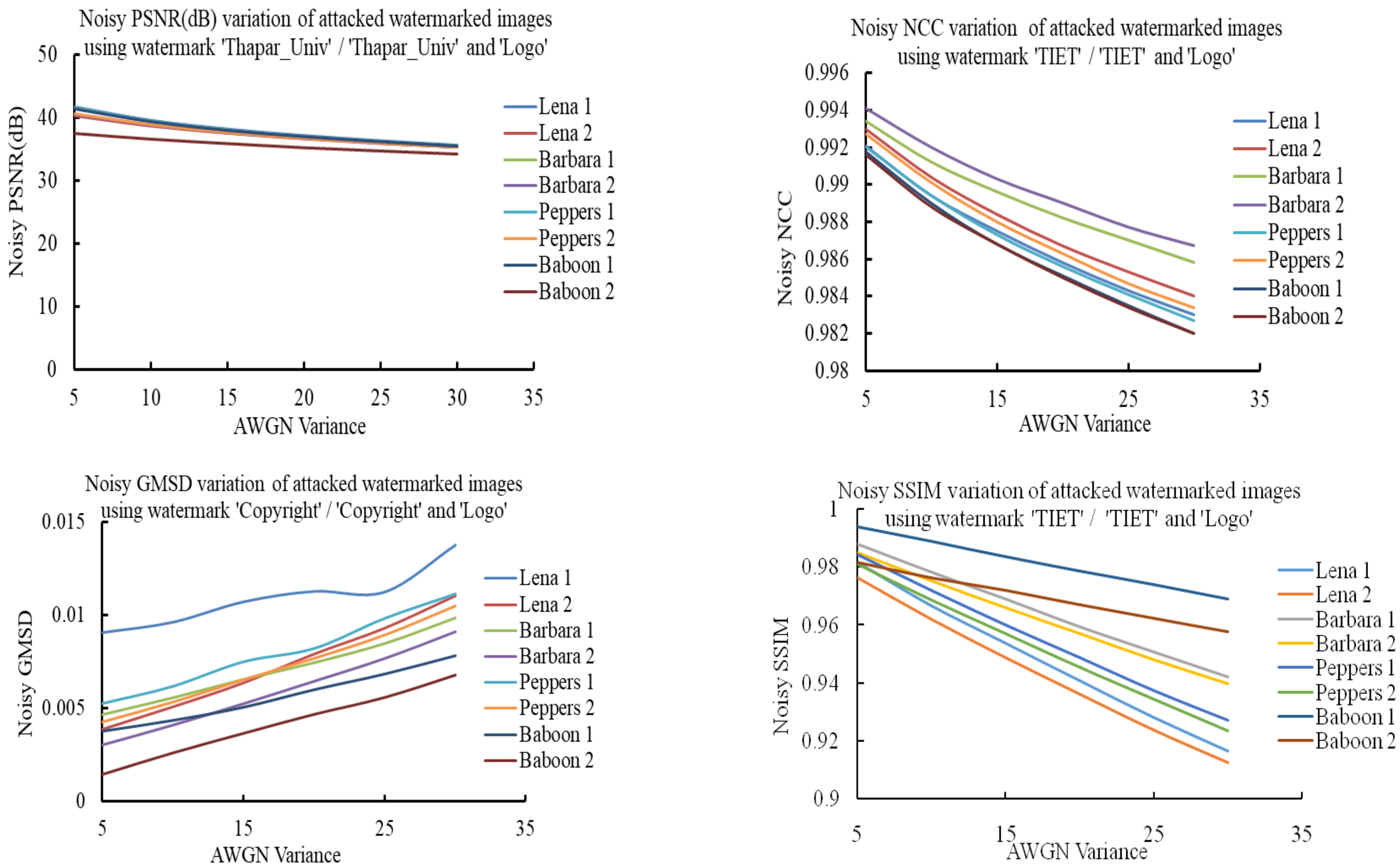

Figure 4.8 Noisy PSNR, NCC, GMSD and SSIM variation of attacked watermarked images under AWGN attacks respectively.

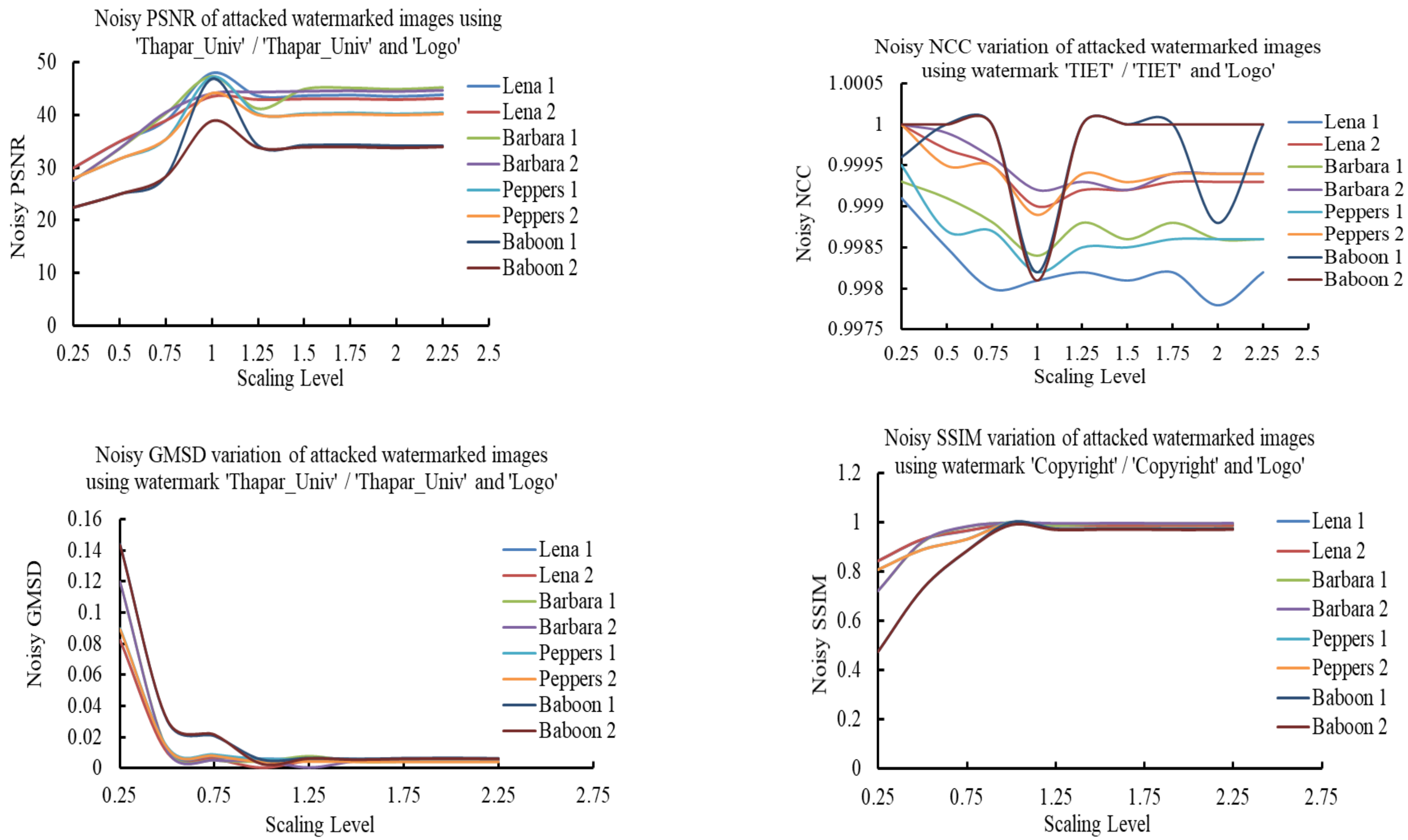

Figure 4.9 Noisy PSNR, NCC, GMSD and SSIM variation of attacked watermarked images under Scaling attacks respectively.

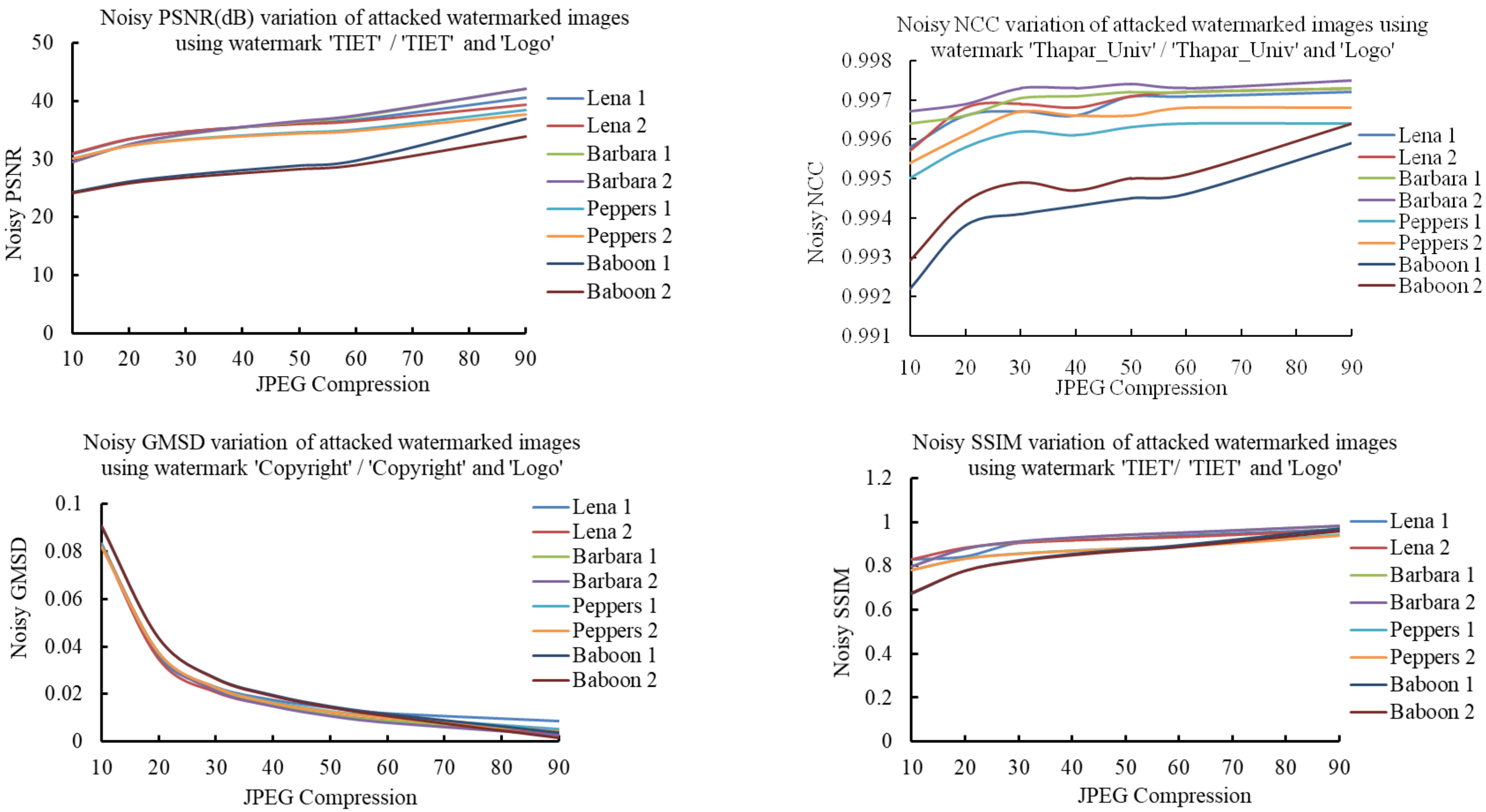

Figure 4.10 Noisy PSNR, NCC, GMSD and SSIM variation of attacked watermarked images under JPEG Compression attacks.

also displayed the success and robust characteristics of the proposed technique. The images under various assaults with recuperated watermarks are displayed in Table 4.7 and Table 4.8 respectively. Largely, the watermarked images were able to survive through the assaults. This was justified through greater amounts of fortunate watermark extractions.

4.5.2 Comparison with other schemes using single watermark

In this Section, the suggested technique of watermarking utilizing one watermark was compared to three different watermarking schemes. Results highlighted in bold values indicated the better performance of the proposed technique.

4.5.2.1 Comparison with Verma et al. [136]

First of all, the suggested approach was collated against Verma et al. [136]. The combination of 'Lifting Wavelet Transform (LWT)', 'Support Vector Machine (SVM)' as well as 'Principal Component Analysis (PCA)' was used in watermark extraction. Original images with dimensions (512 × 512) were utilized for 512-bit watermark duration with 512 bits. Table 4.7 justifies the potential of the suggested technique for achieving superior NCC values against JPEG Comp. (20% - 50%), Filter as well as Scale assaults.

4.5.2.2 Comparison with Amirmazlaghani et al. [31] and Nezhadarya et al. [124]

Juxtaposition was done with the techniques presented by Amirmazlaghani et al. [31] and Nezhadarya et al. [124] which too utilized natural images with dimension (512 × 512). While the antecedent utilized various watermark spans in watermarking, the subsequent utilized only one watermark with 256 bits for inserting. The merits for BER (%) of the suggested approach were obtained for 'Barbara' and 'Baboon' for watermarks with variable dimensions against Amirmazlaghani et al. [31] in Table 4.8. These merits were again obtained separately for 'Peppers', 'Baboon', 'Barbara', Lena' under JPEG Comp. as well as Gauss and Med. Filters in Table 4.11 for [124]. Finally, collation for various merits of SSIM was displayed in Table 4.12. The emphasized merits designated the supremacy of the suggested scheme utilizing the exclusive watermark.

Table 4.7 Images under various assaults with recuperated watermarks.

'Lena' exposed to Gauss F (3 × 3), Scale (0.5), Med. F (5 × 5), AW GN (σ^2=10) , JPEG Comp. (10%) assaults					
					
'Barbara' exposed to Gauss F (5 × 5), Scale (2), AW GN (σ^2=5), JPEG Comp. (10%) , Wien.F (5 × 5) assaults					
		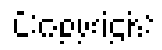			
'Peppers' exposed to JPEG Comp. (60%), AW GN (σ^2=15), Gauss.F (3 × 3), Wien. F (3 × 3) assaults					
					
'Baboon' exposed to Gauss.F (3 × 3) , AW GN (σ^2=20) , Scale (0.75) assaults					
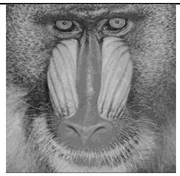		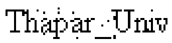			

Table 4.8 Recuperated watermarks with different assaults.

Watermarked Image	Gauss.F (3 × 3)	Scale (0.5)	Med. Filter (5 × 5)	AWGN (variance =10)
			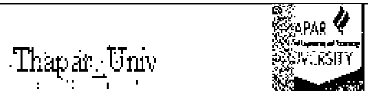	
			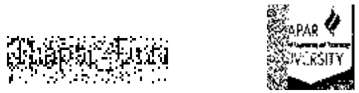	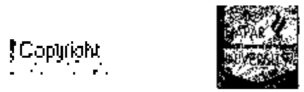
				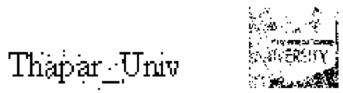
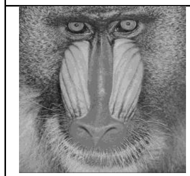		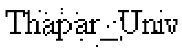		

Table 4.9 Comparison for NCC with recuperated watermarks amongst suggested technique as well as Verma et al. [136] with watermark duration of 512 bits.

JPEG Comp.(%)													
	20	30	40	50	60	90	Median (3 × 3)	Median (5 × 5)	Gauss (3 × 3)	Sharp	Scale 0.5	Scale 0.9	Scale 1.5
'Lena'													
Verma et al.[136]	0 .9063	0.9609	0.9688	0.9805	1	1	0.9258	0.8203	0.9570	0.9648	0.9453	0.9844	0.9961
(Prop)	**0.9950**	**0.9949**	**0.9950**	**0.9954**	0.9953	0.9955	**0.9967**	**0.9977**	**0.9969**	0.6029	**0.9960**	**0.9957**	0.9956
'Peppers'													
Verma et al.[136]	0.9375	0.9453	0.9688	0.9844	1	1	0.9180	0.7773	0.9609	0.9766	0.9414	0.9648	0.9766
(Prop)	**0.9918**	**0.9925**	**0.9923**	**0.9923**	0.9925	0.9925	**0.9934**	**0.9943**	**0.9945**	0.6078	**0.9932**	**0.9930**	0.9931
'Barbara'													
Verma et al.[136]	0.9570	0.9766	0.9688	0.9805	1	1	0.9023	0.8125	0.9727	0.9102	0.9453	0.9805	0.9833
(Prop)	**0.9925**	**0.9930**	**0.9930**	**0.9930**	0.9931	0.9932	**0.9947**	**0.9947**	**0.9946**	**0.6878**	**0.9949**	**0.9935**	**0.9933**

Table 4.10 Comparison for 'BER (%)' of recuperated watermarks amongst suggested technique as well as Amirmazlaghani et al. [31] with watermark duration of 128 bits.

		AWGN (σ_n=10) (σ_n=20) (σ_n=30)	JPEG Comp.(%) (10%) (30%) (50%) (70%)	Med. (3 × 3) Med. (5 × 5)	Gauss (3 × 3) Gauss (5 × 5)	Scaling 2 1.5 0.9 0.75	*(watermark dur.256 bits) AW GN (σ_n=20)*	*(watermark dur. 512 bits) AW GN (σ_n=20)*	*(watermark dur. 1024 bits) AWGN (σ_n=20)*	*(watermark dur. 2048 bits) AWGN (σ_n=20)*
Amirmazlaghani et al.[31]	*Baboon (512×512)*	0.01 0.53 2.36	0 0 0 0	0 8.36	0 0	0 0 0 0	0.14	2.71	0.79	0.9
(Proposed)		**0** **0** **0**	0 0 0 0	0 8.59	0 0	0 0 0 0	**0**	**0**	**0.292**	0.9277
Amirmazlaghani et al.[31]	*Barbara (512×512)*	0.07 0.48 2.03	0 0 0 0	1.21, 5.90	0 0.78	0 0 0.16 0	0.09	1.5	0.97	1.59
(Proposed)		**0** **0,** **0**	0 0 0 0	**0** **1.56**	0 **0**	0 0 **0** 0	**0**	**0**	1.17	**1.26**

Table 4.11 Comparison for' BER (%)' of recuperated watermarks amongst suggested technique as well as Nezhadarya et al. [124] with watermark duration of 256 bits.

		Gauss (3 × 3)	Gauss (5 × 5)	Median (3 × 3)	Median (5 × 5)	JPEG Comp.(%)				
						20	30	40	50	60
Nezhadarya et al. [124] GDWM0	Peppers	0	0.58	1.15	4.92	1.32	0.21	0	0	0
Nezhadarya et al. [124] GDWM1		0	0.58	1.17	6.64	1.41	0.18	0.04	0	0
(Proposed)		0	**0**	**0.3906**	**3.90**	**0.7812**	**0**	**0**	0	0
Nezhadarya et al. [124] GDWM0	Baboon	0	0.92	5.30	21.61	1.53	0.50	0.18	0.07	0
Nezhadarya et al. [124] GDWM1		0	0.96	5.03	19.75	1.41	0.62	0.19	0.07	0
(Proposed)		0	**0**	**1.95**	**13.67**	**0**	**0**	**0**	**0**	0
Nezhadarya et al. [124] GDWM0	Barbara	0	0.13	1.01	6.49	1.56	0.16	0.07	0.01	0
Nezhadarya et al. [124] GDWM1		0	0.13	1.10	8.14	1.69	0.16	0.05	0	0
(Proposed)		0	**0**	**0**	**4.65**	**0**	**0**	**0**	**0**	0
Nezhadarya et al.[124] GDWM0	Lena	0	0	0	5.09	1.90	0.41	0.19	0.05	0
Nezhadarya et al.[124] GDWM1		0	0.17	0	7.10	1.65	0.41	0.22	0.1	0
(Proposed)		0	**0**	**0**	**1.562**	**0**	**0**	**0**	**0**	0

Table 4.12 Comparison for 'BER (%)' and 'SSIM' for recuperated watermark for Gauss Fil., JPEG Comp. as well as AWGN assaults amidst suggested as well as Nezhadarya et al. [124] with watermark duration of 256 bits.

		'Gauss (7 × 7)' SSIM ('BER%')	'JPEG (QF=10%)' SSIM ('BER%')	'AWGN(σ_n=10)' SSIM ('BER%')
Nezhadarya et al. [124] SSGDWM	Peppers	0.98530 (0.02)	0.9918 (0.13)	0.9918 (0.02)
Nezhadarya et al. [124] MSDWM		0.99460 (0.02)	0.9950 (0.13)	0.9955 (0.02)
Proposed		**0.9718 (0)**	**0.7800** (4.68)	**0.9697 (0)**
Nezhadarya et al. [124] SSGDWM	Baboon	0.9974(0.22)	0.9991(0.13)	0.9993(0.02)
Nezhadarya et al. [124] MSDWM		0.9987(0.22)	0.9991(0.13)	0.9991(0.02)
Proposed		**0.9622(0)**	**0.6732**(0.39)	**0.9885(0)**
Nezhadarya et al. [124]SSGDWM	Lena	0.9935(0.02)	0.9944(0.13)	0.9944(0.02)
Nezhadarya et al. [124] MSDWM		0.9962(0.02)	0.9962(0.13)	0.9966(0.02)
Proposed		**0.9827(0)**	**0.8280**(6.25)	**0.9634(%)**

4.5.3 Comparison with additional techniques utilizing duplet watermarks

The suggested approach helped in the simultaneous embedding of twin watermarks into approximately and vertically recurrence parameters of original images utilizing DWT. An amalgamation of various sizes, ('TIET' with 'Logo'), ('Copyright' with 'Logo') as well as ('Thapar_Univ' with 'Logo') were utilized in watermarking. A common comparison of the suggested scheme is displayed in Figure 4.11 against [137] as well as [49].

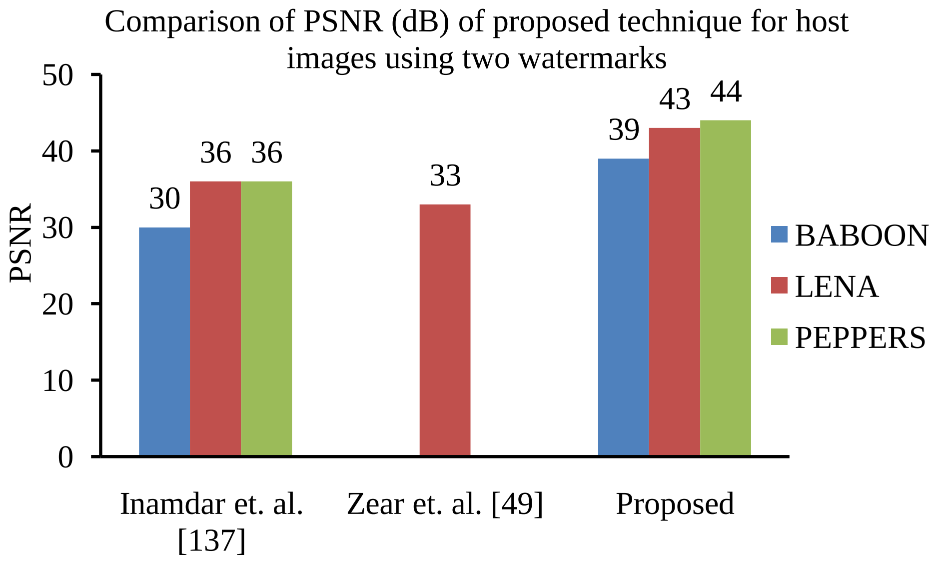

Figure 4.11 Comparison of PSNR (in dB) for suggested technique against Inamdar et al.[137] and Zear et al. [49] utilizing two watermarks.

The experimental results given in Tables 4.1 to 4.12 and Figure 4.11 have manifested excellence for impartial achievement parameters. This has helped to indicate the following important considerations;

a) Though variable dimension watermark amalgamations were utilized, still, the volume for inserting the watermark bits utilized was high.

b) The toughness for the suggested method was much better than the recent techniques.

c) The security for the watermark increased by utilizing duplet undetectable watermarks at the same time. It helped to achieve the double-edged purposes for twin watermarking, that is, avoiding image pilferage along with a rise in integrity on account of double layers of the watermark.

d) Built upon the analytical estimation of parameters, ML Decoder was utilized for watermark recovery, which too enhanced the results accuracy.

Table 4.13 ‘PSNR’, ‘NCC’, ‘SSIM’ as well as ‘GMSD’ variables for medicinal images with dimension (512 × 512).

→ Standard Quality Values ↓ Host image with watermarks	‘PSNR’ (in dB)	‘NCC’	‘SSIM’	‘BER(%)’ for recuperated watermark1	‘BER(%)’ for recuperated watermark2	GMSD
‘Liver’						
(‘TIET’ with ‘ Joint’)	40.20	0.9991	0.9965	1.11	24.21	0.01419
(‘Copyright’ with ‘ Joint’)	49.97	0.9980	0.9996	0.2	47	0.00126
(‘Thapar_Univ’ with ‘Joint’)	52.57	0.9979	0.9998	1.25	56.34	0.000949
‘MRI’						
(‘TIET’ with ‘ Joint’)	50.87	0.9988	0.9985	0.44	26.95	0.00111
(‘Copyright’ with ‘ Joint’)	48.68	0.9956	0.9988	0.4	54.1	0.00441
(‘Thapar_Univ’ with ‘Joint’)	50.15	0.9954	0.9990	0.25	56.83	0.00299
‘X-Ray’						
(‘TIET’ with ‘ Joint’)	46.08	0.9976	0.9965	0	26.95	0.00906
(‘Copyright’ with ‘ Joint’)	43.44	0.9956	0.9940	0	51.95	0.0153
(‘Thapar_Univ’ with ‘Joint’)	41.82	0.9939	0.9910	0	52.53	0.0186
‘Liver’ (‘Patient watermark’ with ‘Joint’)	40.10	0.9997	0.9961	0.66	20.01	0.00103
‘X-Ray’ (‘Patient watermark’ with ‘ Joint’)	42.81	0.9980	0.9910	0	26.95	0.0238
‘MRI’ (‘Patient watermark’ with ‘Joint’)	49.59	0.9990	0.9982	0.22	25.29	0.000239

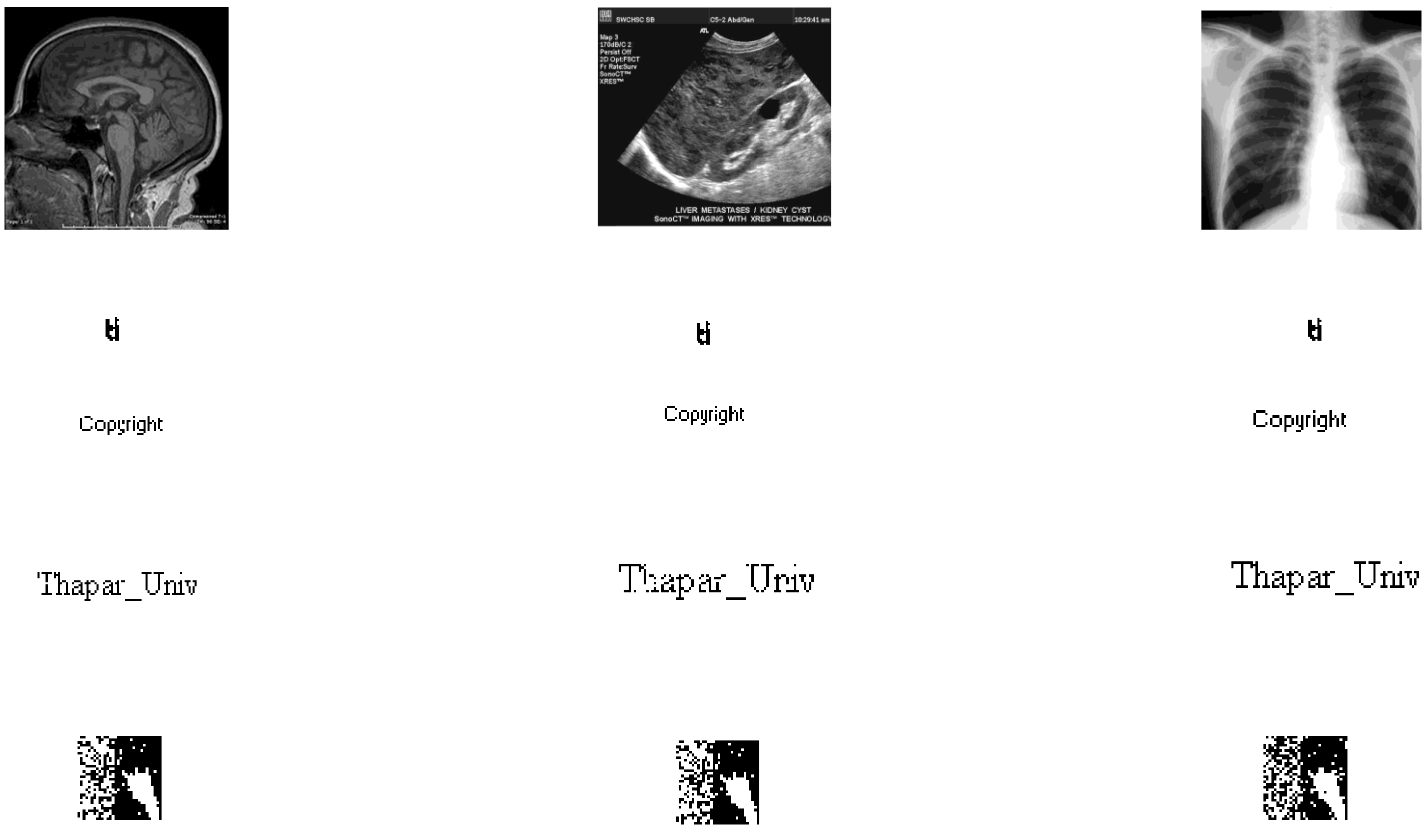

Figure 4.12 Medicinal images with recuperated watermarks.

Table 4.14 'PSNR', 'NCC', 'SSIM' as well as 'GMSD' values for watermarked medicinal images for various assaults.

Assault	PSNR	NCC	SSIM	GMSD	Watermark Combination	Host image
JPEG (QF= 20%)	27.10	1	0.9060	0.0349	('TIET' with 'Joint')	'Liver'
Med.Fil (5 × 5)	18.26	1	0.7284	0.1472		
Gauss Fil. (3 × 3)	30.82	1	0.9836	0.0498		
JPEG (QF= 20%)	27.24	1	0.9068	0.0348	('Copyright' with 'Joint')	'Liver'
Med. Fil. (5 × 5)	18.26	0.9986	0.7297	0.1469		
Wiener Fil. (3 × 3)	3137	1	0.9123	0.0277		
Gauss Fil. (3 × 3)	30.89	1	0.9844	0.0498	('Thapar_Univ' with 'Joint')	'Liver'
Wiener Fil. (3 × 3)	31.39	1	0.9125	0.0277		
Gauss Fil. (5 × 5)	45.82	1	0.9965	0.002749	('TIET' with 'Joint')	'MRI'
Median Fil. (7 × 7)	29.67	1	0.8763	0.08848		
Scaling (0.75)	44.53	0.9963	0.9950	0.004469	('Copyright' with 'Joint')	'MRI'
Wiener Fil. (5 × 5)	36.39	1	0.9413	0.03882		
Gauss Fil. (5 × 5)	45.21	0.9980	0.9964	0.00382	('Thapar_Univ' with 'Joint')	'MRI'
Wiener Fil. (5 × 5)	36.46	1	0.9414	0.0389		
Median Fil. (3 × 3)	44.59	0.9981	0.9900	0.00966	('TIET' with 'Joint')	'X-Ray'
Sharp	10.66	0.6640	0.6905	0.1901		
AWGN (σ_n=10)	39.41	0.9900	0.9585	0.01187		
Scaling (2)	45.99	0.9978	0.9954	0.0103		
Median Fil. (3 × 3)	42.61	0.9958	0.9884	0.0132	('Copyright' with 'Joint')	'X-Ray'
AWGN (σ_n=10)	38.32	0.9877	0.9568	0.0161		
Sharp	10.59	0.6623	0.895	0.1928	('Thapar_Univ' with 'Joint')	'X-Ray'
Scaling (2)	41.76	0.9937	0.9908	0.0173		

Table 4.15 Medicinal images with recuperated watermarks for different assaults of Gauss Filter (3 × 3), Median Filter (5 × 5), JPEG (QF=20%), and AWGN (σ_n=10).

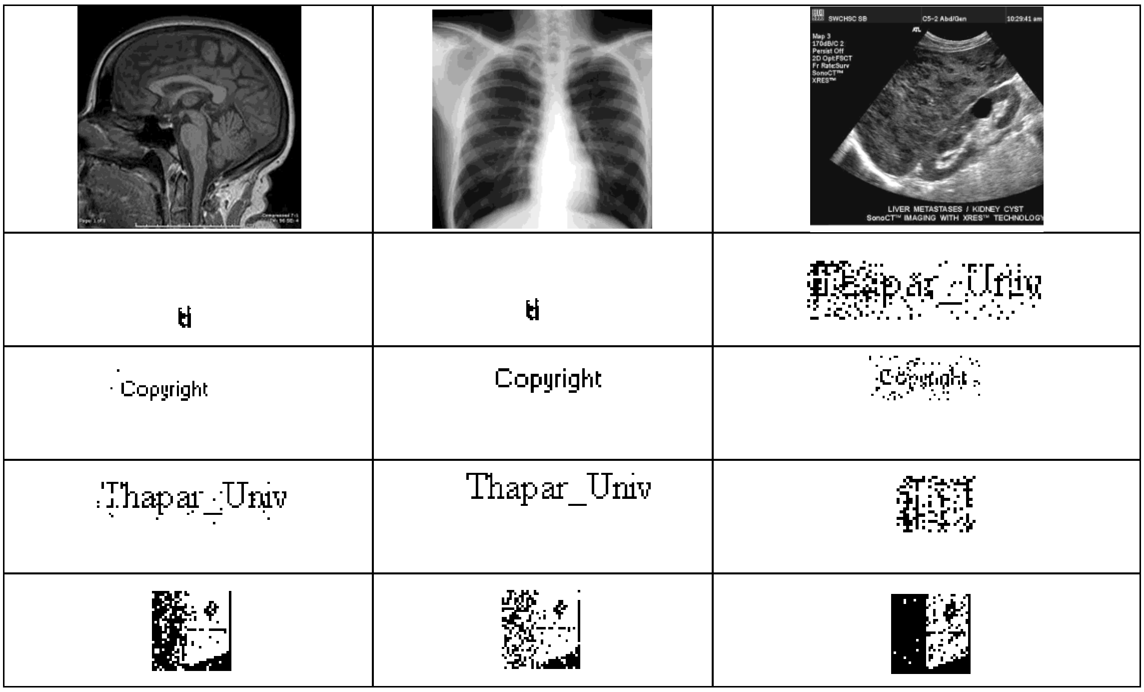

Table 4.16 Collation of 'PSNR (in dB)' for the suggested method with multifold watermarking techniques.

	Parah et al.[19]	Singh et al.[20]	Zear et al.[49]	Proposed technique
Number of watermarks utilized	02	02	03	02
'PSNR(in dB)'	48.285	31.230	34.340	**55.570**
'NCC'	48.285	-	0.9888	**0.9994**

Thus, the suggested technique found suitable applications in medicine water marking.

4.6 APPLICATION FOR TELEMEDICINE

Medicinal images are more complicated than natural images. The sensitive examination details conserved within medical images must be ascertained with accuracy. Also, the safety of such information was also a significant step.

The suggested technique proved effective in inserting the particulars of the patient (as watermark1) as well as the intimate details, like, photo of the medical practitioner or the sick person (as watermark2) into the prognosis (as original image). The idea for duplet watermarking seemed purposeful in conserving the uncommon features of security and robustness of medical images. This approach has helped to maintain the secrecy for details of the patient as well as the reduction in the instances of medicinal crime.

The metrics for execution like, ‘PSNR’, ‘SSIM’, ‘NCC’ or ‘GMSD’ for the images after watermarking are presented in Table 4.13. It was noticed that different watermark amalgamations presented preferable merits for graded coefficients. The potentiality of the suggested scheme for medicinal watermarking was too inspected under different assaults in Table 4.14. The assaulted merits for ‘NCC’ as well as‘SSIM’ approximated to one. Superior merits for ‘PSNR’ confirmed the invisibility with minimal merits of ‘GMSD’ for JPEG Comp., AWGN, Scale, Sharp as well as Filter assaults. Table 4.15 displayed the assaulted images with recuperated watermarks.A collation for ‘PSNR(dB)’ as well as ‘NCC’ merits for the suggested medicinal technique of watermarking is also presented in Table 4.16. While, Parah et al. [19] utilized (32 × 32) and (47 × 47) dimension watermarks accompanying the data of 1024 characters of EPR, Singh et al. [20] utilized characters of size 104 and 60 for content watermark within various sub-bands of DWT. Zear et al. [49] too utilized a watermark with dimension (256 × 256) and content of size 190 characters detailing the signature of the doctor as well as other indications. It was noticed that the suggested technique gave provided excellent invisibility with strong as well as safe watermarks.

4.7 SUMMARY

The presented chapter proposed a strong image-adaptive technique for watermarking utilizing duplet watermarks. DWT was utilized for watermark insertion into approximated and vertically recurrence parameters for (8 × 8) slabs with large entropy of the original image. Using kurtosis, ASF was calculated in the range 0.0040 to 0.07, which was utilized in insertion of watermarks. The modeling of Gaussian distribution was utilized for embedding three watermark combinations into the sub bands of the transformed image. Besides, an analytical approach established upon ML Decoder was utilized in successful watermark extraction. The effectiveness of the suggested technique was proved through the detailed examination built upon durability and perceptivity. The use of the fourth statistical moment in the calculation of ASHF for inserting two watermarks also confirmed the desirable values of PSNR (45-54 dB), and minimum BER(%) as well as GMSD values. The merits of NCC, SSIM and UIQI too approached unity under various attacks. The results demonstrated that the suggested technique was greatly safe and dependable. The algorithm found acceptable applications in medicinal watermarking by accomplishing a significant equilibrium amidst the advisable crucial features of invisibility, toughness as well as volume.

The next chapter focuses upon another proposed watermarking technique using two Transforms and a hybrid combination of strength factors for embedding various watermarks. The technique was also proposed for medicine applications as it proved highly robust against common and geometric attacks.

CHAPTER 5

USE OF HYBRID STRENGTH FACTORS FOR ROBUST IMAGE-ADAPTIVE WATERMARKING

This chapter presents the latest image-adaptive watermarking technique using two transforms, namely DWT and FWHT. This combination was used to augment the imperceptibility and robustness for purpose of proprietary rights protection. The watermark was added into the standard image using a modifiable Hybrid Strength Factor (HSF), which was computed using mean, standard deviation, entropy, and kurtosis of the transformed coefficients of high entropy blocks. Four HSF's were used for embedding the watermarks with the help of limited side information consisting of locations of high entropy blocks and parameters of Gaussian distribution. Similar to the previous techniques, watermarks were extracted using the statistical approach of the ML decoder using the partially blind approach. The efficacy of the technique was proved by better results using the performance metrics of PSNR, SSIM, NCC, GMSD, and UIQI.

5.1 INTRODUCTION

In the field of image watermarking, many techniques had been used for copyright protection. Though robust watermarking could be attained by either spatial or transform domain techniques [138], the latter offered better resistance against attacks [139]. Hence, many researchers used various combinations of transforms [140] to increase the robustness [141]. Still, the approaches failed to optimize the trade-off between desirable robustness [142] and imperceptibility [143]. Hence, the proposed hybrid image-adaptive watermarking technique helped to embed the watermark using a modifiable HSF with the help of two transforms.

The proposed technique drew the benefits of two transforms simultaneously to modify the performance of the watermarked image [144]. Here, DWT provided excellent localization property in the spatial-frequency domain [145] by dividing the image along two dimensions to obtain four frequency sub bands, namely Low-Low, Low-High, High-Low, and High-High [146]. The transform also helped to identify the possible areas of embedding watermark effectively [147] within the host image without being perceptible to the human vision[148]. Generally, it was termed that most of the energy [149] of the image lay in the Low-Low sub band (LL) which helped to provide good robustness against various attacks [150] (shown in Figure 5.1). Hence, the proposed hybrid technique used low frequency coefficients for embedding the watermark. Similar to the advantages of the above transform, FWHT used a simple framework of +1 and -1 basis vectors which too helped to concentrate the main features of the image in a small area. This also helped in hiding the watermark bits imperceptibly with high robustness. The benefit of processing the image bits using a fast calculation approach helped the technique to combine the advantages of both DWT and FWHT to escalate the imperceptibility and robustness of the below watermarking using four hybrid strength factors and obtaining better parameters

5.2 PROPOSED HYBRID APPROACH OF WATERMARKING

In this section, the suggested hybrid image-adaptive technique of watermarking was explained in two different sub sections, the namely hybrid process of watermark embedding and watermark extraction respectively. Section 5.2.1 described the procedure of inserting the watermark within the original image. It resulted in the watermarked image which was subjected to various attacks before it reached the receiver. The attacked watermarked image was received by the statistical decoder for successful elicitation of the watermark in Section 5.2.2.

5.2.1 Hybrid Process of Watermark Embedding

The proposed technique of inserting the watermark (shown in Figure 5.2 (a)) is elucidated in the points below

1: Host Image (HI) was segmented towards blocks of size 8 × 8.

2: High entropy blocks were selected: Entropy (H) defined as the average information present per output source, is expressed mathematically as

$$H = -\sum_{j=1}^{J} P(b_j).\, logP(b_j) \qquad (5.1)$$

where, b_j exhibits a discrete group of random probable events whose possibility of occurrences are inclined as $P(b_j)$. Here, entropy for all blocks was computed to determine the average value. Since the value of high entropy indicated the certainty of the invisible information present, hence only those entropy blocks were selected whose value was higher than the average value. The order of these blocks was preserved in a cell array by scanning one row at a time. This became the first side information of the proposed semi-blind approach as given in Step 8.

Original Image and Watermark (s) used	Sub-band used	Watermarked Image	Recovered watermark(s)	PSNR of watermarked image (dB)
  ‘TIET’  ‘Cameraman’	LL			45.01-45.07
	LH			14.10-11.23
	HL			14.11-11.24
	HH		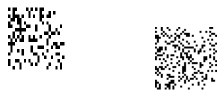	14-11.22

Figure 5.1 Illustration of Multi resolution of DWT on original image ‘Lena’ into LL, LH, HL, and HH sub bands.

3: DWT was applied on blocks with high entropy: Due to the very good spatial-frequency localization characteristic of DWT, the watermark was inserted invisibly in different realms of the host image. Hence, single level DWT was practiced on chosen blocks with large entropy to decompose into four frequency sub bands. These were expressed like, $(HI)^{LL}$, $(HI)^{LH}$, $(HI)^{HL}$, and $(HI)^{HH}$. The less frequency (or $(HI)^{LL}$) coefficients are the most crucial carriers of information and thus were used to embed the watermark bits imperceptibly as verified from Figure 5.1.

4: FWHT was applied on LL sub band coefficients: FWHT transformed the low frequency coefficients $(HI)^{LL}$ obtained through DWT as they were less sensitive to noise. These modified coefficients, assumed as W, concentrated the features of an image into a very small area. This allowed perfectly invisibly hiding the watermark bits in an invisible manner. It also increased the toughness of the suggested technique when such an image was subjected to various attacks.

5: FWHT coefficients (W) were modeled using Normal (or Gaussian) distribution: It was assumed by Mihcak et al. [121] that the less frequency coefficients can be shaped by Gaussian disintegration. Also, the PDF of a normal distribution expressed in (5.2) uses mean (μ) and standard deviation (σ) as its Gaussian parameters in image watermarking.

$$f(z|\mu\,,\sigma^2) = \frac{1}{\sqrt{2\pi\sigma^2}} e^{\frac{-(z-\mu)^2}{2\sigma^2}} \tag{5.2}$$

Thus, FWHT coefficients (W) were also modeled using Gaussian distribution as $W \sim N(\mu, \sigma^2)$. This analytical way helped to determine the values of μ and σ accurately, though they can be calculated from (5.3) also.

$$\bar{X}(or\mu) = (\sum_{i=1}^{N} x_i)/N \quad , \quad \sigma = \sqrt{\frac{\sum_{i=1}^{N}(x_i - \bar{X})}{N}} \tag{5.3}$$

Here for a set of observations (x), the total number of observations is given by N. The square of standard deviation (σ) is known as variance (σ^2). These statistical parameters formed the second important side information along with Step 2. The side information is prepared in Step 8.

6: HSF was calculated using transformed LL coefficients: The value of the hybrid strength factor was calculated using the image-adaptive characteristics of the host image. HSF was determined from the mean, std. deviation, entropy as well as kurtosis of W parameters obtained through the blocks with high entropy of the original image. In the prospective technique, four HSF's were calculated. They are expressed as,

$$HSF_1 = \sigma_i/(\mu_{max})^\rho, HSF_2 = \mu_i/(\sigma_{max})^\rho$$

$$HSF_3 = H_i/(\sigma_{max})^\rho, HSF_4 = Kurtosis_i/(H_{max})^\rho \tag{5.4}$$

Here, σ_i , μ_i , H_i and $Kurtosis_i$ were the std. deviation, mean, entropy, and kurtosis of FWHT coefficients (W) for each i^{th} slab. μ_{max} ,σ_{max} and H_{max} were the maximum mean, std. Deviation, as well as entropy of entire FWHT coefficients (H), slabs selected. ρ was the changeable criterion in the denominator used in the embedding of watermark bits. These were called Hybrid Formulae H1, H2, H3, and H4, given in (5.4).

7: Watermark bits were embedded into W coefficients: The Algorithm for Embedding the watermark was given by the subsequent rules,

Rule1: Calculated HSF defined by (5.4). The calculated number of blocks, B= (size of host image M×M)/(size of blocks)
Rule2: The following Embedding Algorithm was used.

Input-W, HSF, B, wm

1.	for i_d=1:B
2.	while i_d<= length (wm)
3.	If wm(1,id)==1
4.	W=W(1+HSF)
5.	else if wm(1,id)==0
6.	W=W(1-HSF)
7.	end (if)
8.	end (while)
9.	end (for)

Output- Hybrid Watermarked image(WI), μ, σ^2

Here, W was modified FWHT coefficients, wm represented watermark bits and HSF denoted hybrid strength factor.

Thus, the FWHT coefficients (W) were modified by bits '1'and'0' according to the following embedding rules

$$W = W.(1 + HSF), W = W.(1 - HSF) \tag{5.5}$$

8: Side Information was prepared: Since the proposed technique is partially blind, finite side information was also transported with the watermarked image to the destination. Thus, the supporting information was prepared from Steps 2 and 5 consisting of positions of blocks with high entropy and means, variances of W coefficients.

9: Inverse FWHT and Inverse DWT were applied: Once the watermark bits were embedded, IFWHT and IDWT were enforced on the transformed slabs to get $(WI\_HI)^{LL}$, $(WI\_HI)^{LH}$, $(WI\_HI)^{HL}$, and $(WI\_HI)^{HH}$. The selected numeral of blocks with high entropy was always equivalent to the numeral of bits of the watermark to be embedded. All the transformed blocks were later re-coupled along the resting blocks to obtain the image after watermarking in (5.6).

$$WI = \{\iint_{m=0}^{M-1} WI\_HI^{LL}, WI\_HI^{LH}, WI\_HI^{HL}, WI\_HI^{HH} \} \tag{5.6}$$

10: Final watermarked image was transmitted: The final watermarked image was communicated to the receiver along with the sidewise information arranged in Step 8.

5.2.2 Hybrid Process of Extraction of Watermark

The proposed technique of watermark extraction (shown in Figure 5. 2(b)) is depicted in the steps below,

1: Watermarked image (WI') was segmented with M rows and M columns ($M \times M$) in blocks of dimension (8×8).

2: Blocks with large entropy were selected: The supporting information communicated with the image after watermarking contained positions of blocks with large entropy of the host image. This information helped in resolving the blocks of high entropy in the accepted watermarked image also.

3: DWT was applied upon blocks with high entropy in the watermarked image: Similar to the process of embedding, a single level DWT was again enforced upon the blocks of large entropy of the received watermarked image to disintegrate into four sub bands. These were expressed as, $(WI')^{LL}$, $(WI')^{LH}$, $(WI')^{HL}$, and $(WI')^{HH}$. The low frequency coefficients were used as quoted in Step 3 of Section 5.2.1.

4: FWHT was applied on LL sub band coefficients: Again, FWHT was applied in the lowest frequency coefficients of the watermarked image $(WI')^{LL}$, which were obtained from DWT. The watermark bits were concentrated into a small area of the transformed coefficients W' in an imperceptible manner.

5: FWHT coefficients (W') were modeled using Normal (or Gaussian) distribution parameters: Similar to Step 5 of Section 5.2.1, mean and variance were again obtained from FWHT coefficients (W') of the received watermarked image using the assumption of Gaussian distribution as $W' \sim N(\mu', \sigma^{2'})$. These were assumed as (μ') and ($\sigma^{2}{}'$) respectively.

6: Statistical Modeling of ML decoder for extraction of watermark: The parameters of Gaussian distribution transmitted in the side information (μ and σ^2) were compared with the Normal distribution parameters of the received watermarked image (μ' and $\sigma^{2'}$). Similar to the use of ML decoder in [135] and [151], watermark bits '1' and '0' were embedded in W frequency coefficients using multiplicative embedding as,

$$W_{i/0} = W_i.(1 - HSF) \sim N(\mu_{\frac{i}{0}}, \sigma_{\frac{i}{0}}) , \; W_{i/1} = W_i.(1 + HSF) \sim N(\mu_{i/1}, \sigma_{i/1}) \tag{5.7}$$

Thus, the W parameters for every slab having N coefficients w_1, w_2, w_3,…..w_N, assumed as identical and independent distributed (i .i .d.) in embedding bits '0' and '1' were given as,

$$P(W_1, W_2, W_3, \ldots W_N|0) = \prod_{i=1}^{N} \sqrt{2\pi\sigma_{W|0}^2} \frac{1}{e^{-(W)_i - (1-HSF)\mu)^2} / 2\sigma_{(W)|0}^2}$$

$$P(W_1, W_2, W_3, \ldots W_N|1) = \prod_{i=1}^{N} \sqrt{2\pi\sigma_{W|1}^2} \frac{1}{e^{-(W)_i - (1+HSF)\mu)^2} / 2\sigma_{(W)|1}^2} \tag{5.8}$$

Thus, the maximum likelihood decision for W coefficients is given as,

$$P(W_1,\, W_2,\, W_3, \ldots WN|1) \underset{<0}{\overset{>1}{}} P(W_1,\, W_2,\, W_3, \ldots WN|0) \tag{5.9}$$

Substituting (5.8) in (5.9), it is observed

$$\prod_{i=1}^{N} \sqrt{2\pi\sigma_{W|1}^2} \frac{1}{\frac{e^{-(W)_i - (1+HSF)\mu)^2}}{2\sigma_{w|1}^2}} \underset{<0}{\overset{>1}{}} \prod_{i=1}^{N} \sqrt{2\pi\sigma_{W|0}^2} \frac{1}{\frac{e^{-(W)_i - (1-HSF)\mu)^2}}{2\sigma_{w|0}^2}} \tag{5.10}$$

Applying Logs,

$$\frac{(-N)}{2} \ln\left(\sigma_{w|1}^2\right) \frac{1}{\sigma_{w|1}^2} \sum_{i=1}^{N} (w)_i - (1 + HSF)\mu)^2 \underset{<0}{\overset{>1}{}} \frac{(-N)}{2} \ln\left(\sigma_{w|0}^2\right) \frac{1}{\sigma_{w|0}^2} \sum_{i=1}^{N} (w)_i - (1 - HSF\mu)2 \tag{5.11}$$

Simplifying the above equation,

$$\left(\frac{1}{\sigma_{w|0}^2} - \frac{1}{\sigma_{w|1}^2}\right) \sum_{i=1}^{N} (w)_i^2 - 2\mu \left\{\frac{(1-HSF)}{\sigma_{w|0}^2} - \frac{(1+HSF)}{\sigma_{w|1}^2}\right\} \sum_{i=1}^{N} (w)_i \underset{<0}{\overset{>1}{}} N \ln\left(\frac{\sigma_{w|1}^2}{\sigma_{w|0}^2}\right) - N\mu^2 \left\{\frac{(1-HSF)^2}{\sigma_{w|0}^2} - \frac{(1+HSF)^2}{\sigma_{w|1}^2}\right\} \tag{5.12}$$

When the merit of noisy variance approximated zero for a restrained instance of large SNR, then

$$\sigma_{w|1}^2 = (1 + HSF)^2\sigma^2 \quad , \; \sigma_{w|0}^2 = (1 - HSF)^2\sigma^2 \tag{5.13}$$

Thus (5.12) was rewritten for bits 'zero' and 'one' respectively as,

$$\frac{1}{\sigma^2(1-HSF)^2}\sum_{i=1}^{N} w_i^2 - \frac{2\mu}{(1-HSF)\sigma^2}\sum_{i=1}^{N} w_i < (-2N)\{\ln\sigma + \ln(1-HSF)\} - N\frac{\mu^2}{\sigma^2} \tag{5.14}$$

$$\frac{(-1)}{\sigma^2(1+HSF)^2}\sum_{i=1}^{N} w_i^2 + \frac{2\mu}{(1+HSF)\sigma^2}\sum_{i=1}^{N} w_i > (2N)\{\ln\sigma + \ln(1+HSF)\} + N\frac{\mu^2}{\sigma^2} \tag{5.15}$$

Again, the ML decoder became independent of the HSF as the latter approached zero at high SNR for the successful watermark. The Algorithm for the Extraction of the watermark is given below.

The following Watermark Extraction Algorithm was used.

Input-W', length(wm), B, μ, σ^2

1.	for i_{dx}=1:B
2.	while i_{dx}<= length (wm)
3.	If $\mu > \mu'$ *then*
4.	recovered_watermark RW(1, i_{dx})==1
5.	else recovered_watermark RW(1, i_{dx})==0
6.	i_{dx}= i_{dx}+1
	Recovered_watermark={(wm)*length(wm)}
7.	end (if)
8.	end (if)
9.	end (for)

Out put- Recovered watermark

Here, W' represented the modified FWHT coefficients for watermarked image (WI), length (w_m) represented the duration of watermark bits, (μ, σ^2) were the Gaussian distribution parameters (mean and variance) of host image (HI).

7: Recovered Watermark was generated.

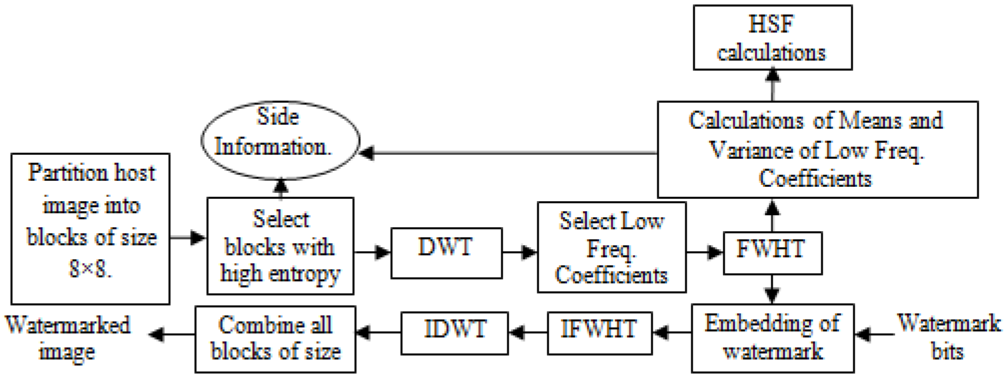

(a)

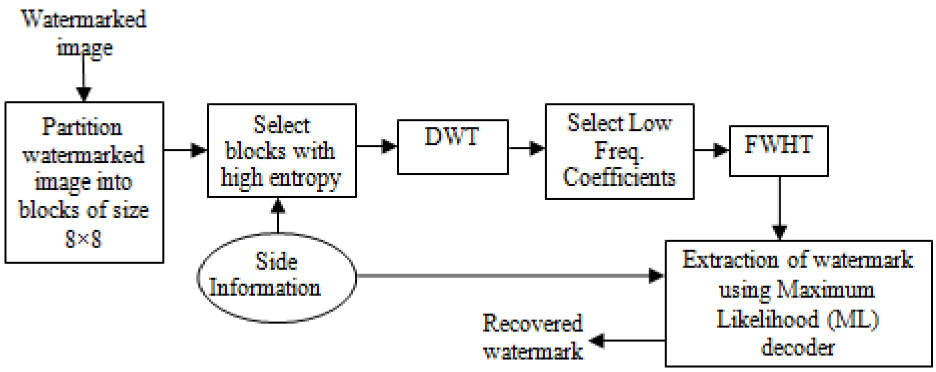

(b)

Figure 5.2 The Embedding and Decoding process of the proposed watermarking scheme.

(a)

(b)

(c)

(d)

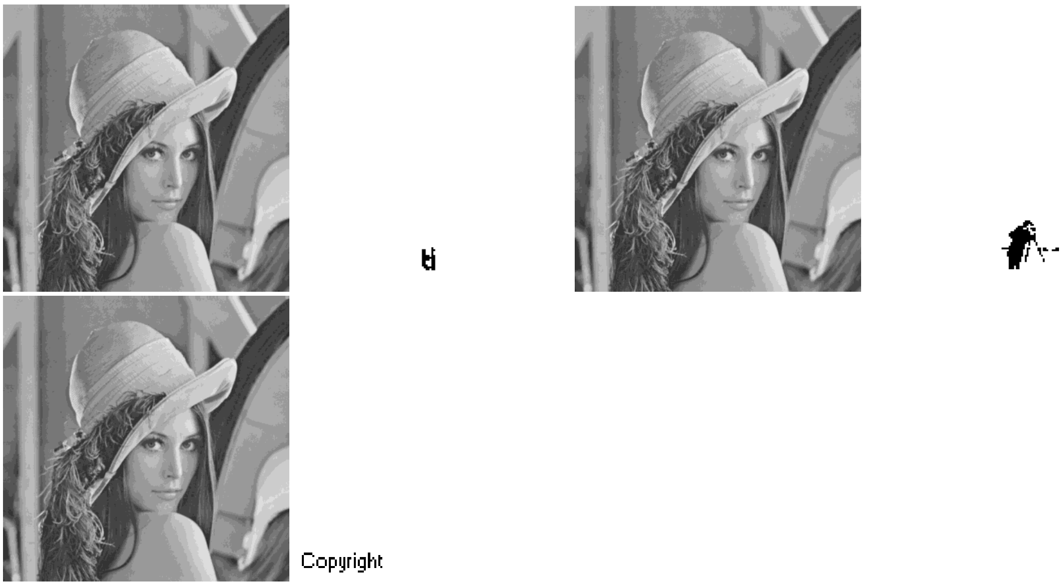

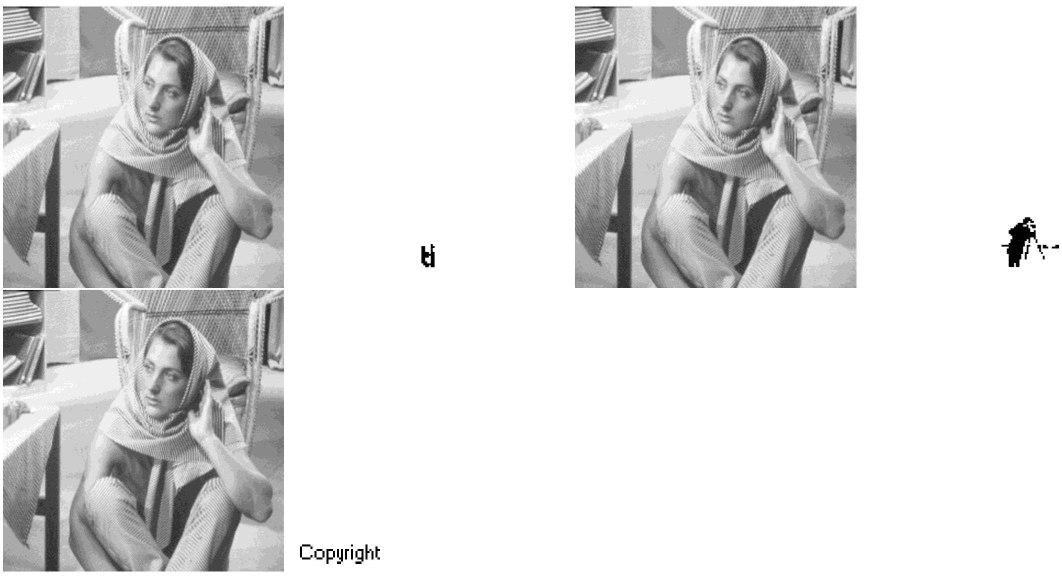

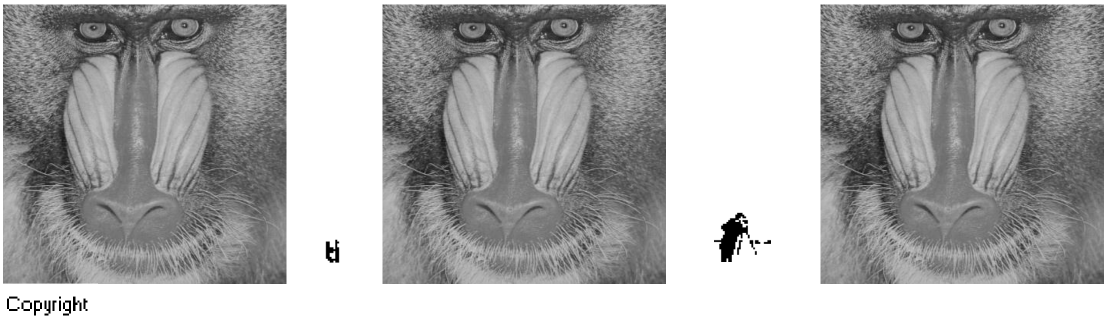

(e)

Figure 5.3 (a) Standard Images (b) Original watermarks (c) watermarked Images (d) Recovered watermarks (e) Attacked Images and retrieved watermarks under Gauss(3x3), Scaling (1.1), AWGN (σ^2=25) and JPEG (QF=40%) attacks.

5.3 SIGNIFICANCE OF HYBRID STRENGTH FACTOR (HSF 1 TO HSF 4)

The proposed hybrid technique successfully achieved invisible watermarking when HSF was highly adaptive with the changing coefficient values (W) of the transformed host image. The adjusting parameter (ρ) in the power of H1, H2, H3, and H4 was a very useful factor in HSF for achieving high values of PSNR.

In this chapter, three standard host images, 'Lena', 'Barbara' and 'Baboon' were used along with variable dimension watermarks 'TIET' (25 × 18), 'Copyright'(20 × 50), and 'Cameraman'(32 × 32) as shown in Figure 5.3. The size of all host images was (512 × 512). Figures 5.4, 5.5, and 5.6 demonstrated the variation of PSNR and BER with ρ for natural images 'Lena', 'Barbara' as well as 'Baboon' utilizing all watermarks. It was observed that as ρ increased, BER increased exponentially much later, with initially a linear increase in PSNR. Using (5.4), the values of ρ for host image 'Lena' using watermarks 'TIET', 'Copyright' and 'Cameraman' were (1.816, 1.515, 0.91, 3.23), (1.8752, 1.567, 0.9734, 3.474) and (1.879,1.596, 0.977, 3.484) respectively. Similarly, for host image 'Barbara' the values of ρ were (1.82, 1.52, 0.93, 3.27), (1.9025, 1.594, 0.9987, 3.567) and (1.907, 1.596, 1.001, 3.575) respectively. For image 'Baboon', the values of ρ were (1.7942, 1.503, 0.94, 3.03), (1.8775, 1.572, 1.013, 3.3335) and (1.3822, 1.576, 1.0159, 3.3466). It was observed from Figures 5.4, 5.5, and 5.6 that stable values of high PSNR for the water marked images with minimum BER of recuperated watermark were best obtained using H4.

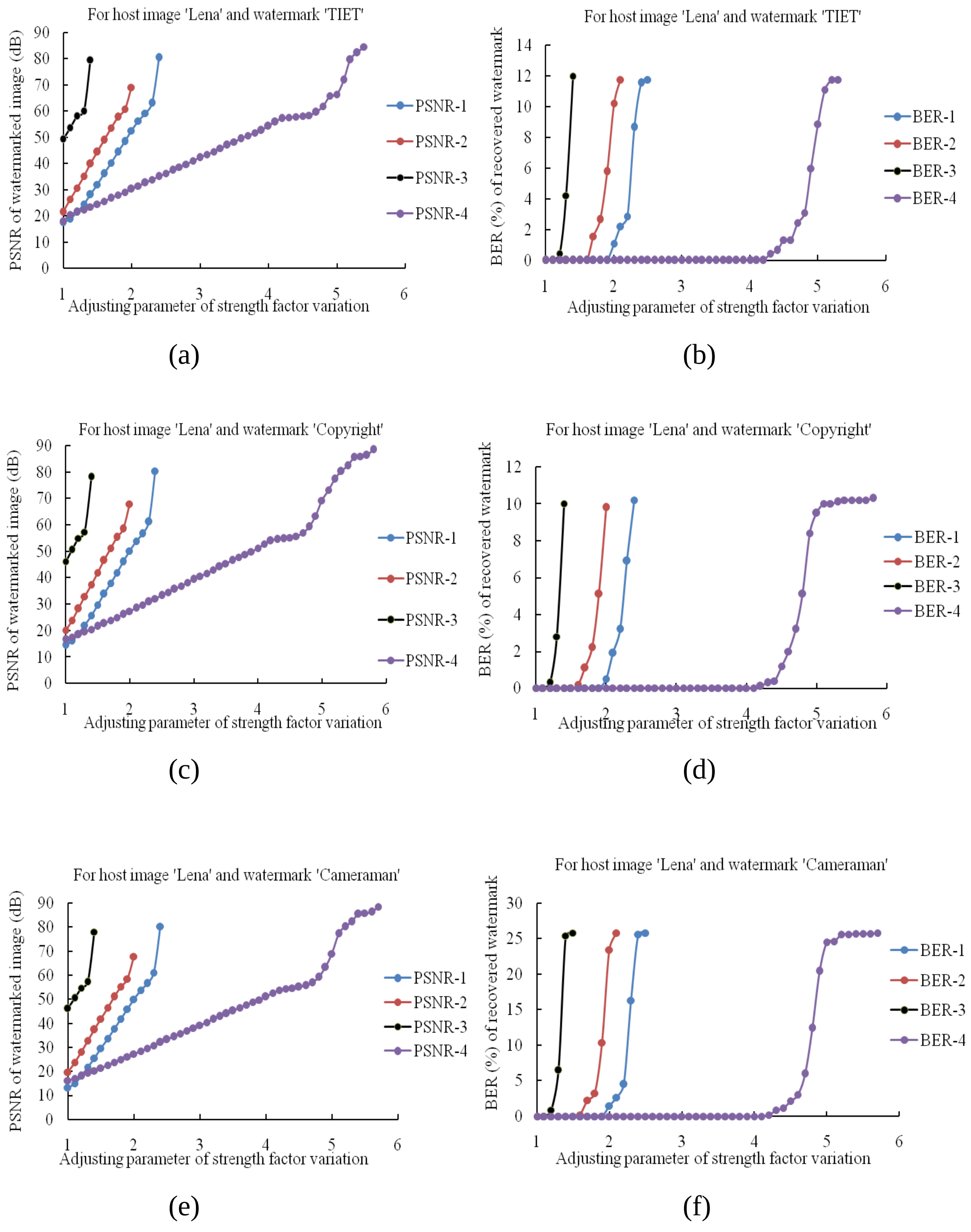

Figure 5.4 Visual representations for 'PSNR (in dB)' of images and 'BER (%)' for extracted watermarks for host image 'Lena'.

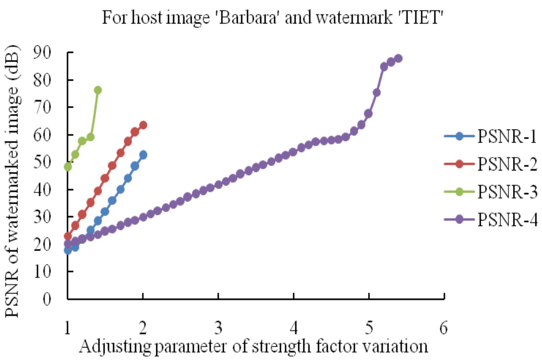

(a)

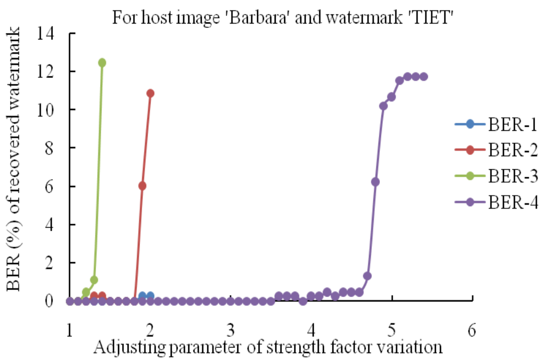

(b)

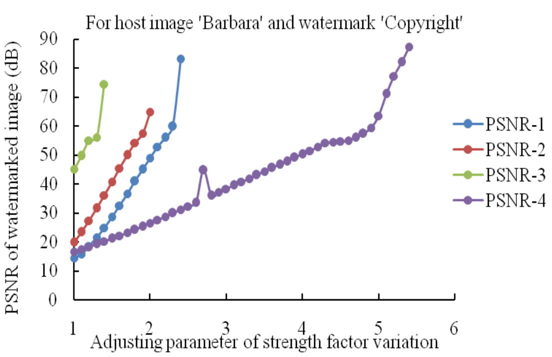

(c)

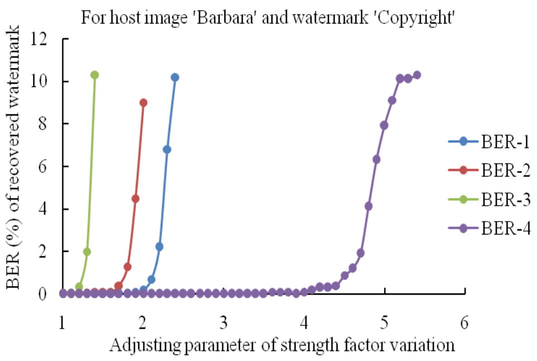

(d)

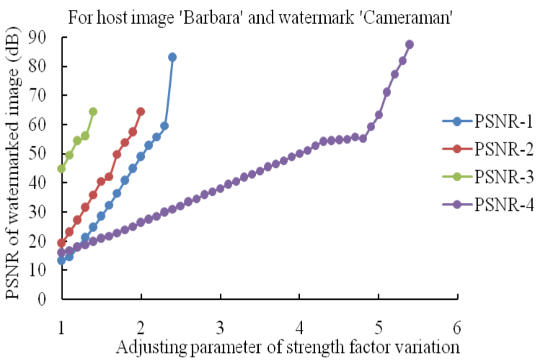

(e)

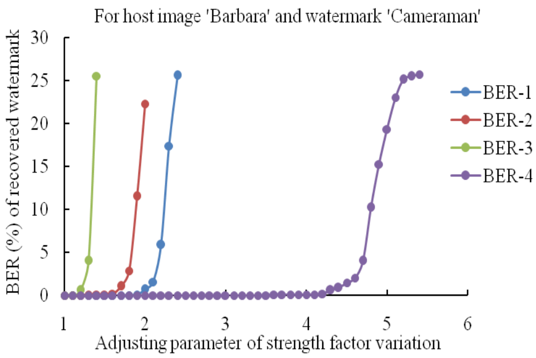

(f)

Figure 5.5 Visual representations for 'PSNR (in dB)' of images and 'BER (%)' for extracted watermarks for host image 'Barbara'.

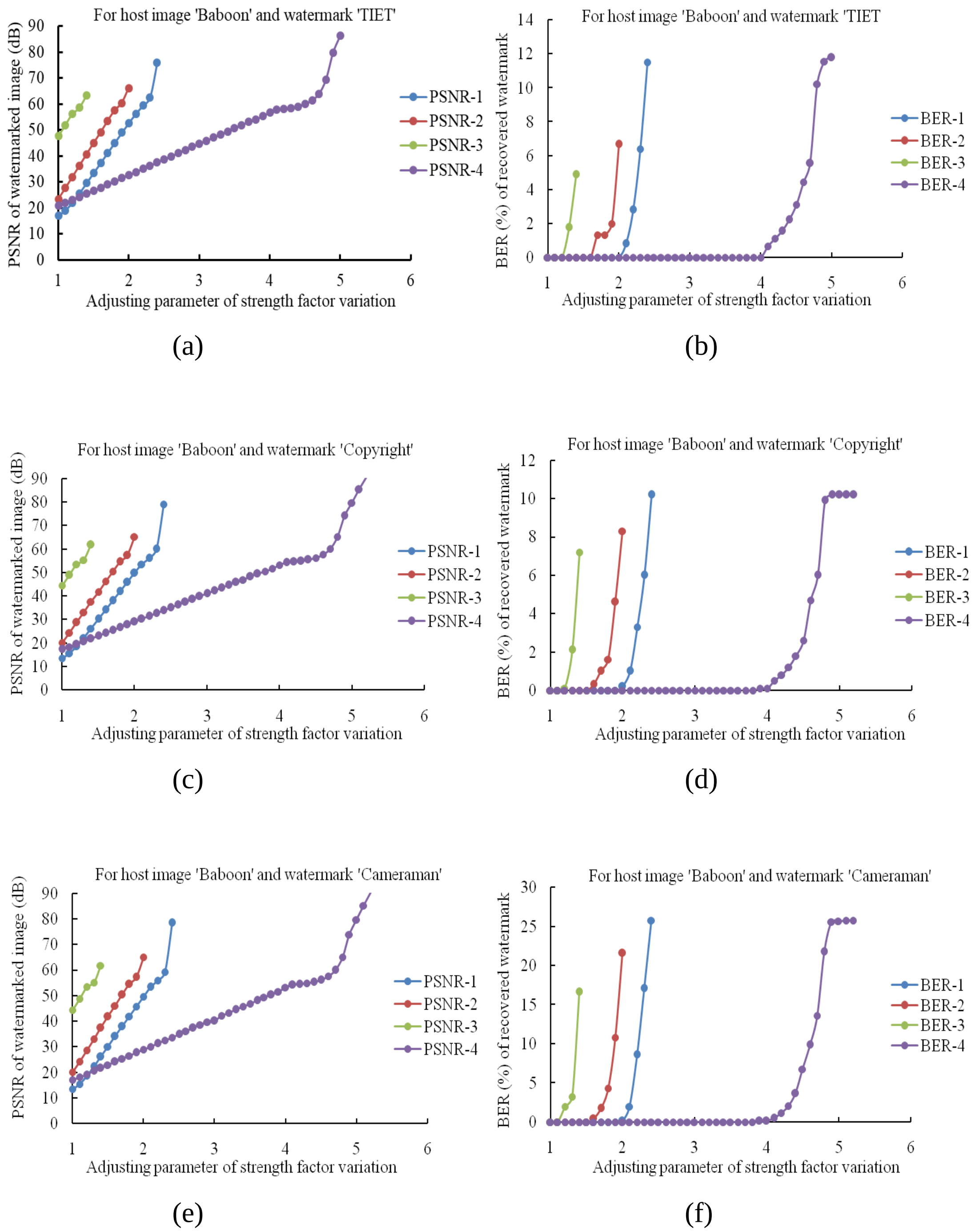

Figure 5.6 Visual representations for ‘PSNR (in dB)’ of images and ‘BER (%)’ for extracted for host image ‘Baboon’.

5.4 SECURITY OF WATERMARK

In the suggested semi-blind hybrid technique, supporting information was transferred with the watermarked image for the successful recovery of the watermark. The locations of blocks with greater entropy proved very important information as they did not relate with the natural image straight forwardly. All the locations were stored temporarily in a cell arrangement structure that increased the security and difficulty for any malicious attacker in concealing the same. Since there were many possible combinations, it became nearly impossible for any attacker to predict the accurate positions of a cell array. The security of the watermark used in this technique was discussed in detail in [135] and [151].

5.5 RESULTS AND INTERPRETATIONS

The simulation of the prospective hybrid watermarking technique was implemented upon three standard images, 'Lena' and 'Barbara' of dimensions (512 × 512) using MATLAB. Three watermarks 'TIET' (25 × 18), 'Copyright' (20 × 50), and 'Cameraman' (32 × 32) were used in the study. Nonetheless, to justify the efficacy of the system, simulation results were also attained from these original images of dimension (1024 × 1024). The original images, watermarks, watermarked images, recovered watermarks and attacked images are shown in Figure 5.3.

5.5.1 Metrics of Performance

The efficiency of the proposed hybrid technique was demonstrated by the quality of the assessment metrics. Additional to PSNR and BER, NCC, SSIM, GMSD, and UIQI were also utilized in judging the quality and toughness of the experiment outcomes. Though our technique proposed to offer high values of PSNR, but similar to [152], [146], and [101], all watermarked images were used at a good PSNR value of 45dB. The proposed technique was highly robust as the scruples of NCC and SSIM approached the perfect merit of one. The experimental results of GMSD and UIQI too closely approximated to zero and one respectively, which indicated the proposed watermarking technique is highly robust.

5.5.2 Analysis of Robustness under various attacks

The tenacity of the prospective technique was proved when the watermarked image

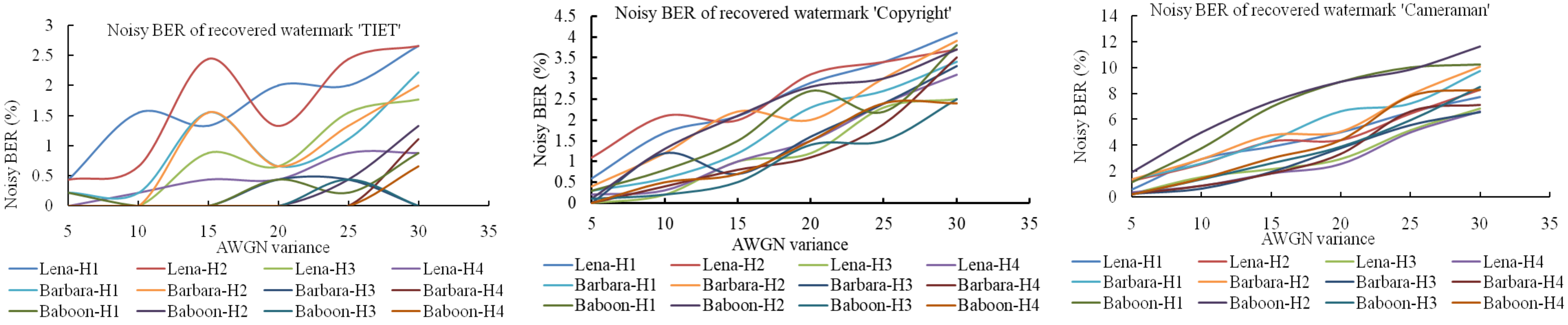

(a) (b) (c)

Figure 5.7 Noisy BER (%) about extracted watermarks from watermarked images of size 512 × 512 at 45dB under AWGN variance attack.

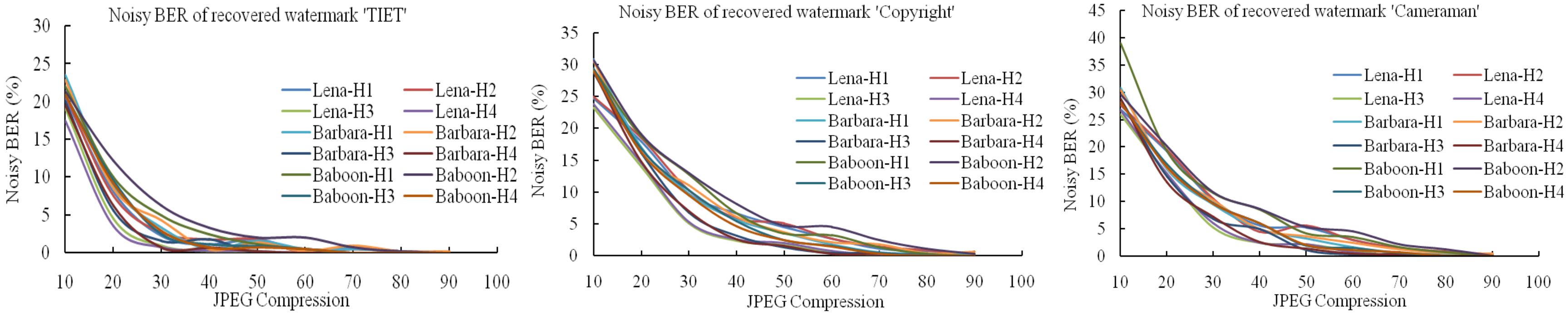

(a) (b) (c)

Figure 5.8 Noisy BER (%) about extracted watermarks from watermarked images of size 512 × 512 at 45dB under JPEG Compression attack.

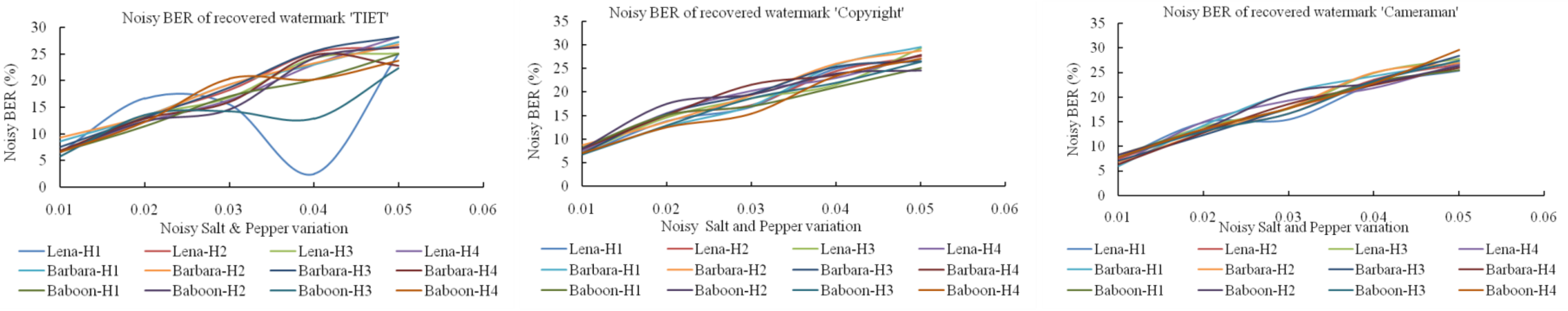

(a) (b) (c)

Figure 5.9 Noisy BER (%) about extracted watermarks from watermarked images of size 512 × 512 at 45dB under Salt & Pepper attack.

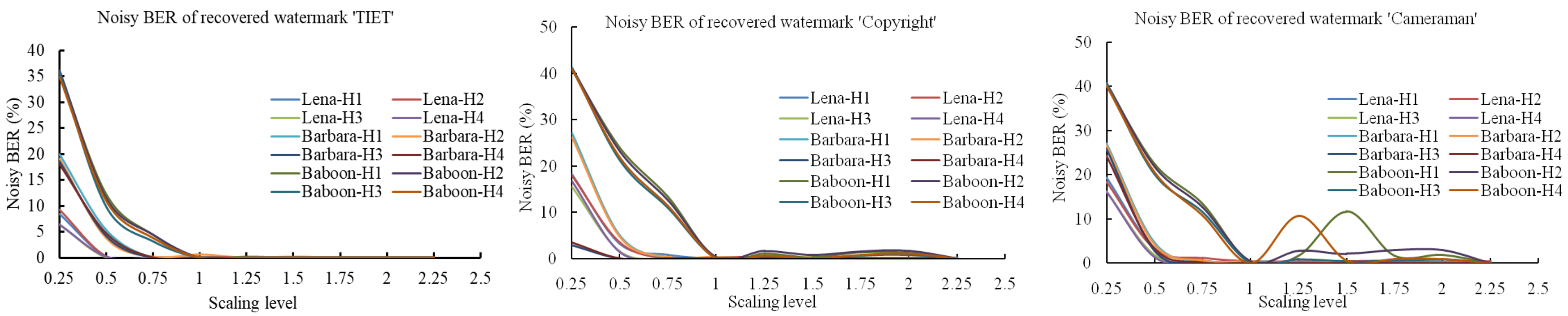

(a) (b) (c)

Figure 5.10 Noisy BER (%) about extracted watermarks from watermarked images of size 512 × 512 at 45dB under Scaling attack.

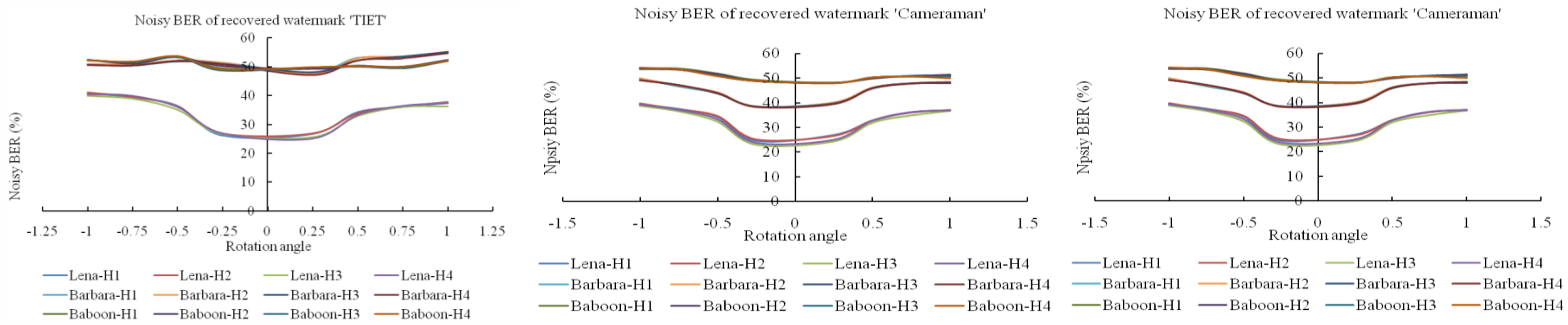

(a) (b) (c)

Figure 5.11 Noisy BER (%) about extracted watermarks ‘TIET’, ‘Copyright’ and ‘Cameraman’ from watermarked images of size 512 × 512 at 45dB under Rotation attack.

was communicated to the receiver. It was attacked by Filtering (Median and Gauss), JPEG Compression, Sharpening and Geometric attacks, etc.

Filtering attacks are familiar signal alteration attacks which are practiced when the watermarked image is transmitted past an insecure communication channel. It was observed that when the Median filter was applied with different filter masks of sizes 3 × 3, 5 × 5, and 7 × 7, the values of PSNR and SSIM decreased gradually for all types of hybrid strength factor formulae. While the quality parameters NCC and UIQI maintained the desirable values approximating to unity, the values of GMSD of watermarked images and BER of recovered watermarks increased using all HSF's. However, when Gauss Filter attacks for identical filter masks were applied, the values of SSIM and NCC were observed to approach desirable values of unity for all sizes of the watermark. While the values of PSNR decreased, the values of GMSD increased slightly. The quality of recovered watermark measured by BER (%) increased for Median filter attacks but remained less than 1% under Gauss filter attacks. The values of UIQI also remained unaffected and highly stable under Gauss (3 × 3), Gauss (5 × 5), and Gauss (7 × 7) filter attacks.

Also, the values of SSIM, NCC, UIQI, and GMSD approached more desirable values of unity and zero respectively under Sharpening attack using all hybrid strength factors H1 to H4. Such useful values are achieved only due to Gaussian modeling of WHT coefficients in HSF calculation. The watermarked images were also levied to different attacks, such as AWGN, JPEG Comp., Scale variation, Rotation, and Salt & Pepper using watermarks 'TIET' and 'Cameraman' for all HSF's. The variation graphs for BER (%) of retrieved watermark concealed by various attacks for both sizes are shown in Figures 5.6 to 5.10.

The robustness of the proposed technique was evaluated by adding white Gaussian noise (AWGN) and Salt & Pepper noise attacks. Such attacks introduced distortion in the watermarked images which complicated the process of watermark recovery. It was noticed that while the results of PSNR and SSIM declined, the values of GMSD, NCC, and UIQI still approached their desirable values of zero and unity respectively using all HSF's.

The BER (%) of the recovered watermarks under AWGN attacks shown in Figure 5.6 varied abruptly for all host images using hybrid strength factors H1 and

H2. Similarly, the BER (%) of the recovered watermarks also increased with the increase in variation of the Salt Pepper attack. It was observed that strength factors H2 and H3 (H3 and H4) caused minimum variations in the value of BER for 'Lena' image (and 'Barbara' image). Thus, the results validated the stability of the prospective technique at lower noise variances and Pepper attacks.

Other common watermarking attacks used in evaluating the performance for the suggested technique were JPEG Compression and Salt & Pepper attacks. When watermarked images were transmitted using different QF's and Salt & Pepper noise variations, it became difficult to extract the watermarks successfully from these corrupted received images. However, the obtained results in Figure 5.7 and Figure 5.8 proved that there was no significant effect of the compression and attack on the desirable values of SSIM, NCC, GMSD, and UIQI for all types of hybrid strength factors in host images using different watermarks. While PSNR of the watermarked image reduced slightly less than 45dB, the values of BER (%) of the recovered watermarks were also observed to be almost zero at maximum compression for both sizes of watermark images.

The robustness of the prospective technique was verified against geometric attacks, such as Scaling and Rotation as shown in Figure 5.9 and Figure 5.10. While the Scaling attack tried to change the values of a bit of the watermarked image, the Rotation attack rotated the image by the value of certain angles. Similarly, under Rotation attack, the desirable values of PSNR, SSIM, and NCC were observed to increase (or decrease) when angles were varied from -1^0 to $+1^0$ (or $+1^0$ to -1^0). However, the response of BER (%) of retrieved watermark decreased for negative variation range of angles and vice versa for all HSF's. Tables 5.1and 5.2 present the values of NCC, SSIM, GMSD, and UIQI for unassaulted and assailed watermarked images using HSF's at minimum values of BER (%) of the extracted watermark(s). It was observed that for all host images, the values of NCC, SSIM, and UIQI approximated the desired value of unity. Similarly, the deviation in the watermarked image and error in watermark recovery was also very close to zero. Such useful values were achieved due to statistical modeling of WHT coefficients in HSF calculation. The images after watermarking and retrieved watermarks were also displayed in Figure 5.3 under various attacks.

Table 5.1 IQA parameters of watermarked images without attacks

IQAParameters → ↓ Standard image with watermark	Formulae used	PSNR (dB)	NCC	SSIM	GMSD	UIQI	BER (%)
'LENA' (Using 'TIET', 'Copyright' and 'Cameraman') at 512 ×512	H1 H2 H3 H4	45,45,45 45,45,45 45,45,45 45,45,45	0.9971,0.9960,0.9981 0.9971,0.9960,0.9981 0.997,0.9960,0.9979 0.9971,0.9959,0.9978	0.9968,0.9968,0.997 0.9968,0.9968,0.997 0.9969,0.9972,0.9974 0.9969,0.9972,0.9973	0.01470,0.01130,0.01087 0.01450.0.01200,01094 0.01293,0.00970,0.009036 0.01264,0.00927,0.008924	0.9999,0.9999,0.9999 0.9999,0.9999,0.9999 0.9998,0.9999,0.9999 0.9998,0.9999,0.9999	0,0,0 0,0,0 0,0,0 0,0,0
'BARBARA' (Using 'TIET', 'Copyright' and 'Cameraman') at 512 ×512	H1 H2 H3 H4	45,45,45 45,45,45 45,45,45 45,45,45	0.9978,0.9968,0.9979 0.9978,0.9968,0.9979 0.9978,0.9967,0.9979 0.9978,0.9968,0.9979	0.9989,0.9986,0.9985 0.9989,0.9987,0.9985 0.9991,0.9988,0.9986 0.999,0.9987,0.9985	0.00845,0.00751,0.00779 0.00840,0.00749,0.00788 0.00690,0.00644,0.00707 0.00849,0.00690,0.00708	0.9999,0.9999,0.9999 0.9999,0.9999,0.9999 0.9998,0.9999,0.9999 0.9998,0.9999,0.9999	0,0.1,0.195 0.22,0.1,0 0,0,0 0,0.1,0
'BABOON' (Using 'TIET', 'Copyright' and 'Cameraman') at 512 ×512	H1 H2 H3 H4	45,45,45 45,45,45 45,45,45 45,45,45	0.9975,0.9960,0.9971 0.9976,0.9960,0.9972 0.99750.9960,0.9972 0.9975,0.996,0.9972	0.9997,0.9996,0.9995 0.9997,0.9996,0.9995 0.9996,0.9996,0.9995 0.9996,0.9996,0.9995	0.00591,0.00587,0.00630 0.00593,0.00589,0.00643. 0.00568,0.00538,0.00582 0.0055,0.00544,0.00591	0.9999,0.9999,0.9999 0.9999,0.9999,0.9999 0.9998,0.9998,0.9998 0.9998,0.9998,0.9998	0,0,0 0,0.1,0.195 0,0,0 0,0,0

'LENA' (Using 'TIET', 'Copyright' and 'Cameraman') at 1024 ×1024	H1 H2 H3 H4	45,45,45 45,45,45 45,45,45 45,45,45	0.9986,0.9978,0.9987 0.9986,0.9978,0.9987 0.9986,0.9979,0.9987 0.99850,0.9978,9987	0.9964,0.9961,0.9956 0.9964,0.9961,0.9955 0.9965,0.9963,0.9959 0.9963,0.9960,0.9954	0.02130,0.01840,0.02044 0.02120,0.01800,0.02056 0.01960,0.01600,0.01720 0.02040,0.01640, 0.01811	0.9999,0.9999,0.9999 0.9999,0.9999,0.9999 0.9998,0.9999,0.9999 0.9998,0.9999,0.9999	0.5859,0 ,0 0,0,0.48 8 0,0,0 0,0,0
'BARBARA' (Using 'TIET', 'Copyright' and 'Cameraman') at 1024 ×1024	H1 H2 H3 H4	45,45,45 45,45,45 45,45,45 45,45,45	0.9988,0.9983,0.9989 0.9988,0.9983,0.9989 0.9988,0.9983,0.9989 0.9988,0.9983,0.9989	0.9988,0.9985,0.9983 0.9988,0.9985,0.9983 0.9988,0.9987,0.9983 0.9988,0.9986,0.9983	0.01010,0.00100,0.01131 0.0101,0.00100,0.01135 0.00954,0.00896,0.00962 0.00979,0.00933,0.00100	0.9999,0.9999,0.9999 0.9999,0.9999,0.9999 0.9998,0.9999,0.9999 0.9998,0.9999,0.9999	0,0,0 0,0,0 0,0,0 0,0.1,0
'BABOON' (Using 'TIET', 'Copyright' and 'Cameraman') at 1024 ×1024	H1 H2 H3 H4	45,45,45 45,45,45 45,45,45 45,45,45	0.9985,0.9979,0.9987 0.9985,0.9979,0.9987 0.9985,0.9979,0.9987 0.9986,0.9979,0.9987	0.9996,0.9995,0.9995 0.9996,0.9995,0.9995 0.9995,0.9995,0.9995 0.9996,0.9995,0.9995	0.00723,0.00646,0.00740 0.00725,0.00640,0.00740 0.00755,0.00620,0.00706 0.00736,0.00604,0.00688	0.9999,0.9999,0.9999 0.9999,0.9999,0.9999 0.9999,0.9998,0.9999 0.9999,0.9998,0.9999	0,0,0 0,0,0 0,0,0 0,0,0

Table 5.2 IQA specifications for assaulted images.

Noisy PSNR (in dB)									
Image	Watermark	Without attack	Median (3 × 3)	Median (5 × 5)	Median (7 × 7)	Gauss (3 × 3)	Gauss (5 × 5)	Gauss (7 × 7)	Sharp
		(Using Formula H1,H2,H3 and H4)							
‘Lena’	‘TIET’	45.01,45.08, 45.04, 45	35.82 35.83 35.82 35.83	32.04 32.04 32.04 32.04	29.99 29.99 29.99 30	39.9 39.92 39.91 39.91	39.88 39.9 39.89 39.89	39.88 39.9 39.89 39.89	39.88 39.9 39.89 39.89
	‘Copyright’	45,45,45,45	35.86 35.85 35.88 35.88	32.07 32.07 32.08 32.09	30.02 30.02 30.02 30.03	39.93 39.93 39.94 39.95	39.92 39.92 39.93 39.93	39.92 39.92 39.93 39.93	8.64 8.64 8.63 8.64
	‘Cameraman’	45.07, 45.01, 45.08, 45.03	35.86 35.85 35.88 35.87	32.08 32.07 32.09 32.09	30.02 30.02 30.03 30.03	39.91 39.89 39.92 39.91	39.89 39.88 39.9 39.89	39.9 39.88 39.9 39.89	39.9 39.88 39.9 39.89
‘Barbara’	‘TIET’	45.07, 45.09, 45.22, 45.06	33.69 33.69 33.7 33.69	29.08 29.08 29.08 29.08	26.84 26.84 26.85 26.84	39.49 39.5 39.53 39.48	39.46 39.47 39.5 39.46	39.46 39.47 39.5 39.46	39.46 39.47 39.5 39.46
	‘Copyright’	45.01,45.07,45.03, 45.04	33.69 33.69 33.69 33.69	29.07 29.07 29.07 29.07	26.83 26.83 26.83 26.83	39.47 39.48 39.46 39.46	39.44 39.45 39.43 39.43	39.44 39.45 39.43 39.43	9.87 9.87 9.86 9.86
	‘Cameraman’	45.06, 45, 44.99, 45	33.67 33.66 33.66 33.67	29.06 29.06 29.06 29.06	26.83 26.82 26.83 26.83	39.4 39.39 39.39 39.38	39.37 39.36 39.36 39.35	39.37 39.36 39.36 39.35	39.37 39.36 39.36 39.35

‘Baboon’	‘TIET’	45,45,45,45,45	25 25.03 25.03 25.03	22.62 22.62 22.62 22.62	21.9 21.9 21.91 21.91	32.83 32.83 32.83 32.84	32.81 32.81 32.81 32.82	32.81 32.81 32.81 32.82	8.63 8.63 8.62 8.62
	‘Copyright’	45,45,45,45,45	25.02 25.02 25.03 25.03	22.6 22.62 22.62 22.62	21.9 21.9 21.91 21.91	32.84 32.84 32.85 32.84	32.82 32.82 32.83 32.83	32.82 32.82 32.83 32.83	8.62 8.62 8.61 8.61
	‘Cameraman’	45,45,45,45,45	25.02 25.02 25.02 25.02	22.61 22.61 22.61 22.61	21.89 21.89 21.89 21.89	32.82 32.82 32.82 32.82	32.8 32.8 32.8 32.8	32.8 32.8 32.8 32.8	8.63 8.63 8.62 8.62
Noisy NCC									
Image	Watermark	Without attack	Median (3 × 3)	Median (5 × 5)	Median (7 × 7)	Gauss (3 × 3)	Gauss (5 × 5)	Gauss (7 × 7)	Sharp
(Using Formula H1,H2,H3 and H4)									
‘Lena’	‘TIET’	0.9971 0.9971 0.997 0.9971	0.9981 0.9981 0.9981 0.9981	0.9991 0.9991 0.999 0.999	0.9997 0.9997 0.9996 0.9996	0.9984 0.9984 0.9983 0.9983	0.9984 0.9984 0.9983 0.9984	0.9984 0.9984 0.9983 0.9984	0.9984 0.9984 0.9983 0.9984
	‘Copyright’	0.996 0.996 0.996 0.9959	0.9971 0.9971 0.9970 0.9970	0.9980 0.9980 0.9979 0.9979	0.9986 0.9986 0.9985 0.9985	0.9973 0.9973 0.9973 0.9972	0.9973 0.9973 0.9973 0.9972	0.9973 0.9973 0.9973 0.9972	0.6028 0.6028 0.6026 0.6026

	‘Cameraman’	0.9981 0.9981 0.9979 0.9978	0.9992 0.9992 0.999 0.9989	1 1 0.9999 0.9998	1 1 1 1	0.9994 0.9994 0.9992 0.9992	0.9994 0.9994 0.9992 0.9992	0.9994 0.9994 0.9992 0.9992	0.9994 0.9994 0.9992 0.9992
‘Barbara’	‘TIET’	0.9978 0.9978 0.9978 0.9978	0.9992 0.9992 0.9992 0.9992	0.9991 0.9991 0.9991 0.9991	0.9987 0.9987 0.9987 0.9987	0.9991 0.9991 0.9992 0.9991	0.9991 0.9992 0.9992 0.9917	0.9991 0.9992 0.9992 0.9991	0.9991 0.9992 0.9992 0.9991
	‘Copyright’	0.9968 0.9968 0.9967 0.9968	0.9982 0.9982 0.9981 0.9982	0.9981 0.9981 0.9980 0.9981	0.9977 0.9977 0.9976 0.9976	0.9981 0.9981 0.9981 0.9981	0.9981 0.9981 0.9981 0.9981	0.9981 0.9981 0.9981 0.9981	0.6682 0.6682 0.6681 0.6681
	‘Cameraman’	0.9979 0.9979 0.9979 0.998	0.9993 0.9993 0.9933 0.9994	0.9992 0.9992 0.9992 0.9992	0.9988 0.9988 0.9988 0.9988	0.9993 0.9992 0.9992 0.9993	09993 0.9993 0.9992 0.9993	0.9993 0.9993 0.9992 0.9993	0.9993 0.9993 0.9992 0.9993
‘Baboon’	‘TIET’	0.9975 0.9976 0.9975 0.9975	0.9995 0.9996 0.9995 0.9995	1 1 1 1	1 1 1 1	1 1 1 1	1 1 1 1	1 1 1 1	0.5873 0.5873 0.5872 0.5872
	‘Copyright’	0.9960 0.9960 0.9960 0.9960	0.9980 0.9980 0.9980 0.9979	0.9988 0.9988 0.9988 0.9988	0.9988 0.9989 0.9988 0.9988	1 1 1 1	1 1 1 1	1 1 1 1	0.5871 0.5871 0.5870 0.5870
	‘Cameraman’	0.9971 0.9972 0.9972 0.9972	0.9991 0.9991 0.9992 0.9992	0.9999 0.9999 0.9999 0.9999	0.9999 0.9999 1 0.9999	1 1 1 1	1 1 1 1	1 1 1 1	0.5873 0.5873 0.5873 0.5873

Noisy SSIM									
Image	Watermark	Without attack	Median (3 × 3)	Median (5 × 5)	Median (7 × 7)	Gauss (3 × 3)	Gauss (5 × 5)	Gauss (7 × 7)	Sharp
(Using Formula H1, H2, H3 and H4)									
‘Lena’	‘TIET’	0.9968	0.934	0.8831	0.843	0.9855	0.9854	0.9854	0.9854
		0.9968	0.934	0.8831	0.8429	0.9855	0.9854	0.9854	0.9854
		0.9969	0.9342	0.8833	0.843	0.9856	0.9856	0.9856	0.9856
		0.9969	0.9341	0.8833	0.843	0.9856	0.9855	0.9855	0.9855
	‘Copyright’	0.9968	0.9342	0.8834	0.8432	0.9855	0.9855	0.9855	0.6261
		0.9968	0.9342	0.8834	0.8432	0.9855	0.9854	0.9854	0.6262
		0.9972	0.9345	0.8837	0.8432	0.9859	0.9858	0.9858	0.6256
		0.9972	0.9345	0.8837	0.8833	0.9859	0.9858	0.9859	0.6255
	‘Cameraman’	0.997	0.9343	0.8836	0.8433	0.9857	0.9857	0.9857	0.9857
		0.997	0.9343	0.8835	0.8433	0.9857	0.9856	0.9856	0.9856
		0.9974	0.9347	0.8839	0.8435	0.9861	0.986	0.986	0.986
		0.9973	0.9346	0.8838	0.8434	0.986	0.9859	0.9859	0.9859
‘Barbara’	‘TIET’	0.9989	0.9238	0.7936	0.6949	0.9899	0.9897	0.9897	0.9897
		0.9989	0.9238	0.7936	0.6949	0.9899	0.9897	0.9897	0.9897
		0.9991	0.9239	0.7938	0.6949	0.99	0.9899	0.9899	0.9899
		0.999	0.9238	0.7937	0.6948	0.9899	0.9898	0.9898	0.9898
	‘Copyright’	0.9986	0.9237	0.7934	0.6946	0.9897	0.9896	0.9896	0.5737
		0.9987	0.9237	0.7935	0.6946	0.9897	0.9896	0.9896	0.5737
		0.9988	0.9239	0.7935	0.6946	0.9899	0.9897	0.9897	0.5733
		0.9987	0.9238	0.7935	0.6946	0.9898	0.9897	0.9897	0.5733
	‘Cameraman’	0.9985	0.9234	0.7931	0.6945	0.9894	0.9893	0.9893	0.9893
		0.9985	0.9234	0.7931	0.6944	0.9894	0.9893	0.9893	0.9893
		0.9986	0.9235	0.7932	0.6945	0.9896	0.9895	0.9895	0.9895
		0.9985	0.9235	0.7932	0.6945	0.9895	0.9894	0.9895	0.9894
‘Baboon’	‘TIET’	0.9997	0.7295	0.5076	0.4166	0.9626	0.9625	0.9625	0.5267
		0.9997	0.7295	0.5075	0.4165	0.9627	0.9625	0.9625	0.5267
		0.9996	0.7295	0.5076	0.4165	0.9626	0.9625	0.9625	0.5266

		0.9996	0.7295	0.5076	0.4166	0.9626	0.9625	0.9625	0.5622
	‘Copyright’	0.9996 0.9996 0.9996 0.9996	0.7299 0.7299 0.7299 0.7299	0.5079 0.5078 0.5079 0.5079	0.4170 0.4169 0.4169 0.4170	0.9627 0.9627 0.9627 0.9627	0.9625 0.9625 0.9626 0.9625	0.9625 0.9625 0.9626 0.9625	0.5267 0.5267 0.5266 0.5622
	‘Cameraman’	0.9995 0.9995 0.9995 0.9995	0.7296 0.7295 0.7296 0.7295	0.5075 0.5075 0.5074 0.5074	0.4167 0.4167 0.4166 0.4167	0.9626 0.9626 0.9626 0.9625	0.9624 0.9624 0.9624 0.9624	0.9624 0.9624 0.9624 0.9624	0.5267 0.5267 0.5266 0.5622
Noisy GMSD									
Image	watermark	Without attack	Median (3 × 3)	Median (5 × 5)	Median (7 × 7)	Gauss (3 × 3)	Gauss (5 × 5)	Gauss (7 × 7)	Sharp
		(Using Formula H1,H2,H3 and H4)							
‘Lena’	‘TIET’	0.0147 0.0145 0.01293 0.01264	0.01878 0.001875 0.01789 0.01771	0.05037 0.00888 0.005017 0.005011	0.08889 0.00215 0.008888 0.008877	0.02155 0.00215 0.02062 0.02044	0.02163 0.00215 0.0207 0.02053	0.02163 0.00215 0.0207 0.02053	0.02163 0.02159 0.0207 0.02053
	‘Copyright’	0.0113 0.0112 0.0097 0.00927	0.0175 0.0174 0.0167 0.0165	0.05 0.05 0.0497 0.0495	0.088 0.088 0.088 0.088	0.0199 0.0198 0.0192 0.0190	0.02 0.0199 0.0193 0.0191	0.02 0.019 0.019 0.019	0.1870 0.1870 0.1876 0.1877
	‘Cameraman’	0.01087 0.01094 0.009036 0.008924	0.01715 0.01717 0.01655 0.01653	0.04984 0.04984 0.04959 0.04954	0.08806 0.08807 0.08782 0.08781	0.01968 0.01971 0.01896 0.01894	0.01978 0.01979 0.01903 0.01902	0.01978 0.01979 0.01903 0.01902	0.01978 0.01979 0.01903 0.01902
‘Barbara’	‘TIET’	0.00845 0.008409 0.006904 0.008497	0.02026 0.0202 0.01986 0.02018	0.07247 0.07237 0.07209 0.07218	0.1294 0.1295 0.1292 0.1294	0.01676 0.0167 0.01619 0.01666	0.01686 0.01683 0.01629 0.01675	0.01686 0.01683 0.01629 0.01675	0.01686 0.01683 0.01629 0.01675

	‘Copyright’	0.00751 0.00749 0.00644 0.0069	0.019 0.0197 0.0199 0.0196	0.073 0.0728 0.0728 0.0727	0.1302 0.1303 0.1301 0.1302	0.016 0.0162 0.0159 0.016	0.016 0.016 0.016 0.016	0.016 0.016 0.016 0.016	0.2597 0.2597 0.2599 0.2597
	‘Cameraman’	0.007793 0.007885 0.00707 0.007081	0.01998 0.02 0.01989 0.01982	0.07319 0.07319 0.07306 0.07298	0.1292 0.1293 0.1291 0.1293	0.01653 0.01654 0.01628 0.01628	0.01666 0.01668 0.0164 0.0164	0.01666 0.01668 0.0164 0.0164	0.01666 0.01668 0.0164 0.0164
‘Baboon’	‘TIET’	0.00591 0.00593 0.00568 0.0055	0.0555 0.0555 0.0554 0.0555	0.1180 0.1180 0.1179 0.1180	0.1694 0.1694 0.1695 0.1694	0.0113 0.0114 0.0112 0.0112	0.0114 0.0115 0.0112 0.0113	0.0014 00115 0.0112 0.0113	0.1596 0.1596 0.1597 0.1597
	‘Copyright’	0.00587 0.00589 0.00538 0.00544	0.0553 0.055 0.055 0.0553	0.1177 0.1177 0.1177 0.1177	0.1692 0.1692 0.1694 0.1693	0.0113 0.0113 0.0111 0.0112	0.0114 0.0114 0.0112 0.0112	0.0114 0.0114 0.0112 0.0112	0.1596 0.1596 0.1597 0.1597
	‘Cameraman’	0.0063 0.00643 0.00582 0.00591	0.0556 0.0556 0.0556 0.0556	0.1180 0.1180 0.1181 0.1181	0.1692 0.1692 0.1694 0.1693	0.0117 0.0118 0.0116 0.0116	0.0118 0.0118 0.0117 0.0116	0.0118 0.0118 0.0117 0.0116	0.1597 0.1597 0.1598 0.1598
Noisy UIQI									
Image	watermark	Without attack	Median (3 × 3)	Median (5 × 5)	Median (7 × 7)	Gauss (3 × 3)	Gauss (5 × 5)	Gauss (7 × 7)	Sharp
(Using Formula H1,H2,H3 and H4)									
‘Lena’	‘TIET’	0.9999 0.9994 0.9999 0.9999	0.9999 0.9999 0.9999 0.9999	0.9997 0.9997 0.9997 0.9997	0.9994 0.9994 0.9994 0.9994	0.9999 0.9999 0.9999 0.9999	0.9999 0.9999 0.9999 0.9999	0.9999 0.9999 0.9999 0.9999	0.9999 0.9999 0.9999 0.9999
	‘Copyright’	0.9999 0.9999	0.9999 0.9999	0.9997 0.9997	0.9994 0.9994	0.9999 0.9999	0.9999 0.9999	0.9999 0.9999	0.7503 0.7503

		0.9999	0.9999	0.9997	0.9994	0.9999	0.9999	0.9999	0.7499
		0.9999	0.9999	0.9997	0.9994	0.9999	0.9999	0.9999	0.7499
	‘Cameraman’	0.9999	0.9999	0.9997	0.9994	0.9999	0.9999	0.9999	0.9999
		0.9999	0.9991	0.9997	0.9994	0.9999	0.9999	0.9999	0.9999
		0.9999	0.9999	0.9997	0.9994	0.9999	0.9999	0.9999	0.9999
		0.9999	0.9999	0.9997	0.9994	0.9999	0.9999	0.9999	0.9999
‘Barbara’	‘TIET’	0.9999	0.9999	0.9998	0.9996	0.9999	0.9999	0.9999	0.9999
		0.9999	0.9999	0.9998	0.9996	0.9999	0.9999	0.9999	0.9999
		0.9999	0.9999	0.9998	0.9996	0.9999	0.9999	0.9999	0.9999
		0.9999	0.9999	0.9998	0.9996	0.9999	0.9999	0.9999	0.9999
	‘Copyright’	0.9999	0.9999	0.9998	0.9996	0.9999	0.9999	0.9999	0.8297
		0.9999	0.9999	0.9999	0.9996	0.9999	0.9999	0.9999	0.8297
		0.9999	0.9999	0.9998	0.9996	0.9999	0.9999	0.9999	0.8295
		0.9999	0.9999	0.9998	0.9996	0.9999	0.9999	0.9999	0.8295
	‘Cameraman’	0.9999	0.9999	0.9998	0.9996	0.9999	0.9999	0.9999	0.9999
		0.9999	0.9999	0.9998	0.9996	0.9999	0.9999	0.9999	0.9999
		0.9994	0.9999	0.9998	0.9996	0.9999	0.9999	0.9999	0.9999
		0.9999	0.9999	0.9998	0.9996	0.9999	0.9999	0.9999	0.9999
‘Baboon’	‘TIET’	0.9999	0.9996	0.999	0.9985	0.9998	0.9989	0.9989	0.766
		0.9999	0.9996	0.999	0.9985	0.9998	0.9998	0.9989	0.766
		0.9998	0.9996	0.999	0.9986	0.9998	0.9998	0.9989	0.765
		0.9998	0.9996	0.999	0.9986	0.9998	0.9998	0.9989	0.765
	‘Copyright’	0.9999	0.9996	0.999	0.9985	0.9998	0.9989	0.9998	0.765
		0.9999	0.9996	0.999	0.9985	0.9998	0.9998	0.9998	0.765
		0.9998	0.9996	0.999	0.9986	0.9998	0.9998	0.9998	0.765
		0.9998	0.9996	0.999	0.9986	0.9998	0.9998	0.9998	0.765
	‘Cameraman’	0.9999	0.9995	0.9989	0.9984	0.9998	0.9998	0.9998	0.7661
		0.9999	0.9995	0.9989	0.9984	0.9998	0.9999	0.9989	0.7661
		0.9998	0.9995	0.9989	0.9984	0.9998	0.9998	0.9988	0.7661
		0.9998	0.9995	0.9989	0.9984	0.9998	0.9998	0.9988	0.7661

Noisy BER(%) of Recovered Watermark									
Image	watermark	Without attack	Median (3 × 3)	Median (5 × 5)	Median (7 × 7)	Gauss (3 × 3)	Gauss (5 × 5)	Gauss (7 × 7)	Sharp
(Using Formula H1,H2,H3 and H4)									
‘Lena’	‘TIET’	0	2.44	6.66	13.11	1.33	1.33	1.33	1.33
		0	2.22	6.66	13.11	1.33	1.33	1.33	1.33
		0	1.11	4	11.55	0.88	0.88	0.88	0.88
		0	1.11	4.44	10.66	0.88	0.88	0.88	0.88
	‘Copyright’	0	8.6	16.6	22.6	2	2	2	10.2
		0	8.4	16.2	22.5	1.7	1.7	1.7	10.2
		0	4.9	13.9	21.5	0.6	0.6	0.6	10.2
		0	5.5	14.3	21.2	0.6	0.6	0.6	10.2
	‘Cameraman’	0	8.39	18.26	24.02	1.46	1.56	1.56	1.56
		0	8.1	17.77	23.53	1.36	1.36	1.36	1.36
		0	5.17	15.91	22.16	0.5859	0.5859	0.5859	0.5859
		0	5.46	16.21	22.26	0.6835	0.6835	0.6835	0.6835
‘Barbara’	‘TIET’	0	13.33	26.88	33.55	11.77	11.77	11.77	11.77
		0.22	12.22	26.22	33.77	11.77	11.77	11.77	11.77
		0	12	24.22	31.77	11.33	11.33	11.33	11.33
		0	12	24.22	31.55	11.55	11.55	11.55	11.55
	‘Copyright’	0.1	12.6	25.7	33	6.4	6.6	6.6	10.2
		01	11.8	25.7	33.1	6.1	6.1	6.1	10.2
		0	10	24.3	32.4	6.1	6.1	6.1	10.2
		0.1	11	24.6	32.1	6.1	6.1	6.1	10.2
	‘Cameraman’	0.195	11.8	26.9	33.59	6.25	6.34	6.34	6.34
		0	11.32	26.17	33.49	6.54	6.54	6.54	6.54
		0	9.17	25	32.32	5.56	5.56	5.56	5.56
		0	10.15	24.8	32.61	6.05	6.05	6.05	6.05
‘Baboon’	‘TIET’	0	35.11	49.77	51.77	16.2	16.2	16.2	11.77
		0	34.88	49.33	52.22	16.2	16.2	16.2	11.77
		0	33.33	48.8	50.66	14.4	14.4	16.2	11.77

		0	34.22	48	51.11	14.4	14.4	14.4	11.77
	‘Copyright’	0	38.4	47.59	49.6	13	13.1	13.1	10.2
		0.1	38.2	46.8	49.5	12.4	12.4	12.4	10.2
		0	37.4	47.2	49.2	11.2	11.3	11.3	10.2
		0	37.3	46.9	49.3	112	11.3	11.3	10.2
	‘Cameraman’	0	34.37	42.96	45.8	13.57	13.67	13.67	25.78
		0.195	34.08	42.67	45.99	13.76	13.86	13.86	25.78
		0	33.69	42.18	45.6	11.42	11.7	11.7	25.78
		0	32.91	42.18	45.6	11.52	11.62	11.62	25.78

Table 5.3 Comparison of BER (%) values with Fazlali et al. [144],Kang et al. [153] and Yadav et al. [131].

Baboon						
Attack	Fazlali et al.[144] at 40.06 dB	Proposed	Kang et al.[153] at 37.14 dB	Proposed	Yadav et al.[131]at 45 dB	Proposed
Scaling(0.75)	---------	---------	---------	---------	0	4.44,4.44,3.11,3.33
Scaling(0.8)	1.5	**0,0,0,0**	---------	---------	---------	---------
Scaling(0.9)	---------	---------	---------	---------	0	2,1.77,0.88,1.11
Scaling(1.1)	2.34	**0,0,0,0**	---------	---------	---------	---------
Scaling(2)	---------	---------	---------	---------	1.33	5.3,6.2,4.66,4.44
JPEG Comp. (QF=10%)	5.47	**2.34,1.562,0,0**	11.43	11.62,12.30,**10.25,9.765**	0	0,0,0,0
JPEG Comp. (QF=20%)	2.34	0,0,0,0	3.61	3.61,4.98,**1.953,2.148**	---------	---------
JPEG Comp. (QF=30%)	0	0,0,0,0	0.78	1.953,2.44,**0.4882**,0.7812	2.22	4.66,6.22,2.44,2.88
JPEG Comp. (QF=40%)	0	0,0,0,0	---------	---------	0	2.44,3.33,0.88,0.44
JPEG Comp. (QF=50%)	---------	---------	0.29	**0.1953,0.7812,0,0**	0	1.11,2,0.66,0.66
JPEG Comp. (QF = 70%)	---------	---------	0.10	**0, 0.09765, 0, 0**	---------	---------

JPEG Comp. (QF=80%)	---------	---------	---------	---------	0	0, 0.22, 0, 0
JPEG Comp. (QF=90%)	---------	---------	---------	---------	0	0,0,0,0
Barbara						
Scale (0.75)			---------	---------	0	0,0,0.22,0
Scale (0.8)	0	0,0,0,0	---------	---------		
Scale (0.9)	---------	---------	---------	---------	0.22	0.22,**0**,0.22,**0**
Scale (1.1)	0	0,0,0,0	---------	---------	4.22	8,7.77,6.44,6.22
Scale (2)	---------	---------	---------	---------	0	0,0,0,0
JPEG Comp. (QF = 10%)	5.47	**2.34,5.46,1.562,0.7812**	---------	---------	---------	---------
JPEG Comp. (QF = 20%)	0.78	0.7812,2.34,**0,0**	---------	---------	---------	---------
JPEG Comp. (QF = 30%)	0	0.7812,1.562,0,0.7812	---------	---------	0	3.33,4.22,1.55,0.66
JPEG Comp. (QF = 40%)	0	0.7812,1.562,0,0.7812	---------	---------	0	0.44,1.77,0.66,0.44
JPEG Comp. (QF = 50%)	---------	---------	---------	---------	0.22	1.55,1.33,**0**,0.22
JPEG Comp. (QF = 70%)	---------	---------	---------	---------		
JPEG Comp. (QF = 80%)	---------	---------	---------	---------	0	0.22,0.22,0,0
JPEG Comp. (QF = 90%)	---------	---------	---------	---------	0	0,0.22,0,0
Lena						
Scale (0.75)	---------	---------	---------	---------	0	0,0,0,0
Scale (0.8)	---------	---------	---------	---------	---------	---------
Scale (0.9)	---------	---------	---------	---------	2.22	**0,0,0,0**
Scale (1.1)	---------	---------	---------	---------	9.78	**0,0,0,0**
Scale (2)	---------	---------	---------	---------	0	0,0,0,0
JPEG Comp.	---------	---------	22.66	**15.33,15.82,13.67,13.18**	---------	---------

(QF = 10%)						
JPEG Comp. (QF = 20%)	---------	---------	20.70	**8.1,8, 2.83,3.125**	---------	---------
JPEG Comp. (QF = 30%)	---------	---------	15.82	**4.1,4.78,0.7812,0.6835**	2	2.26,2.26,**0.88,0.66**
JPEG Comp. (QF = 40%)	---------	---------	---------	---------	0.44	1.11,1.77,**0.22,0.22**
JPEG Comp. (QF = 50%)	---------	---------	7.91	**2.63, 3.02,0,0.09765**	0	1.77,1.77,0.22,0.22
JPEG Comp. (QF = 70%)	---------	---------	2.05	0.2929,0.1953,0,0	---------	---------
JPEG Comp. (QF = 80%)	---------	---------	---------	---------	0	0.22,0.22,0,0
JPEG Comp. (QF = 90%)	---------	---------	---------	---------	0	0,0,0,0

Table 5.4 Analogy of NCC of watermarked images with Elshazly et al. [140], Kang et al. [153], Wang et al. [154], Yuan et al. [155], Zhang et al. [156] and Chen et al. [157].

Lena						
	JPEG (QF=10%)	JPEG (QF = 20%)	JPEG (QF = 30%)	JPEG (QF = 40%)	JPEG (QF = 50%)	JPEG (QF = 60%)
Elshazly et al. [140] at 26.87dB	0.0331	0.2688	---------	0.7437	---------	0.9793
Proposed	**0.9631,0.9631, 0.9913,0.9627**	**0.9638,0.9639,0.9917,0.9632**	---------	0.9638,0.9637,0.9917,0.9632	---------	0.9641,0.9641,**0.9921**,0.9634
Kang et al. [153] at 40.07dB	0.8382	0.8502	0.8867	---------	0.9449	---------
Proposed	**0.9952,0.9952,**	**0.9960,0.9961,0.**	**0.9959,0.9959,0.99**	---------	**0.9963,0.9964,0.99**	---------

	0.9950, 0.9949	**9955,0.9954**	**55,0.9955**		**60,0.9958**	
	JPEG (QF = 70%)	Med.Filter (3×3)	Med.Filter(5×5)	SaltPepper (0.01)	SaltPepper (0.02)	
Elshazly et al. [140] at 26.87dB	---------	---------	---------	---------	---------	
Proposed	---------	---------	---------	---------	---------	
Kang et al. [153] at 40.07dB	0.9859	0.9967	0.9486	0.8817	0.8386	
Proposed	**0.9963,0.9963, 0.9960,0.9958**	**0.9977,0.9976,0.9973,0.9972**	**0.9987,0.9987**,0.9983,0.9982	**0.9890,0.9892,0.9882,0.9887**	**0.9810,0.9813,0.9807,0.9803**	
	JPEG (QF = 40%)	JPEG (QF = 70%)	Median (3×3)	SaltPepper (0.02)		
Yuan et al. [155]	0.9929,0.9714	---------	0.9737,0.9451	0.9755,0.9643		
Zhang et al. [156]	---------	0.9467	0.8981	---------		
Proposed	0.9638,0.9637**,** **0.9917,**0.9632	**0.9963,0.9963,0.9960,0.9958**	**0.9977,0.9976,0.9973,0.9972**	**0.9810,0.9813,0.9807,0.9803**		
Goldhill						
	Under No Attack	JPEG (QF = 50%)	JPEG (QF = 70%)	Med.Filter (3×3)	Med.Filter (4×4)	Med.Filter (5×5)
Wang et al. [154] at 51.01dB	0.9978	0.9964	0.9973	0.9955	0.9885	0.9896
Proposed	**0.9987,0.9987,0.9987,0.9979**	**0.9971**,0.9953,0.9954,0.9953	**0.9974**,0.9954,0.9955,0.9953	**0.9994,0.9976,0.9977,0.9975**	**1,0.9982,0.9982,0.9981**	**1,0.9990,0.9991,0.9989**
	Under No	Salt Pepper (0.01)	Scale (0.25)	Scale (0.5)	Scale (0.9)	Scale (1.2)

	Attack					
Host image: Barbara {under Rotation attack (Angle 30 degrees)}						
Chen et al. [158]	0.89					
Proposed	**0.97,0.97,0.97,0.97**					

Table 5.5 Analogy of BER (%) for recuperated watermark among suggested technique and Sun et al. [158] at 42dB, Nezhadarya et al. [124] at 42.26 dB and Amirmazlaghani et al. [31] at 42.65 dB under Rotation attack.

Rot. Ang. (in deg.)	Sun et al. [158] (at 42dB)	Proposed	Nezhadarya et al. [124] (at 42.26 dB)	Proposed	Amirmazlaghani et al. [31] (at 42.65 dB)	Proposed
-0.5	45.31	**39.06, 37.5,34.37, 35.93**	36.75 (GDWM0)	39.06,39.06,**34.37**,39.06	----	**----**
0.5	43.75	**42.18, 40.62, 43.75, 42.18**	----	----	----	----
0.75	54.69	**45.31, 45.31,45.31,45.31**	----	----	----	----
1	53.13	**46.87, 45.31, 46.87, 46.87**	----	----	----	----
2	60.94	**50, 50, 51.5,50**	----	----	----	----
-1	----	----	----	----	49.20	54.68, **46.87, 46.87, 46.09**

Table 5.6 Analogy of BER (%) of recovered watermark among proposed technique and Yadav et. al [101] at 45dB.

Host Image → Attacks ↓	'Barbara'		'Baboon'		'Peppers'	
	Yadav et al. [101]	Proposed	Yadav et al. [101]	Proposed	Yadav et al. [101]	Proposed
Gauss (3 × 3)	1.9	**0.9**	2.3	2.4	2.3	2.3
Gauss (5 × 5)	1.9	**0.9**	2.3	2.3	2.5	2.4
Wiener (3 × 3)	1.1	1.11	1.1	1	1.9	1.87
Wiener (5 × 5)	7.3	**7**	10.8	10.3	7.8	7.6
Median (3 × 3)	5	**4.8**	30.6	27.67	5	5.1
Median (5 × 5)	17.7	**15.3**	45.7	42.15	12.9	11.78
Scale 0.75	0.1	**0**	0.3	0	2.4	1.6
Scale 0.9	2.1	**1.7**	0.6	0.5	5.2	**4.4**
Scale 1.1	12.8	**10.6**	5	4.67	16.8	12.58
Scale 1.5	0	**0**	0	**0**	1.7	**0.7**
Scale 2	0	**0**	0	**0**	1.8	**0.45**

Sharp	8	10.2	10.8	10.77	8.3	10.56
JPEG (10%)	1.56	**1.43**	-----	-----	-----	-----
Salt& Pepper (1%)	0.78	**0.7**	-----	-----	-----	-----
Salt& Pepper (2%)	2.34	**1.8**	-----	-----	-----	-----
Salt & Pepper (3%)	3.91	**3.2**	-----	-----	-----	-----
Salt & Pepper (4%)	4.68	**4.4**	-----	-----	-----	-----
Salt & Pepper (5%)	8.59	**8.1**	-----	-----	-----	-----

5.5.3 Comparison with alternative schemes

Here, the suggested technique was compared with eleven different watermarking schemes. Results highlighted in bold values indicate the better performance of the proposed technique.

5.5.3.1 Comparison with Fazlali et al. [144], Kang et al. [153] and Yadav et al. [131]

Firstly the performance was compared with a hybrid watermarking scheme Fazlali et al. [144]. The images ‘Baboon’, ‘Barbara’ and ‘Lena’ were used to embed a watermark length of 128 bits. Table 5.3 displayed the comparison outcomes for Scaling and JPEG compression attacks. It was perceived that BER (%) of extracted watermark of proposed technique gave better results. The next comparison was done with Kang et al. [153] for host images ‘Baboon’ and ‘Lena’ with a watermark of size 32×32. The values of NCC as well as BER (%) of the proposed technique again outperformed under Compression, Median Filter, and Salt &Pepper attacks as given in Table 5.4. The BER (%) of extracted watermark ‘TIET’ was also compared with Yadav et al. [131] in Table 5.3 for ‘Baboon’, ‘Barbara’ and ‘Lena’ images. The performance was again highlighted under JPEG Compression, Scaling, and AWGN attacks.

5.5.3.2 Comparison with Elshazly et al. [140], Wang et al. [154], Yuan et al. [155] and Zhang et al. [156]

Better values of NCC of watermarked image Lena using watermark Copyright (20×50) were also given by Elshazly et al. [140] under different QF's of Compression in Table 5.4. Finally, different values of NCC of images ‘Lena’ and ‘Goldhill’ using binary watermark of size 64×64 were also compared with Wang et al. [154],Yuan et al. [155] and Zhang et al. [156] . The results in Table 5.4 again outperformed for JPEG Compression, Median Filtering (3×3, 4×4 and 5×5), Salt Pepper, and Scaling attacks.

5.5.3.3 Comparison with Bi et al. [158], Nezhadarya et al. [124], Amirmazlaghani et al. [31], and Chen et al. [157]

Though the achievement of the proposed technique was evaluated across various common intrusions mentioned above, finally the robustness of the technique was tested against the most difficult and practical geometric attack i.e. Rotation. The BER

(%) of the reclaimed watermark (64 bits) of the suggested technique using Formulae H1, H2, H3, and H4 were compared with different angles (in degrees) of rotation attack with Bi et al. [158] for image 'Lena'. They used Multi Wavelet Transform (MWT) and Empirical Mode Decomposition (EMD) method of watermark embedding. The outputs were given in Table 5.5.

The merits of BER (%) of the recovered watermark (256 bits) were also compared with those given by Nezhadarya et al. [124] at -0.5^0 and 0.5^0 under rotation attack given in Table 5.5. Two different methods (GDWM0 &GDWM) were used for image 'Lena'. The Table also lists the values of BER (%) of the recovered watermark (128 bits) for image 'Barbara' when compared with Amirmazlaghani et al. [31].

Lastly, Tables 5.4, 5.5 and 5.6 demonstrated desirable values of NCC and BER(%) for image 'Barbara' using watermarks 'TIET' and 'Cameraman' using Formulae H1, H2, H3, and H4 as compared with the average value given by Chen et al. [157] and Yadav et al. [101]. It was realized that the prospective technique was not much stable facing rotation attacks because the transformation combination was variant to rotation.

5.6 DISCUSSION OF RESULTS

The implementation of the proposed technique was evaluated through the standard for the watermarked images for sizes (512 × 512) and (1024 × 1024) for robustness against various attacks. Filtering and Sharpening attacks using all HSF's have provided more desirable and stable values of IQA parameters with minimum BER of recovered watermarks for (1024 × 1024) size host images than of size (512 × 512). Under AWGN and Scaling attacks too, these parameters displayed profitable values of NCC, SSIM, GMSD, and UIQI for minimum variation in PSNR using all HSF's. However, H3 and H4 provided better BER values of recovered watermarks under these attacks than H1 and H2 for (1024 × 1024) size host images. These parameters were again observed to be useful under JPEG Compression, Salt & Pepper, and Rotation attacks. All HSF's have proved to furnish minimum values of GMSD and BER of watermarked images and recovered watermarks respectively under different geometric attacks shown in the Tables above. The performance was also verified by collating the achieved results with other alternative schemes which exhibited that the proposed technique outperformed against Scaling, JPEG Compression, and Rotation attacks.

5.7 APPLICATION FOR TELE-MEDICINE

The comparison given in Tables 5.3, 5.4, 5.5 and 5.6 demonstrated that though the methods were not much robust against rotation attacks, still the proposed technique exhibited better stability against these schemes. Thus, unlike previous chapters, the proposed technique again found suitable applications in the field of medicine.

In this section, three medical host images, namely, ‘Liver1’, ‘MRI Brain’ and ‘X-Ray’ were used for two watermarks, ‘Copyright’ and ‘Patient watermark’ as shown in Figure 5.11 and Figure 5.12. Similar to the proposed technique, the first degree of disintegration of Daubechies wavelet was utilized for computation of 2-D DWT of medicinal images. The low frequency coefficients were again transformed through FWHT. The watermark bits were inserted into these coefficients to obtain the watermarked images. The watermarked genre of entire medicinal images and the recuperated watermarks using HSF’s were displayed in Figure 5.12.

(a) (b) (c)

Figure 5.12 Medicinal images utilized (a) ‘Liver1’, (b) ‘MRI Brain’, (c) ‘X-Ray’.

(a) (b)

Figure 5.13 Watermarks used (d) ‘Copyright’ (20 × 50) (e) ‘Patient watermark’ (18 × 25).

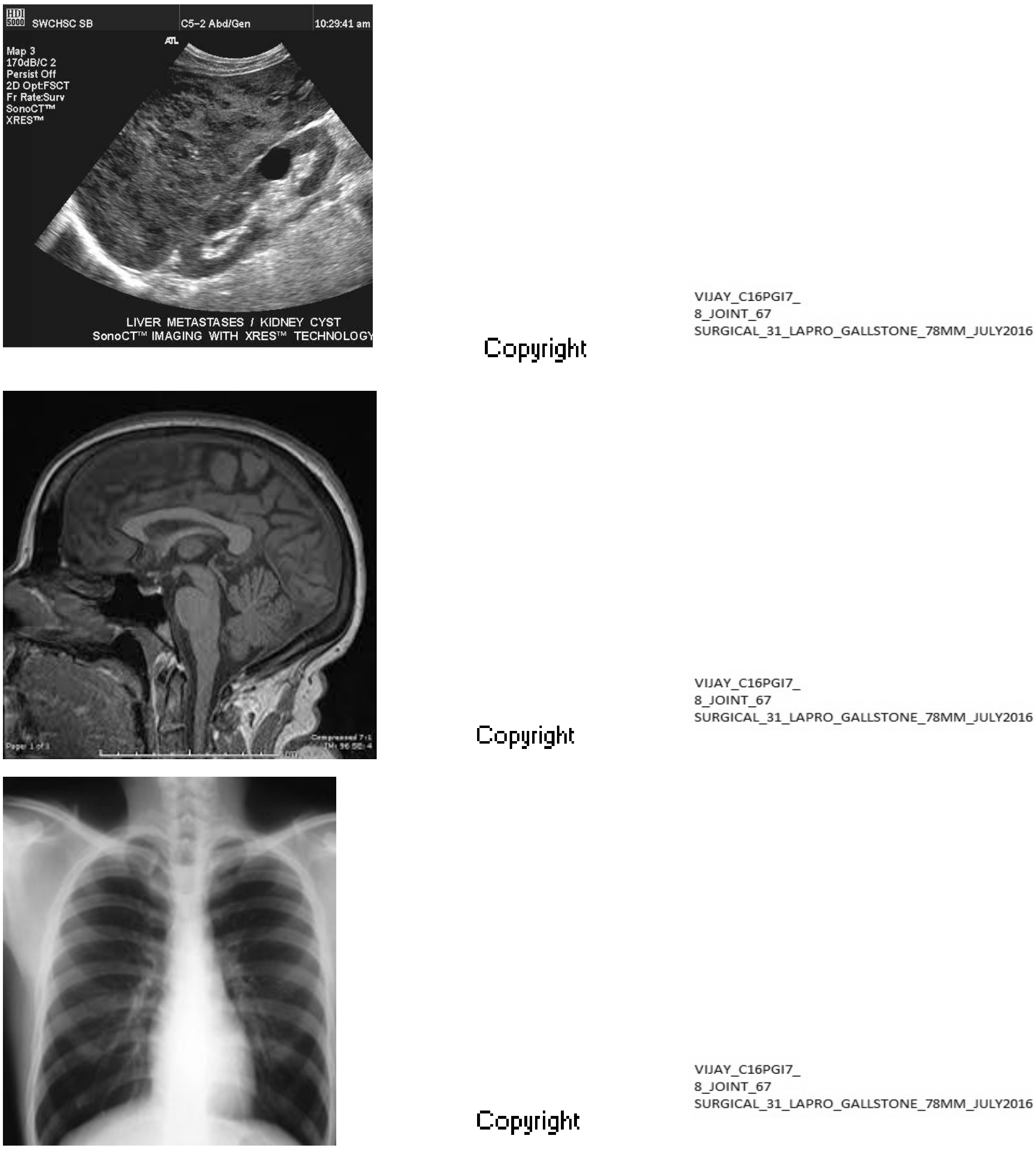

Figure 5.14 Medicinal images after watermarking and recuperated watermarks with HSF (H1, H2, H3 and H4).

Table 5.7 IQA parameters for Medical Host Images for size (512 × 512) under no attacks.

→ IQA Parameters ↓ Standard image with watermark	Formulae Used	PSNR (dB)	NCC	SSIM	GMSD	UIQI	BER (%) of recovered watermark
LIVER 1 (Using 'Copyright', and 'Patient watermark') at 512 ×512	H 1 H 2 H 3 H 4	45,45 45,45 45,45 45,45	0.9996,0.9988 0.9989, 0.9989 0.9955,0.9987 0.9957,0.9988	0.9996,0.9996 0.9996,0.9996 0.9995,0.9994 0.9995,0.9995	0.00483,0.0087 0.00503,0.00683 0.00463,0.00746 0.0046,0.00682	0.9998,0.9999 0.9988,0.9999 0.9998,0.9998 0.9998,0.9987	1.2,1.11 3.9,9.11 0,0 0.1,0
MRI (Using 'Copyright', and 'Patient watermark') at 512 ×512	H 1 H 2 H 3 H 4	45,45 45,45 45,45 45,45	0.9928,0.9974 0.9930,0.9975 0.9924,0.9974 0.9928,0.9973	0.9983,0.9984 0.9982,0.9984 0.9977,0.9973, 0.9979,0.9975	0.00733,0.0085 0.00759,0.00847 0.00746,0.0103 0.00705,0.0103	0.9998,0.9998 0.9998,0.9998 0.9996,0.9995 0.9995,0.9996	1.9,3.33 1.9,5.33 0.4,0.22 0.7,0
XRAY (Using 'Copyright', and 'Patient watermark') at 512 ×512	H 1 H 2 H 3 H 4	45,45 45,45 45,45 45,45	0.9963,0.9984 0.9963,0.9984 0.9962,0.9948 0.9961,0.9984	0.9957,0.9948 0.9954,0.9947 0.9962,0.9949 0.9961,0.9947	0.0122,0.0178 0.0122,0.0183 0.001,0.0162 0.0102,0.0166	0.9999,0.9999 0.9999,0.9999 0.9999,0.9999 0.9999,0.9999	1.4,3.55 1,4.22 0,0 0.3,0

Table 5.8 BER (%) of Medical Watermarked Images under various attacks.

Attacks	Watermark 'Copyright'				Watermark 'Patient watermark"				Host image
	Using (H1)	Using (H2)	Using (H3)	Using (H4)	Using (H1)	Using (H2)	Using (H3)	Using (H4)	
Gauss (3×3)	11.5	12.3	4.39	4.7	8.66	14.8	4.44	5.33	Liver 1
Gauss (3×3)	4.7	4.2	1.5	1.7	7.77	8.88	0.66	1.55	MRI
Gauss (3×3)	7.5	7.5	2.2	2.1	8.38	9.11	4.2	4.2	XRAY
Median (7×7)	48.7	47.7	47	47.5	47.7	48	45.7	46.4	Liver 1
Median (7×7)	26.6	26.5	21.6	21.9	28.6	28.6	22	22.4	MRI
Median (7×7)	17.4	17.8	11.4	11.2	15.3	15.7	11.7	11.3	×RAY
Wiener (5×5)	36.4	36.1	32	33.1	31.55	32.44	28	28	Liver 1
Wiener (5×5)	18.1	16.9	13	13.9	22	20.44	15.11	15.5	MRI
Wiener(5×5)	13.5	13.5	8.3	7.9	11.33	11.33	7.33	6.66	XRAY
AWGN (10)	5.1	5	2.3	1.9	11.55	14.4	4.66	3.32	Liver 1
AWGN (10)	3.3	4	1.5	1.5	9.55	9.77	4.66	4.22	MRI
AWGN (10)	1.8	1.5	1	0.7	6.22	7.11	2.66	1.89	XRAY
JPEG (Q = 20%)	29.6	30.3	21.5	23	28.88	30.22	18.44	22.22	Liver 1

JPEG (Q = 20%)	26.6	26.7	19.1	19.8	23.77	22.44	12.88	13.11	MRI
JPEG (Q = 20%)	20.3	20.6	14.6	14.1	14.8	15.7	8	7.55	XRAY
Scale 0.75	16.9	17.8	9.1	9.8	13.55	17.11	11.33	10	Liver 1
Scale 0.75	6.3	5.8	1.3	1.8	6.44	8.44	0.22	0.66	MRI
Scale 0.75	6.6	5.89	0.20	0	5.11	6.44	0	0	XRAY
Scale 2	8.3	11.8	4.7	4	7.55	13.3	5.33	5.77	Liver 1
Scale 2	4.3	5.2	0.8	1.3	4.4	7.55	0	0.22	MRI
Scale 2	5.5	6.3	0	0.2	4.66	5.33	0	0	XRAY
Sharp	12.1	12.1	12	12	32	32	32.22	32.22	Liver 1
Sharp	10.1	10.1	10.1	10.1	31.11	31.11	31.11	31.11	MRI
Sharp	10.2	10.2	10.2	10.2	31.33	31.33	31.33	31.33	XRAY
Rot. Ang. 5 (in deg.)	52.1	52.6	52	52.7	51	51.6	51.7	51.4	Liver 1
Rot. Ang. 5 (in deg.)	53	53.6	53.9	53.5	52.4	52.3	52	52.1	MRI
Rot. Ang. 5 (in deg.)	53.8	53.7	53	53	52.7	52.2	52.4	52.4	XRAY

Table 5.9 Watermarked Medicinal images with recuperated watermarks against different assaults of Gauss Filter (3×3), Scaling (0.75), JPEG (QF=20%) and AWGN (σ_n=10).

		
		
		
	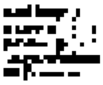	
	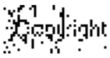	

The accomplishment benchmarks, like, 'PSNR', 'SSIM', 'NCC' as well as 'GMSD' for the watermarked images were listed in Table 5.7. It was again noticed that entire watermark amalgamations presented advisable merits for graded parameters. The capacity of the suggested approach for medicinal watermarking was examined afresh with various assaults in Table 5.8. The assaulted merits for NCC, as well as, SSIM approached the original merit of one. Superior merits for PSNR ascertained invisibility with minimal constants of GMSD against JPEG Comp., AWGN, Scale, Sharp, and Filter assaults. The assailed images after watermarking with their recuperated watermarks were displayed in Table 5.9.

5.8 SUMMARY

In the indicated study, an unfamiliar partially blindfolded hybrid image-adaptive watermarking scheme was proposed for greater robustness. The main benefactions of the proposed scheme using the combination of two transforms, DWT and FWHT included, firstly the calculation of four adjustable hybrid strength factors using the first, second and fourth statistical moments. These factors assisted in embedding the watermark bits at 45dB using Gaussian modeling in LL and LH sub bands simultaneously. Secondly, a statistical decoder established on the convention of maximum likelihood was used for successful watermark eradication at minimum error and deviation values. The results were best obtained using HSF 4. The stability of the technique was also examined across the various common attacks. The results too demonstrated excellent resistance for geometrical attacks such as Salt & Pepper, Rotation, etc with superior performance by NCC, SSIM and UIQI values at unity. A trade-off amongst good imperceptibility and high robustness was easily attained in the proposed method.

In the next chapter, an improvement of the hybrid watermarking technique using DWT and FWHT has been proposed for two watermarks using a new hybrid strength factor. The technique again proves robust against geometric attacks and thus, finds useful applications in the field of telemedicine.

CHAPTER 6

IMPROVED HYBRID IMAGE-ADAPTIVE WATERMARKING WITH TWO WATERMARKS USING STATISTICAL DECODER

This chapter presents an upgraded hybrid image-adaptive watermarking technique where duplet watermarks were inserted simultaneously into the blocks of dimension (8×8) of a natural image. Hybridization of two transforms DWT and FWHT were used to intensify the invisibility of the watermarked images. A new Adaptive Hybrid Strength Factor (AHSF) based upon entropy and kurtosis was used to insert the watermarks to refine the robustness and safety of the proposed watermarking technique. Similar to the previous techniques, a partial blind approach was used to insert the watermarks through Gaussian modeling using AHSF with the help of limited side information. The maximum likelihood approach was used to recover the watermarks with the help of a statistical decoder. The effectiveness of the suggested work was assessed and compared by superior simulation outcomes utilizing different IQA parameters against various assaults. Lastly, the suggested scheme was executed upon medicinal applications due to greater performance over existing methods.

6.1 INTRODUCTION

In the era of digital communication, the rapid use of multimedia information exposed digital images for easy manipulation [159] and duplication [160]. The purpose of robust image watermarking was to protect the owner copyrights with the high security from unauthorized access. In general, a desirable watermarking technique must fulfill the requirements of imperceptibility, robustness, and security with increased capacity. While the robustness and security of the watermarking technique referred to the ability of resistance against various attacks and unauthorized watermark extraction respectively, the increased capacity touched upon a greater number of watermark bits inserted.

In this chapter, a hybrid combination of two frequency transforms were used to embed duplet watermarks for the purpose of protecting copyright, enhancing security as well as improving robust nature. The classification of the suggested approach was partially sighted which omitted the requirement for characteristics of the natural image at the destination. Similar to the previous techniques, the proposed work also the benefits of two transforms to improving the performance of the watermarked image. The ML decoder established upon the model of analytical approach helped in the extraction of the watermarks with recommended performance.

6.2 SIGNIFICANCE OF ADAPTIVE HYBRID STRENGTH FACTOR (AHSF)

The value of the Adaptive Hybrid Strength Factor (AHSF) was calculated using the image-adaptive characteristics of the host image. Similar to the previous technique, AHSF was determined from entropy and kurtosis of FWHT coefficients obtained from the blocks with high entropy of the original image and expressed as,

$$AHSF\ (or\ H_5)\ =\ H_i/(Kurtosis_{max})^{\rho} \tag{6.1}$$

Here, H_i is the entropy of FWHT parameters (F) of each i^{th} slab. $Kurtosis_{max}$ represented the peak value of kurtosis for all chosen blocks of FWHT parameters (F). ρ was the inconsistent criterion in the denominator utilized for inserting bits of watermarks. This was called as Hybrid Formula H5 given in (6.1).

6.3 PROPOSED WATERMARKING APPROACH

The watermarking technique of the upgraded hybrid image-adaptive approach has been explained here in two different sub sections, the namely hybrid process of watermark embedding and watermark extraction respectively. Section 6.3.1 described the process of inserting the two watermarks into the natural image. This image was subjected to various attacks before it reached its destination. The assailed watermarked image was received by the statistical decoder for successful extraction of the watermark in Section 6.3.2.

6.3.1 Hybrid Process of Watermark(s) Embedding

The proposed technique of inserting the watermark (shown in Figure 6.1 (a)) was elucidated in the points below;

1: The Host Image (HI) of dimension (N × N) was partitioned into slabs of proportion (8 × 8).

2: High entropy blocks were selected: Entropy (H) is described as the average details present in every source of the output. It was calculated for each block separately to determine a mean value. It helped in indicating the inclination of the parameters in bunching around restricted merit in a particular disintegration. A cubicle arrangement was devised containing blocks with entropy greater than the mean value. The sequence of these blocks was formed by scrutinizing every row step by step, thus forming the initial supporting information in Step 8.

3: DWT was applied on blocks with high entropy: 2-D DWT was appertained on blocks with high entropy to invisibly embed the watermarks into various regions of the anchor image. Hence, single level DWT was practiced on chosen blocks with large entropy to decompose within four recurrence sub-bands. These were expressed as $(HI)^{LL}$, $(HI)^{LH}$, $(HI)^{HL}$, and $(HI)^{HH}$.

4: FWHT was applied on LL and LH sub-band parameters: The LL, as well as LH recurrence parameters, namely $(HI)^{LL}$ and $(HI)^{LH}$ obtained through DWT, were again transformed using FWHT. These modified coefficients were again assumed as W_{LL} and W_{LH} respectively.

5: FWHT coefficients (W_{LL} and W_{LH}) were modeled using Normal (or Gaussian) distribution: The PDF of the distribution expressed in (6.2) used mean (μ) and standard deviation (σ) as its Gaussian parameters in image watermarking.

$$f(z|\mu\,,\sigma^2) = \frac{1}{\sqrt{2\pi\sigma^2}}e^{\frac{-(z-\mu)^2}{2\sigma^2}} \tag{6.2}$$

Similar to Chapters 4 and 5, the FWHT coefficients (W_{LL} and W_{LH}) were too modeled using Gaussian distribution as $W_{LL}{\sim}N(\mu_{LL},{\sigma^2}_{LL})$ and $W_{LH}{\sim}N(\mu_{LH},{\sigma^2}_{LH})$. This statistical approach helped to determine the values of μ and σ accurately, though the same may be calculated from equation (6.3) also.

$$\bar{X}(or\ \mu) = (\textstyle\sum_{i=1}^{N} x_i)/N \quad , \quad \sigma = \sqrt{\frac{\sum_{i=1}^{N}(x_i-\bar{X})}{N}} \tag{6.3}$$

These parameters formed the second important side information along with Step 2. The side information is prepared in Step 8.

6: AHSF was calculated using transformed LL and LH coefficients: The value of adaptive hybrid strength factor was calculated using the image-adaptive characteristics of the host image. AHSF was determined using (6.1). The calculated value was unique for each sub band.

7: Bits of the First watermark were embedded into W_{LL} coefficients: The Algorithm for embedding the first watermark was given by the following Rules:

Rule 1: Calculated AHSF defined by (6.1).

The calculated number of blocks, BLK= (size of host image N × N)/(size of blocks)
Rule 2: The following Embedding Algorithm was used in LL sub band

Input-W_{LL} , AHSF, BLK, wm

1.	for i_d=1:BLK
2.	while i_d<= length (wm)
3.	If wm(1,id)==1
4.	W_{LL} = W_{LL} (1+AHSF)
5.	else if wm(1,id)==0
6.	W_{LL} = W_{LL} (1-AHSF)
7.	end (if)
8.	end (while)
9.	end (for)

Output- Hybrid Watermarked image(WI $_{LL}$), $\mu_{LL}, \sigma^2{}_{LL}$

Here, W_{LL} were modified FWHT coefficients for LL sub band, wm represented bits of the first watermark and AHSF denoted Adaptive Hybrid Strength Factor.

Thus, the FWHT coefficients (W_{LL}) were modified by bits '1'and'0' according to the following embedding rules

$$W_{LL} = W_{LL}.(1 + AHSF), W_{LL} = W_{LL}.(1 - AHSF) \tag{6.4}$$

9: Bits of the Second watermark were embedded into W_{LH} coefficients: The Algorithm for embedding the second watermark was given by the following Rules:

Rule 3: Calculated AHSF defined by (6.1). The calculated number of blocks, BLK= (size of host image N×N)/(size of blocks)
Rule 4: The following Embedding Algorithm was used in LH sub band

Input-W_{LH} , AHSF, BLK, wm

1.	for i_d=1:BLK
2.	while i_d<= length (wm)
3.	If wm(1,id)==1
4.	W_{LH} = W_{LH} (1+AHSF)
5.	else if wm(1,id)==0
6.	W_{LH} = W_{LH} (1-AHSF)
7.	end (if)

8.	end (while)
9.	end (for)

Output- Hybrid Watermarked image(WI $_{LH}$), $\mu_{LH}, \sigma^2{}_{LH}$

Here, W_{LH} was modified FWHT coefficients for LH sub band, wm represented bits of the first watermark and AHSF denoted Adaptive Hybrid Strength Factor.

Thus, the FWHT coefficients (W_{LH}) were modified by bits '1'and'0' according to the following embedding rules,

$$W_{LH} = W_{LH}.(1 + AHSF), W_{LH} = W_{LH}.(1 - AHSF) \qquad (6.5)$$

10: Side Information was prepared: Since the proposed technique is partially blind, finite side information was also transported with the image after watermarking to the destination. Thus, the supporting information was prepared from Steps 2 and 5 consisting of positions of blocks with large entropy and means and variances for W_{LL} and W_{LH} coefficients.

11: Inverse FWHT and Inverse DWT were applied: Once the watermark bits were embedded, IFWHT and IDWT were appealed upon the transformed slabs to get $(WI\_AI)^{LL,}$ $(WI\_AI)^{LH}$, $(WI\_AI)^{HL}$, and $(WI\_AI)^{HH}$. The quantity of blocks with large entropy selected was always equivalent to the numeral of bits of a watermark to be embedded. All the transformed blocks were later re-coupled along the resting blocks to obtain the image after watermarking in (6.6).

$$WI = \{\iint_{m=0}^{M-1} WI\_HI^{LL}, WI\_HI^{LH}, WI\_HI^{HL}, WI\_HI^{HH}\} \qquad (6.6)$$

12: Final watermarked image was transmitted: The final watermarked image was communicated to the receiver along with the sidewise information arranged in Step 8.

6.3.2 Hybrid Process of Watermark(s) Extraction

The proposed technique of extracting the watermarks (shown in Figure 6.2) was explained in the following steps;

1: Watermarked image (WI') was partitioned with N rows and N columns (N ×N) with (8 × 8) dimension blocks.

2: Blocks with large entropy were selected: The secondary information communicated besides the image after watermarking contained the positions for high entropy blocks of the host image. This information helped to resolve the blocks of large entropy in the collected image also after watermarking.

3: DWT was applied upon blocks with high entropy in the watermarked image: Similar to the steps of embedding, a single level DWT was again applied upon the blocks of large entropy of the received watermarked image to decompose into four sub bands. These were expressed as, $(WI')^{LL}$, $(WI')^{LH}$, $(WI')^{HL}$, and $(WI')^{HH}$. These LL and LH frequency coefficients were used as quoted in Step 4 of Section 6.1.1.

4: FWHT was applied on LL and LH sub band coefficients: The frequency parameters for the image after watermarking as $(WI')^{LL}$ and $(WI')^{LH}$ were obtained from DWT after the application of FWHT. The bits of the first and second watermarks were inserted imperceptibly into a small area of the transformed coefficients.

5: FWHT coefficients ($(WI')^{LL}$ and $(WI')^{LH}$) were modeled using Normal (or Gaussian) distribution parameters: Similar to the process of insertion, mean and variance were again obtained from FWHT coefficients ($(WI')^{LL}$ and $(WI')^{LH}$) of the received image after watermarking using the modeling of Gaussian distribution as $WI_{LL}'\sim N(\mu_{LL}',{\sigma^2}_{LL}')$ and $WI_{LH}'\sim N(\mu_{LH}',{\sigma^2}_{LH}')$. These were assumed as (μ_{LL}', μ_{LH}') and $({\sigma^2}_{LL}', {\sigma^2}_{LH}')$ respectively.

6: Mathematical Modeling of ML Decoder for watermark extraction: The features of Gaussian distribution transmitted in the side information (μ_{LL}, $\sigma^2{}_{LL}$) and (μ_{LH}, $\sigma^2{}_{LH}$) were compared with the Normal distribution parameters of the received watermarked image $(\mu_{LL}',{\sigma^2}_{LL}')$ and $(\mu_{LH}',{\sigma^2}_{LH}')$.The watermark bits '1' and '0' of first and second marks were embedded in W_{LL} and W_{LH} frequency coefficients using multiplicative embedding as,

$$W_{LL\,i/0} = W_{LL\,i}.(1 - AHSF)\sim N(\mu_{\underline{LL\,i}_0}, \sigma_{\underline{LL\,i}_0}),$$

$$W_{LL\,i/1} = W_{LL\,i}.(1 + AHSF)\sim N(\mu_{LLi/1}, \sigma_{LLi/1}) \tag{6.7}$$

$$W_{LH\,i/0} = W_{LH\,i}.(1 - AHSF)\sim N(\mu_{\underline{LH\,i}_0}, \sigma_{\underline{LH\,i}_0}),$$

$$W_{LH\,i/1} = W_{LH\,i}.(1 + AHSF)\sim N(\mu_{LHi/1}, \sigma_{LHi/1}) \tag{6.8}$$

Thus, the W_{LL} parameters in every slab with M coefficients w_{LL1}, w_{LL2}, w_{LL3},…..w_{LLM}, assumed as 'i.i.d.' for embedding bits '0' and '1' are given as,

$$P(W_{LL1}, W_{LL2}, W_{LL3}, \ldots W_{LLM}|0) = \prod_{i=1}^{M} \sqrt{2\pi\sigma^2_{W_{LL}|0}} \frac{1}{e^{-(W_{LL})_i-(1-AHSF)\mu_{LL})^2}/2\sigma^2_{(W_{LL})|0}}$$

$$P(W_{LL1}, W_{LL2}, W_{LL3}, \ldots W_{LLM}|1) = \prod_{i=1}^{M} \sqrt{2\pi\sigma^2_{W_{LL}|1}} \frac{1}{e^{-(W_{LL})_i-(1+AHSF\,)\mu_{LL})^2}/2\sigma^2_{(W_{LL})|1}} \tag{6.9}$$

Similarly, the W_{LH} parameters in every slab with M coefficients w_{LH1}, w_{LH2}, w_{LH3},…..w_{LHM}, assumed as 'i.i.d' for embedding bits '0' and '1' are given as,

$$P(W_{LH1}, W_{LH2}, W_{LH3}, \ldots W_{LHM}|0)$$

$$= \prod_{i=1}^{M} \sqrt{2\pi\sigma^2_{W_{LL}|0}} \frac{1}{e^{-(W_{LH})_i-(1-AHSF)\mu_{LH})^2} / 2\sigma^2_{(W_{LH})|0}}$$

$$P(W_{LH1}, W_{LH2}, W_{LH3}, \ldots W_{LHM}|1) = \prod_{i=1}^{M} \sqrt{2\pi\sigma^2_{W_{LH}|1}} \frac{1}{e^{-(W_{LH})_i-(1+AHSF)\mu_{LH})^2} / 2\sigma^2_{(W_{LH})|1}} \quad (6.10)$$

Thus, the maximum likelihood decision for W_{LL} and W_{LH} coefficients is given as,

$$P(W_{LL1}, W_{LL2}, W_{LL3}, \ldots W_{LL}M|1) \begin{matrix} > 1 \\ < 0 \end{matrix} P(W_{LL1}, W_{LL2}, W_{LL3}, \ldots W_{LL}M|0)$$

and

$$P(W_{LH1}, W_{LH2}, W_{LH3}, \ldots W_{LH}M|1) \begin{matrix} >1 \\ <0 \end{matrix} P(W_{LH1}, W_{LH2}, W_{LH3}, \ldots W_{LH}M|0) \quad (6.11)$$

Substituting (6.10) in (6.11),

$$\prod_{i=1}^{M} \sqrt{2\pi\sigma^2_{W_{LL}|1}} \frac{1}{\frac{e^{-(W_{LL})_i-(1+AHSF)\mu_{LL})^2}}{2\sigma^2_{W_{LL}|1}}} \begin{matrix} >1 \\ <0 \end{matrix} \prod_{i=1}^{M} \sqrt{2\pi\sigma^2_{W_{LL}|0}} \frac{1}{\frac{e^{-(W_{LL})_i-(1-AHSF)\mu_{LL})^2}}{2\sigma^2_{W_{LL}|0}}}$$

and

$$\prod_{i=1}^{M} \sqrt{2\pi\sigma^2_{W_{LH}|1}} \frac{1}{\frac{e^{-(W_{LH})_i-(1+AHSF)\mu_{LH})^2}}{2\sigma^2_{W_{HL}|1}}} \begin{matrix} >1 \\ <0 \end{matrix} \prod_{i=1}^{M} \sqrt{2\pi\sigma^2_{W_{LH}|0}} \frac{1}{\frac{e^{-(W_{LH})_i-(1-AHSF)\mu_{LH})^2}}{2\sigma^2_{W_{LH}|0}}} \quad (6.12)$$

Applying logs, (6.12) is rewritten as

$$\frac{(-M)}{2}\ln\left(\sigma^2_{W_{LL}|1}\right)\frac{1}{\sigma^2_{W_{LL}|1}}\sum_{i=1}^{M}(W_{LL})_i -$$

*1+AHSFμLL)2>1<0(−M)2*ln*σWLL|021σWLL|02i=1M(WLL)i −−AHSFμLL)2*

and

$$\frac{(-M)}{2}\ln\left(\sigma^2_{W_{LH}|1}\right)\frac{1}{\sigma^2_{W_{LH}|1}}\sum_{i=1}^{M}(W_{LH})_i -$$

*1+AHSFμLH)2>1<0−M2*ln*σWLH|021σWLH|02i=1MWLHi −−AHSFμLH)2*

(6.13)

Simplifying the equations above, it is observed

$$\left(\frac{1}{\sigma^2_{W_{LL}|0}} - \frac{1}{\sigma^2_{W_{LL}|1}}\right)\sum_{i=1}^{M}(W_{LL})^2_i - 2\mu_{LL}\left\{\frac{(1-AHSF)}{\sigma^2_{W_{LL}|0}} -\right.$$

(1+AHSF)σWLL|12i=1M(WLL)i>1<0M ln*σWLL|12σWLL|02−MμLL2*

(1−AHSF)2σWLL|02−(1+AHSF)2σWLL|12

and

$\left(\frac{1}{\sigma^2_{W_{LH}|0}} - \frac{1}{\sigma^2_{W_{LH}|1}}\right)\sum_{i=1}^{M}(W_{LH})_i^2 - 2\mu_{LH}\left\{\frac{(1-AHSF)}{\sigma^2_{W_{LH}|0}} -\right.$

(1+AHSF)σWLH|12i=1M(WLH)i>1<0M ln*σWLH|12σWLH|02−MμLH2*

(1−AHSF)2σWLH|02−(1+AHSF)2σWLH|12 (6.14)

If the merit for noisy variances approximated null for the restricting instance of large SNR,

$$\sigma^2_{W_{LL}|1} = (1 + AHSF)^2\sigma^2 \quad , \ \sigma^2_{W_{LL}|0} = (1 - AHSF)^2\sigma^2 \qquad (6.15)$$

$$\sigma^2_{W_{LH}|1} = (1 + AHSF)^2\sigma^2 \quad , \ \sigma^2_{W_{LH}|0} = (1 - AHSF)^2\sigma^2 \qquad (6.16)$$

Thus for LL sub band, (6.14) was rewritten for bits ‘zero’ and ‘one’ respectively as,

$\frac{1}{{\sigma_{LL}}^2(1-AHSF)^2}\sum_{i=1}^{M} {W_{LL}}_i^2 - \frac{2\mu_{LL}}{(1-AHSF){\sigma_{LL}}^2}\sum_{i=1}^{M} {W_{LL}}_i < (-2M)\{\ln \sigma_{LL} \ln(1 - AHSF)\} -$

MμLL2σLL2

(6.17)

$\frac{(-1)}{{\sigma_{LL}}^2(1+AHSF)^2}\sum_{i=1}^{M} {W_{LL}}_i^2 + \frac{2\mu_{LL}}{(1+AHSF){\sigma_{LL}}^2}\sum_{i=1}^{M} {W_{LL}}_i > (2M)\{\ln\sigma_{LL} + \ln(1 + AHSF)\} +$

MμLL2σLL2

(6.18)

Similarly, for LH sub band, (6.14) was rewritten for bits ‘zero’ and ‘one’ respectively as,

$\frac{1}{{\sigma_{LH}}^2(1-AHSF)^2}\sum_{i=1}^{M} {W_{LH}}_i^2 - \frac{2\mu_{LH}}{(1-AHSF){\sigma_{LH}}^2}\sum_{i=1}^{M} {W_{LH}}_i < (-2M)\{\ln \sigma_{LH} + \ln(1 -$

AHSF)}−MμLH2σLH2

(6.19)

$\frac{(-1)}{{\sigma_{LH}}^2(1+AHSF)^2}\sum_{i=1}^{M} {W_{LH}}_i^2 + \frac{2\mu_{LH}}{(1+AHSF){\sigma_{LH}}^2}\sum_{i=1}^{M} {W_{LH}}_i > (2M)\{\ln\sigma_{LH} + \ln(1 +$

AHSF)}+MμLH2σLH2

(6.20)

Similar to Chapter 5, the ML decoder again became independent of the AHSF as the latter approached zero at high SNR for the successful watermark. The Algorithm for Extraction of the watermark(s) is given below.

The following Watermark Extraction Algorithm was used for the first watermark.

Input-W_{LL}*’, length(wm1), BLK,* μ_{LL}, ${\sigma_{LL}}^2$

1.	for i_{dx}=1:BLK
2.	while i_{dx}<= length (wm1)
3.	If μ_{LL}> μ_{LL}*’ then*

4.	Extracted_watermark 1 $ERW_{LL}(1, i_{dx})$==1
5.	else Extracted watermark1 $ERW_{LL}(1, i_{dx})$==0
6.	$i_{dx}= i_{dx}+1$
	Extracted_watermark1={(wm1)*length(wm1)}
7.	end (if)
8.	end (if)
9.	end (for)

Output- Recovered Watermark1

The following Watermark Extraction Algorithm was used for the second watermark.

Input-W_{LH}', length(wm2), BLK, μ_{LH}, σ_{LH}^2

1.	for i_{dx}=1:BLK
2.	while i_{dx}<= length (wm2)
3.	If $\mu_{LH} > \mu_{LH}'$ *then*
4.	Extracted_watermark2 $ERW_{LH}(1, i_{dx})$==1
5.	else Extracted watermark2 $ERW_{LH}(1, i_{dx})$==0
6.	$i_{dx}= i_{dx}+1$
	Extracted_watermark2={(wm2)*length(wm2)}
7.	end (if)
8.	end (if)
9.	end (for)

Output- Recovered Watermark2

Here, W_{LL}' and W_{LH}' represented the modified FWHT coefficients of watermarked Image (WI), length (wm1 and wm2) represented the length of first and second watermark bits, (μ_{LL}, μ_{LH},σ_{LL}^2, σ_{LH}^2), were the Gaussian distribution parameters (mean and variance) of Host Image (HI).

7: First and second extracted Watermarks were generated.

6.4 RESULTS AND DISCUSSION

In this chapter, 'Lena', 'Barbara', 'Baboon' as well as 'Peppers' were utilized along with three different gray-scale image watermarks 'TIET'(25 × 18), Copyright' (20 × 50), and 'Thapar_Univ'(80 × 20) as shown in Figure 6.3 to Figure 6.6. The size of all images was (512 × 512).

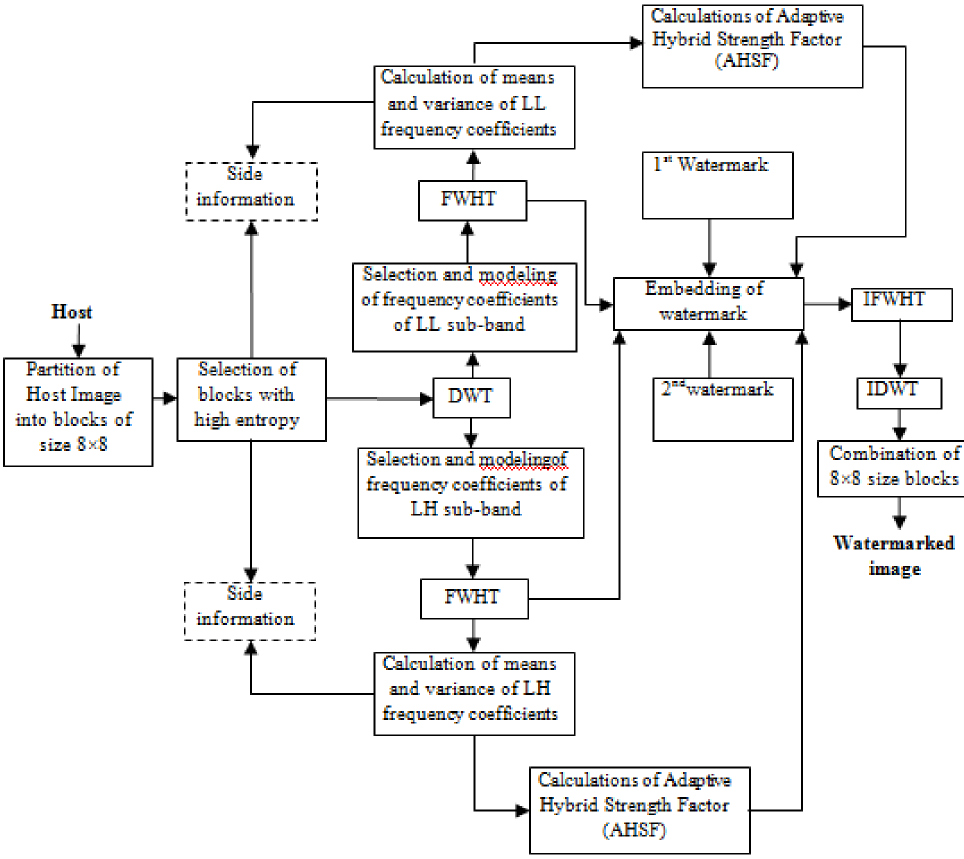

Figure 6.1 Block diagram of suggested work for watermarks insertion.

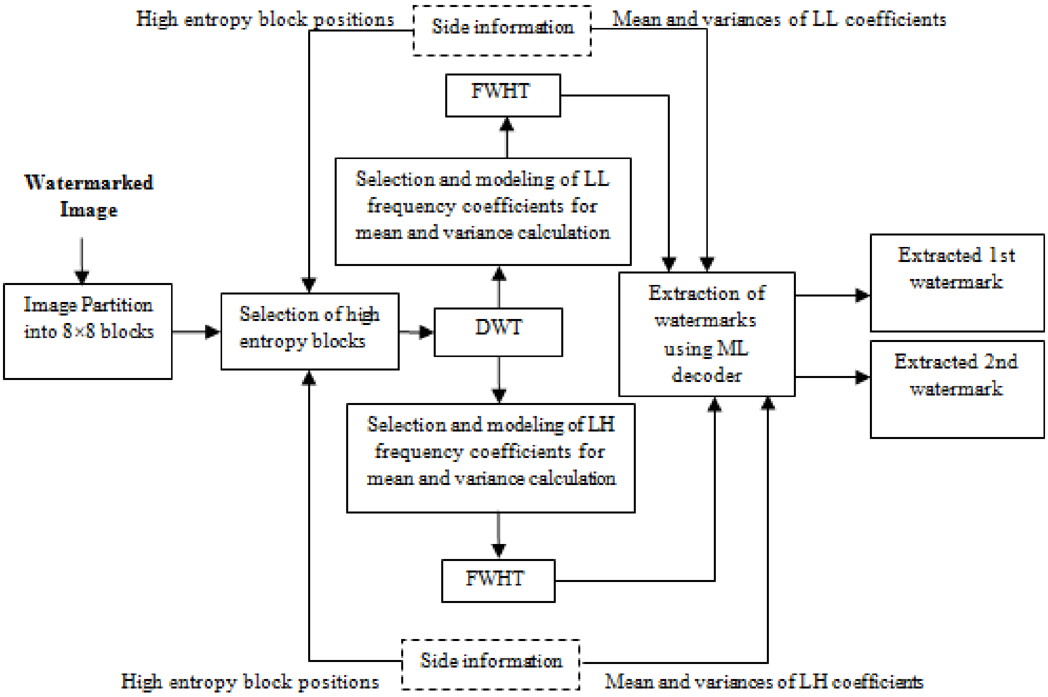

Figure 6.2 Block diagram of suggested work for watermarks recovery.

Similar to Chapter 4, a sole watermark ‘TIET’,’ Copyright’ or ‘Thapar_Univ’ was placed in the coefficients of frequency into the natural image. Subsequently, duplet watermarks were inserted into the approximating and vertically recurrence parameters at the same time, as displayed in Figure 6.1. The initial watermark was either of the above three dimensions introduced, though the secondary watermark utilized was ‘Logo’ (64 × 64).

Hence, overall three watermark combimations were utilized in inserting watermarks, as (‘TIET’ with ‘Logo’), (‘Copyright’ with ‘Logo’) as well as (‘Thapar_Univ with ‘Logo’). Figure 6.3 to Figure 6.5 displays the natural images, watermark(s), and watermark amalgamations utilized in the work. Alike the suggested experiment, ‘Patient watermark’ (18 × 25) as well as ‘Joint’ (32 × 32) [32] too were utilized as the sole amalgamation for inserting the watermarks. Figure 6.6 demonstrates these images.

The variation of ‘PSNR’ and ‘BER (in %)’ with ρ for the host images using all watermarks is displayed in Figure 6.7 to Figure 6.9. It was observed that as ρ increased, BER rises exponentially much later, with initially a linear increase in PSNR. Using (6.1), the values of ρ for ‘Lena’ and ‘Barbara’ utilizing watermarks ‘TIET’, ‘Copyright’ and ‘Thapar_Univ’ are (2.8, 2.8, 2.8) and (3, 3.3, 3.3) respectively. Similarly, for host images ‘Baboon’ and “Peppers’, the values are (3.8, 3.5, 2.7) and (2, 2.1, 2) correspondingly.

Nevertheless, when ‘TIET with ‘Logo’ was placed at the same time in recurrence parameters of every image, the merits of AHSF varied. This variation was different for every sub band in achieving the finest invisible image after watermarking with minimum BER for recuperated watermarks. The merits of ρ chosen for AHSF (s) of both subbands in the first watermark amalgamation were (4.2, 0.8), (4.1, 0.7), (3.1, 0.8) and (5.7, 0.9) for ‘Lena’, ‘Barbara’, ‘Peppers’, ‘Baboon’ correspondingly. Again for embedding ‘Copyright’ and ‘Thapar_Univ’(in LL sub-bands) with Logo (in LH sub-band) in the same host images, the values of ρ were grouped as (3.6,0.7), (3,0.6), (2.7,0.7), (2.9,0.7) and (2.7,0.7), (2.7,0.7), (2.1,0.6) and (3.5,0.6) respectively.

The effectiveness of the proposed technique was also proved by obtaining a few simulation results using host images of size (1024 × 1024). Tables 6.1, 6.2, 6.3, and 6.4 demonstrate the performance metrics of the proposed hybrid watermarking technique using two watermarks. It was noticed that the value of PSNR was obtained above the desired value of 45dB for all host images. The values of NCC, SSIM, and

UIQI of the watermarked images also approached the desirable value of unity for all size watermarks. The deviation in watermarked images and error values in the recovery of watermarks(s) known as GMSD and BER (%) also approached zero in most of the cases. The watermarked images and their extracted watermarks are shown in Table 6.5.

Figure 6.3 Standard images, ‘Lena’, ‘Barbara’, ‘Baboon’, ‘Peppers’.

Figure 6.4 Water marks utilized, ‘TIET’, ’Copyright’, ‘Thapar_Univ’ ,‘Logo’.

(a) (b) (c)

Figure 6.5 Water mark Amalgamations utilized: (a) (‘TIET’, ‘Logo’) (b) (‘Copyright’, ‘Logo’) and (c) (‘Thapar_Univ’, ’Logo’)

(a) (b)

Figure 6.6 Medicinal watermarks (a) ‘Patient watermark’ exhibiting attributes for the doctor, key of the hospital, the numeral of image and prognosis particulars of the victim, as well as (b) ‘Joint’ utilized for medicinal supplications.

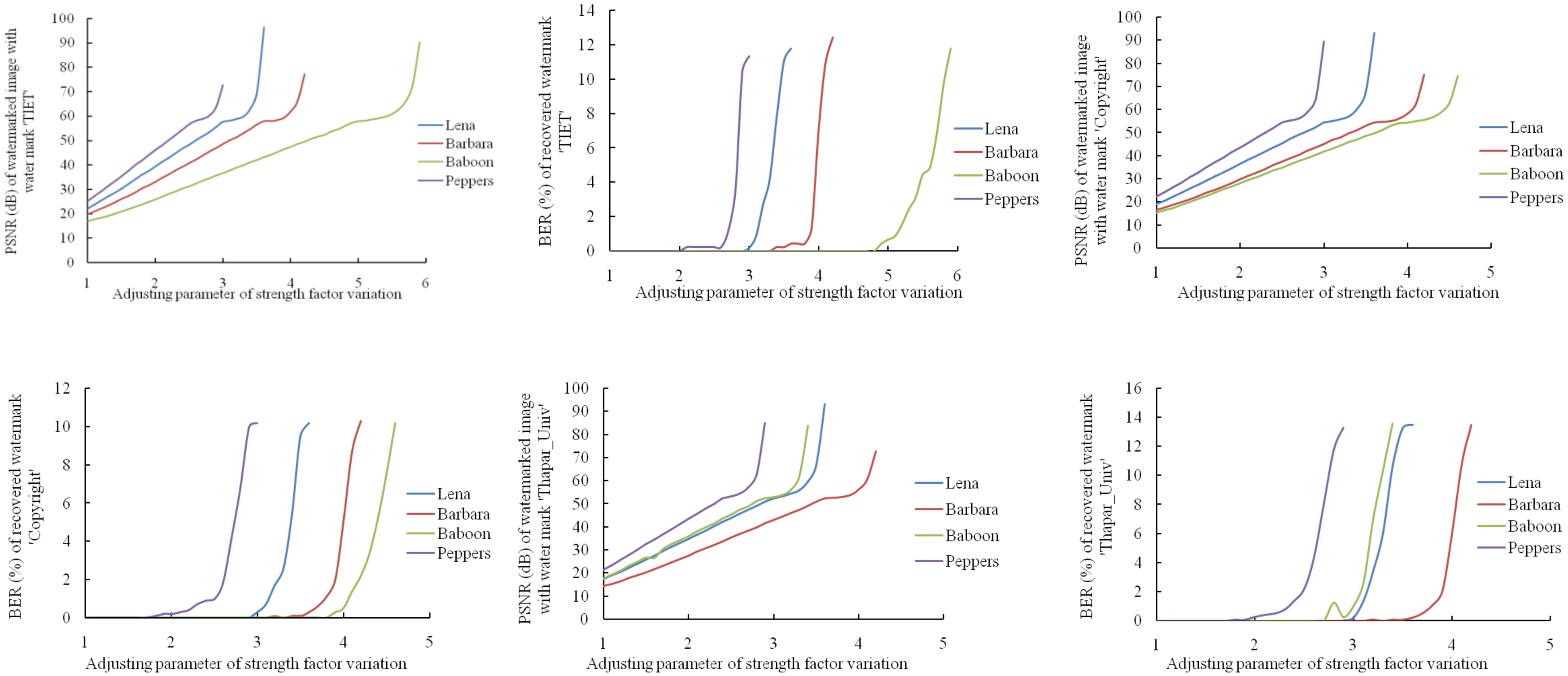

Figure 6.7 Plots of ‘PSNR (in dB)’ for images and ‘BER (%)’ for recuperated watermarks utilizing watermarks ‘TIET’, ‘Copyright’ as well as ‘Thapar_Univ’.

Table 6.1 'PSNR', 'NCC', 'SSIM' as well as 'GMSD' features for images besides 'BER (%)' for recuperated watermarks 'TIET', 'Copyright', 'Thapar_Univ' correspondingly for dimension (512 × 512).

→ Standard Parameters ↓ Host image with watermark	Dimension	'PSNR'	'NCC'	'SSIM'	'GMSD'	'UIQI'	'BER(%)' for recuperated watermark
'Lena'							
('TIET')	(512 × 512)	63.57	0.9989	0.9996	0.0024	0.9999	0
(' Copyright)'		50.61	0.9979	0.9991	0.00317	0.9999	0
('Thapar_Univ')		49.04	0.9972	0.9988	0.00358	0.9999	0
'Barbara'							
('TIET')	(512 × 512)	48.44	0.9985	0.9995	0.0037	0.9999	0
(' Copyright)'		49.64	0.9981	0.9996	0.00229	0.9999	0
('Thapar_Univ')		47.5	0.9972	0.9991	0.00372	0.9999	0
'Peppers'							
('TIET')	(512 × 512)	46.08	0.9974	0.9983	0.0075	0.9999	0
(' Copyright)'		45.74	0.9957	0.9981	0.00647	0.9999	0.3
('Thapar_Univ')		43.49	0.9940	0.9964	0.00948	0.9999	0.25
'Baboon'							
('TIET')	(512 × 512)	45.30	0.9975	0.9997	0.00537	0.00537	0
(' Copyright)'		48.62	0.9974	0.9998	0.00244	0.9999	0
('Thapar_Univ')		48.89	0.9970	0.9997	0.00218	0.9999	0

Table 6.2 'PSNR', 'NCC', 'SSIM' as well as 'GMSD' features for images besides 'BER (%)' for recuperated watermarks 'TIET', 'Copyright', 'Thapar_Univ' correspondingly for dimension (1024 × 1024).

→ Standard Parameters ↓ Host image with watermark	Dimension	'PSNR'	'NCC'	'SSIM'	'GMSD'	'UIQI'	'BER(%)' for recuperated watermark
'Lena'							
('TIET')	(1024× 1024)	50.03	0.9992	0.9986	0.00831	0.9999	0
(' Copyright)'		50.23	0.9988	0.9987	0.00627	0.9999	0
('Thapar_Univ')		51.19	0.9988	0.9988	0.00523	0.9999	0
'Barbara'							
('TIET')	(1024× 1024)	45.17	0.9988	0.9989	0.00931	0.9999	0
(' Copyright)'		51.04	0.9991	0.9996	0.00309	0.9999	0
('Thapar_Univ')		49.18	0.9988	0.9993	0.00414	0.9999	0
'Peppers'							
('TIET')	(1024× 1024)	47.58	0.9988	0.9983	0.0118	0.9999	0
(' Copyright)'		50.96	0.9988	0.9992	0.00428	0.9999	0
('Thapar_Univ')		46.89	0.9978	0.9978	0.00367	0.9999	0.25
Baboon							
(watermark- TIET)	(1024× 1024)	52.67	0.9994	0.9999	0.00195	0.9999	0
(watermark- Copyright)		50.50	0.9989	0.9998	0.00235	0.9999	0
(watermark-Thapar_Univ)		51.3	0.9988	0.9998	0.00179	0.9999	0

Table 6.3 'PSNR', 'NCC', 'SSIM', as well as 'GMSD' features for images (512 × 512) besides 'BER (%)' for amalgamations ('TIET' with 'Logo'), ('Copyright' with 'Logo') and ('Thapar_Univ' with 'Logo') correspondingly.

→Standard Parameters ↓Host image with watermark	Dimension	'PSNR'	'NCC'	'SSIM'	'GMSD'	'UIQI'	'BER(%)' for recuperated watermark 1	'BER(%)' for recuperated watermark 2
'Lena' ('TIET' with 'Logo') ('Copyright' with 'Logo') ('Thapar_Univ' with 'Logo')	(512× 512)	42.04 40.34 42.51	0.9972 0.9950 0.9965	0.9962 0.9902 0.9937	0.0177 0.015 0.00535	0.9999 0.9999 0.9999	0 0 0	8.44 12.67 20.26
'Barbara' ('TIET' with 'Logo') ('Copyright' with 'Logo') ('Thapar_Univ' with 'Logo')	(512× 512)	40.19 38.16 37.19	0.9991 0.9964 0.9916	0.9860 0.9803 0.9841	0.000774 0.00725 0.0255	0.9999 0.9999 0.9999	0.88 0 0	5.63 11.27 18.38
'Peppers' ('TIET' with 'Logo') ('Copyright' with 'Logo') ('Thapar_Univ' with 'Logo')	512× 512	42.22 40.7 38.36	0.9987 0.9985 0.9942	0.9925 0.9896 0.9837	0.001714 0.000889 0.01017	0.9952 0.9997 0.9994	0 4.7 0.375	6.22 10.59 19.04
'Baboon' ('TIET' with 'Logo') ('Copyright' with 'Logo') ('Thapar_Univ' with 'Logo')	(512× 512)	33.42 30.58 30.5	0 .9971 0.9896 0.9922	0 .9772 0.9579 0.9543	0.000264 0.012 0.00442	0.9999 0.9996 0.9998	3.11 0 0	5.76 11.52 18.43

Table 6.4 ‘PSNR’, ‘NCC’, ‘SSIM’, as well as ‘GMSD’ features for images (1024 × 1024) besides ‘BER (%)’ for amalgamations (‘TIET’ with ‘Logo’), (‘Copyright’ with ‘Logo’) and (‘Thapar_Univ’ with ‘Logo’) correspondingly.

→Standard Parameters ↓Host image with watermark	Dimension	‘PSNR’	‘NCC’	‘SSIM’	‘GMSD’	‘UIQI’	‘BER(%)’ for recuperated watermark 1	‘BER(%)’ for recuperated watermark 2
Lena (watermarks- TIET and Logo) (watermarks- Copyright and Logo) (watermarks-Thapar_Univ and Logo)	(1024 × 1024)	 40.27 37 37.78	 0.9975 0.9944 0.9942	 0.9919 0.9845 0.9830	 0.038 0.0519 0.0491	 0.9998 0.9995 0.9996	 0 0 0	 17.65 21.43 26.04
Barbara (watermarks- TIET and Logo) (watermarks- Copyright and Logo) (watermarks-Thapar_Univ and Logo)	(1024 × 1024)	 34.94 37.12 38.41	 0.9960 0.9957 0.9959	 0.9908 0.9918 0.9924	 .0304 .026 .0228	 0.9995 0.9997 0.9997	 0 0 0	 5.37 12.01 20
Peppers (watermarks- TIET and Logo) (watermarks- Copyright and Logo) (watermarks-Thapar_Univ and Logo)	(1024 × 1024)	 39.55 48.83 49.13	 0.9970 0.9993 0.9991	 0.9924 0.9983 0.9984	 0.0342 0.00119 0.00159	 0.9998 0.9999 0.9999	 0 1.2 1.25	 6.27 12.57 19.73
Baboon (watermarks- TIET and Logo) (watermarks- Copyright and Logo) (watermarks-Thapar_Univ and Logo)	(1024 × 1024)	 37.69 36.01 36.99	 0.9971 0.9944 0.9945	 0.9930 0.9927 0.9935	 0.0122 0.0177 0.017	 0.9997 0.9994 0.9995	 0 0 0	 5.68 11.2 18.5

Table 6.5 Images after watermarking with recuperated watermarks

a		ti	Copyright	Thapar_Univ	
b		ti	Copyright	Thapar_Univ	
c		ti	Copyright	Thapar_Univ	
d	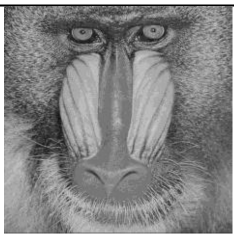	ti	Copyright	Thapar_Univ	

The images for watermarking were initially inserted using watermarks ‘TIET’, ‘Copyright’ and ‘Thapar_Univ’ into the approximated recurrence parameters and exposed to ‘Gauss’ (3 × 3, 5 × 5), ‘Median’ (3 × 3, 5 × 5, 7 × 7), ‘Wiener’ (3 × 3, 5 × 5) Filters as well as ‘Sharp’ assaults. Afterward twin watermarks were utilized for watermarking and exposed to similar assaults. Table 6.6 demonstrates the different merits for ‘PSNR’, ‘NCC’, ‘SSIM’, ‘GMSD’ of assailed images for the various watermarks and their amalgamations. It was observed generally most of the desirable values remained either unaffected or achieved greater values. All highlighted values designated superior outputs.

The effectiveness of the proposed hybrid image-adaptive watermarking technique was proved when both the watermarks were extracted under Salt Pepper, Scaling, and Rotation attacks. These geometric attacks were the most important in an image watermarking technique. As they amended the structure of the watermarked image to a deep extent such that the embedded watermark may weaken permanently. It was a great challenge to extract the watermark under these attacks. The toughness of the prospective technique was reliable against such attacks as shown in Figure 6.8 to Figure 6.10. The charts of variations in ‘PSNR’, ‘NCC’, ‘SSIM’, and ‘GMSD’ were drawn for sole as well as multi folded watermarks. The annotation mentioned in the charts, like, ‘Lena 1’ denoted merits for ‘Lena’ while it was inserted with one watermark while ‘Lena 2’ indicated images with two watermarks.

While the Scaling attack tried to change the bit values for the images after watermarking, the Rotation attack rotated the image with certain angles. Similarly, under Rotation attack, the desirable values of PSNR, SSIM, and NCC were observed to increase (or decrease) when angles were varied from -1^0 to $+1^0$ (or $+1^0$ to -1^0) for both single and combination watermarks. However, the response of BER (%) of retrieved watermarks decreased for negative variation range of angles and vice versa for AHSF.

6.5 COMPARISON

In this Section, the suggested technique for watermarking utilizing an initial watermark was compared with three different watermarking schemes. Results highlighted in bold values indicate the better performance of the proposed technique.

6.5.1 Comparison with Nawaz et al. [161]

First of all, the suggested technique was collated against a scheme for extracting watermarks given by Nawaz et al. [161]. The accelerated feature extraction algorithm of Speed Up Robust Features (SURF) was used with the hybrid combination of Redundant DWT (RDWT) and Singular Value Decomposition (SVD) to improve the watermarking technique against geometric attacks. Images of dimension (512 × 512) were used for inserting the watermark of size (32 × 32). The values of NCC and PSNR were compared under Rotation and Scaling attacks. The results verified the execution of the proposed upgraded hybrid technique.

6.5.2 Comparison with Yadav et al. [131]

The proposed technique was also compared with Yadav et al. [131], who too proposed a hybrid technique of watermarking utilizing the similar combination of

Table 6.6 ‘PSNR’, ‘NCC’, ‘SSIM’, as well as ‘GMSD’ features for assailed images

Noisy PSNR (dB)										
Standard images	Watermark Combination	Under no attack	‘Gauss’ (3× 3)	‘Gauss’ (5× 5)	‘Median’ (3 × 3)	‘Median’ (5 × 5)	‘Median’ (7 × 7)	‘Sharp’	‘Wiener’ (3 × 3)	‘Wiener’ (5 × 5)
‘Barbara’	‘TIET’	48.44	40.2	40.1	33.88	29.0	29.13	9.88	35.57	31.48
	‘TIET’ and ‘Logo’	40.19	38.0	38.34	33.36	29.0	26.8	9.1	35.24	**32.9**
‘Lena’	‘Copyright’	50.61	40.93	40.9	36.22	32.2	30.09	8.64	38.59	35.64
	‘Copyright’ and ‘Logo’	40.34	39.12	39.11	35.34	31.9	29.91	8.63	37.20	35.01
‘Peppers’	‘Thapar_Univ’	43.49	38.45	38.44	34.58	32.10	30.24	9.37	35.96	34.37
	‘Thapar_Univ’ and ‘Logo’	38.36	37.53	38.72	34.11	31.93	30.17	9.34	35.09	34.19
‘Baboon’	‘TIET’	45.30	32.85	32.83	25.03	22.63	21.91	8.62	28.57	26.14
	‘TIET’ and ‘Logo’	33.42	30.85	30.85	24.51	22.39	21.75	8.54	27.43	25.54
Noisy ‘NCC’										
‘Barbara’	‘Copyright’	0.9981	0.9995	0.9995	0.9995	0.9900	0.9994	0.6884	0.9993	1.000
	‘Copyright’ with ‘Logo’	0.9964	0.9786	0.9979	0.9981	**0.9980**	0.9976	0.6812	0.9978	0.9936
‘Lena’	‘Thapar_Univ’	0.9972	0.9986	0.9986	0.9983	0.9992	0.9998	0.6027	0.9986	0.9993
	‘Thapar_Univ’ with‘Logo’	0.9965	0.9979	0.9979	0.9976	0.9986	0.9991	0.6026	0.9958	0.9966
‘Peppers’	‘TIET’	0.9974	0.9990	0.9990	0.9979	0.9986	0.9994	0.6084	0.9985	0.9997
	‘TIET’ with‘Logo’	0.9987	0.9961	0.9961	0.9950	0.9958	0.9965	0.6070	0.9954	0.9967

'Baboon'	'Copyright'	0.9974	1	1	0.999	1	1	0.5873	1	1
	'Copyright' with 'Logo'	**0.9896**	0.9962	0.9963	0.9944	0.9984	0.9986	0.5862	0.9981	1
Noisy 'SSIM'										
'Barbara'	'Thapar_Univ'	0.9991	0.9901	0.9899	0.9241	0.7937	0.6948	0.5742	0.9321	0.8191
	'Thapar_Univ' with 'Logo'	0.9841	0.9833	0.9832	0.9190	0.7904	0.6925	0.5635	0.9319	**0.8202**
'Lena'	'TIET'	0.9996	0.9878	0.9877	0.9360	0.8846	0.8440	0.6275	0.9431	0.9050
	'TIET' with 'Logo'	0.9962	0.9850	0.9849	0.9325	0.8824	0.8421	0.6163	0.9412	0.9042
'Peppers'	'Copyright'	0.9981	0.973	0.9736	0.8886	0.8513	0.8258	0.5321	0.8962	0.8604
	'Copyright' with 'Logo'	0.9896	0.9726	0.9725	0.8860	0.8499	0.8247	0.5172	0.8952	0.8595
'Baboon'	'Thapar_Univ'	0.9997	0.9628	0.9627	0.7299	0.5077	0.4167	0.5265	0.8217	0.6708
	'Thapar_Univ' and 'Logo'	0.9543	0.9458	0.9457	0.7175	0.5015	0.4137	0.4782	0.8157	**0.6716**
Noisy 'GMSD'										
'Barbara'	'TIET'	0.0037	0.01531	0.01541	0.01911	0.07251	0.13	0.259	0.0153	0.0616
	'TIET' and 'Logo'	**0.00078**	0.0271	**0.0149**	**0.0197**	0.0731	0.1314	**0.2521**	**0.0142**	**0.0614**
'Lena'	'Copyright'	0.00317	0.0174	0.0175	0.015	0.0494	0.088	0.1863	0.0086	0.0312
	'Copyright' and 'Logo'	0.015	0.0217	0.0218	0.019	0.0509	0.0892	**0.1844**	0.0129	0.0314
'Peppers'	Thapar_Univ	0.0948	0.0138	0.0138	0.0152	0.0378	0.0675	0.5315	0.01	0.0275
	'Thapar_Univ' and 'Logo'	**0.01017**	0.0142	0.0142	**0.014**	0.0385	0.0676	**0.5131**	**0.0108**	**0.0272**
'Baboon'	TIET	0.00537	0.0111	0.0112	0.05547	0.118	0.169	0.1397	0.0266	0.0753

	'TIET' and 'Logo'	**0.000264**	0.0118	0.0119	0.0654	0.118	**0.1685**	0.1662	0.03	0.0777
Noisy 'UIQI'										
'Barbara'	'TIET'	0.9999	0.9999	0.9999	0.9999	0.9998	0.9997	0.83	0.9999	0.9995
	'TIET' and 'Logo'	0.9999	0.9999	0.9999	0.9999	**0.9999**	0.9997	0.8315	**0.9999**	**0.9999**
'Lena'	'Copyright'	0.9999	0.9999	0.9999	0.9999	0.9997	0.9995	0.7499	0.9999	0.9999
	'Copyright' and 'Logo'	0.9999	0.9998	0.9998	0.9998	0.9996	0.9994	**0.7510**	0.9998	0.9998
'Peppers'	'Thapar_Univ'	0.9999	1	1	0.9968	0.9951	1	0.7318	0.9953	0.9951
	'Thapar_Univ' and 'Logo'	0.9994	1	0.9990	0.9947	0.9924	0.9971	**0.7323**	0.9933	**1**
'Baboon'	'TIET'	0.9999	0.9998	0.9999	0.9996	0.9990	0.9986	0.7659	0.9998	0.9997
	'TIET' and 'Logo'	0.9999	0.9999	0.9999	0.9995	0.9988	0.9984	0.7740	0.9998	0.9997

Table 6.7 Extracted first watermark under different attacks.

<table>
<tr><td colspan="6">‘Lena’ for ‘Gauss Filter’ (3 × 3), ‘Scaling’ (0.5), ‘Median Filter’ (5 × 5), ‘AWGN’ (σ^2=10) , and ‘JPEG’ (10 %) assaults</td></tr>
<tr><td></td><td></td><td></td><td>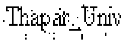</td><td>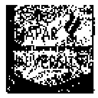</td><td></td></tr>
<tr><td colspan="6">‘Barbara’ for ‘Gauss Filter’ (5 × 5), ‘Scaling’ (2), ‘AWGN’ (σ^2=5), ‘JPEG’ (10 %) and ‘Wiener Filter’ (5 × 5) assaults</td></tr>
<tr><td></td><td></td><td>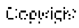</td><td></td><td></td><td></td></tr>
<tr><td colspan="6">‘Peppers’ for ‘JPEG’ (60 %), ‘AWGN’ (σ^2=15), ‘Gauss Filter’ (3 × 3) and ‘Wiener Filter’ (3 × 3) assaults</td></tr>
<tr><td></td><td></td><td></td><td></td><td></td><td></td></tr>
<tr><td colspan="6">‘Baboon’ for ‘Gauss Filter’ (3 × 3) , ‘AWGN ‘(σ^2=20) and ‘Scaling’ (0.75) assaults</td></tr>
<tr><td>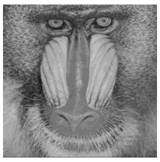</td><td></td><td>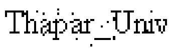</td><td></td><td></td><td></td></tr>
</table>

Table 6.8 Extracted first and second watermarks under various assaults.

Image	'Gauss Filter' (5 × 5)	'Scaling' (1.5)	'Median Filter' (7 × 7)	'Salt & Pepper' (0.01)
				
				
				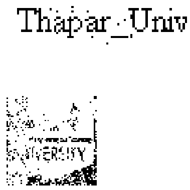
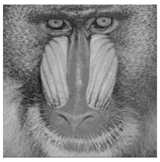			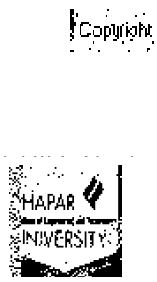	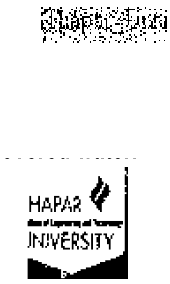

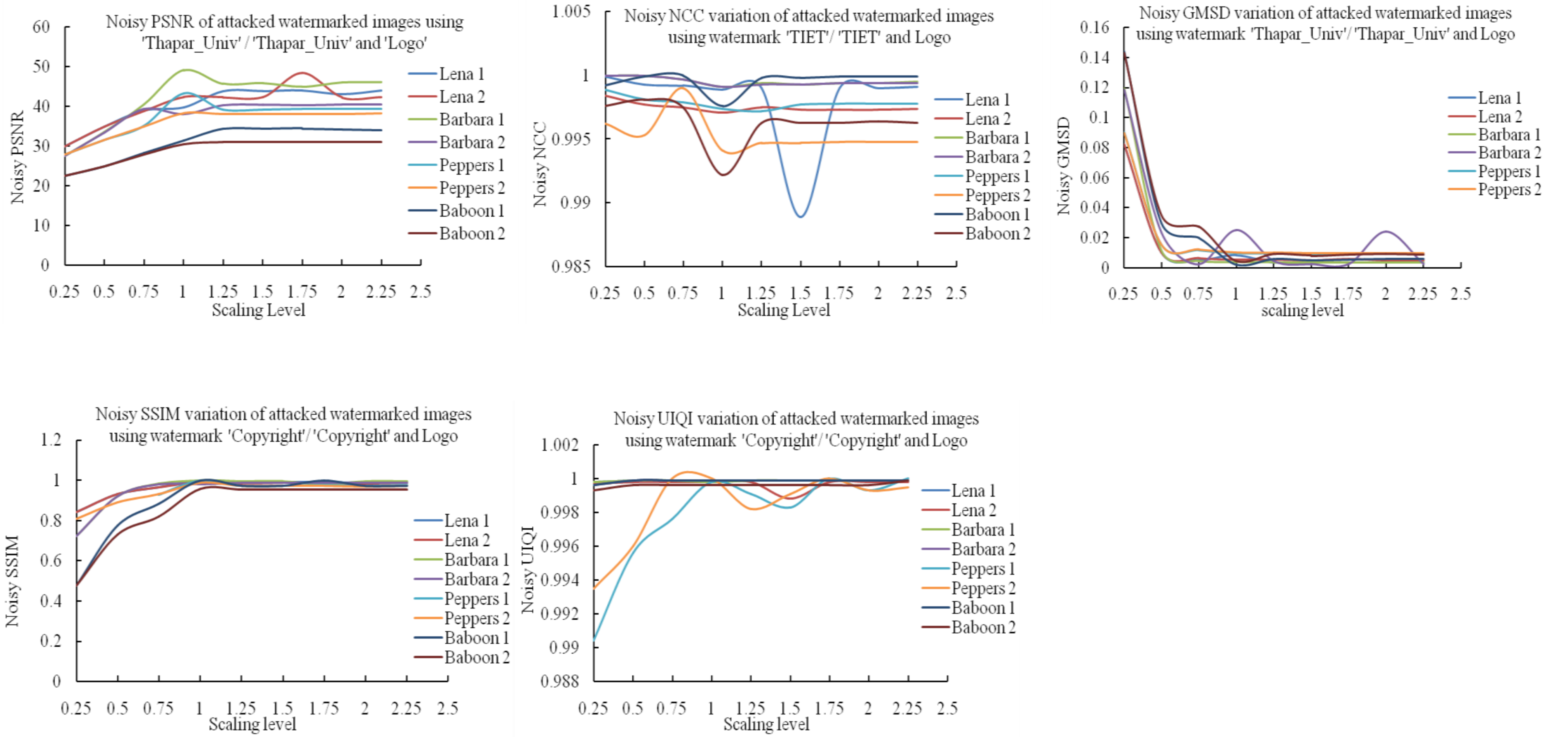

Figure 6.8 Noisy parameter variations for Scaling attack.

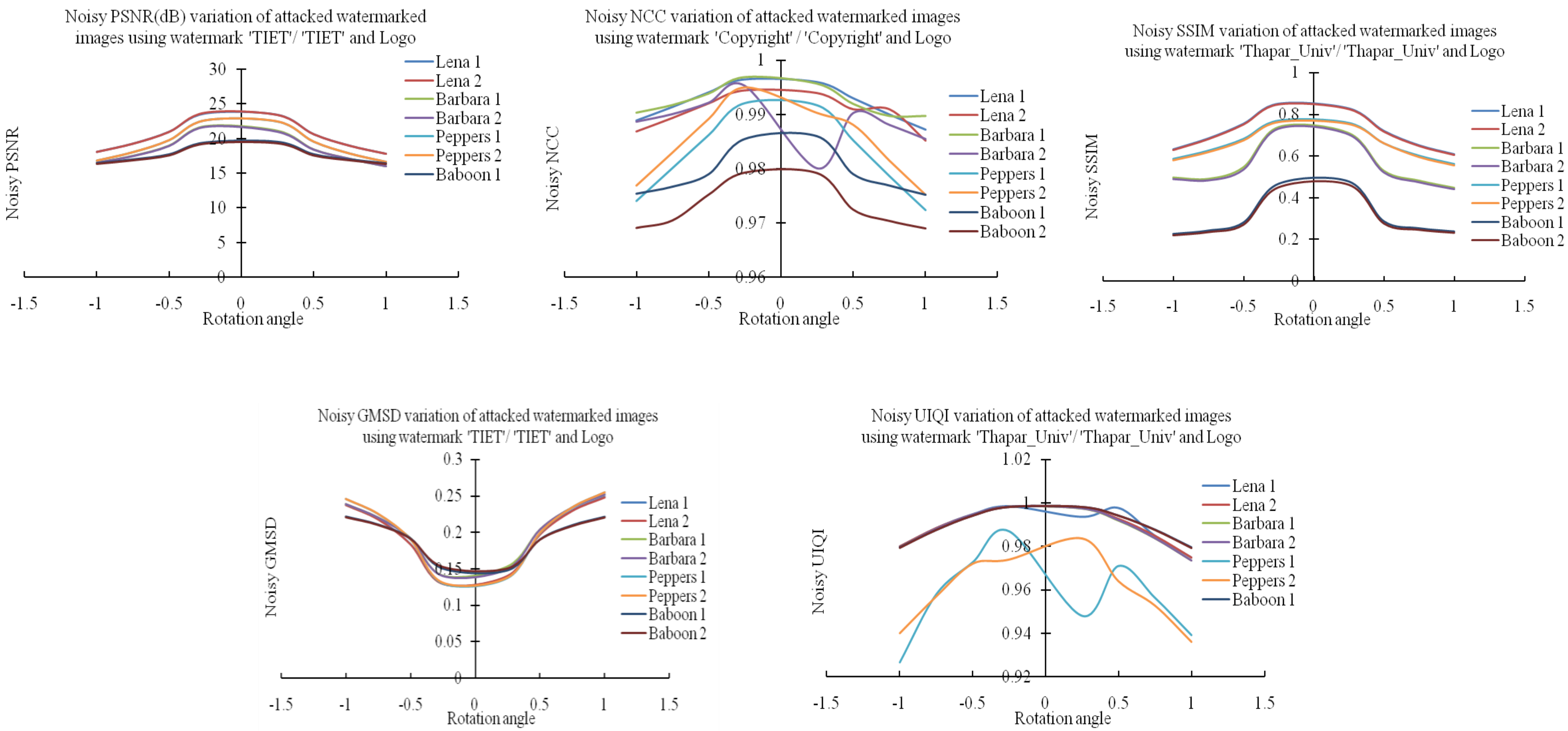

Figure 6.9 Noisy parameters variation for Rotation attack.

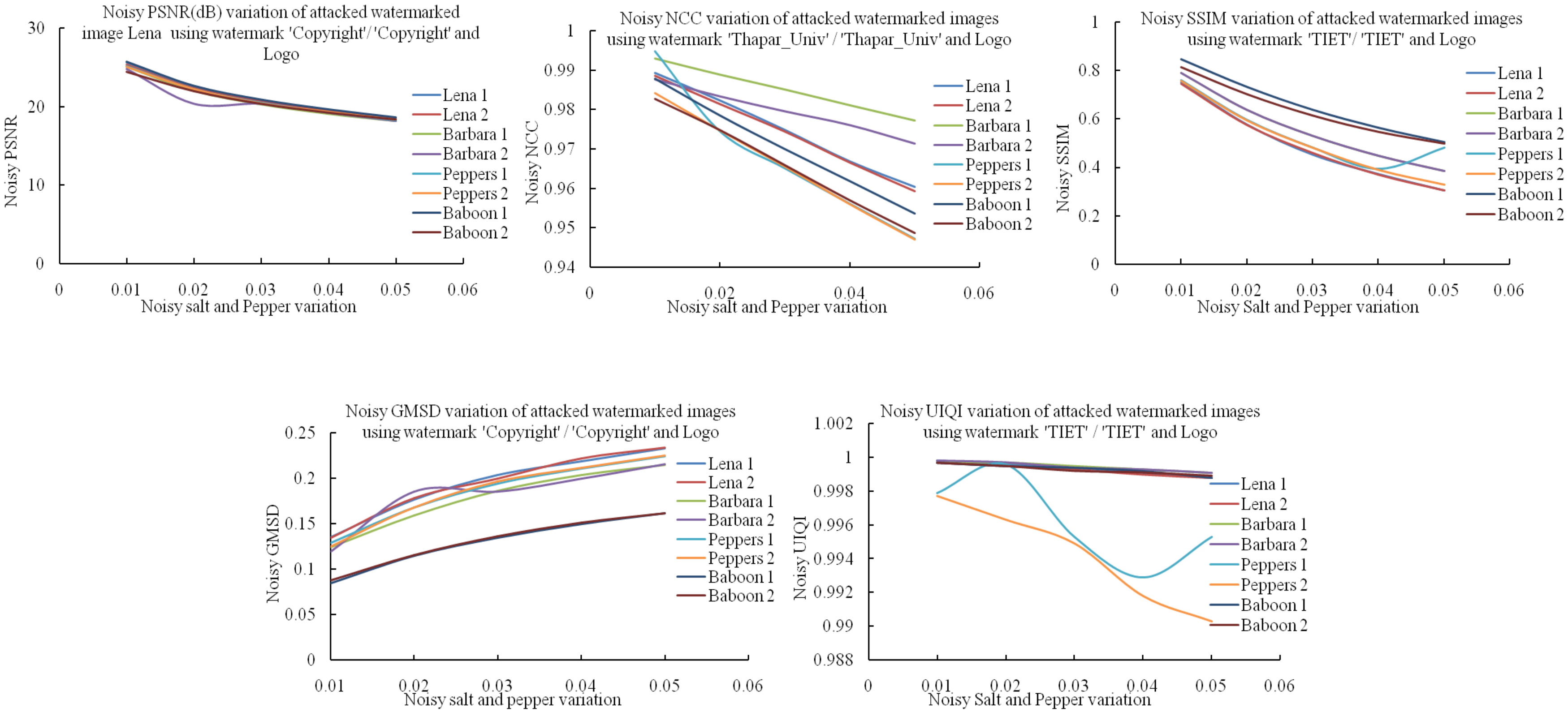

Figure 6.10 Noisy parameters variation for Salt Pepper assaults.

Table 6.9 Comparison of 'PSNR' and 'NCC' of recuperated watermark betwixt suggested technique with Nawaz et al. [161] for watermark dimension (32 × 32) and original images of size (512 × 512).

		Rotation angle									
		+10˚	+30 ˚	+50 ˚	+90 ˚	+120 ˚	-10 ˚	-30 ˚	-50 ˚	-90 ˚	-120 ˚
PSNR	Nawaz et al. [159]	13.35	9.90	7.92	8.42	9.19	13.55	8.94	7.69	8.42	9.23
	Proposed	8.66	7.91	7.84	**9.66**	7.65	9.56	7.78	**7.69**	**10.24**	7.99
NCC	Nawaz et al. [159]	0.92	0.95	0.88	0.86	0.82	0.90	0.91	0.82	0.78	0.86
	Proposed	0.8846	0.9471	**0.9656**	0.8335	**0.9130**	**0.9153**	**0.9304**	**0.9432**	**0.8582**	**0.9566**

		Scaling			
		0.2	0.4	0.6	0.8
NCC	Nawaz et al. [159]	0.76	0.72	0.88	0.30
	Proposed	**0.8851**	**0.8771**	0.8720	0.8672

Table 6.10 Comparison of 'BER (%)' for extracted watermark betwixt suggested technique and Yadav et al. [131].

Host Image → Attacks ↓	'Lena'		'Barbara'		'Baboon'		'Peppers'	
	Yadav et al. [131]	Proposed	Yadav et al. [131]	Proposed	Yadav et al. [131]	Proposed	Yadav et al. [131]	Proposed
Gauss (3 × 3)	0.44	0.88	0.22	11.33	0.44	14.66	0.67	6.22
Gauss (5 × 5)	0.44	0.88	0.22	11.33	0.44	14.66	0.67	6.22
Wiener (3 × 3)	0.22	0.22	0.22	3.55	0.22	5.11	1.11	1.55
Wiener (5 × 5)	1.11	3.33	2.89	11.7	3.78	26.2	2	7.11
Median (3 × 3)	0.44	1.11	0.89	12	21.33	34.44	2	4.22
Median (5 × 5)	3.33	4.88	13.78	24.22	38.67	44.4	9.11	14.6
Scale 0.75	0	0	0	0	0	3.77	1.33	4
Scale 0.9	2.22	**1.1**	0.22	**0**	0	0.88	3.56	**1.11**
Scale 1.1	9.78	**1.55**	4.22	6.41	1.33	5.33	9.11	6.88
Scale 1.5	0	**0**	0	**0**	0	**0**	0.22	**0**
Scale 2	0	**0**	0	**0**	0	**0**	0.44	**0**
Sharp	3.56	11.7	3.33	11.7	9.11	11.7	5.78	11.1
Rotation 0.5°	24.22	33.7	44	52.22	42.67	50	40.89	43.55
Rotation 1°	31.33	37.11	51.33	55.11	48.22	57.2	47.55	49.11

AWGN (5)	0	**0**	0	**0**	0	**0**	1.11	**0**
AWGN (10)	1.11	**0.22**	0.44	**0**	0	0	1.78	**0**
AWGN (15)	1.33	**0.22**	0.67	**0**	0.67	**0**	2	**0.22**
AWGN (20)	1.33	1.33	0.67	**0**	1.33	**0**	3.11	**0.44**
AWGN (25)	2.22	**0.88**	0.67	**0.44**	1.33	**0.22**	2.22	**0.66**
AWGN (30)	2	2.22	1.56	**0.66**	1.56	**0.22**	2	**0.88**
JPEG (10%)	11.56	20	12.44	19.77	12.44	22.6	14.22	22.44
JPEG (20%)	3.33	4.66	1.33	6.44	1.11	9.33	4.67	9.77
JPEG (30%)	2	**0.88**	0	11.77	0.22	2.87	2.22	4.88
JPEG (40%)	0.44	**0.22**	0	0.66	0	0.88	1.33	2.22
JPEG (50%)	0	0.22	0.22	**0**	0	0.66	0.67	1.33
JPEG (80%)	0	**0**	0	**0**	0	**0**	1.11	**0.44**
JPEG (90%)	0	**0**	0	**0**	0	**0**	0.67	**0**

DWT and FWHT with original images of dimension (512 × 512) and watermark (18 × 25). Results for ‘BER (%)’ of recuperated watermark were compared against Filtering, Sharpening, Scale, Rotation, AWGN, and JPEG attacks. The achievement of the proposed technique was again highlighted for Scaling, AWGN, as well as JPEG attacks.

6.5.3 Comparison with Savakar et al. [162] and Ghuli et al. [163]

A general comparison was also done with the latest techniques of Savakar et al. [162] and Ghuli et al. [163]. All these techniques too used the hybrid combination of DWT ad FWHT. It is again observed that the proposed technique gave better PSNR values of watermarked images, as shown in Table 6.9.

Table 6.11 Comparison of PSNR (dB) of watermarked images.

	Yadav et al. [96]	Savakar et al. [162]	Ghuli et al.[163]	Proposed
PSNR(dB)	45	35.0699 to 35.390	43-48	43-53dB

6.6 APPLICATIONS FOR TELE-MEDICINE

The comparison given in Tables 6.9, 6.10, and 6.11 demonstrated that the proposed technique exhibited better stability against different state-of-art schemes. Thus, unlike previous chapters, the proposed technique again found suitable applications in the field of medicine.

In this section, three medical host images, namely, ‘Liver1’, ‘MRI Brain’ and ‘X-Ray’ were used for two watermarks, ‘Patient watermark’ and ‘Joint’ (32 × 32) as shown in Figure 6.7.

Similar to the proposed technique, the first degree of disintegration of Daubechies wavelet was utilized in the computation of 2-D DWT for medical host images. The LL and LH frequency coefficients were again transformed through FWHT. The watermark bits were inserted into these coefficients to obtain the watermarked images. The watermarked images for all medicinal images and the recuperated watermarks were shown in Figure 6.11.

The quality parameters such as, ‘PSNR’, ‘SSIM’, ‘NCC’ and ‘GMSD’ of the images after watermarking were given in Table 6.12. It was noticed that every and each watermark amalgamation presented desirable constants. The competence of the suggested method for medicinal watermarking was inspected against various assaults and dispensed in Table 6.13. The values of NCC and SSIM after attacks too approximated the desirable value of unity. Better values of PSNR ensured imperceptibility with minimum values of GMSD under JPEG Compression, AWGN variances, scaling, sharpening, and filtering attacks.

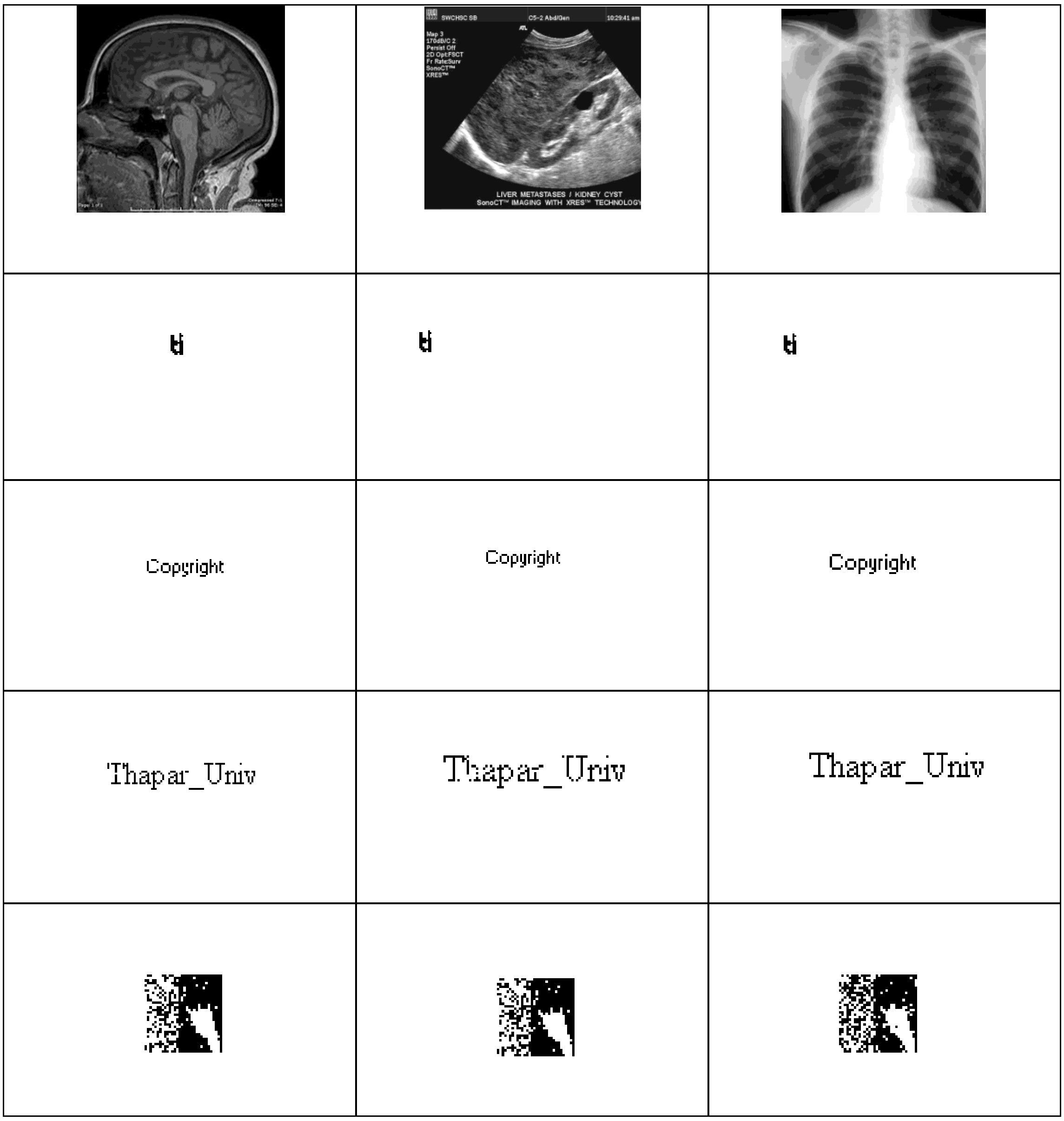

Figure 6.11 Watermarked medicinal images and recuperated watermarks.

Table 6.12 ‘PSNR’, ‘NCC’, ‘SSIM’ as well as ‘GMSD’ features for medicinal watermarked images of dimension (512 × 512).

→ Standard Quality Parameters ↓ Host image with watermarks	‘PSNR’ (in dB)	‘NCC’	‘SSIM’	‘GMSD’	‘UIQI’	‘BER (%)’ of first recovered watermark	‘BER (%)’ of second recovered watermark
‘Liver’							
(‘TIET’ with ‘Joint’)	38.45	0.9987	0.9919	0.00134	0.9999	0	19.82
(‘Copyright’ with ‘Joint’)	41.70	0.9938	0.9984	0.00789	0.9998	0	49.5
(‘Thapar_Univ’ with ‘Joint’)	39.42	0.9894	0.9977	0.00136	0.9999	0	49.7
‘MRI’							
(‘TIET’ with ‘Joint’)	47.30	0.9980	0.9970	0.00158	0.9997	2.88	26.75
(‘Copyright’ with ‘Joint’)	55.36	0.9984	0.9995	.00071	0.9999	5.4	59.66
(‘Thapar_Univ’ with ‘Joint’)	54.17	0.9971	0.9985	.001	0.9996	5.43	58.39
‘X-Ray’							
(‘TIET’ with ‘Joint’)	36.85	0.9922	0.9835	0.0412	0.9994	0	25.09
(‘Copyright’ with ‘Joint’)	33.92	0.9856	0.9661	0.063	0.9988	0	50
(‘Thapar_Univ’ with ‘Joint’)	33.61	0.9829	0.9574	0.0626	0.9987	0	51.46
‘Liver’ (‘Patient watermark’ with ‘Joint’)	38.45	0.9994	0.9919	0.00195	0.9999	0.22	19.92
‘MRI’ (‘Patient watermark’ with ‘Joint’)	46.70	0.9987	0.9966	0.00363	0.9997	2.88	24.31
‘XRAY’ (‘Patient watermark’ with ‘Joint’)	36.85	0.9987	0.9752	0.0533	0.9996	0	25.9

Table 6.13 'PSNR', 'NCC', 'SSIM' as well as 'GMSD' features for medicinal watermarked images against various assaults.

Assault	'PSNR'	'NCC'	'SSIM'	'GMSD'	'UIQI'	Watermark Combination	Host image
Gauss (3 × 3)	30.36	1	0.9779	0.05	0.9988	('TIET' with 'Joint')	'Liver'
Median (7 × 7)	17.51	1	0.6501	0.1984	0.9961		
Wiener (5 × 5)	28.19	1	0.8038	0.0801	0.9994		
Rotation (0.25˚)	16.57	0.9598	0.7182	0.1863	0.9886		
Rotation (-0.75˚)	14.19	0.9237	0.5520	0.2592	0.9618		
Scale (0.5)	22.58	1	0.8740	0.08	0.9993		
Scale (2)	31.25	1	0.9828	0.0367	0.9999		
Salt_Peppers (0.05)	17.53	0.9236	0.4401	0.3062	0.9853		
Gauss (3 × 3)	30.69	1	0.9834	0.05	0.9996	('Copyright' with 'Joint')	'Liver'
Median (7 × 7)	17.49	1	0.6538	0.1976	0.9763		
Wiener (5 × 5)	28.33	1	0.8052	0.079	0.9991		
Rotation (0.25˚)	16.54	0.9548	0.7206	0.1864	0.9884		
Rotation (-0.75˚)	14.17	0.9188	0.5504	0.2594	0.9615		
Scale (0.5)	22.57	1	0.8754	0.08	0.9990		
Scale (2)	31.54	1	0.9877	0.0326	0.9997		
Salt_Peppers (0.05)	17.43	0.9177	0.4361	0.3067	0.9839		
Gauss (3 × 3)	30.47	1	0.9831	0.051	0.9994	('Thapar_Univ' with 'Joint')	'Liver'
Median (7 × 7)	17.49	0.9957	0.6536	0.1979	0.9760		
Wiener (5 × 5)	28.22	0.9975	0.8051	0.079	0.9990		
Rotation (0.25˚)	16.53	0.9506	0.7201	0.1866	0.9883		
Rotation (-0.75˚)	14.15	0.9150	0.5500	0.2594	0.9615		
Scale (0.5)	22.53	0.9976	0.8750	0.081	0.9988		
Scale (2)	31.26	0.9971	0.9872	0.0342	0.9995		
Salt_Peppers (0.05)	17.38	0.9144	0.4372	0.3097	0.9834		
Gauss (3 × 3)	44.95	1	0.9957	0.00301	0.9943	(TIET and Joint)	MRI
Median (7 × 7)	29.66	1	0.8759	0.0886	0.9930		
Wiener (5 × 5)	36.37	1	0.9408	0.039	0.9411		

Rotation (0.25˚)	25.16	0.9858	0.8605	0.1237	0.9048		
Rotation (-0.75˚)	20.32	0.9546	0.6055	0.1963	0.8187		
Scale (0.5)	38.64	1	0.9828	0.00566	0.9796		
Scale (2)	47.94	0.9982	0.9971	0.00146	0.9979		
Salt_Peppers (0.05)	17.61	0.8147	0.3446	0.2578	0.9132		
Gauss (3 × 3)	46.26	1	0.9969	0.00258	0.9945	(‘Copyright’ with ‘Joint’)	‘MRI’
Median (7 × 7)	28.68	1	0.8768	0.0883	0.9511		
Wiener (5 × 5)	36.53	1	0.9416	0.038	0.9426		
Rotation (0.25˚)	25.16	0.9861	0.8611	0.1238	0.9016		
Rotation (-0.75˚)	20.32	0.9549	0.6053	0.1963	0.8139		
Scale (0.5)	38.77	1	0.9830	0.00524	0.9805		
Scale (2)	50.69	0.9985	0.9982	0.00074	0.9980		
Salt_Peppers (0.05)	17.65	0.8160	0.3493	0.2573	0.9242		
Gauss (3 × 3)	46.06	0.9997	0.9969	0.0027	0.9944	(‘Thapar_Univ’ with ‘Joint’)	‘MRI’
Median (7 × 7)	29.68	1	0.8766	0.088	0.9387		
Wiener (5 × 5)	36.54	1	0.9416	0.038	0.9460		
Rotation (0.25˚)	25.16	0.9843	0.8609	0.1238	0.9082		
Rotation (-0.75˚)	20.32	0.9537	0.6050	0.1964	0.8113		
Scale (0.5)	38.72	0.9993	0.9829	0.0054	0.9786		
Scale (2)	49.99	0.9972	0.9981	0.00103	0.9980		
Salt_Peppers (0.05)	17.53	0.8104	0.3395	0.2583	0.9081		
Gauss (3 × 3)	36.55	0.9930	0.9849	0.0423	0.9986	(‘TIET’ with ‘Joint’)	‘X-Ray’
Median (7 × 7)	36.05	0.9934	0.9598	0.04014	0.9928		
Wiener (5 × 5)	36.43	0.9930	0.9670	0.0329	0.9895		
Rotation (0.25˚)	24.63	0.9927	0.9361	0.1064	0.9856		
Rotation (-0.75˚)	19.97	0.9887	0.8372	0.1800	0.9679		
Scale (0.5)	36.81	0.9921	0.9799	0.036	0.9963		
Scale (2)	36.94	0.9920	0.9847	0.039	0.9994		
Salt_Peppers (0.05)	17.82	0.9493	0.2560	0.2481	0.9876		
Gauss (3 × 3)	33.85	0.9865	0.9692	0.0608	0.9980	(‘Copyright’ with’ Joint’)	‘X-Ray
Median (7 × 7)	33.87	0.9872	0.9495	0.0516	0.9922		

Wiener (5 × 5)	34.05	0.9865	0.9574	0.045	0.9897		
Rotation (0.25˚)	24.37	0.9861	0.9201	0.1122	0.9849		
Rotation (-0.75˚)	19.87	0.9822	0.8222	0.1814	0.9674		
Scale (0.5)	34	0.9856	0.9651	0.054	0.9957		
Scale (2)	33.99	0.9855	0.9680	0.06	0.9987		
Salt_Peppers (0.05)	17.78	0.9438	0.2512	0.2443	0.9858		
Gauss (3 × 3)	33.89	0.9838	0.9622	0.0603	0.9978	(‘Thapar_Univ’ and ‘Joint’)	‘X-Ray’
Median (7 × 7)	33.74	0.9847	0.9463	0.0506	0.9921		
Wiener (5 × 5)	33.91	0.9839	0.9545	0.0443	0.9896		
Rotation (0.25˚)	24.32	0.9834	0.9129	0.1122	0.9847		
Rotation (-0.75˚)	19.86	0.9796	0.8149	0.1810	0.9673		
Scale (0.5)	33.73	0.9830	0.9591	0.054	0.9985		
Scale (2)	33.69	0.9828	0.9607	0.0594	0.9986		
Salt_Peppers (0.05)	17.77	0.9412	0.2493	0.2468	0.9845		

6.7 SUMMARY

In this chapter, an improved robust hybrid image-adaptive technique of watermarking was suggested utilizing duplet watermarks. DWT was utilized in simultaneous embedding of the watermarks in LL and LH recurrence parameters of (8 × 8) slabs of the original image with large entropy. Three watermarks of dimensions (18 × 25), (20 × 50) and (80 ×20) were used with (64 × 64) size watermark for insertion into LL and LH sub bands of the image. AHSF was computed through entropy and kurtosis to achieve high values of PSNR (45-63 dB) for watermark embedding. Again, a statistical decoder based upon the concept of ML was used in extracting the watermarks profitably using Gaussian distribution with minimum error and deviation. The efficacy of the suggested technique was verified by the prominent rotation attacks, namely scaling and rotation, in addition to common attacks. The results also demonstrated that the proposed scheme was highly safe and durable, as two watermarks were inserted and recovered successfully. The algorithm also found prospective applications in the sphere of medicinal watermarking by attaining a significant equilibrium between the beneficial and crucial affairs of invisibility, toughness, and capability.

CHAPTER 7

CONCLUSION AND FUTURE SCOPE

This chapter concludes the image-adaptive techniques discussed in the previous chapters. Main highlights and prospects of the research work are also presented.

7.1. CONCLUSION

Digital watermarking is mainly used to shield the intellectual and copyright information of the content owner. In this research work, robust image-adaptive watermarking has been done by employing various techniques using statistical modelling based on Gaussian distribution.

A DWT based semi-blind image-adaptive technique has been used to insert three watermarks, namely ‘TIET’ (18×25), ‘Copyright’ (20×50) and ‘Thapar_Univ’ (20×80) into (8 × 8) blocks with large entropy of the natural image. The bits were embedded in the low frequency coefficients for good human perception.The proposed algorithm used ML decoder for accurate extraction of watermarks with minimal error rates from natural as well as medical images. Thus, the technique found suitable applications in the field of telemedicine by embedding different watermarks to accommodate data of patients into their separate medicinal images. In the suggested technique, the versatile dynamic strength factor (αd) was altered utilizing the equations concurrently to achieve the high PSNR values and less BER (0-1%). Greater resistance towards geometrical assaults was too noticed which proved the toughness of the suggested technique with the leading un-detectability against intentional and unintentional attacks.

An improved, strong image-adaptive technique of watermarking was also proposed utilizing twin watermarks. Three watermark combinations utilizing ‘TIET’, ‘Copyright’ , ‘Thapar_Univ’ and ‘Logo’ (64×64) were used for embedding. DWT was utilized to insert the watermarks in LL and LH recurrence parameters of (8 × 8) slabs with large entropy of the original image using a flexible strength factor based on kurtosis. The use of the fourth statistical moment, kurtosis helped to achieve high PSNR (45-54 dB) values with minimum distortion for both simultaneous recovery of watermarks. The values of NCC, SSIM and UIQI too approached the desirable limit of unity with least GMSD values (in 10^{-3}). Again, a statistical procedure standing upon the concept of ML decoder was used in extracting the watermarks profitably.

The outputs depicted the high security and reliability of the suggested scheme. Real-time applications in the area of medicinal watermarking were again achieved by attaining a significant equilibrium betwixt the beneficial and crucial affairs of invisibility, toughness, and capability.

The hybrid combination of DWT and FWHT too helped to achieve high robustness against common as well as important geometrical attacks while embedding a single watermark. Four adaptive hybrid strength factors based upon the combination of different statistical moments of mean, standard deviation, entropy and kurtosis were utilized in insertion of watermarks with minimum BER (%) . The transforms combination was again used to insert two image watermarks simultaneously with desirable PSNR. The hybrid techniques too found suitable applications in the field of medicine by attaining a good trade-off amongst high imperceptibility and robustness.

7.2. FUTURE SCOPE

This work has proposed four image-adaptive watermarking techniques applicable to digital natural and medical images but there is still a scope of further improvements in the implementation of proposed techniques. This section discusses some of the possible directions that can improve image-adaptive watermarking techniques.

- Many other hybrid techniques may be implemented using different transform combinations.
- Different statistical approaches or modeling techniques may be used for watermark extraction.
- The proposed techniques are semi blind in nature. The techniques may be proposed for the blind approach of watermark extraction too.
- The use of proposed techniques may be extended to audio and video watermarking also.
- Various encryption or encoding methods may be used to enhance the safety of the side information used in the proposed work.

REFERENCES

[1] C. H. Yang, “Inverted pattern approach to improve image quality of information hiding by LSB substitution,” *Pattern Recognit.*, vol. 41, no. 8, pp. 2674–2683, 2008, doi: 10.1016/j.patcog.2008.01.019.

[2] A. Malik, G. Sikka, and H.K. Verma, "A high capacity text steganography scheme based on huffman compression and color coding," *J. Info. Optim. Sci.*, vol. 38, no. 5, pp. 647-664, 2017, doi: 10.1080/02522667.2016.1197572.

[3] I. J. Cox, J. Kilian, F. T. Leighton, and T. Shamoon, “Secure spread spectrum watermarking for multimedia,” *IEEE Trans. Image Process.*, vol. 6, no. 12, pp. 1673–1687, 1997, doi: 10.1109/83.650120.

[4] N. A. Al-Otaibi and A. A. Gutub, “2-Leyer security system for hiding sensitive text data on personal computers,” *Lect. Notes Inf. Theory*, vol. 2, no. 2, pp. 151–157, 2014, doi: 10.12720/lnit.2.2.151-157.

[5] A. A. Abdelwahab and L. A. Hassaan, "A discrete wavelet transform based technique for image data hiding," *Nat. Radio Sci. Conf*, pp. 1-9, 2008, doi: 10.1109/nrsc.2008.4542319.

[6] D. Baby, J. Thomas, G. Augustine, E. George, and N. R. Michael, “A novel DWT based image securing method using steganography,” *Procedia Comput. Sci.*, vol. 46, pp. 612–618, 2015, doi: 10.1016/j.procs.2015.02.105.

[7] D. Artz, “Digital steganography: Hiding data within data,” *IEEE Internet Comput.*, vol. 5, no. 3, pp. 75–80, 2001, doi: 10.1109/4236.935180.

[8] C. C. Chang, C. Y. Lin, and Y. Z. Wang, “New image steganographic methods using run-length approach,” *Inf. Sci. (Ny).*, vol. 176, no. 22, pp. 3393–3408, 2006, doi: 10.1016/j.ins.2006.02.008.

[9] A. A. A. Gutub, F. Al-Haidari, K. M. Al-Kahsah, and J. Hamodi, “E-text watermarking: Utilizing ‘Kashida’ extensions in Arabic language electronic writing,” *J. Emerg. Technol. Web Intell.*, vol. 2, no. 1, pp. 48–55, 2010, doi: 10.4304/jetwi.2.1.48-55.

[10] K. Tanaka, Y. Nakamura, and K. Matsui, "Embedding Secret Information into a Dithered Multilevel Image," *Proc. IEEE Military Commun. Conf.*, pp. 216-220, 1990, doi: 10.1109/milcom.1990.117416.

[11] K. Tanaka, Y. Nakamura, and K. M. Members, “Embedding the attribute information into a dithered image,” *Syst. Comput. Japan*, vol. 21, no. 7, pp. 43–50, 1990, doi: 10.1002/scj.4690210705.

[12] A. Z. Tirkel, G. A. Rankin, R. M. V. Schyndel, W. J. Ho, N. R. A. Mee, and C. F. Osborne, “Electronic Watermark,” *Digit. Image Comput. Technol. Appl.*, pp. 666–673, 1993.

[13] H. Singh, L. Kaur, and K. Singh, “Fractional M-band dual tree complex wavelet transform for digital watermarking,” *Sadhana - Acad. Proc. Eng. Sci.*, vol. 39, no. 2, pp. 345–361, 2014, doi: 10.1007/s12046-013-0217-2.

[14] N. Yadav and K. Singh, “Robust image-adaptive watermarking using an adjustable dynamic strength factor,” *Signal, Image Video Process.*, vol. 9, no. 7, pp. 1531–1542, 2015, doi: 10.1007/s11760-013-0607-2.

[15] H. Singh, L. Kaur, and K. Singh, “A novel robust logo watermarking scheme using fractional M-band wavelet transform,” *J. Commun. Technol. Electron.*, vol. 59, no. 11, pp. 1234–1246, 2014, doi: 10.1134/s1064226914110199.
[16] N. Yadav, K. Singh, "Transform Domain Robust Image-AdaptiveWatermarking: Prevalent Techniques and Their Evaluation," *IEEE Int. Conf. on Comput., Commun. and Automat.* (ICCCA2015), 2015, pp. 1121–1126, doi: 10.1109/ccaa.2015.7148543.
[17] M. Kallel, J.C. Lapayre, and M.S. Bouhlel, "A multiple watermarking scheme for medical image in the spatial domain," *Int. J. Graphic Image Process.,* vol. 7, no. 1, pp. 37–42, 2007.
[18] A. Giakoumaki, S. Pavlopoulos, and D. Koutsouris,"Secure and efficient health data management through multiple watermarking on medical images," *Med. Biol. Eng. Comput*., vol. 44, pp. 619–631, 2006, doi: 10.1007/s11517-006-0081-x.
[19] A.S. Parah, A.J. Sheikh, F. Ahad, A. N. Loan, and G. M. Bhat, " Information hiding in medical images: a robust medical image watermarking system for E-healthcare," *Multimed. Tools Appl.*, vol. 76, no. 8, pp. 10599–10633, 2015, doi: 10.1007/s11042-015-3127-y.
[20] A. K. Singh, M. Dave, A. Mohan, "Multilevel encrypted text watermarking on medical images using spread-spectrum in DWT domain", *Wireless Personal Comm*., vol. 83, no. 3, pp. 2133–2150, 2015, doi: 10.1007/s11277-015-2505-0.
[21] W. Lu, W. Sun, H. Lu, "Novel robust image watermarking based on subsampling and DWT", *Multimed. Tools Appl.*, vol. 60, pp. 31–46, 2012, doi: 10.1007/s11042-011-0794-1.
[22] K. Rangel-Espinoza, E. Fragoso-Navarro, C. Cruz-Ramos, "Adaptive removable visible watermarking technique using dual watermarking for digital color images", *Multimed. Tools Appl.*, vol. 77, pp. 13047–13074, 2018, doi: 10.1007/s11042-017-4931-3.
[23] S. Roy, A. K. Pal, "A robust blind hybrid image watermarking scheme in RDWT-DCT domain using Arnold Scrambling", *Multimed. Tools Appl.* , vol. 76, pp. 3577–3616, 2017, doi: 10.1007/s11042-016-3902-4.
[24] M. Hamghalam, S. Mirzakuchaki, and M. A. Akhaee, “Geometric modelling of the wavelet coefficients for image watermarking using optimum detector,” *IET Image Process.*, vol. 8, no. 3, 2014, pp. 162–172, doi: 10.1049/iet-ipr.2013.0386.
[25] A. Valizadeh and Z. J. Wang, “An improved multiplicative spread spectrum embedding scheme for data hiding,” *IEEE Trans. Inf. Forensics Secur.*, vol. 7, no. 4, pp. 1127–1143, 2012, doi: 10.1109/TIFS.2012.2199312.
[26] D. Patel, N. Chitaliya, M. Pandya, P. Trivedi, M. B. Potdar, and P. Thakkar, “Digital Video Watermarking : A Retrospective,” *Int. J. Sci. Eng. Res.*, vol. 5, no. 12, pp. 1–11, 2014.
[27] M. A. Akhaee, S. M. E. Sahraeian, B. Sankur, and F. Marvasti, “Robust scaling-based image watermarking using maximum-likelihood decoder with optimum strength factor,” *IEEE Trans. Multimed.*, vol. 11, no. 5, pp. 822–833, 2009, doi: 10.1109/TMM.2009.2012922.
[28] S. M. E. Sahraeian, M. A. Akhaee, B. Sankur, and F. Marvasti, “Information hiding with maximum likelihood detector for correlated signals,” *Digit. Signal Process. A*

Rev. J., vol. 36, pp. 144–155, 2015, doi: 10.1016/j.dsp.2014.09.003.
[29] C. H. Chen, Y. L. Tang, W. S. Hsieh, and M. S. Hwang, “Image tamper detection and recovery by intersecting signatures,” *Telkomnika (Telecommunication Comput. Electron. Control.),*vol. 12, no. 4, pp. 1123–1131, 2014, doi: 10.12928/telkomnika.v12i4.1009.
[30] M. Begum and M. S. Uddin, “Digital image watermarking techniques: A review,” *Inf.*, vol. 11, no. 2, 2020, doi: 10.3390/info11020110.
[31] M. Amirmazlaghani, M. Rezghi, and H. Amindavar, “A novel robust scaling image watermarking scheme based on Gaussian Mixture Model,” *Expert Syst. Appl.*, vol. 42, no. 4, pp. 1960–1971, 2015, doi: 10.1016/j.eswa.2014.10.015.
[32] M. Barni, F. Bartolini, A. Piva, "Improved wavelet-based watermarking through pixel-wise masking", *IEEE Trans Image Process*, vol. 5, pp. 783–791, 2001, doi: 10.1109/83.918570.
[33] C. I. Podilchuk and W. Zeng, “Image-Adaptive watermarking using visual models,” *IEEE J. Sel. Areas in Commun.*, vol. 16, pp. 525 - 539, 1998, doi: 10.1109/49.668975.
[34] A.B. Watson, "DCT quantization matrices optimized for individual images", *Proc. SPIE*, pp. 1-15, 1993.
[35] A. B. Watson, R. Borthwick, and M. Taylor, "Image quality and entropy masking", *Proc. SPIE,* , pp. 295–300, 1997.
[36] Q. Su, Z. Yuan, and D. Liu, “An approximate schur decomposition-based spatial domain color image watermarking method,” *IEEE Access*, vol. 7, pp. 4358-4370, 2018, doi: 10.1109/access.2018.2888857.
[37] C.C. Chang, P. Y. Lin, and J. S. Yeh, “Preserving robustness and removability for digital watermarks using subsampling and difference correlation”, *Inf. Sci.*, vol.179, no. 3, pp. 2283-2293, 2009, doi: https://doi.org/10.1016/j.ins.2009.03.003
[38] C. Qin, H. Wang, X. Zhang, and X. Sun, “Self embedding fragile watermarking based on reference-data interleaving and adaptive selection of embedding mode,” *Inf. Sci.*, vol. 373, no. 516, pp. 233–250, 2016, doi: 10.1016/j.ins.2016.09.001.
[39] Q. Su, D. Lie, Z. Yuan, G. Wang, X. Zhang, B. Chen, and T. Yao, “New rapid and robust color image watermarking technique in spatial domain,” *IEEE Access*, vol. 7, pp. 30398–30409, 2019, doi: 10.1109/access.2019.2895062.
[40] R. Roy, T. Ahmed, and S. Changder, “Watermarking through image geometry change tracking,” *Vis. Informatics*, vol. 2, no. 2, pp. 125-135, 2018, doi: 10.1016/j.visinf.2018.03.001.
[41] S. Sarreshtedari, A. Abbasfar, and M. A. Akhaee, “A joint source–channel coding approach to digital image self-recovery,” *Signal, Image Video Process.*, vol. 11, no. 7, pp. 1371–1378, 2017, doi: 10.1007/s11760-017-1095-6.
[42] U. A. Bhatti, Z. Yu, K. U. N. Zhang, G. S. Member, and L. Yuan, “Hybrid watermarking algorithm using clifford algebra with arnold scrambling and chaotic encryption,” *IEEE Access*, vol. 8, pp. 76386–76398, 2020, doi: 10.1109/access.2020.2988298.
[43] A. Amiri and S. Mirzakuchaki, “A digital watermarking method based on NSCT transform and hybrid evolutionary algorithms with neural networks,” *SN Appl.*

Sci,vol. 2, 1669, August, 2020, doi: 10.1007/s42452-020-03452-0
[44] H. Hu and L. Hsu, “Collective blind image watermarking in DWT-DCT domain with adaptive embedding strength governed by quality metrics,” *Multimed. Tools Appl.*, vol. 76, pp. 6575-6594, 2017, doi: 10.1007/s11042-016-3332-3.
[45] I. Assini, A. Badri, K. Safi, A. Sahel, and A. Baghdad, “Hybrid multiple watermarking technique for securing medical image using DWT-FWHT-SVD”, Int. Conf. Adv. Technol. Signal and Image Processing (ATSIP), pp. 1–6, 2017, doi: 10.1109/atsip.2017.8075569.
[46] M. Mardanpour, M. A. Z. Chahooki, “Robust hybrid image watermarking based on discrete wavelet and shearlet transforms,” *ar Xiv e-prints* (2016): arXiv-1603. pp. 1–23, 2016.
[47] G. Cetinel, L. Cerkezi, “Robust Chaotic Digital Image Watermarking Scheme based on RDWT and SVD,” *Int. J. Imag. Graph. Signal Process.*, vol. 8, , pp. 58–67, 2016, doi: 10.5815/ijigsp.2016.08.08.
[48] T. T. Takore, P. R. Kumar, and G. L. Devi, “A new robust and imperceptible image watermarking scheme based on hybrid transform and PSO,” *Int. J. Intell. Syst. Appl.*, vol. 10, no. 11, pp. 50–63, 2018, doi: 10.5815/ijisa.2018.11.06.
[49] A. Zear, A. K. Singh, and P. Kumar, “A proposed secure multiple watermarking technique based on DWT, DCT and SVD for application in medicine,” *Multimed. Tools Appl.*, vol. 77, no. 4, pp. 4863–4882, 2018, doi: 10.1007/s11042-016-3862-8.
[50] P. Garg, L. Dodeja, and M. Dave, “Hybrid color image watermarking algorithm based on DSWT-DCT-SVD and Arnold transform,” *Adv. Signal Process. Comm., Lecture Notes Elect. Eng.*, vol. 526. pp. 327–336, doi: 10.1007/978-981-13-2553-3.
[51] Y. Zhang, Y. Li, and Y. Sun, “Digital watermarking based on joint DWT – DCT and OMP reconstruction,” *Circuits Syst. Signal Process,* vol. 38, pp. 5135-5148, 2019, doi: 10.1007/s00034-019-01112-2.
[52] A. Elsafty, A. Gamal, P. Kreidl, and G. Merckel, “Structural Health Monitoring: Alarming System,” *Wireless Sensor Netw.*, vol.5, no. 5, pp. 105-115, 2013, 10.4236/wsn.2013.55013.
[53] X. Yu, C. Wang, and X. Zhou, “A robust color image watermarking algorithm based on APDCBT and SSVD”, *Symmetry*, vol. 11, no. 10, pp. 1-18, 2019. doi: 10.3390/sym11101227.
[54] R. Pizzolante, A. Castiglione, B. Carpentieri, A. De Santis, and A. Castiglione, “Protection of microscopy images through digital watermarking techniques,” *Proc. - 2014 Int. Conf. Intell. Netw. Collab. Syst. IEEE INCoS 2014*, pp. 65–72, 2014, doi: 10.1109/incos.2014.116.
[55] Z. Zhou, S. Chen, and G. Wang, “A robust digital image watermarking algorithm based on DCT domain for copyright protection,” *Lect. Notes Comput. Sci. (including Subser. Lect. Notes Artif. Intell. Lect. Notes Bioinformatics)*, vol. 9317 LNCS, pp. 132–142, 2017, doi: 10.1007/978-3-319-53838-9_11.
[56] A. K. Singh, B. Kumar, S. K. Singh, S. P. Ghrera, and A. Mohan, “Multiple watermarking technique for securing online social network contents using Back Propagation Neural Network,” *Futur. Gener. Comput. Syst.*, vol. 86, pp. 926–939, 2018, doi: 10.1016/j.future.2016.11.023.

[57] R. Srivastava, R. Tomar, M. Gupta, and A. K. Yadav, “Image Watermarking Approach Using a Hybrid Domain Based on Performance Parameter Analysis”, *Information*, vol. 12, no. 8, pp. 1-19, 2021.

[58] W. Xiang-yang, P. Niu, T. Jing, Y. Hong-ying, and X. U. Huan, "A blind watermark decoder in NSST domain using BKF vector HMT model," *J. Acta Electronica Sinica*, vol. 49, no. 1, pp. 40-49, 2021, doi: 10.1007/s11042-020-09621-y.

[59] P. Niu, L. Wang, J. Tian, S. Zhang, and X. Wang, "A statistical color image watermarking scheme using local QPCET and Cauchy–Rayleigh distribution", *Circuits Syst. Signal Process*., vol. 40, pp. 4516–4545, 2021, doi: 10.1007/s00034-021-01678-w.

[60] X. Y. Wang, X. Shen, J. Tian, P. Niu, and H. Yang, "Statistical image watermark decoder based on local frequency-domain Exponent-Fourier moments modeling," *Multimed. Tools Appl.*, vol 80, pp. 27717–27755, 2021, doi: 10.1007/s11042-021-11056-y.

[61] D. Ariatmanto and F. Ernawan, “An improved robust image watermarking by using different embedding strengths,” *Multimed. Tools Appl.*, vol. 79, no. 17–18, pp. 12041–12067, 2020, doi: 10.1007/s11042-019-08338-x.

[62] D. Ariatmanto and F. Ernawan, “Adaptive scaling factors based on the impact of selected DCT coefficients for image watermarking,” *J. King Saud Univ. - Comput. Inf. Sci.*, 2020, doi: 10.1016/j.jksuci.2020.02.005.

[63] Q. Zheng, N. Liu, and F. Wang, “An adaptive embedding strength watermarking algorithm based on shearlets’ capture directional features,” *Mathematics*, vol. 8, no. 8, 2020, doi: 10.3390/math8081377.

[64] X. Wang, J. Tian, J. Tian, P. Niu, and H. Yang, “Statistical image watermarking using local RHFMs magnitudes and beta exponential distribution,” *J. Vis. Commun. Image Represent.*, vol. 77, 2021, doi: 10.1016/j.jvcir.2021.103123.

[65] P. Niu, X. Shen, Y. F. Song, Y. N. Liu, and X. Y. Wang, "Locally optimum watermark decoder in NSST domain using RSS-based Cauchy distribution", *Multimed. Tools Appl.*, vol. 79, 2020, doi: 10.1007/s11042-020-09621-y.

[66] T. M. Ng and H. K. Garg, “Maximum likelihood detection in image watermarking using generalized gamma model,” *Conf. Rec. - Asilomar Conf. Signals, Syst. Comput.*, vol. 2005, no. 2, pp. 1680–1684, 2005, doi: 10.1109/acssc.2005.1600055.

[67] T. M. Ng and H. K. Garg, “Maximum-Likelihood detection in DWT domain image watermarking using Laplacian modeling”, *IEEE Signal Processing Letters*, vol. 12, pp. 285-288, 2005, doi: 10.1109/lsp.2005.843776.

[68] M. A. Akhaee, S. M. E. Sahraeian, and F. Marvasti, “Contourlet-based image watermarking using optimum detector in a noisy environment,” *IEEE Trans. Image Process.*, vol. 19, no. 4, pp. 967–980, 2010, doi: 10.1109/tip.2009.2038774.

[69] M. A. Akhaee, S. M. E. Sahraeian, and Jin C, “Blind image watermarking using a sample projection approach”, *IEEE Trans. on Inf. Forensics and Secur.*,” vol. 6, pp. 883-893, 2011, doi: 10.1109/tifs.2011.2146250

[70] Y. F. Zhu, “A robust blind image watermarking based on generalized Gaussian distribution”, *Inf. Tech. J.*, vol. 13, pp. 1427-1430, 2014, doi: 10.3923/ijt.2014.1427.1430

[71] R. Cogranne, C. Zitzmann, F. Retraint, I. V. Nikiforov, P. Cornu, and L. Fillatre, "A local adaptive model of natural images for almost optimal detection of hidden data," *Signal Processing*, vol. 100, pp. 169–185, 2014, doi: 10.1016/j.sigpro.2014.01.027

[72] M. Hamghalam, S. Mirzakuchaki, and M. Ali Akhaee, "Vertex angle image watermarking with optimal detector," *Multimed. Tools Appl.*, vol. 74, no. 9, pp. 3077–3098, 2015, doi: 10.1007/s11042-013-1769-1.

[73] M. A. Akhaee and S. M. Ebrahim Sahraeian, "Scaling-based watermarking with universally optimum decoder," *Multimed. Tools Appl.*, vol. 74, no. 15, pp. 5995–6018, 2015, doi: 10.1007/s11042-014-1904-7.

[74] H. Sadreazami , M.O. Ahmad, and M. N. S. Swamy, "Multiplicative watermark decoder in Contourlet domain using the normal inverse Gaussian distribution," *IEEE Trans Multimed.*, vol 18, no. 2, pp. 196–207, 2016, doi: 10.1109/TMM.2015.2508147.

[75] A. Haar, "Zur Theorie der orthogonalen Funktionensysteme," *Math. Ann., vol.* 69, 1910.

[76] A. Grossmann and J. Morlet, "Decomposition of Hardy functions into square integrable wavelets of constant shape," *SIAM J. Math. Anal.*, vol. 15, no. 4, pp. 723-736, 2006, doi: 10.1137/0515056.

[77] I. Daubechies, "Orthonormal bases of compactly supported wavelets," *Fundam. Papers Wavelet Theory*, pp. 564-652, 2009, doi: 10.1515/9781400827268.564.

[78] Y. Meyer, "Orthonormal wavelets," *Wavelets* , pp. 21-37, 1989, doi: 10.1007/978-3-642-97177-8_2

[79] E. E. Abdallah, A. F. Otoom, A. E. Abdallah, M. Bsoul, and S. Awwad, "A hybrid secure watermarking scheme using Nonnegative Matrix Factorization and FastWalsh-Hadamard Transform," *J. Appl. Secur. Res.*, vol. 15, no. 2, pp. 185–198, 2020, doi: 10.1080/19361610.2019.1624100.

[80] T. Khanam, P. K. Dhar, S. Kowsar, and J. M. Kim, "SVD-based image watermarking using the fast Walsh-Hadamard transform, key mapping, and coefficient ordering for ownership protection," *Symmetry*, vol. 12, no. 1, pp. 1–20, 2020, doi: 10.3390/sym12010052.

[81] Y. Zhang, C. Wang, X. Wang, and M. Wang, "Feature-based image watermarking algorithm using SVD and APBT for copyright protection," *Futur. Internet*, vol. 9, no. 2, 2017, doi: 10.3390/fi9020013.

[82] A. Al-Haj and H. Barouqa, "Copyright protection of e-government document images using digital watermarking," *Int. Conf. Inf. Manag. (ICIM)* , pp. 441–446, 2017, doi: 10.1109/infoman.2017.7950424.

[83] F. Ernawan, M. N. Kabir, and Z. Mustaffa, "A blind watermarking technique based on DCT psychovisual threshold for a robust copyright protection," *Int. Conf. Internet Technol. Secur. Trans. (ICITST)*, pp. 92–97, 2017, doi: 10.23919/ICITST.2017.8356354.

[84] B. Lei, X. Zhao, H. Lei, D. Ni, S. Chen, F. Zhou, and T. Wang., "Multipurpose watermarking scheme via intelligent method and chaotic map", *Multimed. Tools Appl.*, vol. 78, no. 19, pp. 27085–27107, 2019, doi: 10.1007/s11042-017-4743-5.

[85] S. P. Ambadekar, J. Jain, and J. Khanapuri, " Digital Image Watermarking Through Encryption and DWT for Copyright Protection," *In book: Recent Trends in Signal and Image Processing*, pp. 187-195, 2019, doi: 10.1007/978-981-10-8863-6_19.

[86] S. Koley, M. R. Nayak, S. N. Bal, and S. K. Sarkar, *Implementation of a Feature-Adaptive Colour Image Copyright Protection Scheme*. *Adv. Comm., Devices Netw., Lecture Notes Elect. Eng.*, vol. 537, pp. 201-211, 2019, doi: 10.1007/978-981-13-3450-4_23.

[87] Q. Su, Y. Niu, G. Wang, S. Jia, and J. Yue, “Color image blind watermarking scheme based on QR decomposition,” *Signal Process.*, vol. 94, pp. 219–235, 2014, doi: 10.1016/j.sigpro.2013.06.025

[88] Q. Su, G. Wang, S. Jia, X. Zhang, Q. Liu, and X. Liu, “Embedding color image watermark in color image based on two-level DCT,” *SIViP*, vol. 9, pp. 991–1007, 2015, doi: 10.1007/s11760-013-0534-2.

[89] T. Huynh-The, C. Hua, N. A. Tu, T. Hur, J. Bang, D. Kim, M. B. Amin, B. H. Kang, H. Seung, and S. Lee, "Selective bit embedding scheme for robust blind color image watermarking", *Inf. Sci.*,vol. 426, pp. 1-18, 2018, doi: 10.1016/j.ins.2017.10.016.

[90] H. Agarwal, B. Raman, and I. Venkat, “Blind reliable invisible watermarking method in wavelet domain for face image watermark,” *Multimed. Tools Appl.*, vol. 74, no. 17, pp. 6897–6935, 2015, doi: 10.1007/s11042-014-1934-1.

[91] X. Wang, Y. Liu, H. Xu, A. Wang, and H. Yang, "Blind optimum detector for robust image watermarking in nonsubsampled shearlet domain," *Inf. Sci.*,vol. 372, pp. 634–654, 2016, doi: 10.1016/j.ins.2016.08.076.

[92] S. Sharmin, M. Khaliluzzaman, M. Mahiuddin, and A. Kafi, "Blind Digital Image Watermarking for Copyright Protection Based on Hadamard Transform", *Adv. Intell. Syst. Comput.*, vol. 814, pp. 215-225, 2019,doi: 10.1007/978-981-13-1501-5_18.

[93] N. A. Loan, N. N. Hurrah, S. A. Parah, J. W. Lee, J. A. Sheikh, and G. M. Bhat, “Secure and robust digital image watermarking using coefficient differencing and Chaotic encryption,” *IEEE Access*, vol. 6, pp. 19876–19897, 2018, doi: 10.1109/access.2018.2808172.

[94] P. R. K. Varma, V. V. Kumari, and S. S. Kumar, "A survey of feature selection techniques in intrusion detection system: A soft computing perspective", *Progress Comput., Anal. Netw.*, vol. 710. , pp. 785-793, 2018, doi: 10.1007/978-981-10-7871-2_75.

[95] A. A. Arrasyid, D. R. I. M. Setiadi, M. A. Soeleman, C. A. Sari, and E. H. Rachmawanto, “Image watermarking using triple transform (DCT-DWT-SVD) to improve copyright protection performance,” *Int. Semin. Res. Inf. Technol. Intell. Syst. ISRITI 2018*, pp. 522–526, 2018, doi: 10.1109/isriti.2018.8864461.

[96] X. Zhou, H. Zhang, and C. Wang, “A robust image watermarking technique based on DWT, APDCBT, and SVD,” *Symmetry*, vol. 10, no. 3, 2018, doi: 10.3390/sym10030077.

[97] W. Xue, L. Zhang, X. Mou, and A. C. Bovik, “Gradient magnitude similarity deviation: A highly efficient perceptual image quality index,” *IEEE Trans. Image Process.*, vol. 23, no. 2, pp. 684–695, 2014, doi: 10.1109/tip.2013.2293423.

[98] F. P. Lestari, C. Anam, Y. Hardiyanti, and F. Haryanto, “Automated Universal

Image Quality Index Measurement vs. Automated Noise Measurement: Which Method is Better to Define CT Image Quality?," *J. Penelit. Fis. dan Apl.*, vol. 9, no. 2, p. 132, 2019, doi: 10.26740/jpfa.v9n2.p132-139.

[99] S. M. R. Islam, X. Huang, and K. Le, "A novel image quality index for image quality assessment," *Lect. Notes Comput. Sci.*, vol. 8228, no.3, pp. 549–556, 2013, doi: 10.1007/978-3-642-42051-1_68.

[100] F. Ernawan and M. N. Kabir, "A blind watermarking technique using redundant wavelet transform for copyright protection," *Int. Colloq. Signal Process. Appl. (CSPA),* pp. 221–226, 2018, doi: 10.1109/cspa.2018.8368716.

[101] N. Yadav and N. Goel, "An effective image-Adaptive hybrid watermarking scheme with transform coefficients," *Int. J. Image Graph.*, vol. 20, no. 1, 2020, doi: 10.1142/S0219467820500023.

[102] R. Pizzolante, A. Castiglione, B. Carpentieri, A. De Santis, and A. Castiglione, "Protection of microscopy images through digital watermarking techniques," *Proc. - 2014 Int. Conf. Intell. Netw. Collab. Syst. IEEE INCoS 2014*, pp. 65–72, 2014, doi: 10.1109/incos.2014.116.

[103] S. Liu, Z. Pan, and H. Song, "Digital image watermarking method based on DCT and fractal encoding," *IET Image Process.*, vol. 11, no. 10, pp. 815–821, 2017, doi: 10.1049/iet-ipr.2016.0862.

[104] S. Jia, Q. Zhou, and H. Zhou, "A novel color image watermarking scheme based on DWT and QR decomposition," *J. Appl. Sci. Eng.*, vol. 20, no. 2, pp. 193–200, 2017, doi: 10.6180/jase.2017.20.2.07.

[105] P. H. Vo, T. S. Nguyen, V. T. Huynh, and T. N. Do, "A robust hybrid watermarking scheme based on DCT and SVD for copyright protection of stereo images," *4th NAFOSTED Conf. Inf. Comput. Sci.*, pp. 331–335, 2017, doi: 10.1109/nafosted.2017.8108087.

[106] B. Harjito and E. Suryani, "Robust image watermarking using DWT and SVD for copyright protection," *AIP Conf. Proc.*, vol. 1813, 2017, doi: 10.1063/1.4975968.

[107] O. Juarez-Sandoval, E. Fragoso-Navarro, M. Cedillo-Hernandez, M. Nakano, H. Perez-Meana, and A. Cedillo-Hernandez, "Improved unseen-visible watermarking for copyrigth protection of digital image," *Proc. 5th Int. Work. Biometrics Forensics,* 2017, doi: 10.1109/iwbf.2017.7935084.

[108] A. Phadikar, P. Jana, and H. Mandal, "Reversible data hiding for DICOM image using lifting and companding," *Cryptography,* vol. 3, no. 3, pp. 21, 2019, doi: 10.3390/cryptography3030021.

[109] H. Chen and W. Xu, "Secure and robust color image watermarking for copyright protection based on lifting wavelet transform," *25th Int. Conf. Mechatronics Mach. Vis. Pract. (MMViP)* , pp. 1–5, 2019, doi: 10.1109/m2vip.2018.8600889.

[110] J. Abraham and V. Paul, "An imperceptible spatial domain color image watermarking scheme," *J. King Saud Univ. - Comput. Inf. Sci.*, vol. 31, no. 1, pp. 125–133, 2019, doi: 10.1016/j.jksuci.2016.12.004.

[111] M. F. Khan, S. M. G. Monir, and I. Naseem, "A novel zero-watermarking based scheme for copyright protection of gray scale images," *Mehran Univ. Res. J. Eng. Technol.*, vol. 38, no. 3, pp. 627–640, 2019, doi: 10.22581/muet1982.1903.09

[112] M. V. Malayil and M. Vedhanayagam, “A novel image scaling based reversible watermarking scheme for secure medical image transmission,” *ISA Trans.*, vol. 108, pp. 269–281, 2021, doi: 10.1016/j.isatra.2020.08.019.

[113] Q. Su, “Novel blind colour image watermarking technique using Hessenberg decomposition,” *Image Procss.*, vol. 10, no. 11, pp. 817–829, 2016, doi: 10.1049/iet-ipr.2016.0048.

[114] N. Mir, “Copyright for web content using invisible text watermarking,” *Comput. Human Behav.*, vol. 30, pp. 648–653, 2014, doi: 10.1016/j.chb.2013.07.040.

[115] D. Rosiyadi, S.-J. Horng, N. Suryana, and N. Masthurah, “A comparison between the hybrid using genetic algorithm and the pure hybrid watermarking scheme,” *Int. J. Comput. Theory Eng.*, vol. 4, no. 3, pp. 329–331, 2012, doi: 10.7763/ijcte.2012.v4.476.

[116] S. Sarreshtedari, S. Member, and M. A. Akhaee, “A source-channel coding approach to digital image protection and self-recovery,” *IEEE Trans. Image Process.*, vol. 24, no. 7, pp. 2266–2277, 2015, doi: 10.1109/TIP.2015.2414878.

[117] M. Amini, M.O. Ahmad, and M. N. S. Swamy, "Digital watermark extraction in wavelet domain using hidden Markov model", *Multimed Tools Appl*, vol. 76, no. 3, pp. 3731–3749, 2017, doi: 10.1007/s11042-016-3975-0.

[118] B. Ahmaderaghi, F. Kurugollu, J. M. D. Rincon, and A. Bouridane, "Blind image watermark detection algorithm based on discrete shearlet transform using statistical decision theory", *IEEE Trans Comput Imaging*, vol. 4, no. 1, pp. 46–59, 2018, doi: 10.1109/tci.2018.2794065.

[119] M. Amini, H. Sadreazami, M.O. Ahmad, and M. N. S. Swamy, "A channel-dependent statistical watermark detector for color images" IEEE Trans Multimed, vol. 21, no. 1, pp. 65–73, 2019, doi: 10.1109/tmm.2018.2851447.

[120] F. Thakkar, V. K. Srivastava, "An adaptive, secure and imperceptive image watermarking using swarm intelligence, Arnold transform, SVD and DWT," *Multimed. Tools Appl.* , vol. 80, pp. 12275–12292, 2021, doi: 10.1007/s11042-020-10220-0.

[121] M. K. Mihçak, I. Kozintsev, K. Ramchandran, and P. Moulin, “Low-complexity image denoising based on statistical modeling of wavelet coefficients,” *IEEE Signal Process. Lett.*, vol. 6, no. 12, pp. 300–303, 1999, doi: 10.1109/97.803428.

[122] M. Singh, S. Singh, and S. Gupta, "An Adaptive speckle suppression filter based on local statistics and edge-map for ultrasound images," *Adv. Sci. Lett.*, vol. 19, no. 8, pp. 2375-2379, 2013, doi: 10.1109/42.387710

[123] N. K. Kalantari, S. M. Ahadi, and M. Vafadust, “A Robust Image Watermarking in the Ridgelet Domain Using Universally Optimum Decoder,” vol. 20, no. 3, pp. 396–406, 2010, doi: 10.1109/tcsvt.2009.2035842.

[124] E. Nezhadarya, Z. J. Wang, and R. K. Ward, “Robust image watermarking based on multiscale gradient direction quantization,” *IEEE Trans. Inf. Forensics Secur.*, vol. 6, no. 4, pp. 1200–1213, 2011, doi: 10.1109/tifs.2011.2163627.

[125] M. Hamghalam, S. Mirzakuchaki, and M. Ali Akhaee, “Vertex angle image watermarking with optimal detector,” *Multimed. Tools Appl.*, vol. 74, no. 9, pp. 3077–3098, 2015, doi: 10.1007/s11042-013-1769-1.

[126] M. Singh, "Processing and Analysis of Ultrasound Images for Tissue Characterization," *PhD. Dissertation*, Thapar University, Patiala, 2014.
[127] Xrayimage:http://cdn.innovativelanguage.com/wordlists/media/thumb/8444_fit512.jpg
[128] MRI image: http://www.oaimaging.com/mri.jpg.
[129] Joint image: https://radiopaedia.org/images/14804579.jpg.
[130] A. A. Mohammed, "Advanced Techniques in Multimedia Watermarking: Image, Video and Audio Applications," *In IGI Publisher of Global Knowledge*, 2010, doi: 10.4018/978-1-61520-903-3.
[131] N. Yadav, "DWT–SVD–WHT Watermarking Using Varying Strength Factor Derived From Means of the WHT Coefficients," *Arab. J. Sci. Eng.*, vol. 43, no. 8, pp. 4131–4143, 2018, doi: 10.1007/s13369-017-2793-7.
[132] Kurtosis formula: https://www.macroption.com/kurtosis-formula/.
[133] C. Song, S. Sudirman, and M. Merabti, "A robust region-adaptive dual image watermarking technique," *J. Vis. Commun. Image Represent.*, vol. 23, no. 3, pp. 549–568, 2012, doi: 10.1016/j.jvcir.2012.01.017.
[134] K. Joshi and R. Yadav, "A LL Subband Based Digital Watermarking in DWT," *Int. J. Eng. Manuf.*, vol. 7, pp. 50–63, 2017, doi: 10.5815/ijem.2017.02.05.
[135] P. Bhinder, K. Singh, and N. Jindal, "Image-adaptive watermarking using maximum likelihood decoder for medical images," *Multimed. Tools Appl.*, vol. 77, no. 8, pp. 10303–10328, 2018, doi: 10.1007/s11042-018-5635-z.
[136] V. S. Verma, R. K. Jha, and A. Ojha, "Digital watermark extraction using support vector machine with principal component analysis based feature reduction," *J. Vis. Commun. Image Represent.*, vol. 31, pp. 75–85, 2015, doi: 10.1016/j.jvcir.2015.06.001.
[137] V. S. Inamdar and P. P. Rege, "Dual watermarking technique with multiple biometric watermarks," *Sadhana*, vol 39, no. 1, pp. 3-26, 2014, doi: 10.1007/s12046-013-0208-3.
[138] R. J. Cintra and T. V Cooklev, "Robust image watermarking using non-regular wavelets," *SiViP*, vol. 3, pp. 241–250, 2009, doi: 10.1007/s11760-008-0070-7.
[139] S. Sharma, P. Fulzele, and I. Sreedevi, "Hybrid Model for Lung Nodule Segmentation based on Support Vector Machine and k-Nearest Neighbor," *International Conference on Computing Methodologies and Communication (ICCMC)*, pp. 170-175, 2020.
[140] H. E. Elshazly, S. O. Faragallah, M. A. Abbas, A. M. Ashour, M. E. Sayed, H. Kazemian, A. S. Alshebeili, E. A. E. Fathi, and S. H. El-Sayed, "Robust and secure fractional wavelet image watermarking," *SIViP*, vol. 9, pp. 89-98, 2014, doi: 10.1007/s11760-014-0684-x.
[141] E. Chrysochos, V. Fotopoulos, M. Xenos, and A. N. Skodras, "Hybrid watermarking based on chaos and histogram modification,", *SiViP*, vol. 8, pp. 843-857, 2012, doi: 10.1007/s11760-012-0307-3
[142] S. Singh and N. R. Prakash, "Modified Adaptive Median Filter for Salt & Pepper Noise", *Int. J. Adv. Res. Comp.Comm. Eng.*, vol. 3, no. 1, 2014.
[143] K. Meenakshi, R. Srinivasa, K. S. Prasad, "A Robust watermarking scheme based

on Walsh-Hadamard Transform and SVD using Zig-Zag Scanning," *13th International Conference on Information Technology,* pp. 2–7, 2014, doi: 10.1109/icit.2014.53.

[144] H. R. Fazlali, S. Samavi, N. Karimi, and S. Shirani, "Adaptive blind image watermarking using edge pixel concentration," *Multimed. Tools Appl.*, vol. 76, no. 2, pp. 3105–3120, 2017, doi: 10.1007/s11042-015-3200-6.

[145] M. Hamidi, E. M. Haziti, H. Cherif, and E. M. Hassouni, "Hybrid blind robust image watermarking technique based on DFT-DCT and Arnold transform," *Multimed. Tools Appl.*, vol. 77, pp. 27181-27214, 2018, doi: 10.1007/s11042-018-5913-9

[146] E. Najafi and K. Loukhaoukha, "Hybrid secure and robust image watermarking scheme based on SVD and sharp frequency localized contourlet transform," *J. Inf. Secur. Appl.*, vol. 44, pp. 144–156, 2019, doi: 10.1016/j.jisa.2018.12.002.

[147] R. Noor, A. Khan, A. Sarfaraz, Z. Mehmood, and A. M. Cheema, "Highly robust hybrid image watermarking approach using Tchebichef transform with secured PCA and CAT encryption," *Soft Comput.*, vol. 23, no. 20, pp. 9821–9829, 2019, doi: 10.1007/s00500-019-03838-2.

[148] D. G. Savakar and A. Ghuli, "Robust Invisible Digital Image Watermarking Using Hybrid Scheme," *Arab. J. Sci. Eng.*, vol. 44, no. 4, pp. 3995–4008, 2019, doi: 10.1007/s13369-019-03751-8

[149] Y. Zhang and Y. Sun, "Optik An image watermarking method based on visual saliency and contourlet transform," *Opt. - Int. J. Light Electron Opt.*, vol. 186, pp. 379–389, 2019, doi: 10.1016/j.ijleo.2019.04.091.

[150] Y. Zhang, B. G. Mobasseri, B. M. Dogahe, and M. G. Amin, "Image-adaptive watermarking using 2D chirps," *SIViP*, vol. 4, pp. 105-121, 2010, doi: 10.1007/s11760-008-0102-3.

[151] P. Bhinder, N. Jindal, and K. Singh, "An improved robust image-adaptive watermarking with two watermarks using statistical decoder," *Multimed. Tools Appl.*, vol. 79, pp. 183-217, 2020, doi: 10.1007/s11042-019-07941-2.

[152] K. Fares, K. Amine, and E. Salah, "A robust blind color image watermarking based on Fourier transform domain," *Optik* , vol. 208, 164562, 2020, doi: 10.1016/j.ijleo.2020.164562.

[153] X. B. Kang, F. Zhao, G. feng Lin, and Y. jun Chen, "A novel hybrid of DCT and SVD in DWT domain for robust and invisible blind image watermarking with optimal embedding strength," *Multimed. Tools Appl.*, vol. 77, no. 11, pp. 13197–13224, 2018, doi: 10.1007/s11042-017-4941-1.

[154] C. Wang, Y. Zhang, and X. Zhou, "Robust image watermarking algorithm based on ASIFT against geometric attacks," *Appl. Sci.*, vol. 8, no. 3, 2018, doi: 10.3390/app8030410.

[155] Z. Yuan, D. Liu, X. Zhang, and Q. Su, "New image blind watermarking method based on two-dimensional discrete cosine transform," *Optik* , vol. 204, 2020, doi: 10.1016/j.ijleo.2019.164152.

[156] X. Zhang, Q. Su, Z. Yuan, and D. Liu, "An efficient blind color image watermarking algorithm in spatial domain combining discrete Fourier transform," *Optik*, vol. 219, 2020, doi: 10.1016/j.ijleo.2020.165272.

[157] L. Chen and J. Zhao, "Contourlet-based image and video watermarking robust to geometric attacks and compressions," *Multimed. Tools Appl.*, vol. 77, no. 6, pp. 7187–7204, 2018, doi: 10.1007/s11042-017-4628-7.

[158] N. Bi, Q. Sun, D. Huang, Z. Yang, and J. Huang, "Robust image watermarking based on multiband wavelets and empirical mode decomposition," *IEEE Trans. Image Process.*, vol. 16, no. 8, pp. 1956–1966, 2007, doi: 10.1109/tip.2007.901206.

[159] D. K. Ahmadaliev, A. A. Medatov, M. M. Jo'rayev, and N. T. O'rinov, " Adaptive Educational Hypermedia Systems: AN Overview of Current Trend of Adaptive Content Representation and Sequencing," *Theor. Appl. Sci.*, vol. 71, no. 03, pp. 58-61, 2019.

[160] J. X. Djumanov, F. F. Rajabov, K. T. Abdurashidova, D. A. Tadjibaeva, and N. S. Atadjanova, "Development of the Method, Algorithm and Software of a Modern Non-invasive Biopotential Meter System," *Intell. Human Comp. Interaction. Lect. Notes Comp. Sci.*, vol. 12615, doi: 10.1007/978-3-030-68449-5_10.

[161] S. A. Nawaz, J. Li, U. A. Bhatti, H. Li, B. Han, and A. Mehmood, "Improved watermarking algorithm based on SURF and SVD with wavelet transformation Against Geometric Attacks," *ACM Int. Conf. Proceeding Ser.*, pp. 49–56, 2020, doi: 10.1145/3383812.3383834.

[162] D. G. Savakar and S. Pujar, "Digital Image Watermarking Using DWT and FWHT," *Int. J. Image, Graph. Signal Process.*, vol. 10, no. 6, pp. 50–67, 2018, doi: 10.5815/ijigsp.2018.06.06.

[163] A. Ghuli, D. G. Savakar, S. and Pujar, "Multiple digital image watermarking using SWT, FWHT and R, G, B Channel," *Innov. Comput. Intell. Comput. Vision*, vol. 1189, pp. 343-350, 2021, doi: 10.1007/978-981-15-6067-5_38.

ABOUT THE AUTHOR

Author was born on 5^{th} September 1979 in Chandigarh. Presently, she is a faculty in Department of Electronics and Communication Engineering, University Institute of Engineering and Technology, Chitkara University, Punjab, India since 2005. She did her Bachelors in Technology (Electronics and Communication) in 2001 and Masters in Technology (Electronics and Communication) in 2005 from Punjab Technical University, Punjab, India. She has worked at different positions at various engineering institutes around Chandigarh and has taught different subjects related to Electronics and Communication engineering. She is having wide experience in the field of teaching, learning and administration.